Impact of climate change and stocking rates on pasture systems in SE Morocco – An Application of the SAVANNA Ecosystem Model

Dissertation

zur

Erlangung des Doktorgrades (Dr. rer. nat.)

der

Mathematisch-Naturwissenschaftlichen Fakultät

der

Rheinischen Friedrich-Wilhelms-Universität Bonn

vorgelegt von

Andreas Roth

aus

Hannover

Bonn, im Dezember 2009

Angefertigt mit Genehmigung der Mathematisch-Naturwissenschaftlichen Fakultät
der Rheinischen Friedrich-Wilhelms-Universität Bonn

Erscheinungsjahr 2010

1. Gutachter: Prof. Dr. H. Goldbach
2. Gutachter: Prof. Dr. B. Diekkrüger
Tag der Promotion: 23. April 2010

For my wife *Therese*

and

in loving memory for my mother

Summary

Extensive sheep and goat grazing provides the main income for population in Morocco's semi-arid to arid areas where rainfall does not permit cropping without irrigation. As processes of vegetation dynamics cannot be assessed via short-term approaches, modelling grazing and biomass productivity may provide better information for planning the sustainable use of these ecosystems.

Southern Morocco has faced decreasing annual rainfall over the last two decades, with a strong impact on the sustainability of the regional ecosystems. Increasing herd sizes as a strategy to offset climate-induced variabilities in animal forage leads to an even more enhanced degradation. The aim of this work was to study the vegetation responses to a changing climate and to alternating livestock numbers. We used the spatially explicit, process-oriented ecosystem model SAVANNA© (Coughenour 1993) to formulise the reaction of the grass, shrub and tree plant functional types (PFT) for the period 1980-2000. The goal was to test its functionality and ability to simulate conditions based on elaborated plant, soil, and climate data. Next we evaluated a range of carrying capacity and climate change scenarios for the period 2001-2050 using the regional climate model REMO.

The objective was to determine whether the simulation results obtained are anthropogenic or climate-induced. The outcomes showed on the one hand that the stocking rate highly influenced biomass production and inter-/ intra-PFT competition, thus reflecting the strong anthropogenic impact, and on the other hand that the climatic impact was weaker. However, together, the stocking rates and the increasing variability of rainfall introduced by the IPCC scenarios largely affected biomass production in all scenarios. All three PFT's aboveground net primary production (*ANPP*) values remained constant or even decreased. Animal energy balances showed a high sensitivity to temporal variations in biomass. A high temporal variability was observed for nitrogen content in plants. Water condition related parameters, e.g. potential evapotranspiration, transpiration, and plant-available soil water are strongly related to rainfall, but showed a specific level of adaptation according to the predicted climate scenarios and livestock number. Under the assumptions made, the model simulated animal energy conditions, life-cycles, and forage values to an acceptable degree indicating both a sustainable resource use and human benefit. The simulation results obtained for plant growth parameters and water status agreed with outcomes from similar modelling approaches found in literature. At the end an adequate model structure was developed delivering future carrying capacity information by analysing the most important functional parts, floristic composition, spatial structure, and productivity of a grazed ecosystem in a water-limited environment.

Kurzfassung

In Trockengebieten wird neben der Bewässerungslandwirtschaft die extensive Beweidungswirtschaft zur Haupteinkommensquelle für die Bevölkerung. Seit Ende der 1970' er Jahre werden im Drâa Einzugsgebiet in Südost Marokko abnehmende jährliche Niederschlagssummen beobachtet. Hinzu kommt eine erhöhte Variabilität der Niederschläge, die sich auf die Vegetation auswirkt und zur Erhaltung des Ökosystems eine Anpassung der Herdengrößen erfordert. Im Hinblick auf eine nachhaltige Ökosystemnutzung wurden in dieser Arbeit Auswirkungen der Klimavariabilität und Herdengröße auf die Vegetationszusammensetzung und ihre Produktivität im Untersuchungsgebiet analysiert. Dazu wurden mit Hilfe des Ökosystemmodells SAVANNA© (Coughenour 1993) Langzeitanalysen von Vegetationsdynamiken unter Beweidung durchgeführt.

Dieses prozessorientierte, raumzeitlich hochauflösende Ökosystemmodell wurde für die Analyse von Kraut-, Strauch- und Baumschichtdynamiken als grundlegende funktionale Pflanzentypen (PFT) für die Basisperiode 1980-2000 verwendet. Auf der Grundlage von erhobenen Tierzensus-, Boden-, Pflanzen- und Klimadaten wurde die Plausibilität und Anwendbarkeit des Modells überprüft um anschließend eine Reihe von Tragfähigkeits- und Klimaszenarien auf der Basis des regionalen Klimamodells REMO über den Zeitraum 2001-2050 zu berechnen.

Das Ziel dieser Arbeit ist anhand der Szenarienergebnisse sowohl den klimatischen als auch den menschlichen Einfluss zu identifizieren. Dabei zeigen die Ergebnisse ein bedeutendes menschliches Einflusspotenzial sowohl auf die gesamte Biomasseproduktion als auch auf die PFT Zusammensetzung. Der klimatische Einfluss wird in den Ergebnissen insbesondere durch das Niederschlagsniveau mit der Rückkopplung auf den regionalen Wasserhaushalt deutlich. Insgesamt langfristiger angelegt als der menschliche Einfluss zeigen die Resultate ein bestimmtes Anpassungsniveau z.B. der Transpiration und potentiellen Evapotranspiration an das verwendete Klimaszenario. Zusammengenommen führen der angenommene Beweidungsdruck und die höhere zukünftige Niederschlagsvariabilität zu erheblichen Veränderungen in der Biomasseproduktivität aller Szenarien. Die Nahrungsgrundlage der Tiere, die fressbare oberirdische Biomasseproduktion (*ANPP*) aller drei PFT, zeigt ebenso eine hohe zeitliche Variabilität und nimmt langfristig, auch durch den Entzug der Nährstoffe, ab. Für die Nachhaltigkeit und Tragfähigkeit des Ökosystems bedeuten die im Szenario erzielten Ergebnisse, dass der saisonale Charakter der Beweidung in Zukunft deutlich wichtiger wird und dahingehend eine Anpassung erfolgen sollte.

Die hier berechneten Szenarienergebnisse zu Pflanzenwachstum, beweidbarer Biomasse und Wasserhaushalt eines semi-ariden Untersuchungsraumes liegen in Übereinstimmung mit Literaturwerten. Damit vereint diese Studie eine adäquate Modellstruktur zur Analyse der wichtigsten funktionalen Ökosystemfaktoren: der floristischen Zusammensetzung, der räumlichen Struktur und ihrer Produktivität in einem wasserlimitierten Untersuchungsgebiet.

Contents

List of Figures

List of Tables

Abbrevations

(F)Intkb	(Forage) Intake rate of browse (0-1); value range: 0 (minimum) - 1 (maximum))
(F)Intkg	(Forage) Intake rate of graze (0-1)
°C	Degree Celsius
°K	Degree Calvin
a	Annual
a.s.l.	Above sea level (m)
Act-N:B	Active Nitrogen (N) to Biomass (B) ratio
ANPP	Aboveground net primary production (g m^{-2})
AnppHrb	Aboveground primary production of herbaceous PFT
AnppShb	Aboveground primary production of shrub PFT
Ans_{season}	Birth giving season (1, 2, 3, 4)
$Areaf_{nsub,nfac}$	Area covered by *nfac* (m^2)
$Atrans_{l,nsp}$	Actual water uptake from soil layer *l* by plant species *nsp* (mm H_2O d^{-1})
avg.	Average
$Avlwat_l$	Available water (mm H_2O d^{-1}) per layer *l*
$Avwpet_{nspt}$	Ratio of total available water to weekly *SysPet* (0-1)
Awpet	Ratio of available water (mm d^{-1}) to *SysPet*
B_1	Slope of the precipitation versus elevation regression equation
B	Biomass
Bs	Base-line simulation (used for sensitivity analysis)
Biomtot	Total (herbaceous and shrub) available biomass (g m^{-2})
BNPP	Belowground net primary production (g m^{-2})
BnppHrb	Belowground primary production of herbaceous PFT
BnppShb	Belowground primary production of shrub PFT
Born	Number of animals born
Bp	Barometric pressure (kPa)
$Bsev_{max}$	Maximum bare soil evaporation (mm)
Bsevw	Weekly bare soil evaporation (mm)
Bulldth	Monthly death rate of mature males (0-1)
Bwmn	Below minimum weight as a function of *CI*
Bwmx	Below maximum weight as a function of *CI*
C	Carbon
C:N	Carbon to nitrogen ratio

Ca	Calcium
Calvdth	Monthly death rate of calves (0-1)
CBTHA	Commissariat pour la Biodivèrsité et Transhumance au Haute Atlas
Cdigst	Current annual stems (0-1)
CI	Condition index (0-1)
cm	Centimetre
CO_2	Carbon dioxide
Conges	Gestation period (number of months)
$Crmx_{nsp}$	Maximum intake rate (kg kg^{-2} d^{-1}) of plant type *nsp*
Cs	Stomatal Conductance (mmol cm^{-2} s^{-1})
Cs-act	Actual simulated stomatal conductance (mmol m^{-2} s^{-1})
Csmx	Maximal Stomata Conductance (mmol cm^{-2} s^{-1})
Cs-pot	Potential simulated stomatal conductance (mmol m^{-2} s^{-1})
$Cvpgr_{nsp}$	Constant cover of root biomass for *nssp* (m^2 g^{-1})
Cvrfac	Fraction of ground (in the grid cell) covered by the facet type (kg ha^{-1})
Cwtkg	Current animal body weight (kg)
d	Day
Dayln	Day length (hours)
Ddigst	Dead leaf digestibility (0-1)
Delwt	Animal weight gain/loss rate (kg d^{-1})
Digest	Mean digestibility of forage (0-1)
Dish	Horizontal travel distances (m)
Distmn	Minimum distance to water (km)
Disv	Vertical travel distances (m)
DMD	Dry matter digestibility
DRH	Direction régionale hydrolique/ Regional hydrology Bureau
Drphmp	Death rate (number d^{-1}) vs. *Phen*
Drtmpp	Death rate (number d^{-1}) vs. T_{avg}
Drtmpsh	Death rate (number $month^{-1}$) vs. T_{avg}
Drwatp	Death rate (number d^{-1}) vs. *Awpet* ratio
Drwatsh	Death rate (number $month^{-1}$) vs. *Awpet* ratio
$Dthnum_{nsp}$	Herbaceous plant mortality (number)
$Dthr_{ageclass}$	Number of animals dying each month per age class
DWT	Dry Weight (g m^{-2})
E	Elevation (m)
e	Daytime vapour pressure (kPa)

Ebal	Predicted animal energy balance as indicated by *CI*
e_c	Vapour pressure in the cuvette (kPa)
Ecbirth	Birth rate per mature female (0-1)
Ecintk	Intake rate decrease when animals are very near their maximum body weight (0-1)
Ecov	Fraction of a subarea that is available for shrub establishment (kg ha^{-1})
Edep	Depth of bare soil evaporation (mm)
Eff-L	Limitation of vegetation growth by light
Eff-N	Limitation of vegetation growth by nitrogen
Eff-T	Limitation of vegetation growth by temperature
Eff-W	Limitation of vegetation growth by water
Eflp	Effect of light (0-1)
Efnp	Effect of nitrogen (0-1)
Efsr(sre)	Effect of shoot:root ratio (0-1)
Eftp	Effect of temperature (0-1)
Efwp	Effect of plant water pressure reducing Cs due to water stress (0-1)
Ehrbeb	Function of total live and dead herbaceous standing crop of all species (0-1)
Ehrbes	0-1 function of *Herbm*
e_l	Vapour pressure in the leaf (kPa)
Elev	Index of elevation suitability (0-1)
Emetab	Product of the gross energy content of digestable plant matter and metabolizability (number)
Eminr	Preference for fresh water (1.0-3.0)
Enal	Function of *Pnb* (0-1)
Enintk(Digest)	Expresses the effect of low digestibility (0-1)
Enintk(N)	Reduction in the intake rate due to low N (protein) content (0-1)
Enup	Function of plant N concentration (0-1)
Epal	Function of *Phen* (0-1)
Epnup	Function of phenophase (*Phen*) (0-1)
e_{sat}	Saturation water vapour pressure (g H_2O m^{-2})
Eseas	Effects of rainfall to water discharge (0-1)
$Estnum_{nsp}$	Number of plants established due to germination
Etgrmb	Germination as a function of T_{avg} (0-1)
Etnup	Function of average daily temperature (T_{avg}) (0-1)
Etrvh	Energy costs of horizontal travel (MJ d^{-1})

Etrvv	Energy costs of vertical travel (MJ d^{-1})
Ewal	Function of the ratio of total available water to *SysPet* (0-1)
Ewgrmb	Germination as a function of *Awpet* (0-1)
Fcp	Volumetric field capacity (%Vol.)
Femaldth	Monthly death rate of mature females (0-1)
Fme	Energy intake rate (MJ d^{-1})
Forragb	Total densities of forage browse in grid-cell (g m^{-2})
Forragg	Total densities of forage graze in grid-cell (g m^{-2})
Frc	Suitability forced by external factors (e.g. fencing) (0-1)
Frg	Forage intake (0-1)
Frkmb	Browse forage densities (g m^{-2}) at half of the daily maximum intake rate
Frkmg	Graze forage densities (g m^{-2}) at half of the daily maximum intake rate
g	Gram
G	Grazing simulation experiment
Gbiom	Green leaf biomass (g m^{-2})
Germrb	Maximal daily germination rate (0-1)
Germrs	Maximum number of new shrubs established per month as a function of *Shbsz*
GIS	Geographic Information System
GLai	Green leaf area index (m^2 m^{-2})
Gr	"Mulch" factor (0.5-1.0)
$Grinis_{nsp}$	Seed germination (g $m^{-2}d^{-1}$)
Grlf	Leaf growth (g m^{-2} d^{-1})
$Grmsa_{nsp}$	Grams of shrub roots per m^2 subarea for *nssp*
ha	Hectare
Hdep	Depth of the herbaceous rooting zone (mm)
Herbm	Total live and dead herbaceous standing crop of all species (g m^{-2})
Hnfor	Number of animals using the forage type *nsp*
$Hpop_{narea}$	Population number in grid cell *narea* (number ha^{-1})
Hpopt	Total population size (number)
Hrbspp1	Sedentary herbaceous biomass consumption (g m^{-2})
Hrbspp2	Nomadic herbaceous biomass consumption (g m^{-2})
Hsf	Habitat suitability affected by forage (0-1)
Hsi	Overall grid cell habitat suitability index (0-1)

IMPETUS	Integratives Management Projekt für den effizienten Umgang mit der Ressource Süßwasser
Intkg(t)	(Total) intake of graze forage (kg d^{-1})
Intkmx	Maximum quality limited intake rate per *nsp* (0-1)
IPCC	International Panel on Climate Change
K	Potassium
k	Extinction coefficient
kg	Kilogram
km	Kilometer
kt	Kilo ton
l	Liter
Lai	Total plant leaf area index (m^2 m^{-2})
leaf	Morphometric proportion of shoot allocation to leaves (0-1)
Lf-N:B	Leaf level- nitrogen to biomass ratio
m	Meter
Mp	Megapascal
Mio	Million
MJ	Megajoule
mmol	Millimol
Mndy	Number of days per month
mol	Mol
N	Nitrogen
N:B	Nitrogen to biomass ratio
Ndtmn	Mean number of days between rainy days plus the rain day itself
NDVI	Normalized digital vegetation index
Ndymx	Maximum number of rainy days
nfac	Number of diagnostic PFT facet (herbaceous (1), shrub (2), tree (3))
NG	Non grazing simulation experiment
N_I	Soil inorganic N concentration (g N m^{-2})
Noise	Term to introduce randomness into spatial distributions, it is a multiplier ranging in values minimum (0) to maximum (1)
NPP	Net primary production (g m^{-2} d^{-1})
nrl	Number of rooting layers
nsp	Number of PFT subspecies (1, 2, 3)
nspt	Number of plant species *nsp* at time *t*
nssp	Shrub species number of sub species
Nstorm	Number of rainy storms in a month

Nstrmw	Mean number of stormy rain days
nsub	Number of diagnostic subarea (1, 2, 3)
Nup_l	Nitrogen uptake at layer *l* (g N $m^{-2}d^{-1}$)
Offtake	Removal of graze forage (g m^{-2} d^{-1})
ORMVAO	Office Régional de Mise en Valeur Agricole Ouarzazate
P	Phosphor
Pdisw	Preference value as a function of *Distmn* (0-1)
Pforage(Tforage)	suitability index for forage abundance (0-1)
PFT	Plant functional types
Phen	Phenophase (1-7)
Phys	Suitability index of the physical habitat (0-1)
$Pinfl_l$	Fraction of rainfall that is infiltrated to each layer *l* (0-1)
Pl-N:B	Plant level-nitrogen to biomass ratio
$Plnum_{nsp}$	Plant density (number per m^2)
Pnb	Plant nitrogen content (g N)
Ppt	Monthly rainfall (mm)
$Ppte_{ij}$	Computed precipitation estimate (mm) at *i*th precipitation datum and *j*th unknown grid point
Ppton	Actual water infiltration into the soil (mm $week^{-1}$)
Pptwk	Fraction of monthly precipitation that occurs in the current week (0-1)
Prefarea	Index for preferred areas included by maps of preferred areas (0, 1)
Prefwater	Suitability index for water (0-1)
Prfb	*nsp* preference-weighted rank value (0-1)
Prfl	Herbaceous shoot growth allocated to reproduction (g m^{-2} d^{-1})
Prfwt	Preference weight parameters for the *nsp* plant type
Prlf	Herbaceous shoot growth allocated to leaves (g m^{-2} d^{-1})
$Proot_l$	Proportion of total roots in soil layer *l*
Prrt	Maximum fraction of *NPP* that can be allocated to roots (0-1)
Ps	Photosynthetic activity (µmol m^{-2} s^{-1})
Psnow	Function of snow depth (cm)
P_{strmn}	Probability of a rainy day (0-1)
Pwatr	Habitat suitability for water distance and quality (0-1)
Rad	Solar radiance (W m^{-2})
Radgl	Monthly sum of daily global shortwave radiation (W $m^{-2}d^{-1}$)
Relh	Relative humidity (%)
Reqnm	Total metabolizable energy required (MJ d^{-1})
Rnemel	Ratio of net to metabolizable energy for weight change (0-1)

Roots	Total root mass density (g m^{-2})
ROSELT	Réseau d´Observatoire et de Surveillance Ecologique à Long Terme
Rsize	Mean root biomass (g m^{-2})
Rtgr	Root growth (g m^{-2}) per month
rwc	Root water content (mm)
s	Second
SD	Statistical Standard Deviation
Sdep	Total simulated soil depth (mm)
$Seedpg_{nsp}$	Maximum number of established plants per gram of germination seed biomass
$Seeds_{nsp}$	Seed biomass in soil (g m^{-2})
Sgrl	Allocation of shoot growth to leaves (0-1)
Shade	Index of shade suitability (0-1)
Shbmx	Simulated maximum size of shrubs (g/plant)
Shbssz	Simulated mean size of shrubs (g/plant)
Shbsz	Shrub size (mm)
Shcvr	Fraction of a subarea that is covered by shrubs (kg ha^{-1})
Shdth	Shrub mortality (number)
Shestb	Shrub establishment (number)
Shgr	Aboveground shoot growth (g m^{-2} d^{-1})
Shnum	Number of shrubs per hectare
Slope	Index of slope suitability (0-1)
Slwat(t)	Soil water (cm) at time *t*
Sm0	Porosity (%)
Sninf	Additional water infiltration input due to snow melt (0-1)
Snrun	Additional water infiltration runoff due to snow melt (0-1)
Sprun	Fraction of runoff during a mean rainy day (0-1)
$Swat_l$	Water (cm) in layer *l*
Swatr 1	Plant available soil water (mm H_2O)
Swatr 2	Field capacity (mm H_2O)
Swatr 3	Wilting point (mm H_2O)
SysPet	Computed potential evapo-transpiration (mm d^{-1})
SysPpt	Simulated rainfall amounts (mm d^{-1}) during model run
t	Simulated time
$T_{atm}max$	Temperature at leaf surrounding atmosphere (°C)
Tavg	Total available graze (g m^{-2})
T_{avg}	Average daily temperature (°C)

Tcons	Total forage intake per animal (kg d^{-1})
Tdelwt	Total weight change rate (kg d^{-1})
$Tdem_{l,nsp}$	Total water demand at layer *l* and *nsp* (mm H_2O d^{-1})
Tfac1N	Total Nitrogen budget of herbaceous PFT
Tfac2N	Total Nitrogen budget of tree PFT
Tfac3N	Total Nitrogen budget of shrub PFT
Tforage	Includes vegetation in animals diet only
Thc	Index of thicket cover suitability (0-1)
$T_{leaf}max$	Maximum temperature at leaf surface (°C)
T_{max}	Maximum daily temperature (°C)
T_{min}	Minimum daily temperature (°C)
Tothrb	Total herbaceous biomass (g m^{-2})
Totshb	Total shrub biomass (g m^{-2})
Totwdy	Total woody biomass (g m^{-2})
trans	Predicted Transpiration (regional) (mm)
$trans_{(l)}$	Predicted Transpiration (mmol cm^{-2} s^{-1}) per layer $_l$
Trvcsh	Horizontal travel costs (J per kg body weight per m)
Trvsv	Vertical travel costs (J per kg body weight per m)
Ungrzb	Ungrazable leaf biomass density (g m^{-2})
Upmx	Maximal N uptake rate (g N/root d^{-1})
Upnkm	Michaelis Menten half saturation constant (g N m^{-2})
Vdef	Vapour pressure deficit (g H_2O m^{-3})
VPD_{max}	Vapour pressure deficit (kPa)
W	Watt
w(k)	Week
Wdcvr	Fraction of a subarea that is covered by trees (kg ha^{-1})
Wdgr	Stem growth (g m^{-2} d^{-1})
Wdigst	Old stem digestibility (0-1)
wlt	Wilting point (Mpascal)
Wltp	Water (cm) held at 5 Mp
WUE	Water use efficiency (g m^{-2} mm^{-1} H_2O)
Youngdth	Monthly death rate of newborns (0-1)
α	Initial slope of the function *Eflp* of *Rad* (mmol m^{-2} sec^{-1})
µmol	Micromole

1 Introduction

The impacts of climate change are brought to the forefront of world agendas primarily by the United Nations Convention on Climate Change (UNFCCC 1992) in the early nineties. This document stimulated discussions worldwide about the effects of climate change and counteractions even beyond the scientific community. Moreover the impacts of climate change (an increase of 0.74°C since 1850 is verified and an increase up to 4°C to 2100 is predicted by UNFCCC (2006)) will affect tremendously water availability around the planet. Since the UNFCCC enacted the Kyoto protocol in 1997, it has been widely proven and accepted that the trends in climate change described in the newest IPCC report from 2007 (IPPC 2007a) will have large impacts on the vulnerability and sustainability of fresh water resources. This is supported by recent research, i.e., (Bates *et al.* 2006; Freeman *et al.* 2007). Arid and semi-arid regions around the globe are particularly affected by fresh water shortages. The environmental and economic costs of climate change will have tremendous impacts on human welfare and lifestyles. It will affect human income and livelihood from animal husbandry and cropping. Especially in arid and semi-arid environments, the availability of water resources is the most important factor limiting family income. Many regions suffer from an increasing water demand under conditions of a likewise increasing water shortage. This applies to many regions in Northern and Eastern Africa. It is believed that by the end of the 21st century, 50% of the human population in Africa may not have adequate access to fresh water (IMPETUS 2003). The United Nations Environmental Program (UNEP) anticipates that by 2025, 25 African countries, including Morocco, will suffer from water shortages if current water consumption trends persist (WRI 1998). From a global viewpoint, grazing areas are the most important land use form practised by humans. As land use is part of an interactive coupling function between atmospheric and terrestrial flows of energy, e.g., water, human decisions will directly affect these coupled processes. In the last decade, the region of Ouarzazate and its rangelands have faced severe episodes of drought (Schulz 2007), and the rangelands have been degraded to various extents. This degradation is not only a result of water scarcity, but also of an inappropriate increase of animal density, which is responsible for overgrazing of rangelands (Ramdane, 2006, Service d´élevage, personal communication). These phenomena are further aggravated by biomass collection for fuel wood, although limited to more lignified parts of vegetation, i.e., branches, and roots (El Moudden 2005). Hence, the way natural resources are handled will affect human welfare in the near future.

1.1 Scientific placement

Climate and land use changes have been identified as the major components of the global change complex (Alverson *et al.* 2000), and it is now widely accepted that they closely interact. Land use and vegetation are the main agents responsible for the coupling of atmospheric and terrestrial processes. The physio-chemical processes involved in the vegetation-climate interface are integrated at the individual plant level (Boulain *et al.* 2006). This is based on the abundance of vegetation in space and time, which is responsible for the coupling and which highly influences energy fluxes between the atmosphere and the land.

Predicting the impact of land management on the hydrology of agricultural areas and rangeland ecosystems will become essential as public demand for water increases and water-related conflicts arise (Reisner 2001; Bremer *et al.* 2001). Globally, the fraction of grassland utilized for pasture is about 70%. This area plays a key role as a nutrient pool and biomass producer for both human needs and herbivores. Grazing affects transpiration and evaporation of water from the soil by removing significant amounts of vegetation (Wraith *et al.* 1987; Bremer *et al.* 2001). This is substantiated, e.g., by REMO simulations for Western Africa, which predict a substantial risk of precipitation decrease if vegetation cover is reduced by more than 50% (IMPETUS 2003). The most important factor determining ecosystem structure, function and productivity in most grassland is the balance between precipitation and evapotranspiration (Gresens 2006).

Managed grazing occupies more than 33 Mio. km^2, or 25% of the global land surface, representing the single most extended form of land use on the planet (Asner *et al.* 2004). Consequently, grazing potentially affects key ecosystem processes over large areas, e.g., the water budget. In Morocco, the overall agricultural area comprises 85,000 km^2, and rangeland totals 210,000 km^2, with 190,300 km^2 of steppes and 19,700 km^2 of forests (FAO 2000). Agriculture in Morocco is under serious pressure: annual reduction of farmer's household income (in US$) due to climatic effects (drought) for livestock and crop production in a semi-arid area are balanced to 82% for livestock and 80% for small (<5 ha) farmsizes (IFAD 1999). Heidecke and Schulz (2008) estimated agriculture (cultivation and breeding) as the major activity for people in the Drâa Region. Accordingly more than 80% of the total surface is used for agriculture and as rangelands. Managing the grazing of rangelands is a major key to assessing the shortage of water resources. Moreover, the Wadi Drâa region (Wadi: Arabic for River Bed) has faced continued drought in the recent decades, leading to a decrease in seasonal animal fodder availability and consequently a decrease in animal numbers (Roth and Heidecke 2008). Irrigated agriculture, most common in the oases of the area, faces severe production losses due to rainfall variability (Ramdane, 2006, Service d´élevage, personal communication). A rainfall gradient has been found for the region which

influences vegetation forms and growth (Hübener *et al.* 2005; Gresens 2006). To avoid a shortage of animal feed due to drought, transhumance tendencies increase. Transhumance is defined as a division into partly agricultural and partly nomadic herding activities to ensure income security. This trend attended decreasing rainfall since the 1980s and so raises territorial conflicts between growing settlements and nomadic pathway zones. Resource saving, traditional herding strategies with seasonal recovery zones (Agdal), were altered, and the environment is endangered by increasing stocking rates, e.g., animal trampling paths, which facilitate soil erosion. More substantial and sustainable strategies must be found, based on a reliable diagnosis of the temporal and spatial development of biomass and its abundance.

A key function of resource management to assess the vulnerability of vegetation is to create comprehensive regional databases. To extrapolate from the plot or field scales (Upscaling), multiple model concepts with various scopes have been developed in recent decades. For example, Wiegand *et al.* (2004) investigated the relationships of phytomass production, plant ground cover and precipitation in a semi-arid South African grassland. The results showed that mean phytomass production per unit of plant ground area does not vary to a major extent on rangelands under similar environmental conditions. A decline in biomass production with an increase in degradation is a first order effect of reduced phytomass ground area. Ecological models have been used worldwide in a wide range of arid, semi-arid and humid locations to determine concurrence, interactions and extinction in annual and perennial grass, shrub and tree plant communities. Vegetation responses to drought, climate change and elevated CO_2 levels have been analysed (Hunt *et al.* 1991; Bonan 1993; Chen *et al.* 1996; Riedo *et al.* 1998; Grant *et al.* 1999; Gillet *et al.* 2002). Other models have been used to analyse the spatial distributions of animals and their nutritional requirements, as well as their roles as interactive determinants of environmental change (White 1984b; Howden *et al.* 1996; Wu *et al.* 1996; Dumont and Hill 2001; Wang *et al.* 2001; Boone *et al.* 2002). Moreover, a large array of modelling approaches has been used to assess plant species distribution and performance, and carbon and nitrogen turnover (Wook and Kim 1997; Latore *et al.* 1999; Wang *et al.* 2001).

A large number of research studies have been conducted to study transpiration as the key parameter for the description of dynamic processes in agro-ecosystems (Kappen *et al.* 1972; Schulze 1972; Zaady *et al.* 2001; Orthmann 2005; Williams and Albertson 2005; Gresens 2006). This inter-linking feature between the system compartments of soil, plants, and the atmosphere is of crucial importance. Therefore, much effort has to be expended on the accurate calculation of transpiration over space and time and if modeled to the the chosen resolution. The main transpiration measurement methods applied are the steady state porometer method (Foetzky 2002; Zhang *et al.* 2002; Gresens 2006) and sap flow

measurements (Hogg and Hurdle 1997; Lundblad *et al.* 2001; Foetzky 2002; Gresens 2006). The accuracies of transpiration measurement methods strongly depend on the research focus, and the appropriate transpiration term, leaves of small plants or sap flow area of trees has to be detected first. Additionally, the understory and overstory effects of trees on shrubs or herbaceous plants must be considered. Accordingly, measurements can reveal large differences in the spatio-temporal resolution. Canopy conductance is a reliable parameter to characterize transpiring biomass (Gresens 2006; Ainsworth and Rogers 2007). The water status of plants is a suitable measure to describe drought stress. Plants use different strategies of water consumption, e.g. stomata closure to overcome periods of drought stress (Nadezhdina 1999; Gresens 2006). Accordingly plant groups of different water consumption strategies may be grouped to functional types and investigated as done in this study.

1.2 The SAVANNA© Model

The SAVANNA© ecosystem model is capable of improving our knowledge of ecosystem interactions, plant responses to drought, nutrient cycling, herbivores and water balance dynamics in arid to semi-arid ecosystems. Its strength is that it simulates all of these processes “at once”; therefore, this model is at the forefront of ecosystem modelling. The aim of this study is to evaluate the responses and dynamics of plant populations facing climate change, grazing intensities and human management alternatives with the given model.

The SAVANNA© ecosystem model was one of the first models capable of simulating the full range of processes that lead to ecosystem changes, such as plant growth, animal population growth and nutrient cycling by soil micro-organisms (Coughenour 2005). It is a powerful model, and like the MUSE-TREEGRASS model (Simioni *et al.* 2000), it is a comprehensive tool, as well. The SAVANNA© model has been applied to mutiple research topics in several regions (Coughenour 1993). Application studies have been conducted in national conservation areas, e.g., Ngorongoro National Park in Kenya (Boone *et al.* 2002) as well as Yellowstone National Park (Coughenour 2005) in the USA. It was further used for the evaluation of carrying capacity of livestock in Australian grazing lands (Ludwig *et al.* 2001), livestock and wildlife in Kruger National Park, South Africa (Kiker 1998), and to manage elk ranges in the Rocky Mountains (Weisberg *et al.* 2002). The aim was to predict the future development of forage and wildlife and to obtain solutions for the enormous pressure on both. It has been used to simulate the effects of different environmental changes, climate change, land-use practises and management strategies. In contrast to many other biogeochemical models, it not only simulates plants, soil, weather and nutrient cycling, but

also includes animals as another layer of complexity. Biogeochemical and other ecosystem models are either static, simulating ecosystem state at a single point in time, e.g., CENTURY, (Parton *et al.* 1992) or have no inherent spatial structure or scale. For example, GRASP (Littleboy and McKeon 1997) and GrazPlan (Moore *et al.* 1997) assumes a homogenous vegetation canopy from which fluxes are simulated in the vertical dimension only (Scurlock *et al.* 2002). In contrast, SAVANNA© represent a dynamic model style by demonstrating the interactions of processes over space and time. Different parts of the landscape are simulated independently but simultaneously, rather than averaging the values for the landscape as a whole.

1.3 The GLOWA IMPETUS project

The GLOWA[1] IMPETUS[2] project is an interdisciplinary project that is run by the Rheinische Friedrich-Wilhelms-University in Bonn and the University of Cologne and financed by the Federal German Ministry of Education and Research (BMBF) under grant No. 01 LW 0103A and by the Ministry of Science and Research (MWF) of the federal state of Northrhine-Westfalia under grant No.223-21200200. The overall objective of this project is the analysis, quantification, and simulation of scarce water resources in two water basins, the Wadi Drâa basin (Morocco) and the Upper Ouéme basin (Benin) in western Africa (Speth *et al.* 2005). About 50 scientists from a wide array of disciplines, from the natural sciences to human and social sciences, work together in this framework to increase understanding of all important aspects of the hydrologic cycle. This work is embedded in the project working group for the Wadi Drâa catchment in south-eastern Morocco.

The main hypothesis of this project is the existence of a meteorological link between the ITC (Inner Tropical Convection Zone) and Northern Africa. In addition, strong evidence has been found for tropical-extra-tropical interactions, where moisture packages originating from West Africa could be associated with precipitation events in the Atlas Mountains. Atmospheric meteorological modelling points to the important role of tropical soil surface temperatures (SST) and the vegetation for the decadal-scale drought conditions observed in West Africa during the 1970s and 80s (Paeth 2004; Christoph and Speth 2000).

---

[1] GLOWA–Global Change and the Hydrological Cycle, Federal Ministry of Education and Research, www.glowa.org

[2] IMPETUS-german: “Integratives Management Projekt für einen effizienten und tragfähigen Umgang mit der Ressource Süßwasser”, english: “An integrated Approach to the Efficient Management of Scarce Water Resources”

At the start, the project's research concentrated on intensive data collection by all disciplines to improve the basic understanding of all compartments of the hydrological cycle in the project area. Each discipline individually identified accurate parameters influencing the water cycle. Next, the project works were dominated by the parameterisation and calibration of appropriate models, followed by the development of appropriate scenarios of land use and human decision-making for each discipline individually. This led to the simulation of identified key problem clusters for climate change. During this phase, field experiments were also used to generate validation parameters. In the final phase, "Spatial Decision Support Systems" (SDSS) and "Information Systems" (IS) were created. These systems are aimed at providing data sets from field experiments and model results according to the individual problem cluster for local decision-making purposes (IMPETUS 2006). Moroccan decision makers, scientists or administrative groups from all disciplines may use these data to solve resource allocation problems related to the fresh water cycle. This concept includes local and regional capacity building programs in the final phase and data sets will be delivered to the counterparts by the end of the project.

The listing below shows the IMPETUS project interdisciplinary work structure for (B) the Wadi Drâa catchment in Morocco[3] (IMPETUS 2006):

Subproject B1: atmospheric variability

Subproject B2: continental hydrosphere

Subproject B3: vegetation ecology and functional relationship

Subproject B4: socio-economic development

Subproject B5: anthropology conditions

This interdisciplinary framework was essential for this study because meteorological scenario data, soil data, remote sensing and eco-physiology databases are essential to obtaining successful ecosystem simulations. However, this study is embedded in the vegetation ecology group (B3) studying vegetation dynamics and its role on the catchment's fresh water cycle. The work presented here will emphasise the complex spatio-temporal dynamics of vegetation under pasture and climatic change.

1.4 Description of the study area

The study area is the hydrological catchment of the Wadi Drâa. This catchment is found in the south-eastern region of the kingdom of Morocco. The High Atlas is orographically the

[3] The project in Benin (A) is organized in a similar way

most dominant part of the research area. It defines the altitudinal top peak (Jebel M'Goun, 4071 m a.s.l.) as well as the floristic, climatic and cultural border towards northern and western parts of the country (Oldeland 2006). This mountain massif is divided into the High-, Middle- and Anti-Atlas (about 1300 m a.s.l.). Mountains cross the country at a length of 700 km from south-west to the north-east. Between the High- and Anti-Atlas is located the basin of Ouarzazate. The city of Ouarzazate is the administrative capital at the province level. Further south the neighbouring province of Zagora, with its capital Zagora, was added to the total area of research. Geographically the study area is located south of the central High Atlas Mountain in south-eastern Morocco (Figure 1).

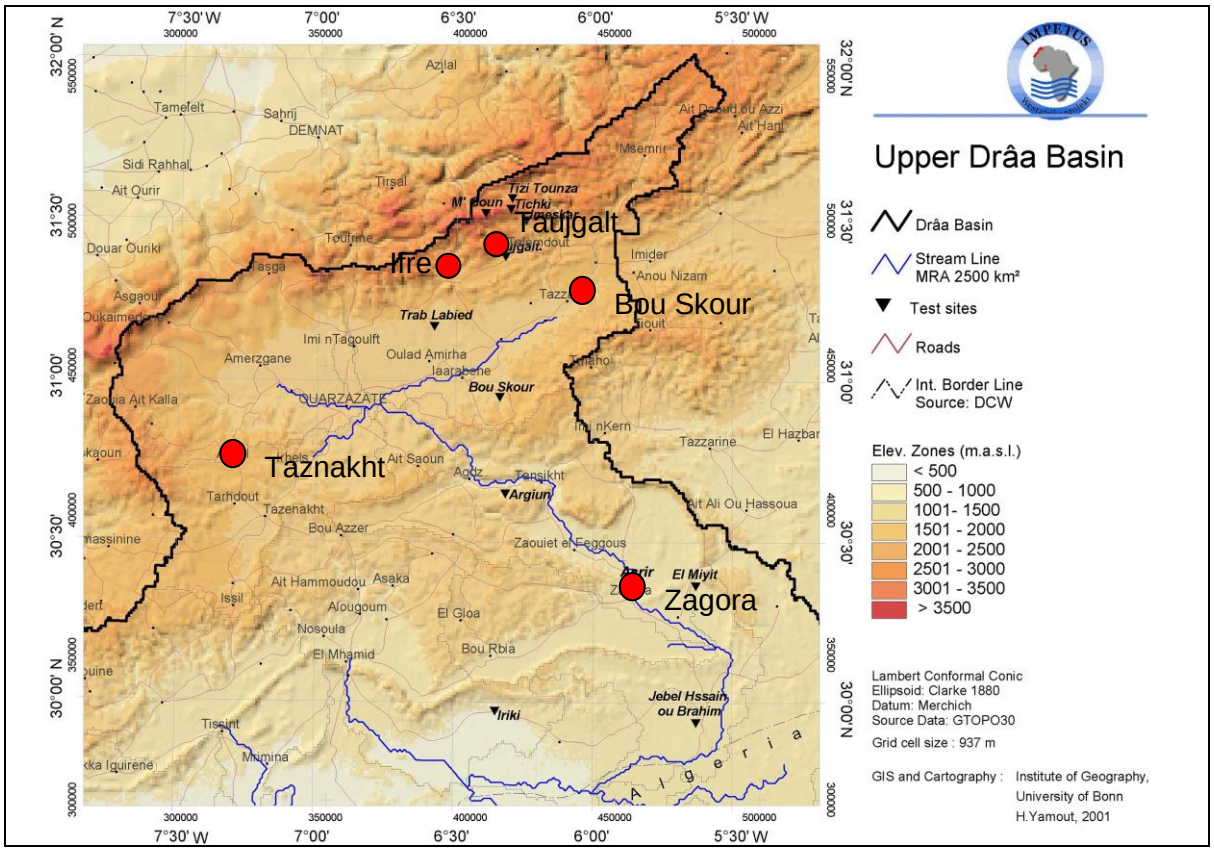

Figure 1: IMPETUS study area: the upper Drâa Basin, elevation zones (m a.s.l.), test-site names (red dots) and stream lines (blue lines) of the Drâa, Ouarzazate, M`Goun and the Dades rivers (Yamout 2007).

Streams using the discharge system of the rivers Dades and M´Goun and originating from the M´Goun Mountain delimitate the research area hydrologically. Next to the city of Ourzazate both rivers compose the river, or Wadi Drâa and are pooled in the reservoir Mansour Eddahbi constructed in 1972. The reservoir with an initial capacity of 560 Mio. m^3 was reduced due to an enhanced sedimentation rate to a recent capacity of 440 Mio. m^3 and is used for irrigation water supply for the downstream oases in the middle Drâa valley (see chapter 1.4.3 and Figure 1). The area is approximately 32,000 km^2, stretching (from north to south) from the top of the M´Goun massif southward to the Ouarzazate basin at approx.

1300 m a.s.l. and further south to the Lac Iriki clay pan at approx. 448 m a.s.l. at the margins of the Sahara desert which is the terminal lake of the Drâa river.

1.4.1 Climate Conditions

Morocco has highly diverse climate conditions over the country. Climatic conditions are regionally differentiated by aridity gradients and the effects of orographic phenomena, in the case of the Drâa catchment the High Atlas mountain massif. In Northern Africa climatic differentiation is mainly due to temperature and precipitation conditions. The Atlas mountain massif divides the country climatically into a north-western oceanic part and a south-eastern Saharan part. The north-western country is characterised by a more maritime, humid-cold climate, whereas the Saharan part has a more continental, dry-hot climate.

During winter the precipitation events in northern Morocco are based on the western drift of cyclones coming from the Atlantic Ocean on their way towards the eastern Mediterranean Sea (Weischet 1991). However, the orographic barrier of the Atlas Mountains largely prevents these hibernal humid air masses from entering and precipitating in the Draa catchment. In the summer the Azoric anticyclone prevents humid air masses from entering the region and instead diverts only dry and hot air. During this period, precipitation is only delivered by extraordinary storm events. Nevertheless, these events (and their intensities) are essential for the regions rainfall balance (Knippertz 2003). In spring and especially autumn, hot subtropical air convections take place. These subtropic humidities lead to extreme precipitation events because of orographic forced advections by the High Atlas Mountains. Sometimes these heavy rains contribute about 75% of total annual precipitation (Schulz 2007). The highest precipitation (Rauh 1952) usually occurs in October/November and February/March. In the Wadi Drâa, from north to south, the gradient of aridity and precipitation variability increases.

The Drâa region is classified as a transition zone between semi-arid and arid climate in the classification scheme (Emberger 1938). According to this classification, an arid climate has precipitation < evaporation for 10 to 12 months annually, whereas for a semi-arid climate this relationship lasts 6 to 9 months a year. A typical index for an arid climate is the lack of perennial streams and an average annual precipitation of <80 mm. Mean temperatures in the upper Drâa catchment (the basin of Ouarzazate) range from –7°C in winter to 40°C in summer. Temperature values in the research area increase from north to south. The above described tendencies are shown in Figure 2 and Figure 3 (below), the monthly averages of precipitation and temperature at the DRH (DRH 2004) station Ifre (see Figure 1) located in the High Atlas Mountains and the IMPETUS climate station at Zagora (located in the

southern Drâa valley). The rainfall regime for both stations is bimodal, dominated by the second half of the year in the longterm perspective. At Ifre station average precipitation amounts are higher, whereas at Zagora station the temperature average is higher.

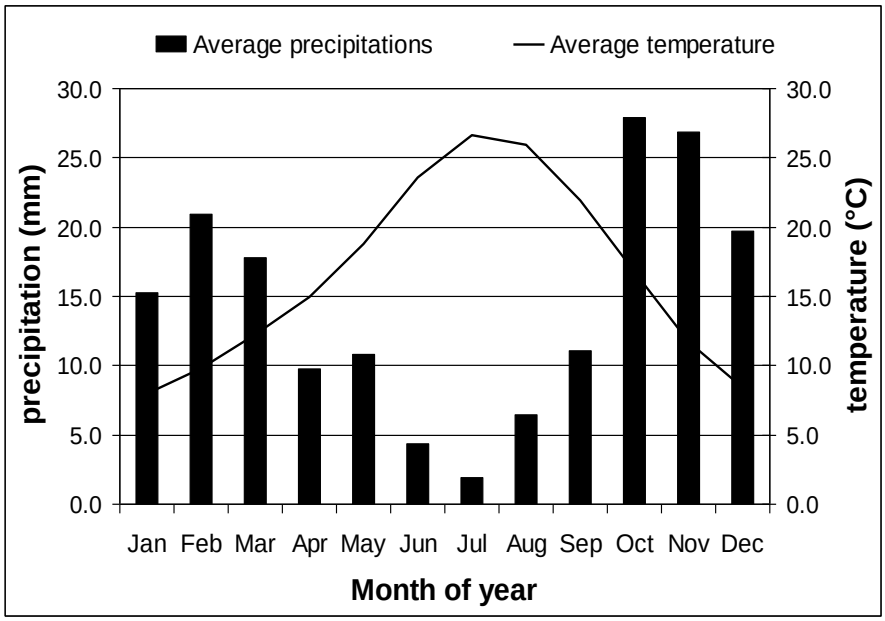

Figure 2: Ifre climate station average monthly temperatures (°C) and precipitation (mm) from 1964-1998 (DRH 2004).

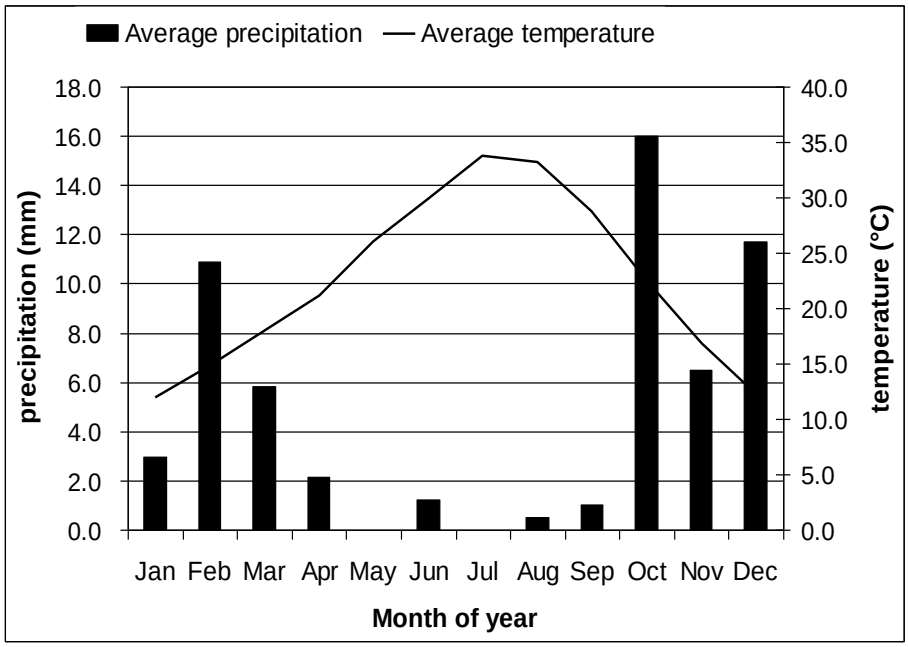

Figure 3: Zagora climate station average monthly temperatures (°C) and precipitation (mm) from 1975-1998 (DRH 2004).

The rainfall amounts decline further southwards with average annual amounts at DRH stations (DRH 2004) of 215 mm at M´semir, to 173 mm at Ifre and 163 mm at Ait Mouted. In the basin of Ouarzazate, annual precipitation amounts rarely exceed 100 mm. South of Ouarzazate, the Anti-Atlas ridge reaches average rainfall amounts of about 200 mm. Further

south the annual precipitation averages decline sharply to 70 mm (Zagora station, Figure 3 and 53 mm at the Foum Z´guid climate station on the border of the Sahara. Most of this rainfall takes place from September to May with an average of 30 to 40 rainy days (DRH 2004).

Another important meteorological feature in semi-arid and arid areas is the amount of water lost in the regional water balance by evaporation. This either occurs by transpiration of plants, which is defined as the water transformation from the fluid to gaseous phase at the boundary layer of plants against water vapour deficit, or water evapo-transpirates from bare soil absorbed by dry air masses depending on temperature, radiation, wind and the vapour deficit (Strasburger *et al.* 1991).

In the Drâa catchment these both influence to a major part the regional water budgets. Potential evaporation was measured in a range of 2000 to 3000 mm yearly (DRH 2004). Following the hypothesis that 90 to 100% of precipitation in arid to semi-arid areas is redistributed to the atmosphere via evaporation and transpiration, vegetation in this area contributes a large proportion of the actual evapotranspiration rate (Gresens 2006).

1.4.2 Pedology

Information on soil textures, bulk densities, soil organic matter and C:N ratio are provided in the project database (Klose 2009). Soil properties vary largely over the catchment. Whereas soil organic matter is relatively high in the High Atlas Mountains, it rapidly decreases further south following the aridity gradient. Soil depth varies with the relief: shallow on tops and ridges and increasing in the basins. Field capacity varies accordingly. Thus, fragments and the skeleton content determine considerably soil hydraulic properties in the area (Klose 2009). These soils are frequently subject to continuing erosion processes. Due to sparse vegetation cover, top soils are removed by soil erosion, especially with extreme precipitation events (IMPETUS 2003) on steep slopes with a high relief energy, chiefly at higher altitudes. Moreover, these soils show a high variance of infiltration capacity (Weber 2004). Channel regimes, such as the Wadis in the south and creeks in mountainous areas, have a high relative percentage of sandy and coarse grained material and thus high infiltration but low water holding capacity, whereas colluvial pediments and topographic depressions with accumulations of fine-textured soils have the highest water holding capacity but the slowest infiltration rates. A third lithological unit was identified on steep rocks and topographic convexities with shallow soil, low infiltration losses and low moisture contents.

Soil types

Different soil types are found in the study area. Based on the above description of soil properties and according to the WRB classification scheme, the following soils have been classified: Anthrosols, Cambisols, Fluvisols, Regosols, Leptosols, Luvisols, Kastanozems, Solochaks, Solonetz, Calcisols and Vertisols. Predominant are Calcisols (~32% of the profiles) and Regosols (~19%), followed by Leptosols (~13%) (Klose 2009). Calcisols are found all over the catchment area on all hillside positions, but 54% of Calcisols are identified in the high Atlas Mountains. Regosols are mainly restricted to the southern part (Anti-Atlas and Sahara foreland) and the lower slope positions of the Drâa catchment. This group represent a poorly developed soil group often found in arid environments. Leptosols occur on upper slope positions (backslope and summit) and are very shallow and rich in brash and gravel (<10% fine material). Consequently ~79% of Leptosols are detected in the mountainous areas of the High Atlas and Anti-Atlas with steep slopes and high erosion rates.

1.4.3 Vegetation

The potential natural vegetation in the study area can be roughly separated into three categories: forests, dry steppes and desert communities (Benabid and Fennane 1994; Msanda *et al*. 2002). Forests are only of marginal importance in the research area as they are largely absent. A compound of trees in the meaning of forests is found only in the oases in terms of fruit trees, i.e., walnut and palm trees (see the latter section). Semi-natural steppes and deserts cover approximately 95% of the Drâa catchment area (IMPETUS 2003). Deserts and steppes are differentiated either by the average annual rainfall (Brovkin *et al.* 1997) or magnitude of evapotranspiration (Noy-Meir *et al.* 1970) and abundance of perennial plants (Le Houérou 1995).

Vegetation cover in turn is highly variable and depends on precipitation, soil conditions and disturbances (mostly grazing). Vegetation abundance largely influences the fate of rainfall water in this area. Moreover spatial patterns and temporal dynamics of vegetation cover influence to a great extent, important features of the water balance such as transpiration, infiltration and run-off (IMPETUS 2003). Besides climatic conditions, vegetation patterns are linked to surface variations and anthropogenic disturbances. High temperatures and radiances, frost in mountainous areas and salty, shallow soils complicate floristic composition for specialists. Vegetation is composed as a consequence of multiple adaption strategies (Müller-Hohenstein and Popp 1990). Vegetation types in the study area are affected to varying degrees by human influence such as fuel wood cutting, agriculture and husbandry.

Primary floristic descriptive works in this area was published by Quézel and Santa (1962) and Le Houérou (1972).

According to the above statements of determents of vegetation, shapes in the following predominant plant communities are introduced. The description of plants follows the gradient of aridity increasing from north to south and an altitudinal gradient decreasing in the same direction. Furthermore, a differentiation between mountainous, steppe and desert vegetation types is made. Agricultural areas and the oases production areas are introduced separately. The principal plant species components, their environmental characteristics, and abundance data of such species are presented here.

Oro- Mediterranean

Dorn bare/dense spiny cushion shrub vegetation and carbonic debris with the predominant vegetation units *Platycapnion saxicolae* and *Arenarion pungentis* cover the upper vegetation belts of the High Atlas. Quézel and Santa (1962) described them between 2800 m and 3400 m a.s.l., above the forest belt. The association of *Arenarion pungentis* is mainly constituted by the thorny cushion shrubs: *Alyssum spinosum, Cytisus balansae, Erinacea anthyllis, Bupleurum spinosum,* and *Vella mairei*. Carbonic debris scones are sparsely populated by hemicryptophytes e.g., *Raffenaldia primuloides, Platycapnion saxicola,* und *Veronica rosea* (Oldeland 2006). This area is characterized by night-day temperature differences of up to 30°K, frosts all year long, high net radiation and laminar soil erosion.

***Juniper thurifera* – *Quercion* tree communities**

Forests composed of *Quercus rotundifolia* and *Juniperus* sub-species (ssp.) in the mountains have largely been destroyed due to fuel wood cutting, and have been replaced by the sub-Saharan sclerophyllus (sage) shrub community. Formerly, the *Quercus* communities largely dominated the area and functioned as the key structural species. They dominate due to their tolerance against fractured terrains with steep slopes and low temperatures, as well as low nutrient and/or water contents in soil. Further plant species include xerophile species, mainly *Juniperus phoenicea* and *Buxus balearica* in the High Atlas Mountains, whereas *Juniperus thurifea* is found in the Anti-Atlas Mountains. Today, population numbers have decreased to a great extent due to human influence. Plant communities now only exist in degradation forms in a close refugium.

***Artemisia ssp. herba-alba* and *Artemisia ssp. mesatlantica* steppes**

The sagebrush *Artemisia* species, here *Artemisia herba-alba* and *Artemisia mesatlantica* belong to the family of *Asteraceae–Anthemideae*. The genus *Artemisia* is species rich and widely distributed in the study area. Large areas at the southern slope of the High Atlas Mountains are dominated by sagebrush steppes. The sagebrush flowering period is autumn

(September-October), when precipitation increases to about 200 mm but estival elevated radiation and temperatures are reduced to match the optimum temperatures for *Artemisia* growth of about 20 °C (see chapter 2.5.1.3). These steppes are found at altitudes between 1,300 – 2,300 m a.s.l. and exhibit a long intensive grazing history (El Moudden 2005).

Artemisia populations compete with other predominant plants for nutrients, water and space. *Artemisia* steppes are secondly dominated by *Theucrium mideltense* shrubs. Both shrubs avoid concurrence by differing flowering seasons. The flowering period of *Theucrium* takes place in spring, whereas the *Artemisia* flowering period is in autumn. This situation can be confirmed by the water consumption measurements of these plants conducted in different campaigns in 2001 to 2003 (Gresens 2006). Further details of water consumption and metabolic characteristics of rangeland plants in the region are found in Gresens (2006). Figure 4 indicates the seasonal development of leaf area (m^2) for *Teucrium mideltense* and *Artemisia herba-alba* from autumn 2001 to spring 2003. The growth period of *Artemisia herba-alba* in autumn is underlined by its enhanced leaf development. Whereas *Teucrium mideltense* illustrates accelerate leaf development in spring period. These features display the individual vegetative growth period and thus the water demands for plant growth are high. Plant water consumption shows a large seasonal variation depending on rainfall. For example the year 2002 was extraordinary because of a reduced annual sum of rainfalls showed by plant water consumption, too.

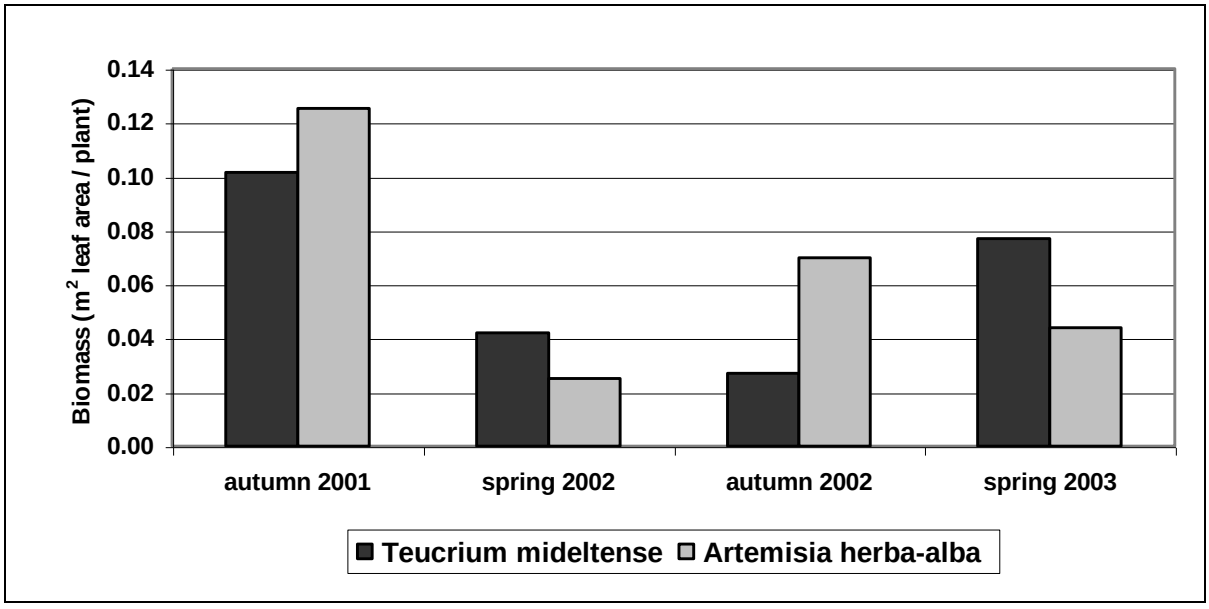

Figure 4: Seasonal development of leaf area (m^2) per plant for *Teucrium mideltense* (n=31) and *Artemisia herba-alba* (n=33) at Taoujgalt test-site comparison between autumn and spring (2001-2003) by Gresens (2006).

Hamada scoparia steppes

The predominant species *Hamada scoparia* grows on shallow soils at higher altitudes of the Anti-Atlas ridge. The species *Hamada scoparia* is a *Chenopodiaceae* desert species and is

the major component of wide ranges of the *Hamada* steppes in the semi-arid study area. According to the GEFWEB[4] classification scheme, it is an endangered species. Noy-Meir *et al.* (1970) compared different transpiration characteristics of *Artemisia herba-alba* and *Hamada scoparia* in the Negev desert (Israel). *Hamada scoparia* shows different shapes compared to *Artemisia herba-alba* as it develops, e.g., tight-fitting green branches instead of tissued leaves to reduce transpiration losses in hot, dry environments. These steppes can generally be defined as degraded steppic landscapes, low in species numbers with different secondary dwarf shrub compositions (Staudinger and Finckh 2005). The second important plant type in most *Hamada* steppes is *Convolvulus tributianus* or *Farsetia occidentalis*. These species have developed other adaptation strategies towards drought, nutrient or water acquisition. For this reason the coexistence of these species is feasible in most parts of the *Hamada* steppes.

Stipa ssp.

The predominant *Gramineae* species found in the mid-altitude southern slopes of the High Atlas Mountains is *Stipa cf. parviflora*. It is a major constituent of the western Mediterranean Halfa grass steppe. At niches of higher altitudes of the High Atlas Mountains the *Gramineae Stipa tenacissima* is found. In mountainous areas this species are considerably endangered by anthropogenic progress such as grazing. Further south at the arid border to the Sahara, *Stipa tenacissima* is the main *Gramineae* structure forming agent at higher altitudes (CBTHA 2002).

Spiny cushion shrubs- and the oro-mediterranean communities

These communities are mostly located in higher altitudes of the High Atlas Mountains. There are few references in the literature for this type of vegetation. Main common characteristics are the multiple defence strategies against high temperatures and high radiation as well as low nutrient and water inputs (Staudinger and Finckh 2005). The cushion and spiny structure protect these pastures from intensive grazing. Other strategies are niche and co-existence characteristics of species using the poor resource pool successfully. Adapted species of the oro-mediterrenean category described are *Platycapnion saxicolae*, *Arenarion pungestis* (found at altitudes >2300 m a.s.l.) and *Ormenion scariosae* (1900 – 2400 m a.s.l.) on calcareous soils. These are often replaced due to grazing activities and human biomass withdrawal by *Artemisia herba-alba/mesatlantica* steppe and a mixture of *Bupleurum spinosum* (indifferent substrate occupation at 1700 m – 2100 m a.s.l., in the Anti-Atlas ridge). The species *Allysum spinosum*, *Erinacetalia anthyllidis* and *Vella marei* (southern slope of

[4] GEFWEB- Global Environment Facility; www.gefweb.org/Council/Morocco

High Atlas >2300 m a.s.l.) are joined as the spiny cushion belt in the category of oro-mediterranaen communities. The terms of direct or indirect influence between species are discussed intensively in the literature (e.g. Palmer 1994). A direct influence is indicated when different species affect each other in growth or reproduction rates, which decreases inter-specific and increases intra-specific competition. Through indirect influence one species or PFT profits from the micro scale biotic advantages given by a certain other species (Staudinger and Finckh 2005). So these key species provide ecological niches according to their specific morphology or growth attributes and provides a favourable environment for their development.

***Zyghophyllum gaetulum*, halophyte species and sand dune vegetation**

The dwarf shrub *Zygophyllum gaetulum* dominated clay pan areas are found mostly in valleys with fine sediments transported by the Drâa River through the mountain ridges of the southern Drâa catchment. This species is characterised by CAM metabolism. Plants of this metabolism type open their stomata at night for respiration (CO_2 uptake) at lower temperatures and higher relative humidity. CAM and C_4 metabolisms had resemblances, C_4 in contrary concentrates CO_2 spatialy in a bundle sheath cell being inundated with CO_2. Plants with CAM and C_4 photosynthesis fixtion mechanisms are adaption specialists to hot dry environments.This vegetative strategy minimises water loss, unlike C_3 metabolism plants, which must use other sophisticated strategies to overcome water shortage. All other plants described in this section and simulated belong to the C_3 metabolism. In arid climates, clay soils get enriched with salt by capillary rise so this dominant species can be described as halophytic (IMPETUS 2003). These species are specialists best adapted to environmental difficulties as extreme drought and salt stresses. Spatial distribution of *Zygophyllum* is closely associated with clay pans in the Saharan sector, as are halophytes. Here, especially in the former Drâa lake Lac Iriki, which is now a large clay pan, their abundance is linked to the water storage capabilities of clay. Halophytic species, like *Frankenia pulverulenta*, *Mesembryanthemum nodiflorum* and *Limonium sinuatum*, are well adapted to high salinity contents. Annuals (ephemeral) species using the irregular precipitation events for onset flowering and possess extremely short vegetation phases belong to this category, too.

***Panico turgidi-Acacion* / *Acanthorhino-Zillion* communities**

Panico-turgidi-Accacion, *Acanthrhino-Zillion,* and *Tamarix-Nerium* communities are trees restricted to the Wadis and their direct borders (dunes) in the southern Drâa catchment area. The group of *Panico turgidi-Acacion* may be further differentiated into two subtypes according to their exposure to salinity. In the group affected by salinity, *Accacia raddiana* and *Panicum turgidum* are the dominant species in the bigger Wadis around the towns of

Tamgroute and M´Hamid. Accompanying species such as *Zygophyllum gaetulum* and *Zilla macroptera* indicate the potential saline influence. These areas are an important biomass resource for forage supply to local nomadic and sedentary sheep, goats and dromedary herds. Whereas many former nomads of the southern ranges have become sedentary to ensure income stability.

The group not affected by salt is mainly dominated by *Accacia raddiana*, located south of the Anti-Atlas ridge basins in depth contours on the pediments and glacis. These Wadis upper flow regions with deep aquifers do not show any saline effect so the vegetation is composed of species of the dry steppes type such as *Asteracea Anvillea raddiata* and the dwarf shrub *Convolvulus tributianus*. The vegetation is concentrated mainly in the gorges and ravines surrounding Regs (Arabic for pediments) are practically free of perennial species (IMPETUS 2003).

Isotope C^{14} studies at the El Miyit test-site have shown that the roots of the trees are capable of reaching the ground water table (Gresens 2006). According to earlier plant water consumption studies, it was considered reasonable to divide tree species into different height classes as water consumption depends on plants leaf area. This helped to obtain meaningful values for estimating regional water consumption when extrapolating from single plant measurements (Gresens 2006). These outcomes are used in this work for a better evaluation of plant water consumption amounts of southern ranges that are found rarely in the literature.

***Tamarix-Nerium* communities**

In this association one has to differentiate between two groups, the association on terraces of perennial water flows and sand dune sites. Sites with a perennial (ground as well surface) water flow are dominated on their terraces by the bushes *Tamarix amplexicaule*, *Tamarix africana* and *Nerium oleander*.

Sand dunes with accumulated *Tamarix aphylla* stands with access to aquifers inside the dunes are found south of Zagora and at the Sahara desert borderline. *Tamarix* populations are under threat of biomass collection for fuel. Removing *Tamarix* leads to re-mobilization of sand and thus to further desertification. Besides *Tamarix aphylla* no further predominant higher species are identified. Sand dune off-side areas are sometimes populated by other *Tamarix* species such as *Tamarix zygophyllum*, *Nitria retusa* and *Zygophyllum*-dominated clay pans (IMPETUS 2003).

Date palm oases

The date palm oases in the middle Drâa valley are located between the Anti-Atlas ridge and the Lac Iriki near the Algerian border. The overall surface area along the river Drâa is about 600 km^2. Their ecological and socioeconomic importance is based on their comparatively high agricultural productivity and the correlated economic benefits for the local population.

Income is mainly based on date production by *Phoenix dactylifera*. Thus date palms are the macro- and micro-scale dominant agricultural cash crop. As date palms constitute most of the standing biomass, their water use and transpiration has been studied before in the context of IMPETUS (Gresens 2006).

Cropland

Agriculture is still the most important economic factor in the region (following remittances from work migrants = 69% of total income: Heidecke, 2008, personal communication). Most farmers cultivate their land in semi-subsistence. The cropped area in the Drâa basin is mainly concentrated in six large oases, located in a line in the river Drâa valley (e.g. Roth 2008). In 1996 the cultivated area was estimated at approximately 37000 ha, for the province of Zagora (Heidecke and Schulz 2008). Farm size varies from small plots of <1 ha to large farms of over 20 ha. As management intensity is related to farm size, yields for the most relevant cereals, wheat, maize and barley, are of a maximum of 4000 kg ha^{-1}.

In recent years the leguminous *alfalfa* has grown in popularity, in 2002 reaching 125 kt (ORMVAO 2002). Date yields for the agricultural years 2001-2002 reached 1900 kt, whereas the mean date yield is estimated at approximately 1630 kt (ORMVAO 2003). This emphasizes the unique role of the so called “palmeraies” (French: palm garden). They can be separated into three different vertical agricultural production layers. The lowest ground layer comprises annual crops, mostly cereals (wheat, barley and maize). Additionally, vegetables such as tomatoes, potatoes and peppers, plus additional cash crops such as henna, are cultivated. Leguminous species play an important role for N fixation in crop rotation. The importance of alfalfa is shown by the fact that in 2001-2002 agricultural campaigns, 9,450 ha were cultivated with alfalfa (ORMVAO 2003). However as water scarcity in the region increases, alfalfa production, as water demanding crop, may decrease. The intermediate layer is formed by fruit trees, e.g., walnut, olive, henna and apples. The upper-most layer is made up exclusively of date palms. It is important to mention that dates are not usually separately irrigated; they profit from crop water supplies at lower layers. The crop rotation varies in the oasis according to water availability. Irrigation water supply is provided by wells and water drainage by Mansour Eddabhi reservoir.

In two oases south of Zagora, crop areas have been recently reduced due to limited water resources. Wheat and barley crop rotations are the dominant crops cultivated. However in the surrounding rangeland only small scale cultivation on fluvial pediments is possible. These are mainly situated in the small basins around the oasis. At the extreme southern catchment border in the Lac Iriki pan, rain fed agriculture is the main agricultural technique. However, that is only the case in those years when substantial rainfalls provide sufficient water for the area.

In the High Atlas regions, farm sizes are smaller, mostly below 5 ha, with an average area of about 1.2 ha (Gresens 2006). The crop rotation here mainly consists of maize and barley. Arable land at higher altitudes, however, is completely different from the Drâa valley oases. Besides its size, water availability is far better due to perennial flows. Additionally, vegetables for subsistance such as potatoes, beets and shallots are cultivated (Gresens 2006). Lower temperatures enable the cultivation of fruit trees such as walnuts, apples and olives. Apples for example are often grown as a cash crop to generate additional income.

Open gravel areas

These areas define a spatial surface descriptive unit rather than a vegetation unit. Open gravel beds originate from fluvial sediment transport. They are found partly north of the Mansour Eddabhi reservoir (located near the city of Ourzazate) along the main streams heading towards the rivers Ouarzazate, M'Goun and Dades in the basin of Ouarzazate (Figure 1). In the Anti-Atlas region Wadis heading towards the river Drâa are likewise filled by gravel. Due to the very coarse texture, shallow soils and sporadic fluvial disturbance, they are covered by extremely sparse (annual grass) vegetation.

1.4.4 Herbivores

As indicated above, this study concentrates on the effects of grazing on biomass production in the rangelands. Hence in the following the most important animals in the research area are described and subsummed to herds.

Sheep and Goats

This category is the far most important regional animal species according to its numbers as livestock units. As herds are mostly composed of both species, below, they will be subsummed to one herd. Dominant goat breeds are the local species "Rahali" and "Drâa" (Ramdane 2006). "Rahali" is a small rustic animal adapted for long walks. The breed "Drâa" is a highly reproductive and lactating breed originating from the middle Drâa valley. "D´Man" is the local dominant sheep breed from the Central Drâa valley, less suited for long migrations but highly reproductive (Boujenane and Kansari 2002). Numbers of total sheep and goats in the study area were 1,466,000 heads in 1980 and decreased to 768,550 heads in 2003 (ORMVAO 2003) in the Ouarzazate province. Variability of sheep and goat numbers are strongly related to annual precipitation rates as seen in Figure 5.

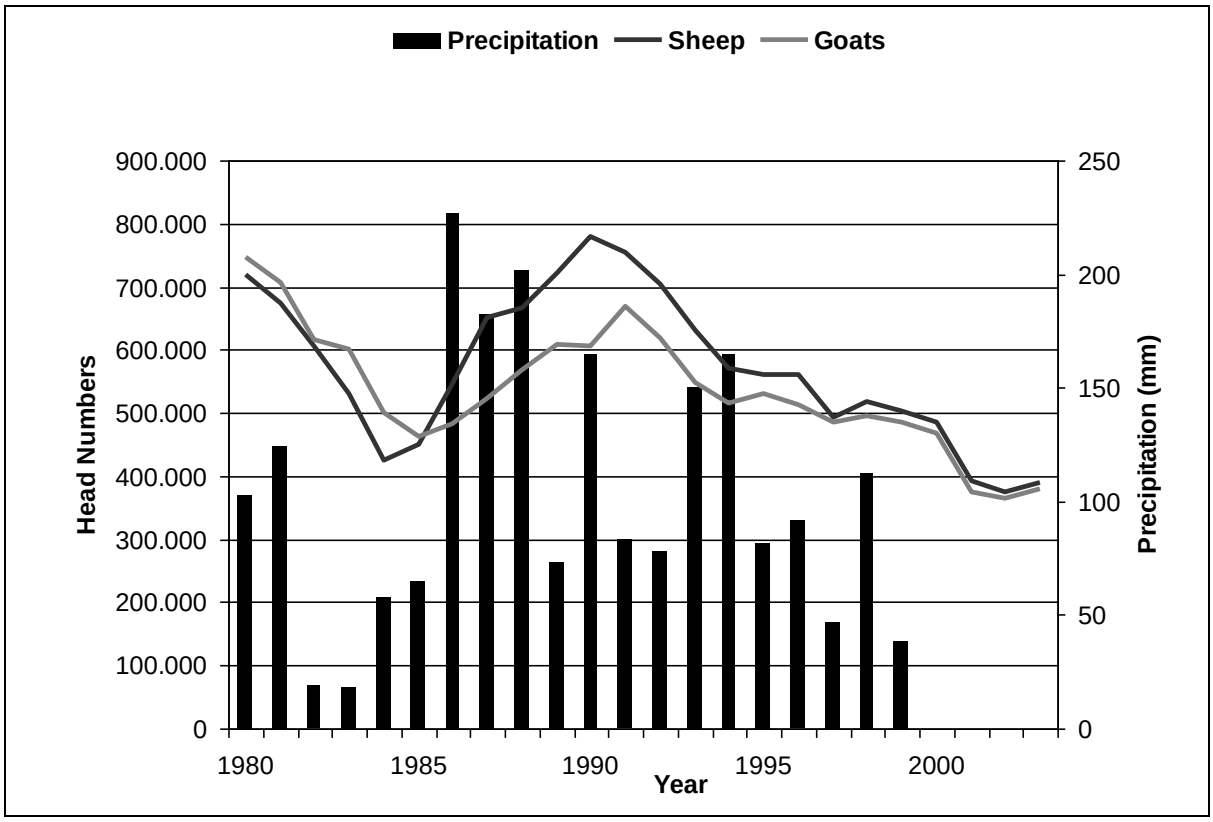

Figure 5: Livestock numbers for Ouarzazate province for 1980-2003 and annual precipitation (mm) sum 1979-1999. Data from the Office régionale de mise en Valeur Agricole Ouarzazate (ORMVAO 2005).

Sheep and goats usually are mixed in one herd. Sedentary herds only graze areas within a certain radius, a few km^2 around villages, whereas nomadic herds seasonally range for food consumption and thus are regionally more relevant. These two herd types generally differ in head numbers, nomadic herds usually exceeding sedentary herds. Thus these two are in a competitive situation for natural distribution of feed. One driving factor for both herds is the distribution of water wells, which determines their daily shifts.

Dromedaries

The Dromedary (*camelus dromedarius*) is an even-toed ungulate, one-humped camel species adapted to arid environments (Rachid 2004). In contrast to goats and sheep, dromedary numbers are not subject to large variations. These herds are concentrated in the southern part of the study area, basically south of the Anti-Atlas ridge. This ridge is nevertheless often used in springtime by goats, sheep and dromedary breeders because of annual grass floor dispersal resulting from exceptional rains here. Individual herd numbers are variable reaching from <10 to >100 heads, depending whether the animals are used for husbandry or are subject to transportation issues. The latter is mainly the case for the large herds (>100 heads) of dromedaries travelling through the Sahara desert for the transportation of goods.

Human biomass withdrawal

Biomass collection is carried out by women in the surroundings of villages with an increasing tendency to extend the activities in a wider radius. It is mainly used for fuel for cooking purposes (83%), water heating for baths (11%), and the stoking of houses (6%) (El Moudden 2005). Human biomass removal differs from animal grazing as much as it is usually stocked for longer time and thus more sporadic, but its intensity is higher. Benchekroun (1988) reported biomass withdrawal at about 65 to120 kg per household and week in winter. These figures strongly depend on the temporal resolution, season and localisation of research. This estimation is over-assessed as amounts for the southern Fezouata rangeland area shows. Rachid (2004) found total biomass production of about 1170 kg ha^{-1} during the high productive months April to May in an area of 100 ha. Biomass collection is limited to woody parts (stems, branches, and roots) of vegetation and has a long tradition. In the past mainly tree cutting (e.g., *Juniperus thurifera*, *Buxus ssp.*, *Quercus ilex*) was practised, but is prohibited since hardly any trees are left in the region. Hence this technique concentrates on plant species with acceptable woody biomass, e.g., *Artemisia herba-alba*, *Artemisia mesatlantica*, *Theucrium middeltense or Adenocarpus baquie.*

1.5 Study objectives and working hypotheses

Core issues in tracking the vulnerability of ecosystems are climate conditions and anthropogenic-induced land use changes. These processes will alter ecosystems tremendously if the present usage continues and will lead to severe changes in the coming decades. Precipitation amounts, water budgets and grazing intensities are often studied separately. However, as inter-connecting processes occur comprehensive modelling studies on many components are best suited to enhance ecosystem understanding. In order to understand vegetation responses to a changing climate and land-use and their impacts on local hydrological cycles, ecosystem models are used. The aim of this work is to analyze the vulnerability and resilience of vegetation in a semi-arid to arid ecosystem under the influences of grazing intensities and climate scenarios.

The vulnerability and resilience of vegetation are evaluated in terms of:

-floristic composition of vegetation in the future,

-spatial structure of vegetation in the future, and

-development of vegetation productivity.

In order to evaluate the above objectives, two factors are introduced to distinguish whether the research hypotheses are induced by either the livestock number as an anthropogenic

factor or a climatic factor, represented by the amount of predicted evapotranspiration and stomata conductance. The following three working hypotheses have been created: The anthropogenic and/or the climatic impact will:

1. change the spatio-temporal production features of plant functional types;
2. permit a continous vegetation growth and meet the requirements for future human needs even by altered stocking rates;
3. lead to changes of regional water budgets.

2 Materials and Methods

This section primarily gives the following: (1) an overview of methods used for transpiration measurements; (2) a description of nutrient cycling in the research area; (3) a detailed model description of SAVANNA©; and (4) the parameterisation procedure for data sets introduced to the model.

2.1 Measurement test sites

Measurement campaigns during this study were conducted next to three out of 13 test sites located in the High Atlas Mountains, within the Drâa basin and at the margin of the Sahara desert. Test sites are equipped with automatic climate stations and are built along the gradient of aridity from north to south and west to east. Next to these stations fenced grazing exclusion areas were built.

The oasis of Ameskar is located in the Assif-Ait Achmed valley in the High Atlas Mountains (2150 m a.s.l.) on 31.50093°N, -6.27161°E. This valley was formed by a perennial river (Assif) streaming downward from the top of M´Goun (Figure 1). The small oasis of Tichki (Figure 6) is located in the Assif valley, too, underneath the southern slope of the M´Goun mountain top at 2350 m a.s.l. at 31.50040°N and –6.31654°E. The entire oasis surface of Ameskar is 20.2 ha and Tichki is 21.2 ha. These relatively small agricultural surfaces of arable land are cultivated by 36 (Ameskar) and 47 (Tichki) owners (Choukri 2005). Besides the cropping scheme indicated in chapter 1.4.3., the riparian Aspen (*Populus canescens*) is often found here. These trees are planted in the sandy sediment banks of perennial waterways and are used for the construction material and fuel wood (El Moudden 2005).

The Taoujgalt test site is located in a rangeland area in the northern Drâa river catchment (1900 m a.s.l.) at the southern slope of the High Atlas Mountains, at 31.38994°N and -6.32203°E (Figure 7). The area belongs climatological to the Basin of Ouarzazate. Mean annual precipitation from 2002 - 2005 was 250 mm (Campbell automatic IMPETUS climate station at Taoujgalt).

Figure 6: Upper Tichki Oasis, agricultural fields.

Figure 7: Taoujgalt test site, *Artemisia herba-alba* and *Artemisia mesatlantica* steppe.

The Taoujgalt plain is grazed frequently by migratory nomadic sheep and goat herds and is also used by sedentary herds from neighbouring villages. Agriculture is limited to small fluvial pediment sites (Figure 7, middlepart).

2.2 Transpiration measurements

Plant transpiration was measured via leaf conductance using a zero balance steady-state porometer equipped with a cylindrical chamber to accommodate leafy shoots of different plant types (LI-1600 Instruction Manual, (LI-COR 1999)). This method accounts for transpiration (*trans*) as a one-sided leaf area measurements (Eq. 1). Gresens (2006) reported that measurement of in-situ *trans* was often difficult because of the small leaf areas (0.5 to 1.0 cm^2) studied. The LI-1600M used here calculated *trans*, as follows:

$$trans = Cs\frac{(e_l - e_c)}{Bp} \qquad \text{(Eq. 1)}$$

High solar radiation and temperatures affected the gas exchange measurements, resulting in erroneous results at temperatures above 42°C (Gresens 2006). So measurement campaigns had to be carried out in spring or autumn to receive reliable data. Most LI-COR measurements were conducted near the villages of Ameskar and Tichki in the Assif Ait-Achmed river valley (Table 1 and Table 2). Radiances (W m^{-2}) and temperatures (°C) for the calculation of transpiration rates (l m^{-2}) were taken from the nearby located IMPETUS weather stations Ameskar and Tichki.

Tree sap flow measurements were conducted with the PROSALog-DL2[5] system (UP-GmbH 2000) using the Granier system (Granier *et al.* 1990). We used a mobile xylem constant heating sap flow measuring system with the heat pulse method. Two thermocouples were installed symmetrically 0.75 cm above and below a 2 cm long heater with 2 W cm^{-1} power output. Probes had a diameter of 1.6 mm and were inserted in boreholes drilled with the same diameter into the trees. The depth of thermocouples probes was 1.5 cm, at a tree diameter of approximately 20 cm. The probes were inserted 1.5 m above ground on the north side of the tree (UP-GmbH 2000) and thermally insulated by wrapping with white polyethylene packing material. At each experiment, a data logger PROSALog (powered by a battery recharged with solar power) was installed to record temperature changes at the upper (t_U) and lower (t_l) thermocouples. Three thermocouples pairs were distributed on three Aspen trees (*Populus canescens*) with the above-mentioned configurations. Initial voltage on each of the three was 20 mV.

A multi-week set of measurements on a riparian Aspen (*Populus canescens*) population was conducted. Due to the time needed for experimental construction and quality controls, one series of sap flow measurements was obtained in the oasis of Ameskar between March 24th and April 9th 2005. Another experiment was conducted in the oasis of Tichki between June

[5] UP GmbH - Umweltanalytische Produkte GmbH, Ibbenbühren, Germany

18th and August 15th 2005. Table 1 and Table 2 describe parameter settings used for these measurements.

The trees for these measurements were chosen within a riparian stand to match variation in height, circumference and size. At maximum three trees could be chosen due to the number of thermocouples. Error measurements and interruptions in data logging occurred and were discussed for each experiment separately (see chapter 4.2).

Table 1: Parameter settings for sap flow measurements in Tichki.

Tichki	Aspen 1	Aspen 2	Aspen 3
Circumference at breast height (cm)	24.5	19.8	37.5
Circumference, Granier measuring point (cm)	24.5	19.8	37.5
Height above ground, Granier measuring point (cm)	150	150	150
Xylem depth, Granier measuring point (cm)	4.0	3.4	3.7
Sapwood area, Granier measuring height (cm)	1.0	1.0	1.0
Tree height, approximate (m)	5.5	6.5	8.5
Crown height, approximate (m)	5.0	6.0	8.0
Averaged leaf size (cm^2)	3.3	3.3	3.3
Electrode length (cm)	2.0	2.0	2.0

Table 2: Parameter settings for sap flow measurements in Ameskar.

Ameskar	Aspen 1	Aspen 2	Aspen 3
Circumference at breast height (cm)	17.8	24.1	28.3
Circumference, Granier measuring point (cm)	17.8	24.1	28.3
Height above ground, Granier measuring point (cm)	150	150	150
Xylem depth, Granier measuring point (cm)	2.9	3.2	3.5
Sapwood area, Granier measuring height (cm)	1.0	1.0	1.0
Tree height, approximate (m)	5.0	5.5	6.5
Crown height, approximate (m)	4.5	5.0	6.0
Averaged leaf size (cm^2)	3.0	3.0	3.0
Electrode length (cm)	2.0	2.0	2.0

2.3 Plant nutrients

Plant nutrients C, N, P and K were analysed in tissues of selected predominant plant species. Both leaf and stem material from *Artemisia herba-alba, Theucrium mideltense, Farsetia occidentalis* and *Hamada scoparia, Acacia raddiana* and *Zizifus lotus* was collected and prepared for analyses. These plants are dominant species: *Artemisia herba-alba* and *Theucrium mideltense* are found on the southern slopes of the High Atlas Mountains; *Hamada scoparia* and *Farsetia occidentalis* are widely distributed in the Basin of Ouarzazate, the Anti Atlas ridge and the southern ranges and *Acacia raddiana* and *Zizifus lotus* are predominant species for Wadi beds in the hot and dry southern rangelands.

The nutrient status of plants is important: Primarily, it is an indicator of the environmental growth conditions. Secondly, it must be considered while evaluating simulation results. Last but not least, N content is an important model input parameter.

Leaf stem dry weight material was analysed with the gas chromatograph *Elementar Analyzer EA* (EuroVector Instruments & Software). The measurement results are shown in chapter 4.3.

N distribution and its potential limitations to rangeland plants in arid ecosystems is a key feature of nutrient status. In rangelands globally, a tremendous proportion of nitrate is provided by animal dung. These facts and the unique role N plays in plant´s growth mark its importance. Accordingly, this work later focuses on plant N contents and its implications.

2.4 SAVANNA© Model description

The model *SAVANNA*© is composed of interacting sub-models that combine to adapt to a given environment. Figure 8 gives a general overview of the sub-models used in the present study. Primary environmental factors are conditions of weather, soil and water balance, which determine plant population dynamics and primary production in the region. These factors affect forage availability to animal populations and thus the distribution of these populations. Finally, human activities also affect animal distribution and population dynamics.

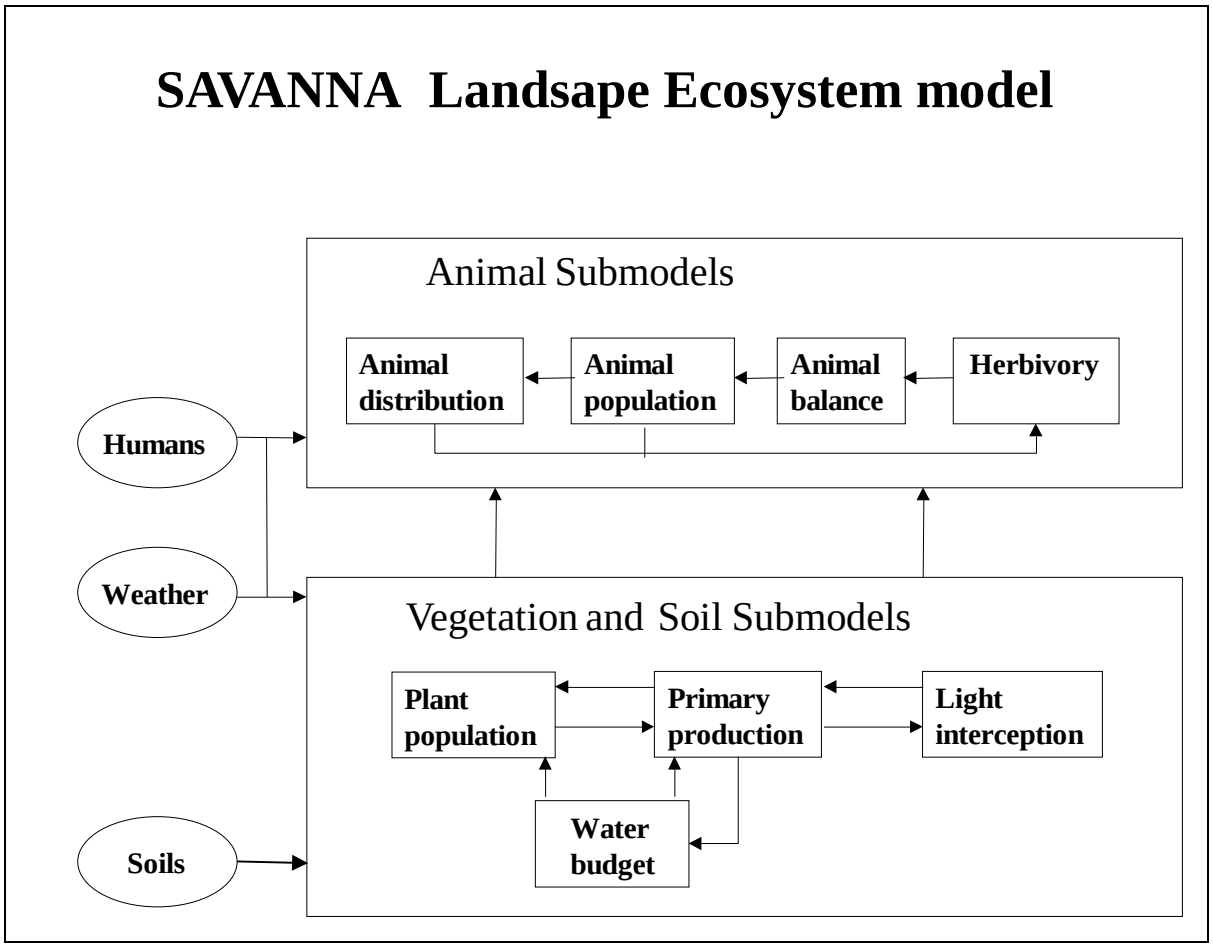

Figure 8: Conceptual diagram of SAVANNA© model components (Coughenour and Chen 1997).

2.4.1 Vegetation sub-model

In this section the main vegetation sub-models gathered from Coughenour (1993) are described: net primary production (*NPP*), biomass allocation and plant population. The primary production sub model belongs to the vegetation and soil sub model group. The *NPP* model primarily simulates light penetration through tree, shrub and herbaceous plant canopies using Beer's law. Hence leaf areas and extinction coefficients are summed across species and tissue types. Beer's law is used to calculate the radiation that passes through the overstory, which is then used as incident radiation in the next lower canopy layer.

Potential Transpiration rates

SAVANNA© computes potential *NPP* as a product of a computed rate of water use through transpiration (*trans*) and water use efficiency (*WUE*). Stomatal conductance (*Cs*) is calculated as

$$Cs = Csmx \times Efwp(Awpet) \times Eflp(Rad) \times Eftp(T_{day}) \times \min[Efnp(Pnb), Efsr(Sre)] \quad \text{(Eq. 2)}$$

The concept of *Awpet* (Eq. 2) is used rather than actual soil water content for two reasons: First, because of weekly simulation time steps, substantial amounts of water may be added to the soil which would not otherwise be usable until the next week. Second, the amount of water that is available during a week may exceed the soil water holding capacity due to within-week cycles of rain-days followed by plant water uptake. Most importantly, scaling up to *SysPet* accounts for drought stress on daily stomatal closure.

Eflp is used to compute the effects of light on photosynthesis and *trans* as

$$Eflp = \frac{\alpha \times Rad}{\sqrt{1 + (\alpha \times Rad)^2}} \quad \text{(Eq. 3)}$$

$$trans = Cs \times Vdef \times Day\ln \times 0.0036 \times Gbiom \quad \text{(Eq. 4)}$$

The constant 0.0036 is used to convert units[6]. Transpirational water demand from soil water layers is distributed similarly to available soil water.

Net primary production (*NPP*)

The potential plant water demand of all plants rooted in a soil layer may exceed the actual quantity of available water due to the weekly simulation resolution. On a daily time step, stomata would gradually close as soil water is depleted. An approximation is derived by assuming that each plant´s competitive abilities for water are proportional to its potential rate of water use. Thus when total plant water demands in a layer exceed available water the availabe water is partitioned among competitors in proportion to their demands:

$$Atrans_{l,nsp} = \frac{Tdem_{l,nsp}}{\sum_{nsp=1}^{nspmx} Tdem_{l,nsp}} \times Avlwat_l \quad \text{(Eq. 5)}$$

If total water demand does not exceed available water, then actual water uptake equals potential water uptake. Finally, the actual *NPP* rate is

$$Npp_{nsp} = \sum_{l=1}^{nlay} Atrans_{l,nsp} \times WUE_{nsp} \quad \text{(Eq. 6)}$$

[6] 0.0036=3600 (seconds hour^{-1}) x 10^3 (mg g^{-1}) x 10^{-6} (m^3 cm^{-3}) x 10^{-3} (mm g^{-1} H_2O m^{-2})

Nitrogen uptake

Nitrogen uptake (*Nup*) is calculated by the Michaelis-Menten function of soil inorganic N concentration

$$Nup_l = (\mathrm{Pr}oot_l \times Roots) \times Enup(Pnb) \times Etnup(T_{avg}) \times Epnup(Phen) \times \frac{N_l \times Upmx}{N_l + Upnkm} \quad \text{(Eq. 7)}$$

The weekly time step creates situations where the total plant demand for N can exceed the available soil N supply. An approximate solution is to apportion N uptake among species according to their demand.

Biomass allocation - herbaceous plants and shrubs

NPP of herbs and shrubs is allocated between shoots and roots. Then shoot growth is allocated among leaves, stems and reproductive tissues. Belowground net primary production (*BNPP*) of herbaceous plants and shrubs is calculated as

$$Rtgr = Npp \times \mathrm{Pr}rt \times Efsr(sre) \times Ewal(Awpet) \times Enal(Pnb) \times Epal(Phen) \quad \text{(Eq. 8)}$$

The remainder of *NPP* is used for aboveground shoot growth (*Shgr*)

$$Shgr = Npp - Rtgr \quad \text{(Eq. 9)}$$

Herbaceous shoot growth is allocated to leaves in the proportion *Prlf* and to reproduction in the proportion *Prfl*, while the remainder is allocated to the stem. Hence leaf growth is

$$Grlf = Shgr \times \mathrm{Pr}lf \quad \text{(Eq. 10)}$$

while stem growth (*Wdgr*) constitutes the balance

$$Wdgr = Shgr \times (1 - \mathrm{Pr}lf - \mathrm{Pr}\ fl) \quad \text{(Eq. 11)}$$

Allocation of *Shgr* by shrubs depends on the current fraction of shoots that are leaves. As growth begins, the model assumes highest priority to allocation to leaves until the morphometric leaf:stem ratio is attained. Hereafter allocation to leaves is in the morphometric proportion

$$leaf = \mathrm{Pr}lf \times (Wdgr + Gbiom) - Gbiom \quad \text{(Eq. 12)}$$

is the current deficit of leaf mass relative to the morphometric leaf mass, and

$$\begin{aligned} Sgrl &= Min(leaf, Shgr), Defl > 0 \\ Sgrl &= \mathrm{Pr}lfxShgr, leaf \le 0 \end{aligned} \quad \text{(Eq. 13)}$$

Is the allocation of shoot growth to leaves to meet the leaf mass deficit, if any, or it is the allocation to leaves in the proportion *Prlf* if there is not.

Plant Population sub-models

Herbaceous plant population sizes are calculated on the basis of the number of plants per m^2. There is a single plant size class; however, plant size varies in response to tissue growth and mortality. Shrub populations are modelled on the number of plants per hectare. Shrubs that do not grow beneath trees are referred to as overstory shrubs, a distinction used in this study. Shrub population dynamics are computed using a weekly time step and a single size class. However plant size is variable. Tree population dynamics are computed as the number of plants per km^2. Tree cover defines the woody zone. The tree population in each grid cell subarea is divided into six classes, simulated on an annual time step. There exist three main points of connection between *NPP* and the plant population sub-model: seed germination, plant size determination and plant mortality. The latter two are straightforward; when plant biomass increases relative to plant number, plants must increase in size, and when plants die, live tissue biomass is converted to dead tissue biomass.

Seed germination and recruitment of shrubs is modelled in demographic terms in this approach. However, a more complex approach is needed to compute the dynamics of short-lived or annual herbaceous plants. The time lag for short-lived herbaceous plants associated with seed development and transfer to soil can lead to significant errors. Here, the biomass of seeds that germinate and become established is used.

Biomass-based seed germination and establishment

This sub-model tracks seeds from allocation of *NPP* to seeds on the plant to seeds in the soil, to establishment. Seed biomass on the plant is distinguished from seed biomass in soil (*Seeds*). *Seeds* are transferred from the shoots to the soil at a daily rate. Soil seeds also originate from an external seed source, representing seed rain from outside the study area. Seeds that become inviable are removed from the soil seed bank. Seed germination ($Grinis_{nsp}$) proceeds at the rate

$$Grinis_{nsp} = Seeds_{nsp} \times Germrb_{nsp} \times Etgrmb(T_{avg}) \times Ewgrmb(Avwpet_{nsp}) \quad \text{(Eq. 14)}$$

Newly established seed biomass is converted to leaf and root tissue in equal proportions. The number of plants established ($Estnum_{nsp}$) due to germination is

$$Estnum_{nsp} = Seedpg_{nsp} \times Grinis_{nsp} \times Ehrbeb_{nsp}(Herbm) \quad \text{(Eq. 15)}$$

The function *Ehrbeb* computes shading or other competitive effects from established plants.

Demographic seed dynamic sand establishment

The demographic model calculates establishment, which depends on the number of plants already established, abiotic factors and competition from herbaceous plants. Shrub establishment (*Shestb*) in a given month, from seed or vegetative spread, is

$$Shestb = Shnum \times Germrs(Shbsz) \times Etgrms(T_{avg}) \times Ewgrms(Awpet) \times Ehrbes(Herbm) \times E\,\mathrm{cov} \quad \text{(Eq. 16)}$$

Ecov of the overstory is then

$$E\,\mathrm{cov} = 1 - Wdcvr - Shcvr \quad \text{(Eq. 17)}$$

Plant Mortality

Plant mortality is differentiated between herbs and shrubs due to differences in their time scales, absence or presence of size classes. Herbaceous plant mortality ($Dthnum_{nsp}$) rate is

$$Dthnum_{nsp} = P\ln um_{nsp} \times Max(Drwatp(Awpet), Drtmpp(T_{avg}), Drphnp(Phen)) \quad \text{(Eq. 18)}$$

Shrub mortality (*Shdth*) is

$$Shdth = Shnum \times Max\left\lfloor Drwatsh(Awpet), Drtmpsh(T_{avg})\right\rfloor \quad \text{(Eq. 19)}$$

Plant size and cover

Mean root biomass (*Rsize*) per plant is a measure of herbaceous plant size,

$$Rsize = \frac{Roots_{nsp}}{P\ln um_{nsp}} \quad \text{(Eq. 20)}$$

Overstory shrub cover (*Shcvr*) is calculated at

$$Shcvr = \sum_{nssp=1}^{nsspt} Grmsa_{nssp} \times Cvpgr_{nssp} \quad \text{(Eq. 21)}$$

Important to mention is root mass as it defines the cover of the overstory shrub level, the biomass densities of shoot and other state variables per m^2 of subarea. Since these may change in response to changes in total root biomass and facet cover.

2.4.2 Soil sub-model

Soil profiles are divided into three layers in this model. The total simulated soil depth (*Sdep*) is here the maximum plant rooting depth. The depth of the herbaceous rooting zone (*Hdep*)

generally defines the bottom of the second layer, while the third and deepest layer is often only used by large woody plants (c.p. chapter 9 Appendix). The middle layer is occupied by roots of both trees and herbaceous plants. The top layer must be at least as deep as the depth of bare soil evaporation (*Edep*, cm). Layer thickness (cm), volumetric field capacity (*Fcp*), 1.5 Mp wilting point (*Wlt*), and porosity (*Sm0*) are used to calculate soil moisture holding capacities and the maximum quantity of water available for plants.

Bare soil evaporation is simulated using the model developed by Ritchie (1972). This model must be implemented using a daily time step. It is applied here on a weekly basis, by calculating the evaporation following a mean weekly rain day. The approach is to calculate the *fraction* of rainfall that evaporates in a mean weekly rain day. Then apply that fraction to the weekly rainfall total. Dummy soil layers are first initialized at start of simulation with values equal to the current soil water contents. Water from precipitation and runon minus runoff is infiltrated into the top dummy soil layer. Crack flow and water in excess of field capacity is drained from each dummy layer. Water is drained into successively deeper layers, filling each with drainage from the layer above, up to field capacity. Excess water above field capacity is drained. This approach is applied with the mean weekly rain day to determine the fraction of rainfall that is infiltrated to each layer ($Pinfl_l$). Each week the actual water infiltration into the soil (*Ppton*) is computed as

$$Ppton = \left(\left[Pptwk \times Ppt\right] + Runonw\right)\left(1 - Sprun\right) + \left(Sn\inf - Snrun\right) \quad \text{(Eq. 22)}$$

The maximum quantity of $Avlwat_l$ to plants in each soil layer for the week is

$$Avlwat_l = \left(Swatr_l - Wltp_l\right) + Ppton\left(P\inf l_l\right) \quad \text{(Eq. 23)}$$

The total water available to a given plant species is the sum of *Avlwat* over all layers *l* where the plant is rooted. The ratio of total available water to weekly *SysPet,* $Avwpet_{nspt}$ for a given plant species is

$$Avwpet_{nspt} = \frac{\sum_{l=1}^{nrl} Avlwat_l}{SysPet_{wk}} \quad \text{(Eq. 24)}$$

$Avwpet_{nspt}$ is used to affect plant growth and death (see plant submodels). At the end of each weekly time step, the weekly soil water budget for each layer is updated with

$$Slwat_l(t+1) = Slwat_l(t) + (Ppton \times P\inf l_l) - trans_l \quad \text{(Eq. 25)}$$

Weekly bare soil evaporation (*Bsevw*) is also subtracted from the top soil layer. The total water available for evaporation is the fraction of water in the top dummy layer regulated by the layer thickness. Evaporation proceeds in two stages. During the first stage it is limited

only by *SysPet*, while in the second stage it is limited by soil water content. Evaporation may proceed for a maximum number of rainy days (*Ndymx*):

$$Ndymx = \frac{Ndtmn}{Min(1, Nstrmw)} \quad \text{(Eq. 26)}$$

Total weekly evaporation (*Bsevw*) is found as evaporation per the number of rain days per week. Maximum bare soil evaporation ($Bsev_{max}$) is

$$Bsev_{\max} = SysPet \times Min(e^{-LAI \times K}, Gr) \quad \text{(Eq. 27)}$$

The value *Gr* is the the minimum reduction in *SysPet* due to surface litter shading (Wight and Skiles 1987).

2.4.3 Weather sub-model

Estimated rainfall (*Ppte*) at each grid point is estimated as a function of nearby rainfall and elevation *i*, computed each month. For each grid point (cell), the four nearest weather stations are consulted. Thus, for the i^{th} known precipitation datum (i=1, 2, 3 or 4) and the j^{th} unknown grid point, thus

$$Ppte_{i,j} = Ppt_i + B_1(E_j - E_i) \quad \text{(Eq. 28)}$$

If the precipitation versus elevation regression produces a low correlation coefficient, elevation is not used and interpolation is based only on the inverse distance function. Spatial variations in temperature and water vapour pressure are computed during a model run based upon elevation of the monthly weather data station. Minimum and maximum temperatures are assumed to lapse at the same rate. Mean monthly values of daily global shortwave radiation (*Radgl*) and relative humidity (*Relh*) are used in each simulation. Daytime saturation water vapour pressure (e_{sat}) is calculated from temperature (T_{day}) as

$$\begin{aligned} e_{sat} &= 4.89 + 0.33T_{day} + 0.0695T^2{}_{day}, T_{day} \geq 5.0 \\ e_{sat} &= 6.33T_{day} - 0.748T_{day} + 0.0301T^2{}_{day}, T_{day} \leq 5.0 \end{aligned} \quad \text{(Eq. 29)}$$

Daytime vapour pressure (*e*) is then

$$e = \mathrm{Re}lh \times e_{sat} \quad \text{(Eq. 30)}$$

Since temperature varies with elevation so does water vapour. *SysPet* rate is calculated using the Priestly-Taylor equation (Priestley and Taylor 1972). The size of an individual precipitation event, e.g., per day, strongly affects runoff and bare soil evaporation. Hence there is a need to translate monthly precipitation data into the number and (approximate) size of rain days per week. To accomplish this, the model stochastically determines the number of rain days in each week. The probability of a rainy day (P_{strom}) is

$$P_{storm} = \frac{Nstorm}{Mndy} \quad \text{(Eq. 31)}$$

2.4.4 Animal dynamics sub-models

The animal dynamics sub-models are a complex of four sub-models divided into herbivory, animal energy balance, animal population and animal distribution. These sub-models are described further in that order.

Herbivory sub-model

Animal diet composition and forage intake are described first. Both depend upon the distribution and abundance of available forage. Available herbaceous forage is the standing crop minus ungrazable biomass. Available herbaceous green leaf expressed as *Tavg* is

$$Tavg = Gbiom - Ungrzb \quad \text{(Eq. 32)}$$

The calculation of stem and dead leaf availability is similar. Available shrub green leaf expressed by *Tavg* is computed as

$$Tavg = \left(Gbiom \times Eshsz\left(\frac{Shbssz}{Shbmx} \right) \right) - Ungrzb \quad \text{(Eq. 33)}$$

Dead leaf, current and old stems are calculated similarly.

Diet composition

Animals in a grid cell, as predicted by the distribution submodel (see the latter section), choose among patches and plant types within patches in a cell in order to gain a preferred diet composition. Diet composition is determined by using preference weightings (c.p.Table 22 and Table 23; (Ellis *et al.* 1976). A preference-weighted rank value ($Prfb_{nsp}$) on subarea *n* for facet *n* of a forage species is

$$\Pr fb_{nsp,nsub,nfac} = \Pr fwt_{nsp} \times Tavg_{nsp,nsub,nfac} \times Cvrfac_{nsub,nfac} \quad \text{(Eq. 34)}$$

Thus, *Prfb* responds to the total abundance of forage in a grid cell as well as the preferences of the herbivore.

Forage intake rate

To account for the fact that forage abundance affects forage intake (*Frg*), a type II functional respond is introduced. This is expressed by

$$Frg = \frac{Foragg}{Foragg + Frkmg} \quad \text{(Eq. 35a)}$$

$$Frg = \frac{Foragb}{Foragb + Frkmb} \quad \text{(Eq. 35b)}$$

Total available graze abundance (*Foragg*) per grid cell is

$$Foragg = \sum_{nsp,nsub,nfac} Tavg_{nsp,nsub,nfac} \times Cvrfac_{nsub,nfac} \quad \text{(Eq. 36)}$$

These calculations include only herbaceous plants. However, browse abundance is calculated similarly by summing over shrubs. These are the aggregated responses to the total densities of graze and browse. Responses to individual forage species are not calculated since it is unlikely that functional responses are known at the species level. Forage intake rates for each species of graze (*Fintkg*) and browse (*Fintkb*) are

$$F\text{int}kg_{nsp} = Crmx_{nsp} \times Foragg \times Esnow_{nsp} \times Ec\,\text{int}k(CI) \quad \text{(Eq. 37a)}$$

$$F\text{int}kb_{nsp} = Crmx_{nsp} \times Foragb \times Esnow_{nsp} \times Ec\,\text{int}k(CI) \quad \text{(Eq. 37b)}$$

The total forage intake rate of an animal cannot exceed a rate that is limited by forage quality. This is due to the fact that digestion can be limited by the rate of passage of the plant tissue through the animal rumen, which can decline if forage quality is low. Grazers are more affected by this factor than browsers, because browsers have adapted rumen functionality to "skim" the high quality material even from low quality material. Thus

$$\begin{aligned} Intkmx_{nsp} &= Crmx_{nsp} \times En\,\text{int}k_{nsp}(N) \times Ed\,\text{int}k_{nsp}(Digest) \\ Intkg_{nsp} &= Min(F\text{int}kg_{nsp}, Intkmx_{nsp}) \\ Intkb_{nsp} &= Min(F\text{int}kb_{nsp}, Intkmx_{nsp}) \end{aligned} \quad \text{(Eq. 38)}$$

Green leaf digestibility is given as a function of green leaf N content which varies with plant N content and phenology. Total intake of the graze forage (*Intkgt*), on each facet is

$$Intkgt_{nsp,nsub,nfac} = Intkg_{nsp,nsub,nfac} \times Cwtkg \times Hnfor_{nsp,nsub,nfac} \quad \text{(Eq. 39)}$$

A similar equation is applied to browse items (not shown here). The removal of graze per unit of ground area ($Offtake_{nsp}$) is

$$Offtake_{nsp,nsub,nfac} = \frac{Intkg_{nsp,nsub,nfac}}{Areaf_{nsub,nfac}} \times 10^3 \quad \text{(Eq. 40)}$$

Browse removal is computed in similar ways.

Animal energy balance

The weight dynamics of animals are predicted by modelling their energy balance. Weight is gained when energy intake exceeds requirements, and it is lost when intake is less than requirements. Metabolizable energy intake from forage consumption (*Fme*) is computed by

$$Fme = Tcons \times Digest \times Emetab \quad \text{(Eq. 41)}$$

Energy requirements consist of a “base cost” metabolic energy demand per unit body weight per day. To this, energetic costs of travel and lactation may optionally be added. In this work, lactation costs are not simulated explicitly. Travel costs are computed from simulated values based on simulated mean distance to water. The costs of horizontal and vertical travel (*Etrvh, Etrvv*) are computed by

$$Etrvh = Dish \times Cwtkg \times Trvsch \times 0.001 \quad \text{(Eq. 42a)}$$

$$Etrvv = Disv \times Cwtkg \times Trvsch \times 0.001 \quad \text{(Eq. 42b)}$$

The term 0.001 converts meters to kilometres. Total metabolizable energy required (*Reqnm*) is then

$$\mathrm{Re}qnm = (Cwtkg \times \mathrm{Re}qnm) + Etrvh + Etrv + Elac \quad \text{(Eq. 43)}$$

If *Fme* exceeds R*eqnm*, then the rate of weight gain (*Delwt*) is

$$Delwt = (Fme - Rqenm) \times \frac{Rnemel}{26.0} \quad \text{(Eq. 44)}$$

Here 26.0 is the MJ net energy used per kg of body weight gained. If *Fme* exceed R*eqnm*, *Delwt* (a negative value) is

$$Delwt = (Fme - Rqenm) \times \frac{Rnemel}{26.0 \times 0.84} \quad \text{(Eq. 45)}$$

The value 0.84 is the efficiency of energy metabolism from weight loss. The total weight change rate (*Tdelwt*) of the mean animal in the population is

$$Tdelwt = \sum_{narea} Delwt_{narea} \times \frac{Hpop_{narae}}{Hpopt} \quad \text{(Eq. 46)}$$

Mean body weight cannot exceed the maximum nor be less than the minimum body weight of the mean animal given the current age/sex class distribution. The animal condition index (*CI*) is a dimensionless number between 0.0 and 1.0, the ratio of deviation below maximum weight (*Bwmx*) to the difference between maximum and minimum weight (*Bwmn*). At *CI* of 0.0 animals are at the minimum weight, while at *CI* of 1.0 animals are at maximum weight:

$$CI = \frac{Cwtkg - Bwmn}{Bwmx - Bwmn} \quad \text{(Eq. 47)}$$

Animal Population submodel

The animal population model is an age-sex class model in which birth and death rates respond to the animal *CI*. There are five age-sex classes: (1) newborns (unsexed), (2) immature females, (3) immature males, (4) mature females and (5) mature males. Newborns are classified as younger then the last birthing season. In this study, that class is younger than one year, as there is only one birthing months per year (March) for each animal species. The number of animals born per month (*Born*) is calculated by:

$$Born = Ans_4 \times Ecbirth(Conges) \quad \text{(Eq. 48)}$$

In the month of a birth, the lactation month is set to 1 and increments monthly thereafter. In each birth month, the last cohort of newborns is set to the immature classes.

Mortality is also a function of the *CI*. The number of animals dying per month ($Dthr_l$) in each age/sex class is

$$\begin{aligned} Dthr_1 &= Ans_1 \times Calvdth(Min[CI, Conges]) \\ Dthr_2 &= Ans_2 \times Youngdth(CI) \\ Dthr_3 &= Ans_3 \times Youngdth(CI) \\ Dthr_4 &= Ans_4 \times Femaldth(CI) \\ Dthr_5 &= Ans_5 \times Bulldth(CI) \end{aligned} \quad \text{(Eq. 49)}$$

Animal distribution submodel

The animal distribution model predicts how animal populations are distributed among grid cells per month in the study area in relation to habitat suitability. Instead of modelling animal movement explicitly, the model redistributes the entire population in relationship to the spatial

distribution of habitat suitability. The suitability of habitat in a grid cell is potentially affected by many factors, including forage (*Hsf*) and water as well as tree covers. Suitability indices based on the individual current state are calculated for each of these factors monthly in the grid cell and are combined to yield an overall grid cell suitability index (*Hsi*). The indices are computed by

$$Hsf_{narea} = Pforage(Tforage) \times Phys \times \Pr efarea \times \Pr efwater \times Noise$$
$$Hsi_{narea} = \frac{Hsf_{narea}}{\sum_{narea} Hsf_{narea}} \quad \text{(Eq. 50)}$$

Physical habitat suitability (*Phys*) is computed as

$$Phys = Min(Slope, Elev, Shade, Thc) \times Frc \times Psnow(Sdep) \quad \text{(Eq. 51)}$$

Animal habitat use is often limited by the distribution and quality of water. During this study, we used distance maps of permanent wells. This water type is characterised by two types of maps: one describing the minimum distance to a water source and one describing the effective discharge rate. The effect of distance to water and water quality on habitat suitability ($Pwatr_{nscn}$) are represented by

$$Pwatr_{nscn} = \sum_{nw} Pdisw_{nscn}(Distmn_{nw,nscn}) \times E\min r_{nw,nscn} \times Eseas_{nw} \quad \text{(Eq. 52)}$$

After animals have been distributed in relationship to the distribution of *Hsi*, it is possible that animal density distributions may not be supportable by the available water discharge. This is calculated by a requirement to supply term. The result is the number of animals in grid cell which can be supplied. The excess number of animals is transferred to a pool of dispersers which is redistributed to either a grid cell with unused water quantities or below the animal density limit.

2.4.5 Spatial modelling and landscape characterisation

This chapter describes the model system approach starting with general features of the landscape, which were refined into explicit environmental variables used in the sub-model simulations.

The model simulates ecosystem processes using states (Coughenour 1993), which can only be changed by the flow of materials or energy (Figure 9). Neither matter nor energy is

created or destroyed in this approach. Mathematical equations define these flows (c.p. chapters 2.4.1-2.4.4), as flows vary in response to the amounts of matter or energy stored in different states or in response to inputs of matter or energy from outside the system. Energy from outside the system is referred to as a driving force, and the most important driving force is the climate. The relevant climate factors are *Ppt*, T_{avg}, *Relh*, wind speed and *Rad*, which were calculated by latitude, time and cloud cover data. This dataset was determined by numerous weather stations distributed over the study area. These data are used to create monthly sets of *Ppt* and T_{avg}. A month is the basic unit of time in the SAVANNA© model. An interpolation scheme corrects this data for elevation differences between weather stations and grid-cells (see Figure 10).

A second source of data was derived from Geographic Information Systems (GIS). These data include digital maps of soils, vegetation, elevation, aspect and slope. The term grid-cell has been adopted by GIS developers to identify a certain spatial terrain in a system by a rectangular border containing one value of any unit. Descriptive tables accompany the vegetation and soil maps. Here vegetation is described in terms of tree, shrub and herbaceous cover and height, root biomass and plant species composition (chapter 2.5.1). Soil descriptions, including *Wlt*, soil depth and nutrient content, are described in chapter 2.6.

Primarily, the water budget simulation is described. The first step is the start of the water balance sub-model based on given *Ppt* and soil characteristics, calculating soil moisture dynamics and soil water use for each grid-cell. A soil map is read while initialising the model transporting the water holding capacity for each soil type. The model expands this information over the soil map of the entire study area. The water budget on the grid-cell level includes *Ppt*, interception by leaves and detritus, run-off, run-on, infiltration to subsurface layers, deep drainage losses, *Bsev*, root water uptake and *trans* losses from leaves (Coughenour 1993). Each of these fragments might be controlled, because they are output parameters.

This information is used for the 2nd next step of the simulation, the *NPP* sub-model is run. It simulates plant biomass production and its dynamics. Plant biomass production is affected by light, water, N, temperature and herbivory (Figure 8; see chapter 2.4.1). Water and nutrients are derived from soils and local climate via various pathways. They are allocated in plant species roots and shoots and contribute to biomass production of trees, shrubs and herbs. This biomass is used either by grazers (goats and dromedaries) or browsers (sheep or human withdrawal) as well as decomposers.

Because plants need to transpire, in order to build up biomass through photosynthesis, this sub-model is explicitly linked to the water budget sub-model via transpiration and plant water use.

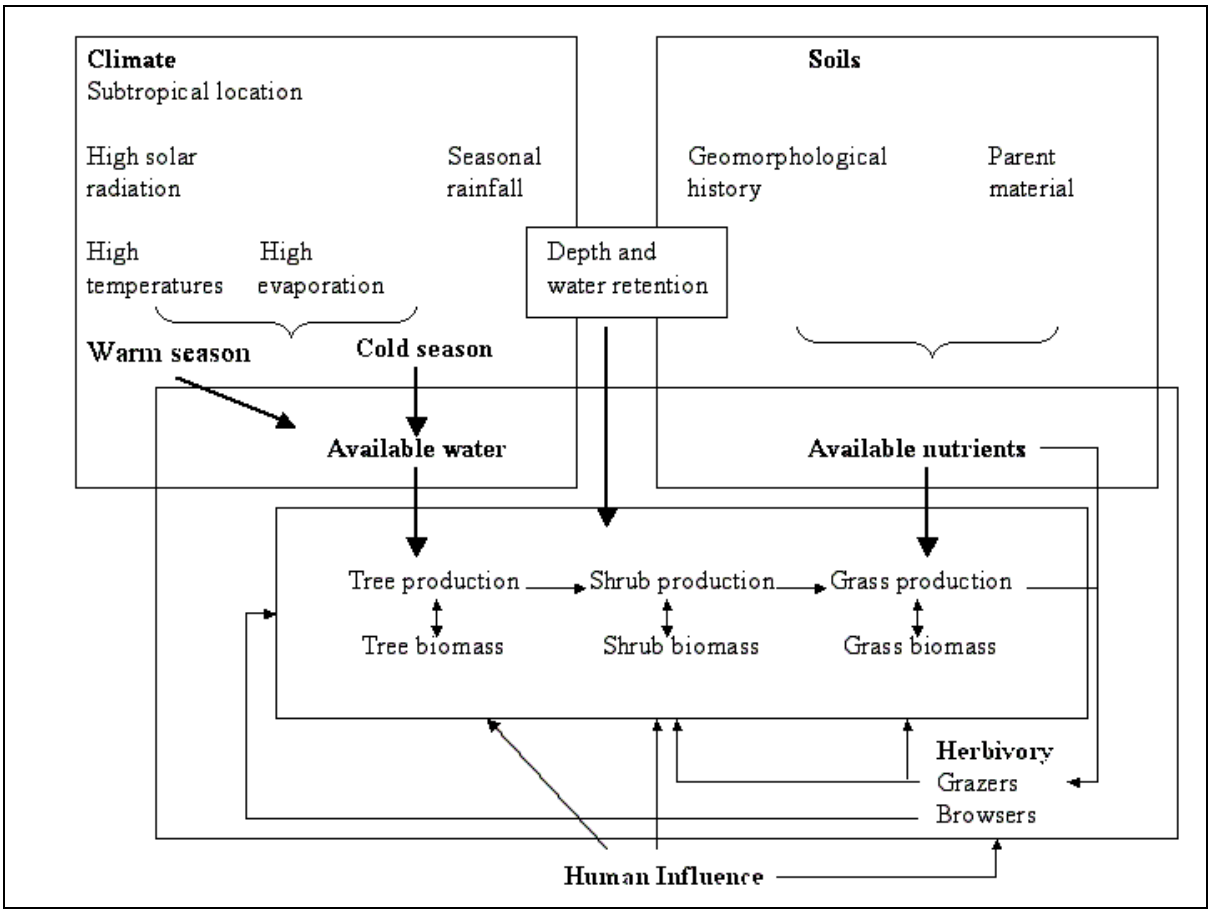

Figure 9: Ecosystem determinants and fluxes of biomass production and herbivores, modified from Coughenour and Chen (1997).

New biomass is produced by vegetation patches (tree, shrub and herbs (grass)) based on available water and nutrients. These are products of the local/regional environmental constraints. Plant life cycles and phenology reflect their maximal longevities in nominal rates. Due to water and/or temperature stresses, the phenology might be corrupted.

N allocation is important in plant life cycles for growth and photosynthetic activity. N is simulated by the litter decomposition and N cycling sub-routine implemented in the primary production sub-model (c.p. chapter 2.4.3).

Nup correlates with the soil N concentration and is calculated by the Michaelis Menten function. *Nup* rates correlates directly with plant N concentration: if plant N increases uptake rate decreases and vice-versa (Coughenour and Chen 1997). Furthermore, N is allocated among shoot tissues of different ages in relation to the age-dependent sink strength or light intensity. If tissues die, N is re-translocated to remaining living tissues. Otherwise, N is released during (litter) decomposition to mineral forms that can be taken up by plants. N in plants is either transferred to soil detritus due to tissue mortality or is relocated from herbivores to soil as urine or faeces. N leaves the system though conversion to gaseous forms during detritus decomposition or through volatilisation of ammonia from herbivore urine. Decomposition depends on soil moisture content and temperature.

Next, important features of landscape simulation based on raster cells and GIS data are prestented. Figure 10 explains the basic simulation procedures of SAVANNA©: (I) Landscape information on soil, vegetation and topography provided by GIS are recalculated to (II) spatially explicit grid-cells of regional extent. A sub-grid cell consists of the three major vegetation components: tree (woody), shrub and herbaceous (grass) patches (Coughenour 1993). These patches are distributed in the landscape as categories of both run-on and run-off areas (III), and vegetation patches modify local water budgets. Inputs are derived from overland as well as aerial run-on, with its parameters *Ppt* and snow. Aerial run-off is a function of *trans* and *Bsev*. Lateral downland drainage as well as vertical soil water movements is part of run-off calculations, too. Snow melt and snow evaporation were not used in these simulations.

Next, the concept of plant functional types (PFT) used in the simulations is described. The groups of PFT´s used here are herbaceous, shrub and tree, summed up as homogenous landscape vegetation identifiers. Each grid-cell has vegetation from these three PFT´s in predefined percentages (c.p. Table 7) and these PFT´s affect run-off and run-on. This concept is described in Coughenour (2005) and determines important pasture features individually and as they interact (e.g., in competition and synergistically).

The simulation results can be visualised in different formats. In a temporal format, one can see the average number of animals or plant biomass in different parts of the simulated landscape. In a spatial-temporal format, the spatial distribution of animals and biomass is lined up in sequential maps, within the simulated time range. In combination with a GIS, *SAVANNA*© provides highly refined mapped information.

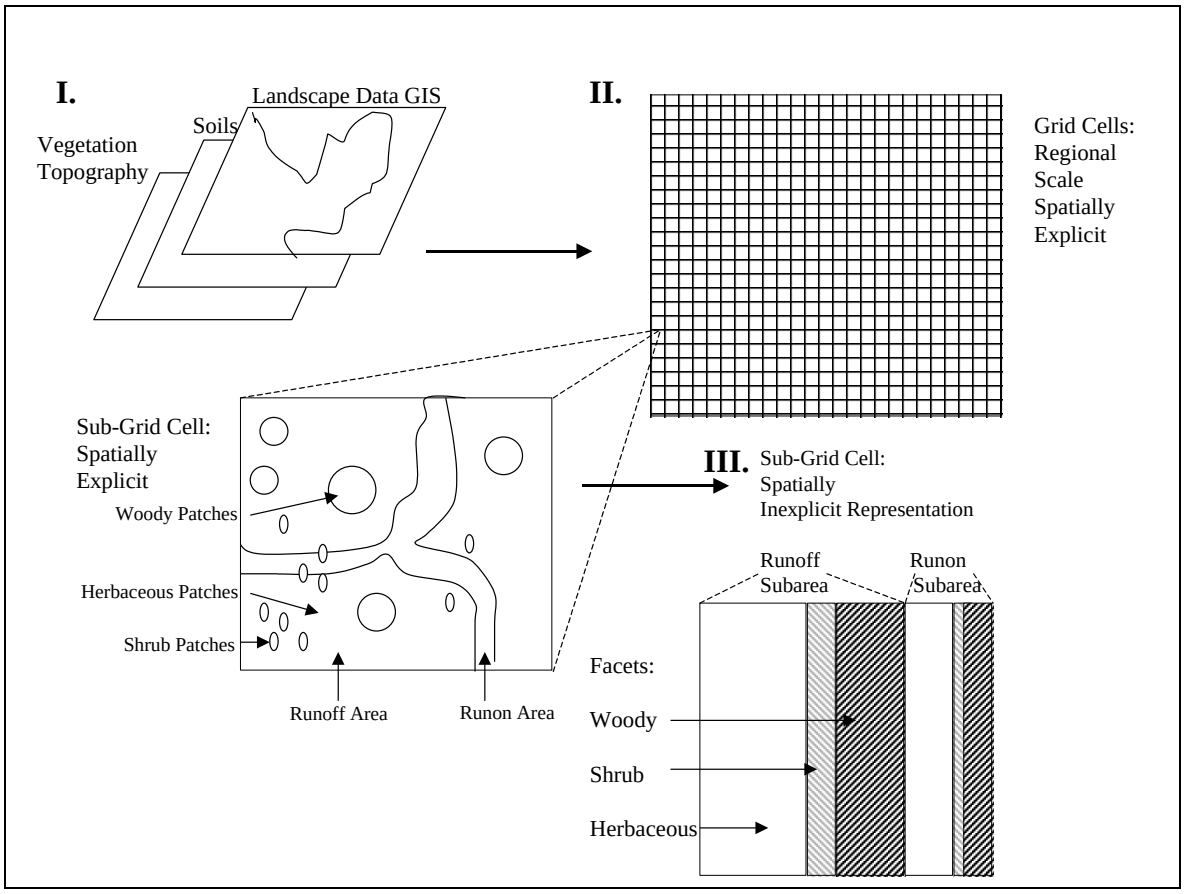

Figure 10: Landscape functionality in the ecosystem model SAVANNA©, modified from Coughenour (1993).

2.4.6 Dataset

The model uses a database provided by several sub-projects within IMPETUS as well as counterparts from Morroco (Table 3). In the following section, the database is presented. All spatial data in the simulations were converted to the same geographical extension in order to confirm proper simulations. The coordinate system is Lambert Conformic Conic with the date Merchich, defined to be used by the entire IMPETUS project (Schulz 2008).

Table 3: Data for SAVANNA© model parameterisation and application.

Map data	**IMPETUS Subproject & Partner**	**Resolution**	**Model Resolution**
SRTM – digital elevation model	Remote sensing (Poete)	30 x 30 m	1 km^2
Vegetation map	Vegetation ecology (Finckh) and Remote Sensing (Poete)	30 x 30 m	1 km^2
NDVI data and model	Remote sensing (Fritzsche)	30 x 30 m	1 km^2
Soil type map	Continental Hydrosphere (Klose)	30 x 30 m	1 km^2
Descriptive data		**Description**	
Animals	ORMVAO service d´elevage (Ramdane)	*O*ffice *r*égional de *M*ise à *V*aleur *A*gronomique *O*uarzazate - Demographics, populations	
Animals	CBTHA-Ouarzazate (Benidir)	Projet de *C*onservation de la *B*iodiversité par la *T*ranshumance dans le versant sud du *H*aut *A*tlas - Livestock numbers	
Climate	Direction Regional Hydrologique (DRH)-Ouarzazate	Monthly climate data	
Climate	Hydrology (Schulz) and own data	Monthly climate data	
Meteorology	Meteorology (Born)	Regional scenarios and IPCC A1 and A1B	
Vegetation	Vegetation ecology (own data; Staudinger and Finckh 2005; Gresens 2006)	Physiological and abundance data	
Soils and Hydrology	Continental Hydrosphere (Klose)	Soil chemical and physical parameters	

2.5 Parameterisation

The aim of this model parameterisation scheme is the provision of parameters for the research area.

2.5.1 Vegetation

The above-mentioned sub-models, primary production and plant population (see chapter 2.4.1), were parameterised with data obtained from new field measurements, the literature, or other IMPETUS sub projects or local partner organisations, namely the ORMVAO in Ouarzazate.

The model was parameterised and calibrated by re-running the simulation after resetting parameters (Christensen *et al.* 2003). A sensitivity analysis was conducted to analyse the influence of one individual parameter.

The model basically simulates three PFT groups: *herbaceous* (grasses and forbs), *shrub* and *trees* (see Figure 10). Different combinations of these groups make up most real ecosystems. The principle is to simulate all functional groups of plants favourable to herbivores in the system, achieving further understanding of the interactions among nutrient and water flows in the system, vertical and horizontal landscape cover and the basic structure of vegetative biomass. Hence, plant groups identified in the study area are classified into the three groups above. Each PFT is further divided into specific plant groups (see Table 4).

As already indicated, the simulated herbaceous PFT consists of grasses and forbs. These plants do not use physical or chemical defence strategies. Secondly, shrub PFT is considered. This feature is important for semi-arid grazed ecosystems as the primary contributor of biomass. Secondly, this PFT consists of herbaceous parts as well as woody structures. Both woody and herbaceous tissues on shrubs are digestible in this study by specialised animals. Trees are also important for biomass production, but are less digestible. Only specialists like goats and dromedaries consume tree leaves.

Table 4: Allocation of specific plant groups to herbaceous, shrub and tree PFT's.

PFT	Plant Group Name - Description	Number
Herbaceous	"fine grass" – annual leafy grasses	(1)
	"coarse grass" – perennial coarse grasses	(2)
	"alpine grass" – perennial alpine grasses	(3)
	"alpine forbs" – perennial alpine herbaceous forbs	(4)
	"fine grass" – herbaceous - annual	(5)
Shrub	"evergreen shrubs"	(6)
	"low DMD (low dry matter digestibility) shrubs" – deciduous shrubs of low dry matter digestibility	(7)
	"sage shrubs" – semi deciduous shrubs	(8)
Tree	"deciduous trees"	(9)
	"aspen trees"	(10)

The next step of parameterisation is allocating specified plant communities found in the study area to the three PFT groups. Finckh and Poete (2008) developed a vegetation map for the region of 25 major plant communities plus one class for water bodies, developed through remote sensing work and field studies (Table 5, Figure 11). This classification was developed by the vegetation ecology (Finckh, Staudinger and Oldeland) and the remote sensing (Poete) groups at Hamburg and Bonn universities using literature research (Quézel and Barbero 1981; Quézel *et al.* 1988) and intense field studies. With these datasets, plant communities are classified in this study to simulate the most abundant species and their genetic relatives. Furthermore, plant groups are structured by geographical position or abundance data (bare or densely structured, etc.) as follows. Note that due to the exclusion of certain communities, the order of numbers is interrupted.

The spatial distribution of the above-mentioned inherent vegetation communities of the model is shown in Figure 11 below.

Table 5: List of plant species in the parameterised SAVANNA© order according to vegetation map elaborated by Finckh and Poete (2008), see Figure 11.

Order	Structure and Scientific Name
1	densely structured *Artemisia mesatlantica-Artemisia negrei* steppe (woody parts)
2	densely structured *Artemisia herba-alba* steppe
3	bare/degraded *Artemisia herba-alba* steppe
4	on rocks *Artemisia herba-alba* steppe
5	dorn dense structured spiny cushion shrubs with *Platycapnion saxicolae*
6	dorn bare, detrital meadow with *Arenarion pungentis*
7	densely structured *Hammada scoparia-Convolvulus tributianus* steppe
8	steppe *Hammada scoparia-Farsetia hamiltonii* steppe
9	bare *Hammada scoparia* steppes, degraded
10	semi desert *Hammada scoparia*
11	Saharan rock communities: *Asterisco-Forsskaoletea*
12	juniper steppe-*Junipero thuriferea, Quercion*
13	lower reaches spiny cushion shrubs *Ormenion scariosae*
14	oro-mediterranean plant communities
15	mobile sand vegetation, *Aristida pungens*, *Caligonum comosum* *Calotropis procera*
16	annual Halophytes, *Frankenia pulverulenta*, *Anastatica hierochuntica* *Mesembryanthemum nodiflorum* and *Limonium sinuatum*
17	water body
19	clay pans, *Zygophyllum gaetulum*
20	dune vegetation
21	Date palm (*Phoenix dactylifera*) oases
22	agricultural areas
23	*Panico turgidi-Acacion* communities
25	*Acanthorhino-Zillion* communities
33	*Tamarix-Nerium* Wadi communities
38	open gravel areas
39	lime detrital meadow

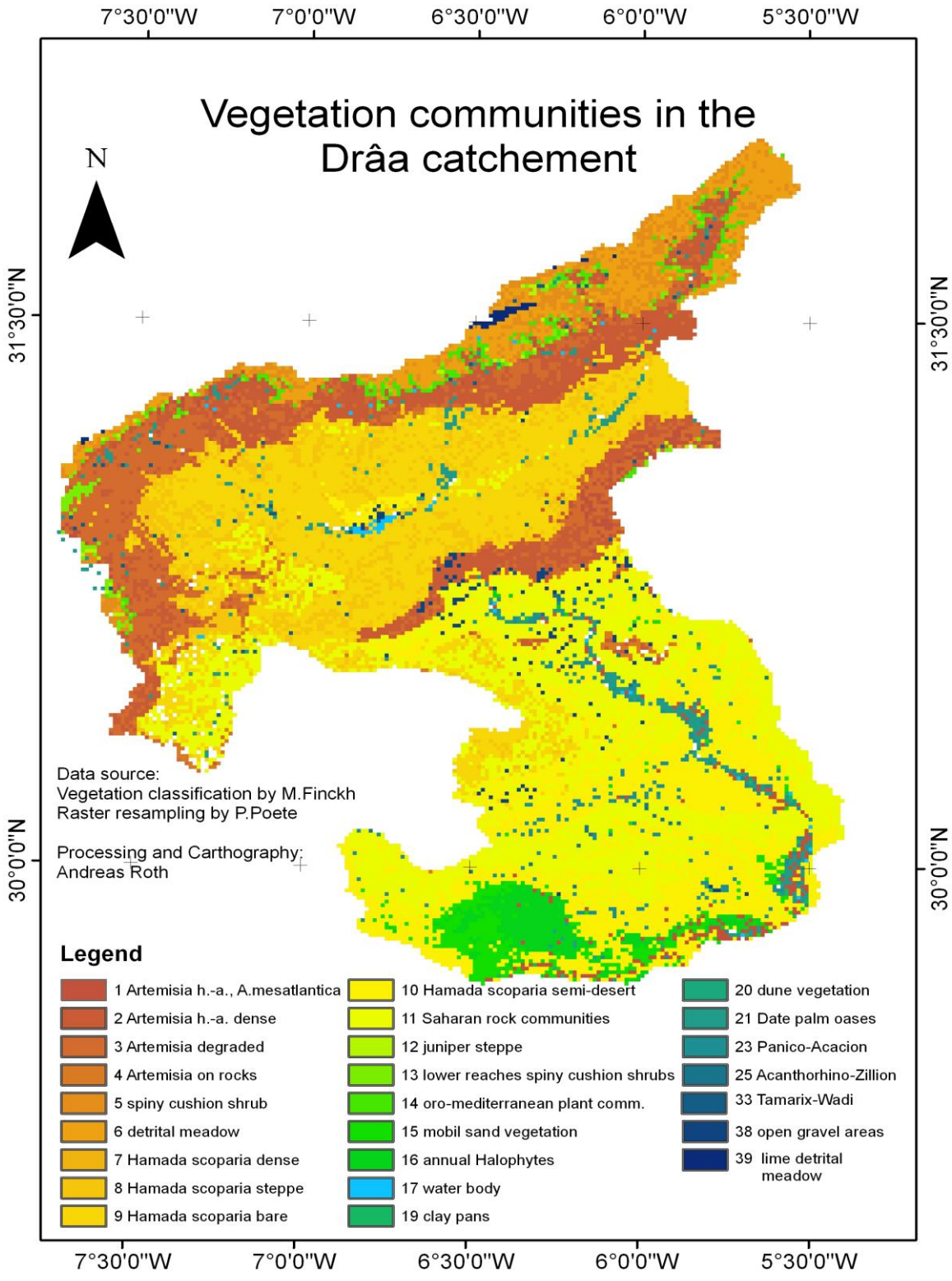

Figure 11: SAVANNA© vegetation dataset of the Drâa catchement (Finckh and Poete 2008), grid cell size 1 km^2 recalculated.

2.5.1.1 Simulations of vegetation communities - the concept of plant functional types

Ground cover data of vegetation is the most important feature of modelling vegetation dynamics (Coughenour 1993; Retzer and Reudenbach 2005). Parameter files were used to describe the relative ground cover of plant functional type (PFT) groups of vegetation. The concept of PFT groups was developed to summarize plant species to groups that reflects certain common strategies towards nutrients, disturbance, grazing or climate change (Allen-Diaz and Bartolome 1998; Körner 1994; Mouillot *et al.* 2001, Boer and Stafford Smith 2003). The combination of PFT groups or layers describes the interaction and concurrence between plant communities in the model. Next the transmission of the PFT concept to the study area is described.

Here, overall three PFT groups are used to calculate plant simulations based on spatial information derived from remote sensing. These PFT groups are herbaceous, shrub and tree. Each of these three groups is allocated to a clearly defined vegetation type, based on field studies, remote sensing and literature data (Table 3). The modeller should choose a reliable combination of PFT groups to simulate a certain target. The listing of plant groups modelled in the system is for herbaceous from (1) “fine grass” annual leafy grasses type to (5) “fine grass” herbaceous-annual type, for shrub from (6) “evergreen shrubs” to (8) “sage shrub” semi-deciduos type and for trees from (9) “deciduos tree” to ((10) “aspen tree” (Table 4), and is the source key for the following descriptions.

Table 6 portrays the figures of plant group acquisition for herbaceous, shrub and tree PFT groups, starting with vegetation type numbers (1-39) based on the vegetation map. This number refers directly to the vegetation map written initially by the model. The model initially aggregates all system numbers (1-39) to one herbaceous plant group type (1-5) (Table 4), else the number is zero. Vegetation type is not fixed to any plant group and can be changed iteratively during parameterisation.

For the shrub PFT, the model allocates one herbaceous and one shrub type (6-10). Because shrubs are estimated as an overstory level above the herbaceous plant group and herbaceous type must not be the same as in herbaceous PFT. This scheme contributes to the competitive situation, e.g., shrubs and herbaceous plants in the same plots are forced to compete for nutrients and sunlight. But at the next higher level the shrub PFT itself competes with herbaceous PFT, too which might be composed by different herbaceous plant type. This concept is applied to all three PFT and the tree (woody) PFT probably increases complexity. Finally for the tree PFT, three plant groups might be chosen. Here, plant group numbers must be different from the herbaceous and shrub numbers. This stipulation acknowledges the overstory character of trees. Due to the spare distribution of trees in the study area, only four vegetation type numbers, 12 and 21-23 (c.p. Table 5), make up the tree PFT group.

Table 6: Plant groups refer to classification (1)-(10) Table 4, Vegetation types refer to Table 5, modelled in herbaceous, shrub and tree PFT.

Vegetation type number	Herbaceous group number	Shrub group number*	Tree group number**
1	3	4 8	0
2	5	5 7	0
3	3	4 8	0
4	3	3 7	0
5	2	2 6	0
6	2	2 8	0
7	3	4 8	0
8	3	4 7	0
9	5	5 7	0
10	5	5 7	0
11	2	2 7	0
12	3	4 6	4 6 8
13	1	1 8	0
14	1	1 8	0
15	1	5 0	0
16	1	5 0	0
17	0	0 0	0
19	5	5 6	0
20	1	1 7	0
21	1	1 0	1 0 10
22	3	4 9	4 9 10
23	2	2 0	2 0 9
25	1	1 7	0
33	3	4 6	0
38	5	5 7	0
39	4	4 7	0

* Composite of 1st position herbaceous group number and 2nd position shrub group number

** Composite of 1st position herbaceous group number, 2nd position shrub group number and 3rd position tree group number

In each vegetation plot simulated in the model, if the plant type group number is > 0, it consists of a combination of herbaceous, shrub and tree plant types.

For example: Vegetation type number 14, identified as oro-mediterranean vegetation community, is calculated with plant type no. 1 (fine grass) in the herbaceous PFT group. Next

column to consider is the shrub PFT group no. 8 (predominant shrub sage) and the tree PFT group no. 0, not present in this vegetation type. Thus, this type is simulated with a fine grass understory and a sagebrush overstory. Based on this information, plant types were initially distributed spatially in the system (c.p. chapter 2.4.4).

In the following section, the ground cover here the percentages per PFT group (Table 4), of vegetation type number are next to be parameterised in the model. This defines the presence and absence of each plant group type. Following the principle of vegetation ground cover (Wiegand *et al.* 2004), the initial model dry matter amount of each plant type (e.g. based on Table 11) is estimated. With the above example, the percentage of ground cover of fine grass for the herbaceous PFT group is 15.7% (Table 7).

All PFT plant growth is primarily calculated with the root to shoot ratio (Eq. 8-13). For herbaceous plants, leaf biomass allocation is the important issue in terms of growth, as it does not possess woody parts. As an example, the dry matter of fine grass may be 50 g m^{-2} per PFT group. Thus, the detailed PFT specific dry matter (g m^{-2}) per cell is calculated by the initial value of for example 50 g m^{-2} referenced to 15.7% (Groundcover of Vegetation type 14) resulting in 7.85 g m^{-2}.

A similar calculation is done for shrub biomass allocation. In additional to the estimates of leaf allocation, woody stem biomass must be calculated for shrubs (Eq. 12). For the example above, vegetation unit no. 14 again contains one shrub PFT. Thus a guess as to the dry matter content for shrub PFT is here 200 g m^{-2}. The percentage of ground cover for shrub sage is 12.9% (Table 7). Following the above made calculation the result for shrub PFT appareance in this cell is 25.8 g m^{-2}.

Thus, within grid cells containing vegetation unit 14, the initial value for fine grass is 7.85 g m^{-2} and for sage shrub 25.8 g m^{-2}.

Table 7: Estimation of ground cover (%) of herbaceous, shrub and tree PFT (Finckh, 2007, personal communication).

Model vegetation type number	Herbaceous PFT groups ground cover (%)	Shrub PFT groups* ground cover (%)	Tree PFT groups** ground cover (%)
1	23.3	23.3 25.4	0.0
2	19.5	19.5 10.6	0.0
3	25.1	25.1 31.1	0.0
4	20.8	20.8 7.3	0.0
5	40.5	40.5 5.6	0.0
6	30.0	30.0 5.1	0.0
7	40.2	40.2 43.2	0.0
8	25.6	25.6 50.3	0.0
9	18.9	18.9 17.6	0.0
10	15.7	15.7 12.7	0.0
11	20.0	20.0 7.2	0.0
12	20.9	20.9 38.5	20.9 38.5 21.0
13	25.2	25.2 20.3	0.0
14	15.7	15.7 12.9	0.0
15	5.1	5.1 2.0	0.0
16	5.8	5.8 14.8	0.0
17	0.0	0.0 0.0	0.0
19	30.8	30.8 33.2	0.0
20	15.0	15.0 1.3	0.0
21	60.5	60.5 0.0	60.5 0.0 34.9
22	50.0	50.0 45.5	50.0 45.5 4.5
23	25.8	25.8 0.0	25.8 0.0 37.3
25	10.6	10.6 22.6	0.0
33	20.8	20.8 20.4	0.0
38	10.4	10.4 10.7	0.0
39	7.1	7.1 5.3	0.0

* Composite of 1st position herbaceous group number and 2nd position shrub group number

** Composite of 1st position herbaceous group number, 2nd position shrub group number and 3rd position tree group number

Next, grid cells containing shrub and tree PFT's had to be defined in their woody height, too, as biomass allocation is calculated by woody stem parts, in addition to leaf allocation.

Table 8 shows woody biomass estimates (mm) for shrub- and tree PFT. As above, this data was used to calculate initial conditions for PFT's ground cover, canopy extensions and biomass.

Table 8: Woody size/height data (mm) for shrub and tree PFT (Finckh, 2007, personal communication).

Model vegetation type number	Shrub PFT group woody height data (mm)	Tree PFT group* woody height data (mm)	
1	300	0.0	0.0
2	230	0.0	0.0
3	300	0.0	0.0
4	250	0.0	0.0
5	400	0.0	0.0
6	300	0.0	0.0
7	310	0.0	0.0
8	270	0.0	0.0
9	110	0.0	0.0
10	180	0.0	0.0
11	180	0.0	0.0
12	1500	400	400
13	1000	0.0	0.0
14	1000	0.0	0.0
15	240	0.0	0.0
16	200	0.0	0.0
17	0.0	0.0	0.0
19	290	0.0	0.0
20	140	0.0	0.0
21	0.0	0.0	7000
22	2000	2000	2000
23	0.0	0.0	4000
25	2000	0.0	0.0
33	2600	0.0	0.0
38	260	0.0	0.0
39	200	0.0	0.0

* Composite of 1st position shrub group number and 2nd position tree group number

Figure 12 portrays annual variations of observed vegetation ground cover (compare Table 7) in the Saharan zone (Oued Mird) of the study area (ROSELT 2004). The inter-annual

vegetation cover variation of approximately a quarter is remarkable. Annual mean rainfall amounts for the corresponding years 2000-2003 is of -70% to -50% at surrounding Zagora station with mean longterm (20 years) annual rainfall of 53 mm (DRH 2004). This trend is interrupted in 2004 by +50% of rainfall amounts compared to the longterm mean. The level of ground cover indicated here was used for the semi-desert vegetation community ground cover.

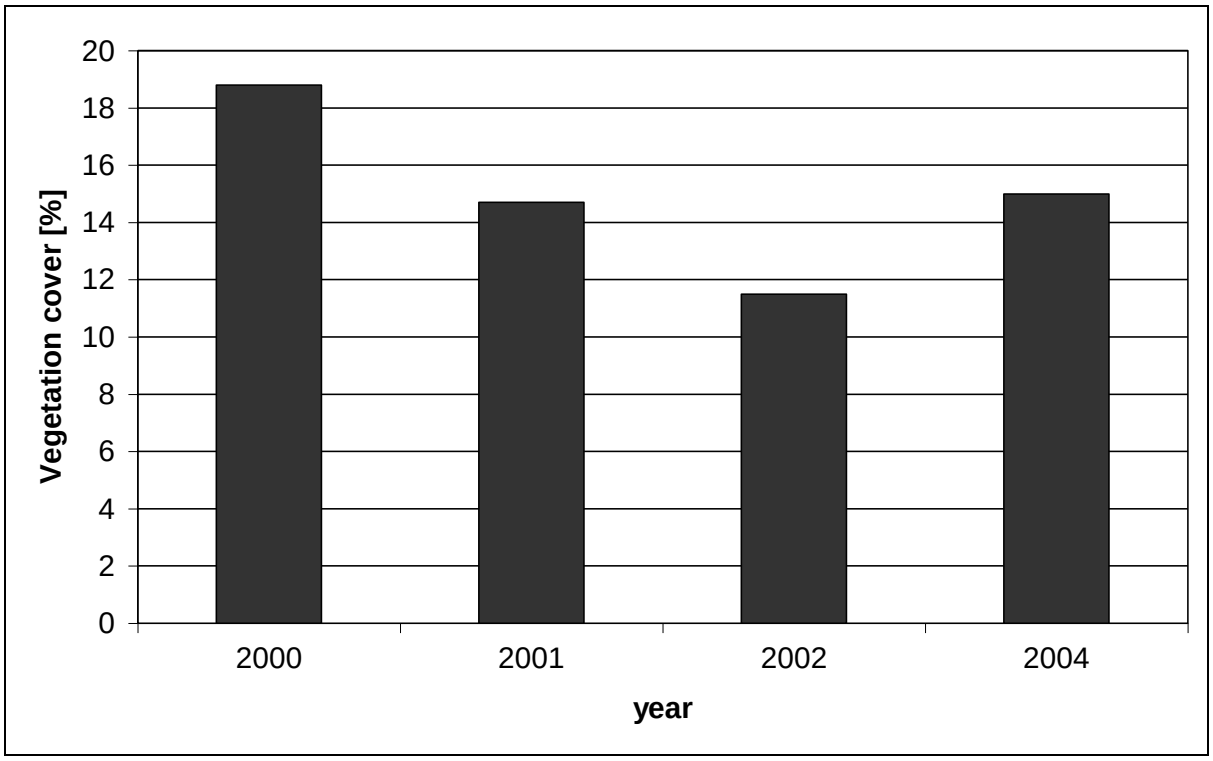

Figure 12: Variation of vegetation cover (%) 2000-2004 at the ROSELT observatory in Oued Mird (ROSELT 2004, modified).

The described parameterisation scheme was undertaken in order to convert elaborate data on the spatial distribution and characteristics of plant communities into PFT´s in a ground cover-based spatially explicit model.

In the following section, the parameterisation scheme for the definition of individual plant types making up the herbaceous, shrub and tree PFT's is given. This is necessary as the model PFT's spatial definition is derived from the spatial localisation of the plant species or communities found in Table 5. The measurement campaign was undertaken in autumn 2006.

2.5.1.2 Herbaceous PFT

Table 9 lists herbaceous PFT subgroup compounds considered in this approach and their characteristic, multiple mentions of plant species or communities are possible. The

herbaceous PFT characterisation is based on ground cover data and a list of functional responses, e.g. phenological cycle of plants. Other than shrub PFT which is parameterised by biomass contents of leaves and roots (next chapter). These responses are described with linear relationships for plant growth, transpiration and nutrient uptake. For example, grass root development is described by a fraction of roots in the soil (not shown). Other relationships describe the shoot to root ratio and water and nutrient uptake by roots. The nitrogen to biomass ratio and population determinants (seed reproduction rates, seed germination and water availability) is estimated with linear relationships, as well. The geographical location of each plant species or community is seen in Figure 11, plant samples are seen in Figure 13 and Figure 14.

Table 9: Herbaceous PFT compounds and characteristics.

Herbaceous PFT	**PFT subgroup**	**Species/communities subsummed**	**Phenology completed (days)**	**ground cover (%) (see Table 7)**
	“fine grass”	*Stipa cf. parviflora*	120	15.0
		Zyghophyllum gaetulum		30.8
		Halophyte species		5.8
		Open gravel areas		10.4
		Mobile sand vegetation		15.0
		Agricultural area		50.0
	“alpine grass”	Spiny cushion shrubs	120	25.2
		detrital meadows		7.1
	“coarse grass”	*Zyghophyllum gaetulum*	60	30.8
	“alpine forbs”	Spiny cushion shrubs	120	25.2
		detrital meadows		30.0

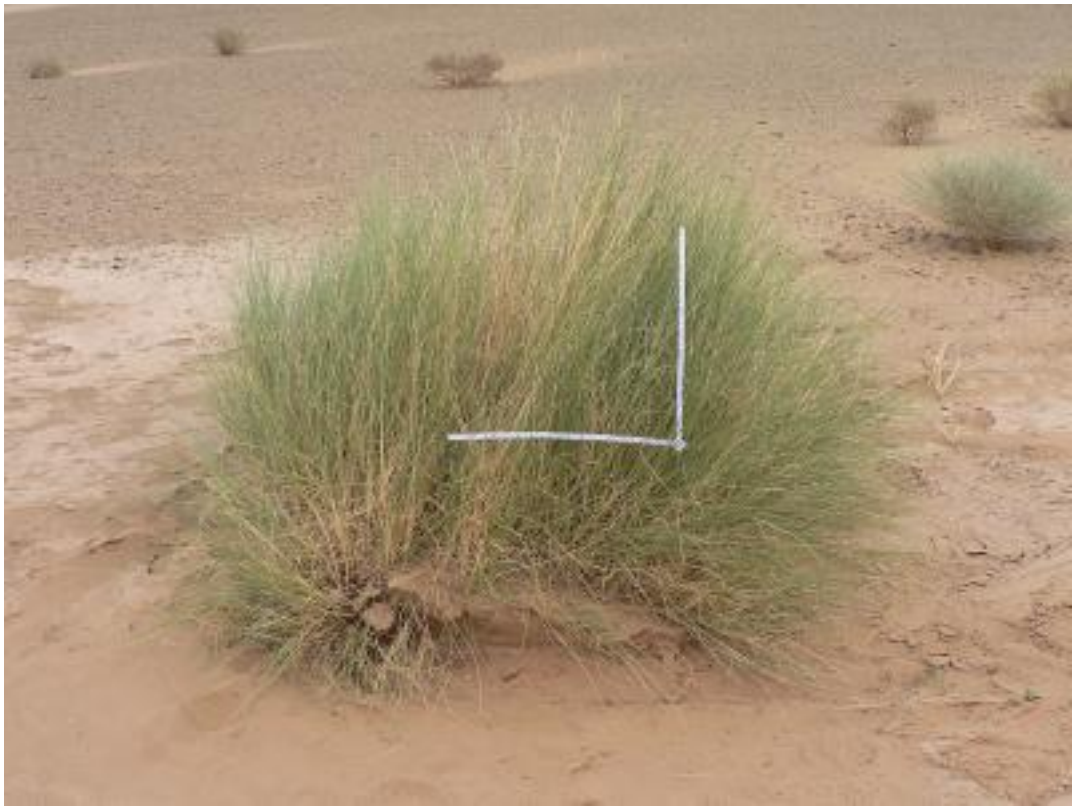

Figure 13: *Stipa grosstis* in the southern range of the study area (Photography A. Linstädter).

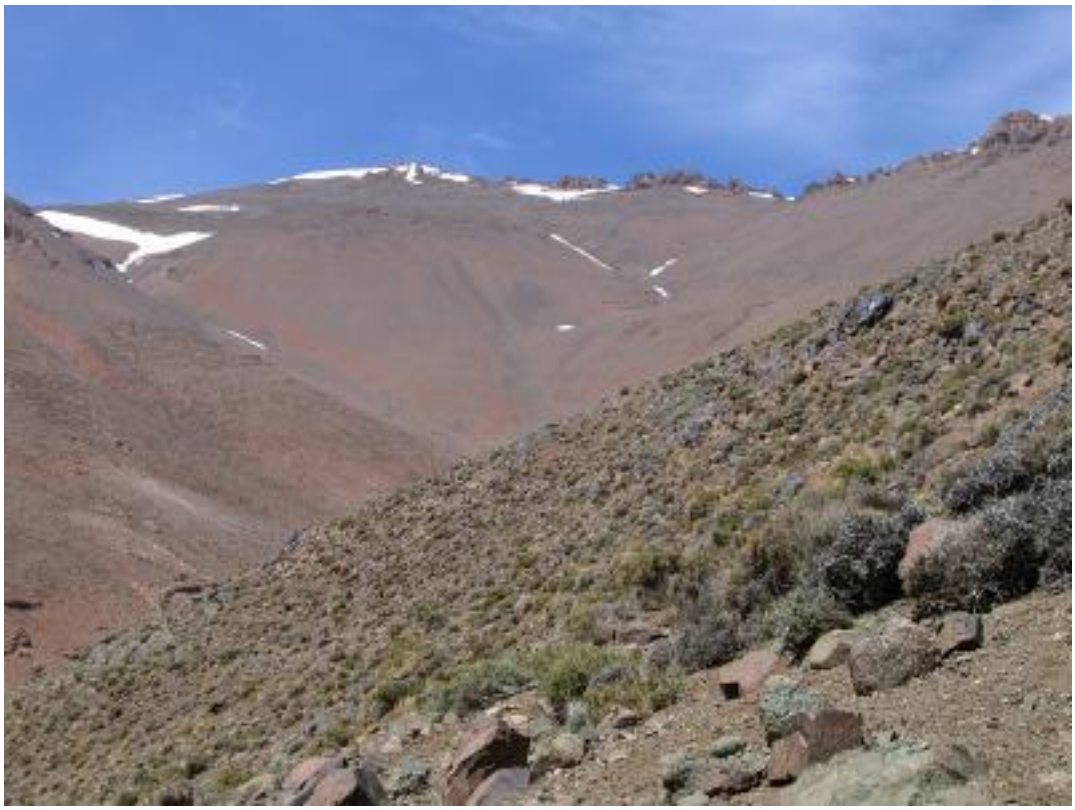

Figure 14: Oro-mediterranean forbs and shrubs in the High Atlas Mountains (Photography A.Linstädter).

2.5.1.3 Shrub PFT

Table 10 lists shrub PFT subgroup compounds considered in this approach and their characteristic.

Table 10: Shrub PFT compounds and characteristics.

Shrub PFT	PFT subgroup	Species/communities subsummed	Temperature (°C) Minimum-, Optimum-, Maximum-,	Phenology completed (days)	ground cover (%) (Table 7)
	"sage shrub"	*Artemisia herba-alba* steppe	0°, 18°, 40°	120	10.6/ 31.1/ 7.3
		Artemisia mesatlantica steppe	0°, 18°, 40°		25.4
	"low DMD shrub"	*Hamada scoparia* steppe	0°, 18°, 40°	120	43.2/50.3/ 17.6/12.7
		Convolvulus tributianus	0°, 18°, 40°		40.2
	"evergreen shrubs"	Spiny cushion shrubs	0°, 18°, 40°	120	25.2
		Oro-mediterrenean communities	0°, 18°, 40°	120	12.9

The sage shrub Group

In this study we used *Artemisia herba-alba* to be the predominat species of semi-deciduous sagebrush steppe in the model. Physiological field studies are used to parameterise the model according to the SAVANNA© user manual. These studies indicated a large spectrum of size and age or weight classes (Table 11). These classifications are necessary for all shrub and tree plant species in SAVANNA© in order to simulate a plant "aging" process and thus a shift from one class to another. Older, or in this case heavier, bigger plants compete better because of the assumed larger canopy on limited nutrients and space. This approach is useful for evaluation of the competitiveness or adaptance between classes of the same plant species to a given environment. Measurements of photosynthesis and leaf transpiration of *Artemisia herba-alba* additionally were used to parameterise the model in terms of transpiration amounts for *Artemisia* steppes.

Figure 15: *Artemisia-herba-alba* (Photography A. Linstädter).

Plant growth is simulated according to ground cover and classified weight data. Biomass data on *Artemisia herba-alba* was obtained from 10 m^2 plot measurements. These sets of data were classified into 6 weight classes, depending on the specific weight of leaves, roots, fine branches and fine roots. Weight classes are the most important biomass information on plant individuals for model simulation.

As Table 11 indicates, dry weight average quantities of plant compartments, especially root and fine root content, is often very low. Therefore, the model had to be parameterised very carefully in order to obtain reliable simulations of plant growth and its constraints in arid regions (see chapter 3.2). For example, estimating rooting depths and root contents is very difficult due to shallow soil depth and the high skeleton content (often >50%) of the soil (see Chapter 2.6). The presented values display the biomass amounts computed at the model start.

Table 11: Dry weight (kg) classes for *Artemisia herba-alba, own data; n.a.= not available*.

Artemisia herba-alba **kg dry weight**	***Shbsz*** **leaf+root**	**leaf**	**root**	**fine branch**	**fine root (est.*)**	**moist weight**
class 1	0.0145	0.0019	0.0009	0.0111	0.0001	0.0211
class 2	0.0107	0.0023	0.0012	0.0061	n.a.	0.0150
class 3	0.0075	0.0018	n.a.	0.0056	n.a.	0.0102
class 4	0.0204	0.0019	n.a.	0.0179	n.a.	0.0274
class 5	0.3372	0.1350	0.1792	0.1591	0.1060	0.4390
class 6	0.0176	0.0031	n.a.	0.0137	n.a.	0.0257

*estimate

Plant digestibility for animals is another important feature in the model. Digestibility is expressed in terms of preference weights and proportions of plant types within animal diets in the range of 0.0 to 1.0 for each plant type and each animal herd. The term preference weight (*Prfwt*) is a research based weighting amount between plant types within the diet (Coughenour 1993, see

Tables 22 and 23). However, *Artemisia* plants are not the first choice of animals, but its numerous defensive mechanisms against drought in summer (Gresens 2006), and consequently its predominant character for northern ranges, make it the main forage in the area.

The low dry matter digestibility (DMD) shrub Group

Table 12 shows the class composition and categorisation of *Hamada scoparia* based on biomass measurements. These values were used to parameterise the model for this kind of plant type. Based on the experiences with class range determination of *Artemisia herba-alba*, we chose here the category of shrub size (S*hbsz*), with the leaf and root weights to be the classifying determinants.

The flowering period of *Hamada scoparia* is in the springtime (see chapter 1.5.3).

Table 12: Dry weight (kg) size classes for *Hamada scoparia; n.a.=not available*.

Hamada scoparia **kg Dry Weight**	***Shbsz*** **leaf+root**	**leaf**	**root**	**fine branch**	**fine root (est.*)**
class 1	0.077	0.0041	0.0400	0.0300	0.021
class 2	0.154	0.0121	0.0716	0.0591	0.070
class 3	0.454	0.0180	0.2892	0.3229	0.160
class 4	0.502	0.0223	0.3511	0.0974	0.240
class 5	0.932	0.1141	0.5682	0.2313	0.061
class 6	0.041	0.0164	0.0209	0.0209	n.a.

*estimate

Figure 16: *Hamada scoparia* (Photography A. Linstädter).

As indicated *Convolvulus tributianus* is the second predominant plant species in the *Hamada* steppes. For that reason, this plant was included in simulations along with *Hamada scoparia*.

Table 13 shows measured biomass values of *Shbsz*, leaves, roots, fine branches and fine roots for *Convolvulus tributianus*.

Table 13: Dry weight (kg) size classes for *Convolvulus tributianus; n.a. = not available*.

Convolvulus tributianus **kg Dry Weight**	***Shbsz*** **leaf+root**	**leaf**	**root**	**fine branch**	**fine root (est*.)**
class 1	n.a.	n.a.	n.a.	n.a.	n.a.
class 2	n.a.	n.a.	n.a.	n.a.	n.a.
class 3	n.a.	n.a.	n.a.	n.a.	n.a.
class 4	0.0341	0.0135	n.a.	0.0185	n.a.
class 5	0.0230	0.0156	n.a.	0.0112	n.a.
class 6	0.0382	0.0111	n.a.	0.0270	n.a.

*estimate

Figure 17: Flowering *Convolvulus trabutianus* (Photography A. Linstädter).

Like *Artemisia herba-alba* plants, neither *Hamada scoparia* nor *Convolvulus trabutianus* are favoured palatable plants (see Table 22 and Table 23).

The evergreen shrub Group

Similar to the description above, this PFT was parameterised by weight and size classes, too. In the following section, the weight and size classes used for the simulation of spiny cushion shrubs and oro-mediterranean plant communities (Table 5) are shown. The parameterisation scheme was similar to *Artemisia herba-alba* and *Hamada scoparia*. Table 14 indicates measured values for the evergreen shrub *Buxus balearicus*, which predominately composes the community of oro-mediterranean plants in the simulations. As with most plant types in the research area, because of marginal rainfall amounts the measured biomass values are low.

For animal digestibilities of this group, see Table 22 and Table 23.

Table 14: Evergreen shrubs: distribution of size and weight classes of *Buxus balearicus*.

"low DMD-" and "evergreen" shrub	**class 1**	**class 2**	**class 3**	**class 4**	**class 5**	**class 6**
Height(Canopy) (m)	0.14	0.17	0.24	0.31	0.35	0.37
Woody weight (kg)	0.037	0.043	0.165	0.205	0.337	0.369
Leaf weight (kg)	0.015	0.017	0.066	0.082	0.135	0.148

2.5.1.4 Tree PFT

Table 15 lists shrub PFT subgroup compounds considered in this approach and their respective ground cover.

Table 15: Tree PFT compounds and ground cover.

Tree PFT	**PFT subgroup**	**Species/communities subsummed**	**ground cover (%) (see Table 7)**
	"deciduos tree"	*Juniper thurifera – Quercion*	21.0
		Tamarix-Nerium communities	<1.0
		Panico turgidi-Acacion / Acanthorhino-Zillion communities	<1.0
		Date palm oasis (*Phoenix dactylifera*)	34.9
	"aspen tree"	*Populus canescens*	4.5

Deciduous trees Group

Similar to the shrub PFT, the tree PFT is decribed by biomass measurements, in this case, measurements of canopy height and leaf weight. Additionally, the woody weights are considered as well.

Juniperus thurifera mean height and weight classes are shown in the Table 16. These parameters were collected from literature research (Montes *et al.* 2002), as we were not able to collect data during this study. Root distribution was estimated at a mean maximum for tree roots at 7 m according to Canadell *et al.* (1996). What might be not representative for species like *Acacia raddiana* with profond root distribution as reported by Gresens (2006).

Table 16: *Juniperus thurifera*: distribution of size and weight classes.

Juniperus thurifera	**class 1**	**class 2**	**class 3**	**class 4**	**class 5**	**class 6**
Height Canopy (m)	2.8	11.5	14.5	16.8	17.9	19.0
Woody weight (kg)	2.8	14.9	41.3	92.2	138.8	226.0
Leaf weight (kg)	0.2	3.5	5.3	8.7	9.8	11.9

Figure 18: *Acacia raddiana* at El Miyet test site in the southern ranges, (Photography A. Linstädter).

As tree communities are of minor interest in this study, the digestibility index of tree biomass was set to low values, except for dromedaries (see chapter 2.5.2.2). The biomass values in

Table 16 were used for *Panico-turgidi-Accacion, Acanthorhino-Zillion* and *Tamarix-Nerium* (c.p. Table 5) and date palm oases.

Figure 19: *Juniperus thurifera* in the High Atlas Mountains, (Photography A. Linstädter).

Aspen trees Group

Aspen tree communities are the predominant species for agricultural areas in the High Atlas Mountains. However, these trees occur in narrow strips in mountain valleys only. Similar to the other parameterisation schemes, *Populus canescens* characterisation was based on height and weight values (Table 17).

Table 17: *Populus canescens*: distribution of height and size classes.

Populus canescens	**class 1**	**class 2**	**class 3**	**class 4**	**class 5**	**class 6**
Height Canopy (m)	2.8	9.5	11.1	13.3	14.5	15.7
Woody weight (kg)	2.5	8.6	19.1	31.7	36.1	47.9
Leaf weight (kg)	0.3	3.0	4.3	7.8	9.4	11.9

Figure 20: *Populus canescens* in the Tichki Oasis in the High Atlas Mountains.

As *Populus canescens* plays no role in animal diets, its disgestibility preference weight was set to zero.

2.5.2 Simulation of Herbivores

Animal distribution is first described by age and sex composition. The model divides each herd into population and age categories, and this information is used to initialise herd dynamics. Herds described here are sheep and goats, dromedaries and humans. First, a specific description of each herd type follows.

2.5.2.1 Sheep and Goats

Population parameters are shown in Table 18 based upon data contributed by ORMVAO (2005) (Service d´élevage/Bureau of Animal Husbandry) (see Eq. 48-49). The maximum age of animals in this herd is set to four years based upon Bureau of Animal Husbandry survey information.

Table 18: Computed herd composition for sheep and goats: ages, survival rates of females and males and births of female per year (modified from Service d´élevage data, ORMVAO 2005).

Age of animals (year)	Survival rate female	Survival rate male	Birthrate of females
1	0.70	0.68	0.00
2	0.77	0.73	0.47
3	0.78	0.75	0.62
4	0.00	0.00	0.00

The table indicates the fraction of male and female survivorship (animal's ≥1 year old) and births of female sheep and goats. For example, the survival rate of female animals increases from 70% at one year old to 78% at three years old. This information is needed to characterise the simulated herd, combined with values of the month of birth and the initial condition index (*CI*) (Eq. 47) during gestation (here = 0.47 (Coughenour 1993)) given in the population parameter file. Together, these factors affect the energy balance of animals (Eq. 41), the nominal survivorship of newborns (Eq. 49), survivorship of female and male animals and the proportion of female births. These relationships are expressed by linear XY pairs. The maximum-minimum daily weight gain and loss affecting *CI* was parameterised to ± 0.15 kg (Coughenour 1993) except for pregnant animals with higher energy costs. The *CI* is the major factor that indicates the range of performance between energy requirements and energy used in herds. In later simulations, this index is evaluated to determine the quality and quantities of nourishment for herds and finally it determines herd sizes.

As animal age and sex is directly related to body weight and thus *CI*, Table 19 illustrates the initial population distributions of the herds (Eq. 50-52). For this herd type, the maximum age of animals is four years. We choose the initial age distribution to be a quarter in each age class with an even sex ratio (which made 1/2 for each male and female), resulting in an equal age - sex distribution (0.125 of the total population in each age-sex class).

Table 19: Computed initial age and sex distribution of sheep and goats - even sex ratio condition.

Age of animals (year)	females	males
1	0.125	0.125
2	0.125	0.125
3	0.125	0.125
4	0.125	0.125

These initial conditions are balanced for each herd type separately, while energy requirements and distribution patterns of herbivores are commonly parameterised for all herd types together. During model runs, these settings are modified by seasonal variations in climate and nourishment of herds.

2.5.2.2 Simulation of dromedaries

The following section describes the configuration of dromedary herds analogous to 2.5.2.1. The initial herd population is described by Table 20. The maximum age of dromedaries is considered here to be ten years (Ramdane, 2006, personal communication).

Table 20: Computed herd composition for dromedaries: age, female and male survival rates and births of female per year (Ramdane, 2006, personal communication).

Age of animals (year)	Survival Rate female	Survival rate male	Birthrates of females
1	0.80	0.77	0.00
2	0.88	0.85	0.40
3	0.90	0.87	0.48
4	0.90	0.87	0.62
5	0.90	0.87	0.64
6	0.90	0.87	0.68
7	0.90	0.87	0.58
8	0.76	0.75	0.45
9	0.28	0.26	0.17
10	0.00	0.00	0.00

Similarly to previous section, Table 20 indicates fractions of 1.0 (or 100%). For example, the survivorship of female dromedaries starts with 80% of one year old females, increases to 90% of three to seven year old females and finally decreases until culling. Birth numbers are highest (62-68% respectively) for four to six year old females (Ramdane 2006, personal communication).

Similar death rate versus *CI* functions as those for sheep and goats are used here to set up initial nominal survivorship for newborns (Eq. 49) and female and male animals and the proportions of female births. However *CI* factor for dromedaries was parametrised giving animals a higher tolerance rate towards poor forage quality and thus lower energy input

compare to sheep and goats. This is primarily due to their adaptation to hot and dry environments. Table 21 shows dromedaries initial proportional age - sex distribution.

Table 21: Computed initial age and sex distribution of dromedaries, Ramdane (2006) modified.

Age of animals (year)	Females	Males
1	0.15	0.15
2	0.15	0.15
3	0.24	0.24
4	0.24	0.24
5	0.44	0.44
6	0.44	0.44
7	0.05	0.05
8	0.05	0.05
9	0.05	0.05
10	0.00	0.00

The initial sex distribution is equal for females and males in each age class. Dromedaries are not culled in reality; animals simply are replaced at the age of ten years.

2.5.2.3 Simulation of humans

Human disturbance in the system was described in section 1.5.4 (El Moudden 2005). As this disturbance is important, we decided to simulate a human herd. Considering humans as herds for biomass withdrawal is critical due to their irregular abundance (on rangelands) and population data (limiting age). This feature thus describes groups of people searching certain areas for woody biomass. In order to not run into system failure and to describe humans properly as a herd, we copied the herd population distribution of sheep and goats (Table 19) but enlarging the life span to 30 years. However the most important difference to other herds is the diet consumption features (Table 22).

2.5.2.4 Energy and diet requirements of herds

Special emphasis is given to parameterisation of the energy budget of each animal type. This is specified in the metabolizable energy intake from forage cosumption of the populations

(Eq. 41). Animal energy costs are strongly related to their *CI*. Energy requirements consist primarily of the basic cost of metabolic energy demand per body weight and day. Additional costs of travel to satisfy that demand may be added (Eq. 42a and 42b). Basically, a balance of weight losses and weight gains is calculated (Eq. 46). These estimates are modified by changes in the age - sex distribution in any herd, which dictate changes in the mean animal body weight as well. Energy requirements are basically satisfied by forage intake (Eqs. 37a and 37b) and forage availability (Eq. 36).

First animal diets for each herd according to the ten groups of PFT (see Table 4) are considered. These are divided into the preference weights (*Prfwt*) and maximum proportions considered in each animal diet (Eq. 34). The weighting factor indicates the proportion of energy intake via shrub and grass to satisfy daily animal energy requirements (MJ kg^{-1} d^{-1}). The plant tissue components are separately divided into different categories (Table 22).

The maximum weighting proportion of a single plant type is 1.0. Thus, each *Prfwt* of 1.0 is the most likely palatable plant for this herd. A value of <1.0 indicates that these parts are of lesser preference for this animal. In detail, sheep and goats are more likely to graze or browse everything except for trees. The most preferred plants are grasses (“fine-“, “coarse-“ and “alpine-“). For shrubs, “evergreen-” are more likely grazed than “sage-” or “low DMD shrubs”. Dromedaries more likely grazed all kinds of tree branches. They are also assumed to graze everything down to “low DMD shrubs”. These herds are configured to be only limited to their area of interest defined by force maps (*Frc*). For the category of humans, their interest is defined to be upon woody (dead) material of shrub and tree plant types.

Tissue preference (for plant parts such as leaves, stems, branches and dead biomass, Table 23) of animals is weighted by values between the minimum 0.0 and the maximum 5.0. The higher the value the more the respective tissues are consumed.

In terms of tissue weighting, sheep and goats graze and browse more for live herbaceous leaves but also for stems and dead plant material. Dromedaries browse for leaves and stem material but less for dead tissues and fine branches. Humans mainly search for dead woody material.

Table 22: Configuration of diet plant group weighting for sheep and goats, dromedaries and humans.

Plant group no.	Sheep and Goats		Dromedaries		Human	
	Preference weight	Maximum proportion	Preference weight	Maximum proportion	Preference weight	Maximum proportion
(1)	1.0	1.0	0.06	1.0	0.0	0.0
(2)	1.0	1.0	0.06	1.0	0.0	0.0
(3)	1.0	1.0	0.06	1.0	0.0	0.0
(4)	0.06	1.0	0.06	1.0	0.05	1.0
(5)	1.0	1.0	0.06	1.0	0.0	0.0
(6)	0.08	1.0	0.08	1.0	1.0	1.0
(7)	0.05	1.0	0.05	1.0	1.0	1.0
(8)	0.06	1.0	0.06	1.0	1.0	1.0
(9)	0.02	1.0	1.0	1.0	0.03	0.5
(10)	0.0	1.0	1.0	1.0	0.03	0.5

Table 23: Configuration of tissue weighting in animal diets for sheep and goats, dromedaries and humans.

Tissue Preference Weights	Sheep and Goats	Dromedaries	Human
herbaceous leaf	5.0	5.0	0.0
herbaceous stem	1.0	1.0	1.0
herbaceous dead	1.0	0.0	1.0
browse leaf	5.0	2.0	0.0
browse dead	1.0	0.5	1.0
browse fine branch	0.0	0.5	0.0

2.5.2.5 Distribution patterns

Indices are used that accounts for forage distribution (*Hsf*) and forage intake rates (dependent on energy requirements and the habitat suitability (*Hsi*)). This index is used as the basis for animal distribution. The habitat suitability index (Eq. 50), over all grid cells, is expressed by linear relations among forage abundance, water availability (Eq. 52) and

physical habitat (Eq. 51). Additionally, animal distributions are shaped by maps of animals “preferred areas“ and of “water availability“.

As the research area is topographically highly heterogenous, we described next the linear relation between the habitat preference index and surface slope (Figure 21). Values are given in XY pairs as above.

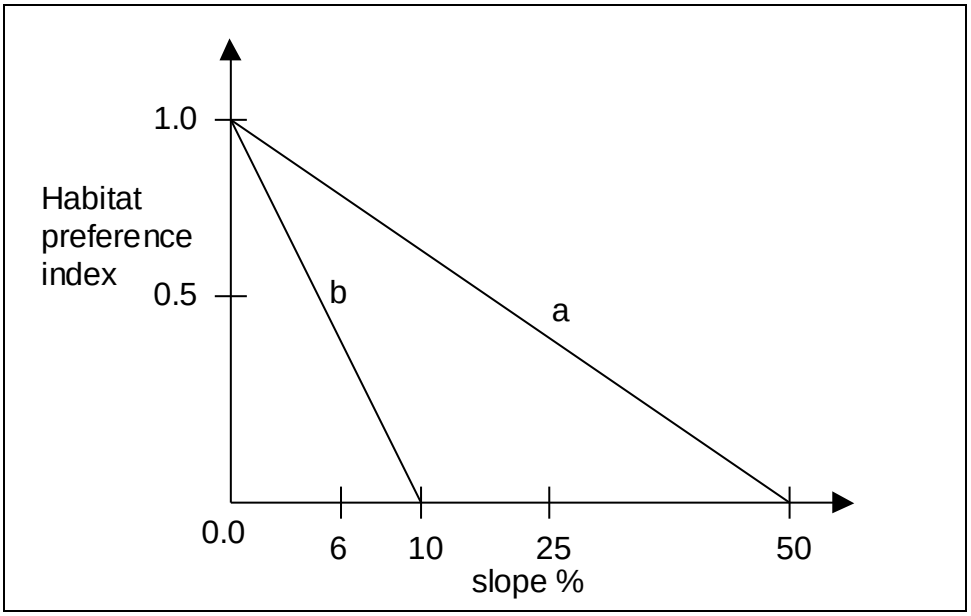

Figure 21: Physical habitat preference index and slope relationship for (a) sheep and goats and (b) dromedaries, SAVANNA©-modified.

Sheep and goats are more adapted to mountainous environments and steep slopes than dromedaries are. This difference is in the habitat preference index, which is set to 0.0 at 50% slope for sheep and goats but at 10% slope for dromedaries.

Water availability is calculated by the distance to water (km), which is introduced with a map of the number of wells accessible to animals. Water distances for animals here are low for the northern catchment and higher for the southern region. The *Hsi* is high if animals possess good access to water resources and low if not.

The spatial herd distribution is computed with a specific distribution map or force maps (*Frc*) indicating herd appearance in a certain grid-cell with 1 and absence with 0. Sheep, goats and humans are distributed over the entire study area. So each grid-cell in the system is labelled 1 for these herds. Dromedaries appear south of the Anti Atlas ridge only; for the northern study area, the respective distribution map is set to 0. These parameters are used to initially distribute animals over the study area and to force animal movement during the simulation.

2.5.3 Soil conditions

Soils are of evident importance to plant growth for provision of nutrients and water. Different parameter files describe soil fertility, C:N ratios, soils depth and soil textures on a grid-cell basis (c.p. Appendix, Tables 35 and 36). Next soil characteristics used in the model are indicated. Data are based on physical and chemical soil analyses (Klose 2009).

In total, 52 different soil characteristics were identified in the reasearch area and listed in a basic spatial map of soil distribution. An initial characterisation of each soil type is assessed with information on soil depth (*Sdep*, mm), *Wlt* (mm), *Fcp* (mm), *sm0* (proportion (%/100)), run-on and run-off (mm) curve numbers (USDA 1972; Wight and Skiles 1987) and *Bsev* (mm). Values were measured for each of three soil layers (see section 2.4.2.). These soil characeristics were transferred to the system's soil parameter files (see Appendix Tables 35 and 36).

The names of soil profiles in these appended lists are due to a newer model version different from the names given in section 2.4.2. Depth 1 refers to the bottom of the top layer (*Edep*) identical to *Bsev* layer with a fix depth of 10 cm for the entire study area. Depth 2 characterises the bottom of the herbaceous and (if appropiate) tree rooting zone (*Hdep*). Total depth is the maximum plant rooting depth (*Sdep*) and refers to the total simulated soil depth.

A second set of soil layers (see Appendix Table 36) describing soil fertility properties is used for model setup. These soil layers characterise C and N content (%), bulk density and thresholds of litter C and N (g m^{-2}) for surface and deeper soils. In addition the soil organic matter (SOM) amounts, as C:N ratios (g m^{-2}) are described. The C:N ratios are separated into the SOM1 fraction (fast availability by microbes), the SOM2 ratio (intermediate availability) and SOM3 (low availability) (Parton 1992). Because the distribution of organic matter is crucial for plant development, each of the ten plant types (see Table 4) has its SOM1, SOM2, and SOM3 fractions defined separately.

The soil files correspond to the numerical labels on the soil map. A spatial generalization of soil characteristics is critical and limitations of the information should be discussed (see section 5.2).

2.5.4 Climate data

The model includes different parameter files for completing an appropriate climate description (see section 2.4.3) for the simulation.

The meteorological station at the Mansour Eddabhi reservoir (DRH) near Ouarzazate was chosen as the central base station. Seven other climate stations (both of DRH and

IMPETUS) in the research area are included here in order to achieve appropriate interpolation schemes. All of the stations contain data on their specific geographic position and altitude.

The climate parameters in the central weather station are the monthly averages of T_{min} and T_{max}, *Relh*, wind speed (m s^{-1}), *Ppt*. These datasets must be provided throughout the entire simulation periode. All other climate stations provide only monthly means of minimum and maximum temperatures and *Ppt*. Table 24 shows parameter values for the Ouarzazate climate base station.

Table 24: Monthly averages of *Relh* (%/100), wind speed (m s^{-1}), T_{min} (C°), T_{max} (C°) and *Ppt* (mm) at Ouarzazate central model climate station. Derived from decadal average values (1997–2007) of these parameters, DRH climate station (DRH 2004).

Parameter Monthly Averages	Jan	Feb	Mar	Apr	May	Jun	Jul	Aug	Sep	Oct	Nov	Dec
Relh (%/100)	0.58	0.53	0.49	0.41	0.37	0.35	0.34	0.36	0.38	0.49	0.58	0.63
Wind speed (m s^{-1})	1.4	1.7	2.5	2.7	2.5	2.6	2.8	3.0	2.0	2.1	2.0	1.6
T_{min} (C°)	-0.6	0.7	2.8	5.7	8.6	13.6	17.4	16.9	13.0	8.6	3.4	0.8
T_{max} (C°)	20.6	23.9	26.6	30.0	34.1	37.9	39.9	39.2	36.8	31.0	25.9	21.3
Ppt (mm)	10.1	12.5	9.5	7.1	6.2	4.1	2.2	6.3	12.9	17.0	17.3	11.5

Based on the configuration of soil, climate, plant types and animal parameters shown in this section, the first model simulations were conducted. The next step in the modelling process was to applicate the model.

3 Model application

In this study, the overall modelling aim was primarily to simulate a dynamic vegetation community under a grazing regime in the long-term.

3.1 Model adaptation to regional conditions

The model was primarely applied to the rangeland area of Taoujgalt (see chapter 2.1). In order to set up an apppropiate simulation, five different soil profiles were distinguished: agricultural, channel, jurrasic, quartenary and tertiary. These soil types were parameterised according to the scheme shown in the previous section. The predominant perennial species modelled are the “sage shrub” plant group type (no. 7), the herbaceous “fine grass” (no. 1) and the “deciduous tree” *Junipero thurifera* (no. 9, cp. Table 5). All three vegetation PFT groups were selected, even though trees are of minor importance for animal diets, to confirm inter-PFT reliability of simulations in its regional context. To analyse the suitability of vegetation patches, we chose grid-cell size of 125 m^2 and a simulation period of ten years from 2002 to 2012.

Data used in this thesis are derived from biomass investigations, transpiration measurements by Gresens (2006); own unpublished data and studies on plant species distribution, development and abundance (Finckh and Staudinger 2002; El Moudden 2005; Oldeland 2006).

For a first application, two types of herds have been distinguished: sedentary and nomadic. These are estimated as fixed numbers of 5,000 and 15,000 head respectively. Table 25 presents climate data at the IMPETUS Taoujgalt station as it was used for parameterisation of the regional climate characteristics.

Initial model application showed that herbaceous plants and shrubs are restricted in their plant growth due to temperature, radiation and rainfall constraints found in the semi-arid environment. The parameterisation of these PFT groups for the research area required substantial modifications of plant soil water uptake and reproduction rates. In a first approach, these functions were used identical to Yellowstone National Park model applications. Expectedtly high plant mortality rates were predicted in response to climate conditions in the Drâa catchment research area. This result suggested that regional herbaceous and shrub species are adapted to high temperatures and radiation amounts and

a high variability of rainfall amounts. A description of the program modification process for plant-available soil water follows.

Table 25: Monthly averages of climate parameters at the IMPETUS Taoujgalt climate station: *Relh* (%/100), wind speed (m s^{-1}), T_{min} (C°), T_{max} (C°) and *Ppt* (mm).

Parameter Monthly Averages	Jan	Feb	Mar	Apr	May	Jun	Jul	Aug	Sep	Oct	Nov	Dec
Relh (%/100)	0.51	0.40	0.37	0.45	0.31	0.18	0.16	0.25	0.31	0.37	0.43	0.63
Wind speed (m s^{-1})	1.4	1.7	2.5	2.7	2.5	2.6	2.8	3.0	2.0	2.1	2.0	1.6
T_{min} (C°)	2.0	2.8	2.7	5.8	7.9	19.9	22.8	19.7	17.3	12.1	4.2	3.3
T_{max} (C°)	10.0	11.3	15.5	16.5	22.4	26.1	27.4	26.0	23.5	17.7	14.3	10.0
Ppt (mm)	2.0	27.8	26.1	48.2	19.8	2.2	2.2	1.8	15.0	2.2	19.6	48.7

3.2 Modification of substantial parameters

The simulations of plant growth in semi-arid to arid environments had to be adjusted to the constraints of the plants and the soil water situation. First, the impact of high radiance and temperature on plant growth was modified by identifying appropriate values for photosynthetic rates (Eq. 3) and leaf mortality rates (Eq. 10). This was done for the “fine grass” and “sage shrub” plant groups to determine whether and how fast these plants grow. If a declining trend in plant growth was still observed after simulating these parameters, then plant growth may be limited by water supply and must be re-parameterised.

Plant-available soil water (*Avlwat*) is a critical function in the model and has been identified as the major limitation to plant growth. Variables defining this function are root water content (*rwc*) and root water uptake. *Rwc* is computed as a weighted value between the mean and the wettest soil layer(s) accessible by plant roots, and is dimensionless. *Avlwat* (Eq. 5) is determined by *rwc* to maintain plant growth and is described by piece linear interpolation.

Rwc is a 0-1 function describing the weighting factor, using either all wettest *rwc* (value 1.0) or all mean *rwc* (value 0.0) based on *Ppt* amounts. The value describes daily *Avlwat* amounts accessible from both soil layers summed to weekly time steps (Eq. 14). The all wettest alternative accounts for dry conditions in which wettest soil layers must be summed to form plant sufficient *rwc*. Else the all mean alternative is adequate to simulate *rwc* in

temperate and humid regions. Where the *rwc* value 0.005 cm d $^{-1}$ (per soil layer) is defined as the minimum *Avlwat* content for alternative (1) all wettest (1.0 weight) and 0.02 cm d^{-1} (0.0 weight) reports the maximum value for alternative (2) all mean conditions (Table 26). If in one simulation week, the maximum *rwc* is supported by *Ppt* amounts, the model distributes 0.02 cm d^{-1} (all mean *rwc*) to plants. However, model application shows that the weekly minimum value (0.005 cm d^{-1}) is more likely in the study area, so we decided to use the *rwc* weighting factor 0.4 to compute an increased tendency to the wettest layer alternative. This decision was made for a variety of reasons: This procedure accounts for the fact that drought stress effects occur as daily stomatal closures. It also accounts for the significant amounts of water which may be added to the soil and would otherwise only be usable the next week because of models weekly time-steps or which may exceed *Wlt* capacities, drain and be lost to plants. In order to obtain a limited water supply to plants in the study region even during drought periods, the basic level of *rwc* is set to 0.4 instead of 0.0. As result of application, this value provides sufficient *Avlwat* by both all wettest and all mean *rwc*.

This relationship is implemented to accurately simulate plant types that are more droughts tolerant in the semi-arid to arid ecosystem.

Table 26: Linear interpolation of the *rwc* function versus plant available water (cm d^{-1}) and the value used for simualtions.

Description	**Mean soil layer *rwc* content**	**All wettest soil layer *rwc***	**applied value**
Linear interpolation scheme	0.0	1.0	0.4
plant available soil water (cm per soil layer d^{-1})	0.02	0.005	-

3.3 Limitations to simulated plant growth

Figure 22 summarises the limitations on plant growth due to N, water, light and temperature, in a “no grazing” (NG) condition model application. For first simualtions two conditions have been distinguished NG and “grazing” (G). The ordinate scale (Y) indicates the degree of influence of these parameters on the simulated plant groups. The value 1.0 represents a low effect, indicating that this parameter does not limit vegetation growth, and a value of 0.4 (at NG condition) indicates a high effect and thus a limiting influence of N, water, light or

temperature. The limiting threshold 0.4 directly refers to the water access determination of *rwc* made in the previous section. The simulated months and years are shown on the X axis. The parameter water is the predominant limiting factor in this environment, followed by N and temperature thresholds limiting plant development. During first applications, the figure for temperature fluctuations was running in a reasonable range. The influence of light intensities is negligible for plant growth in the area. Intra-annual variation in restrictions by water is obvious. In the majority of the months and years simulated, plant growth is limited by water availablity: The water situation in simulations is characterised by a deficit interrupted only by exceptional annual precipitation. Since water is a key feature for plant development, the continuing deficit influences other factors, too. N limitation does not turn out severe constraint compared to the water availability. According to model application outcomes N turned out to be a limiting factor for plant growth especially in the early spring at the onset of plant growth.

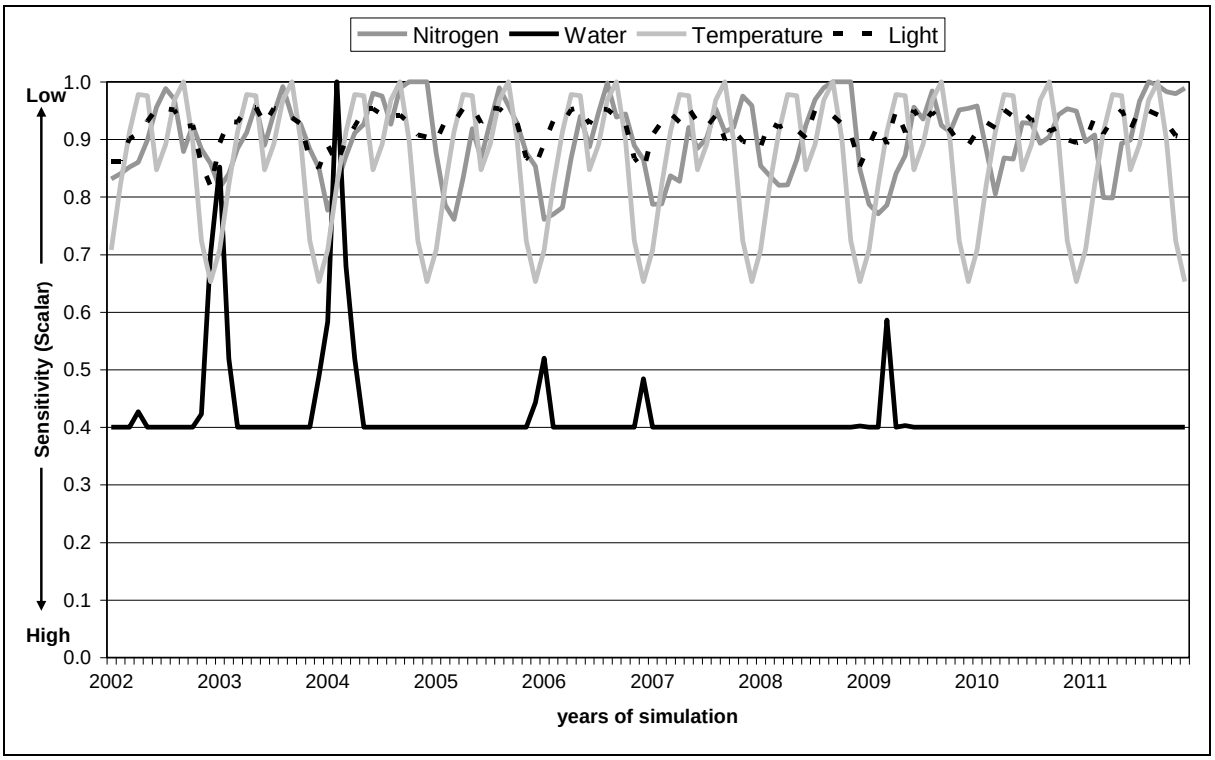

Figure 22: "No grazing" (NG) run (2002-2012) scalar limitation (0.4-1.0) to vegetation growth due to nitrogen *Eff-N*, water *Eff-W*, light *Eff-L* and temperature *Eff-T*. Monthly values are of January to December.

Figure 23 shows the limitation to plant growth simulated under G conditions and is different from Figure 22. Water again is the main limiting factor with equal figures, due to the same *Avlwat* parameterisation. Temperature and light sensitivities are also similar, but N sensitivity increases substantially according to model results. N limitation increases probably due to a higher reallocation rate of N because of animals compare to NG conditions. According to model outcomes N limitation increases coincidenced with decreasing water limitation

(precipitation events), indicating a growing deficit of N probably to due to increased plant growth. Additionally N may be washed out by surface water flows. Severe sediment losses and denudation events are often found in the region (Weber 2004; Gresens 2006).

Model application, however, computes stable vegetation growth and dynamics even under grazing pressure. Otherwise, the computed biomass production would not be sufficient to feed the simulated animals. Further results of these G and NG runs are portrayed in section 4.4.1.

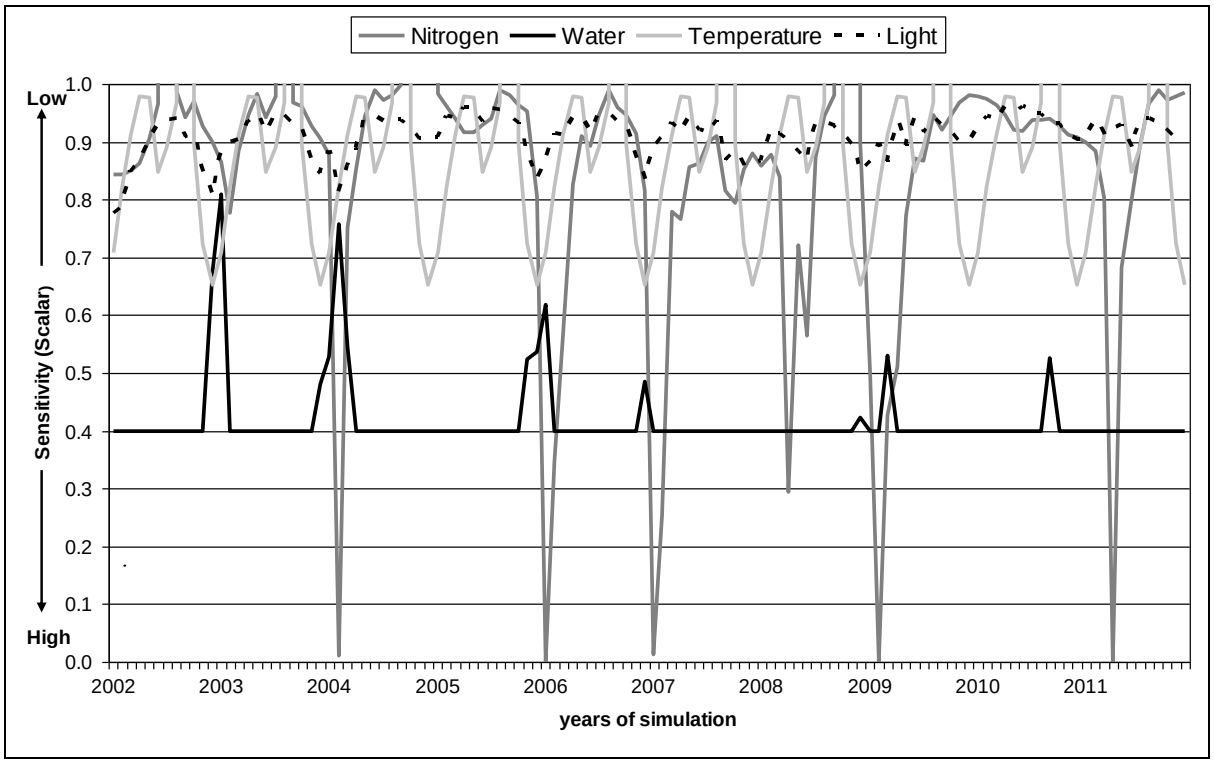

Figure 23: "Grazing" (G) run (2002-2012) scalar limitation (0.0-1.0) to vegetation growth due to nitrogen *Eff-N*, water *Eff-W*, light *Eff-L* and temperature *Eff-T*. Monthly values are of January to December.

3.4 Plausibility analysis

The model plausibility was first tested by comparing simulated numbers of *Artemisia herba-alba* per hectare to aggregated numbers per hectare for the growing season 2002-2003 (Figure 24; Gresens, 2006, personal communication). Simulation yielded a good coincidence compared to direct observation. Note that the simulation starts in 2002, so the first year must be labelled as model "warm-up", which has to be considered for all simulations throughout this study. Past that point, the population increases from spring to autumn and are in agreement with field observations and reflect the shrub flowering peak in autumn. A

timespan of only two years was, however, to short to assess longer-term responses to climate and grazing.

The number of individual plants varies widely per season, at approximately ± 2,000 per ha (Gresens, 2006, personal communication). The observed data on numbers of individuals reflect the high seasonal variability, up to ± 5,000 per ha of *Artemisia herba-alba* populations in the field.

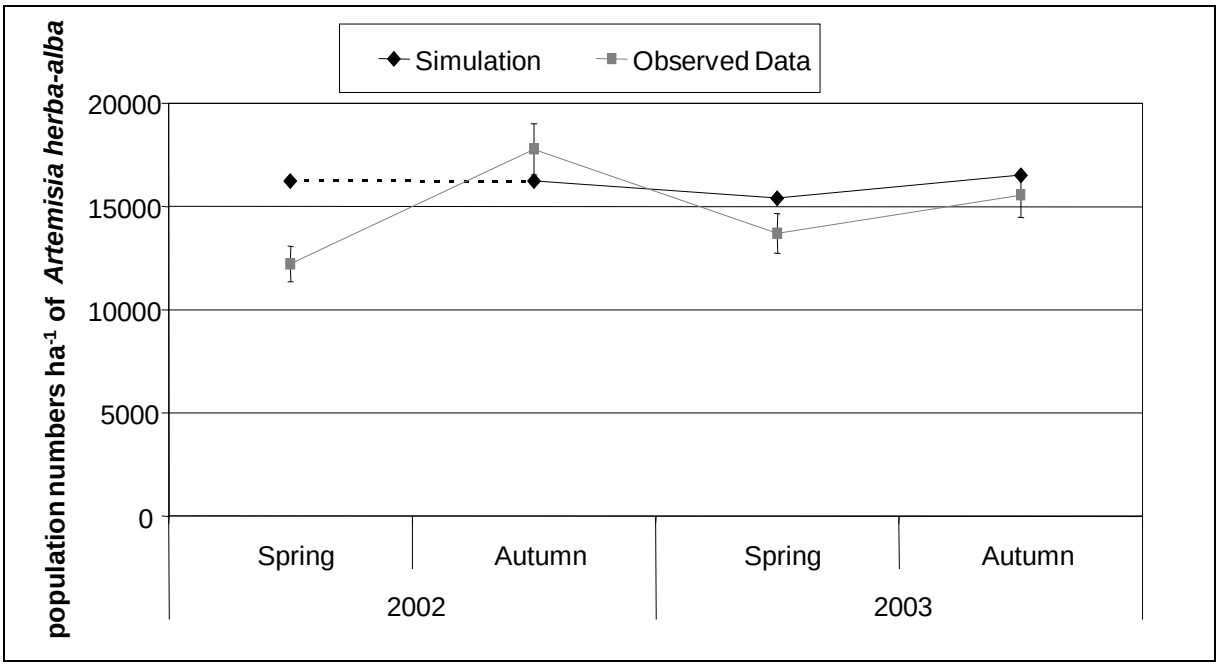

Figure 24: Observed population data (grey line, numbers ha^{-1}) and Standard Deviation (SD) of *Artmesia herba-alba* versus simulated data (black line, numbers ha^{-1}) for spring 2002 until autumn 2003; the dashed black is the model "warm-up".

The next attempt at a plausibility check was based on the parameter leaf area index (*Lai*). Again, simulated values (1998-2006) were compared to surveyed data beginning in autumn 2001 until spring 2004, aggregated to seasonal figures (Figure 25). Apparently, the model climate files did not match the real data thus a comparison is critical. Additionally the regionalisation of observed data as well as the different locations of observation might occur. Model predicted *Lai* "sage shrub" PFT values are very low, at about 0.1 m^2 m^{-2}. Although the first simulated years are omitted as the model "warm up" phase, the predicted *Lai* for "sage shrub" PFT shows a strong decrease from 2000 to 2002: from 0.08 to 0.01 m^2 m^{-2}. Subsequently, the modeled *Lai* lies between 0.03 in spring to 0.06 m^2 m^{-2} in the autumn.

However, observed regionalised *Lai* shows a large inter-seasonal variation of values, from autumn 2001, at 0.35 m^2 m^{-2}, to approximately 0.025 m^2 m^{-2} in spring 2002. Generally, observed *Lai* follows tendencies that are similar to the simulated values, with higher amounts in autumn the flowering period than in spring. An improvement of simulations by *Lai* parameterisation was not possible as modelled *Lai* is calculated by plant shoot growth

(Eq. 12). The reliable seasonal tendency of simulated *Lai* as animal forage indicator is important for simulations.

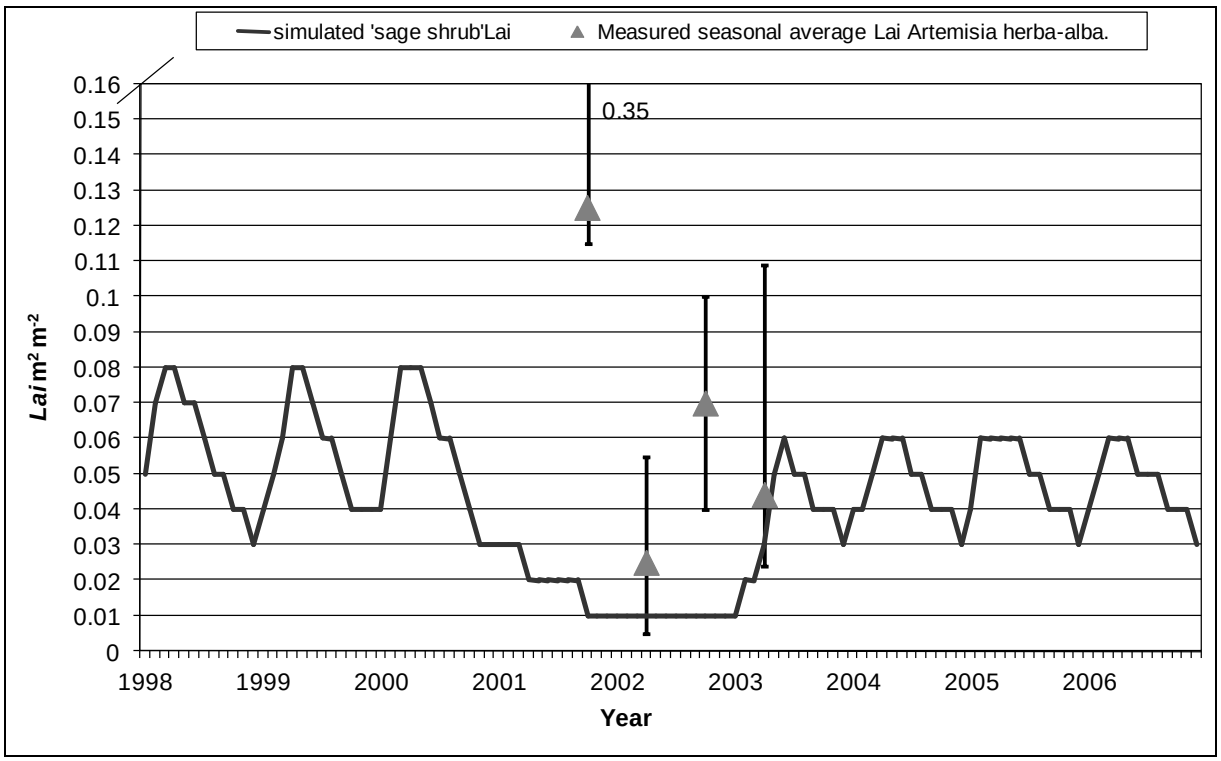

Figure 25: Simulated leaf area index *Lai* (m^2 m^{-2}) for "sage shrub" PFT group for 1998 – 2006 versus measured seasonal (springtime-April; autumn-October) average *Lai* of *Artemisia herba-alba*. The range of variation (SD) is the minimum and maximum *Lai* measurements at Taoujgalt and the months are January to December.

Another possibility to test the model's plausibility is to compare simulated green *Lai* to the computed weekly Normalized Differenced Vegetation Index (*NDVI*) in the same grid-cell (Figure 26). Other than the *Lai* description given above (Figure 24), which comprises total (live and dead) *Lai*, green *Lai* expresses an index of shoot leaf area only. *NDVI* is obtained by remote sensing procedures in a similar 1x1 km grid cell resolution (Fritzsche, 2008, personal communication). The period of observation here is from January 2000 to December 2004 and the diagnostic cell is located in the northern basin of Ouarzazate. Differences among these are on the one hand based on different temporal resolutions: the *NDVI* is based on weekly resolution while the SAVANNA© computes green *Lai* on monthly basis. A result of this is the smoother time-variation curve of SAVANNA© modelled green *Lai*. On the other hand shoot leaf area is seasonally growing over the year as a plant phenological function and reduced to minimum of 0.05 m^2 m^{-2} in winter. Whereas the *NDVI* is calculated as a continuous flux of radiation emitted by surfaces, including a certain percentage of bare soil fractions, so amounts probably do not decrease below approximately 0.08 m^2 m^{-2}. Both indices reported increasing values for the onsetting growing season. Besides that we assume that both factors increases as rainfall induced vegetative growth. Because of the

weekly resolution the *NDVI* signal is probably able to more accurately report these rainfall responses to vegetation. The starting year 2000 and 2001 could be disiguished as a “warm-up phase” for both procedures, as values fluctuated substantially. However, in the spring, the modelled green *Lai* is underestimated compared to *NDVI* probably due to phenological functions involved. While in the autumn simulated green *Lai* is overestimated relative to *NDVI* probably because of modelled rainfall data (see chapter 6.1). As shown by measured *Lai* values, the semi-arid character of the study region leads to a high variance of very low *Lai* amounts, which are hard to reproduce in the *NDVI* data set. For biomass with low *ANPP*, the *NDVI* signal is influenced by soil and can be difficult to separate (Paruelo *et al.* 1997). Thus, it seems hard to determine biomass by detecting *NDVI* in this semi-arid area. This comparison approach had to be declared insufficient for testing model plausibility as error ranges are high for both the *NDVI* and the green *Lai* methods. But we may assume that the behaviour of both factors is similar and is plausible.

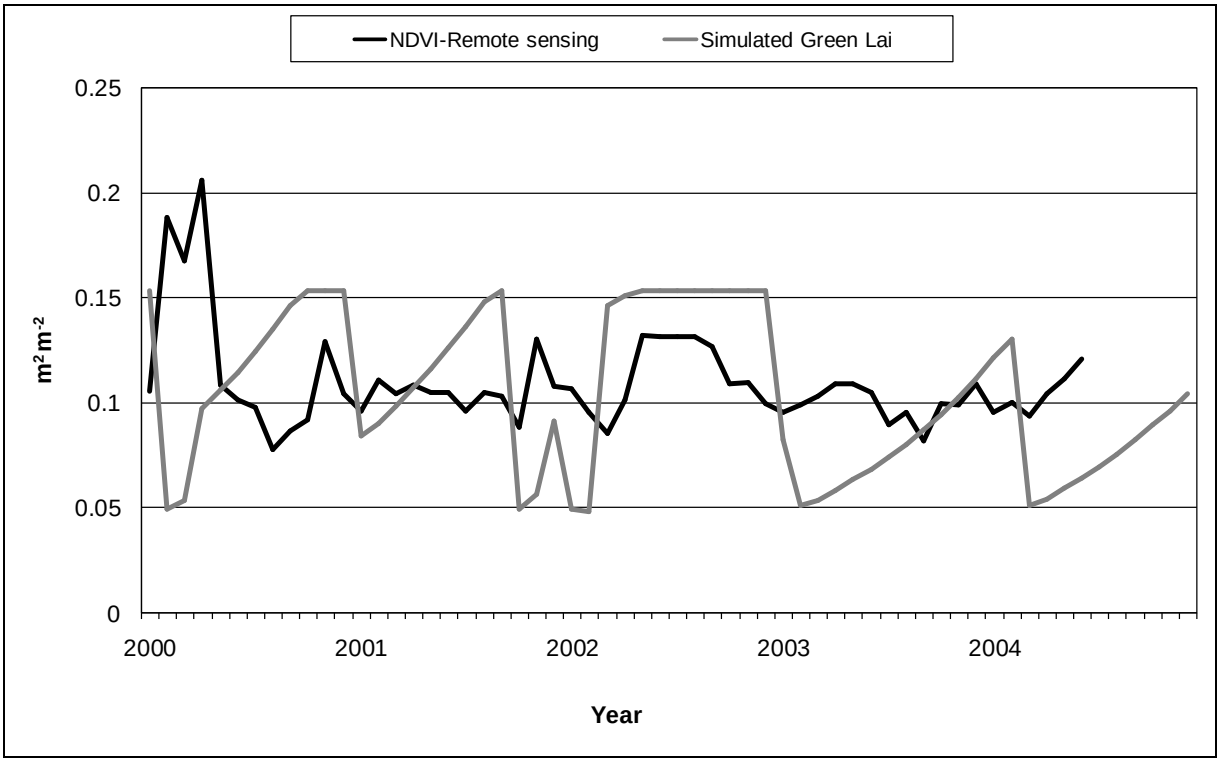

Figure 26: Simulated green leaf area index *Lai* on a subarea (grey line, m^2 m^{-2}) and remote sensing derived *NDVI* (black line, m^2 m^{-2}), both for the same diagnostic cell. Monthly values are from January to December.

Because the availablity of permanent biomass productivity plots is restricted for the plant species modeled, we have to compare the simulation outcomes to the limited number of observation plots in the area and to our own unpublished biomass estimates. Other productivity figures are taken from the literature.

The evolution of mean shrub green leaf mass (kg ha^{-1}) per grid-cell for the month (10) October 1999-2006 (Figure 27) was within the range of base-line simulation from 1975-2006

(see section 4.5). The simulation reflects well the inter-annual changes in green leaf biomass. It is remarkable that in October 2001, the lowest green leaf availability over a wide range is predicted with a mean biomass per grid-cell of only about 16 to 33 kg ha^{-1}. The biomass values of *Artemisia herba-alba* at the Anti Atlas ranges and of *Hamada scoparia* in the southern ranges of the research area are shown in Table 27. Yessef (1996) evaluated the palatable biomass for rangelands as very variable on their growth peak, with values between 5 to 287 kg ha^{-1}.

Table 27: Comparison of *Artemisia herba-alba* and *Hamada scoparia* biomass estimates for the Anti Atlas and the southern Wadi Drâa ranges.

Plant species	Year	own data[7] (kg ha^{-1})	Nording 2008[8] (kg ha^{-1})	Yessef 1996[9] (kg ha^{-1})	ROSELT 2004[10] (kg ha^{-1})
Artemisia herba-alba Anti Atlas ranges	2004	4	-	-	156-324[11]
	2005	10	-	-	-
	2008	-	1-250	-	-
Hamada scoparia Southern ranges	1996	-	-	3-541	-
	2004	22	-	-	7-26
	2008	-	1-500	-	-

Simulated values coincided comparably well with other sources output although high spatio-temporal biomass variation is reported.

The presented figures and tables illustrate the difficulties of comparing among plant species that possess low ground cover and are highly intra-annual variable in their biomass. Above this the comparison is aggregated PFT's to aggregated facies with all implied errors. A further discussion on the uncertainties of the approaches chosen here is given in chapter 5.4.

[7] Our aggregated based on 10 m^2 plots.

[8] Nording (2008) aggregates amounts based on 10m^2 plots.

[9] Yessef (2006) calculates amounts based on species groups, here *Hamada scoparia* for Fezouata ranges

[10] ROSELT (2004) calculates biomass amounts based on transects of predominant species; evaluation at Observatory ranges.

[11] Cumulative perennial phytomass production on 6 transects.

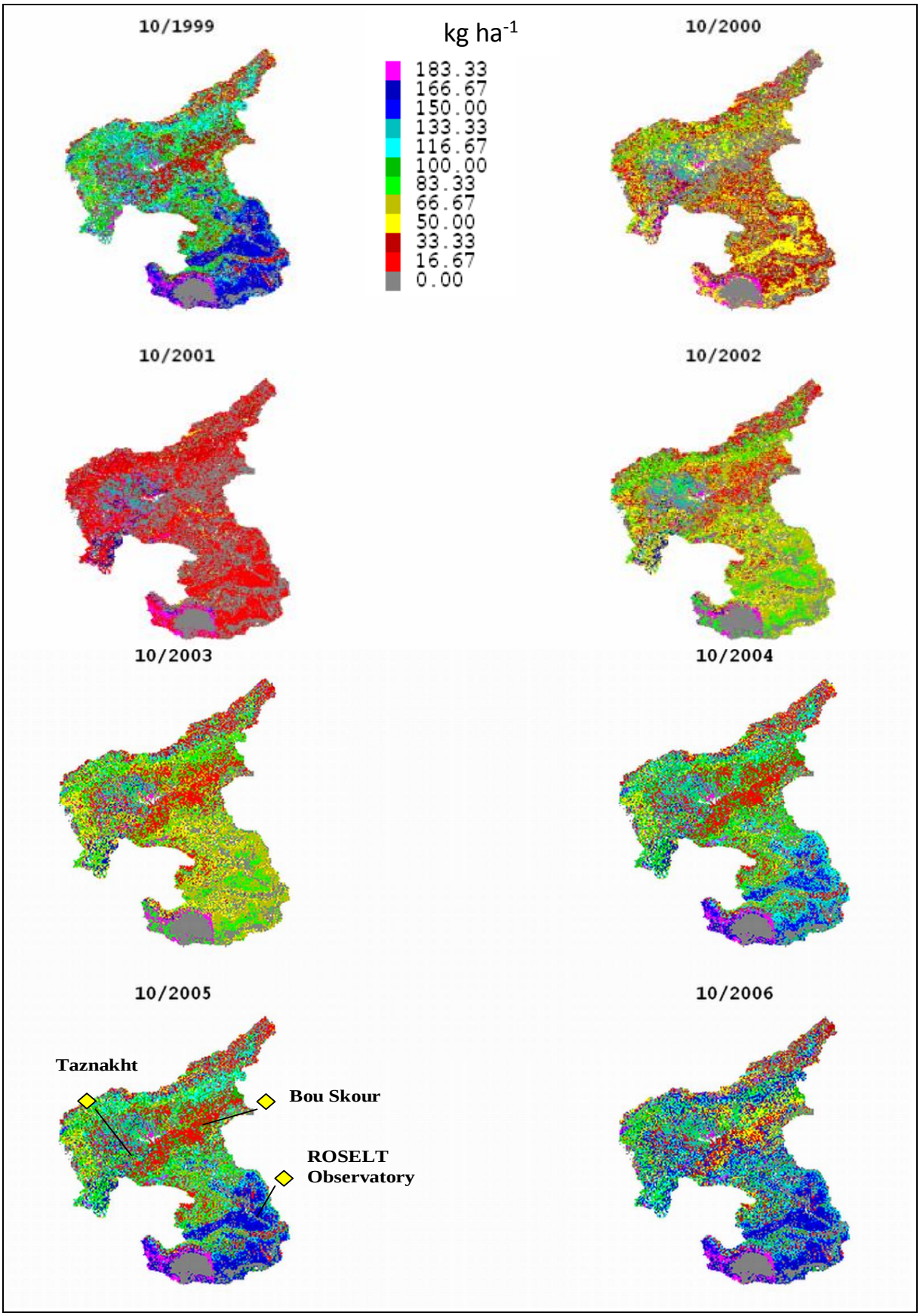

Figure 27: Mean shrub green leaf mass (kg ha^{-1}) per grid-cell for October (10) each year 1999-2006 for the Drâa catchment area.

3.5 Sensitivity analysis

Parameters used to test model accuracy should be chosen carefully for sensitivity analyses. The range of output parameter variation (+/-) expresses the model's behaviour and gives a better understanding of the model's sensitivity. If parameter variation exceeds certain pre-defined limitations in analysis, then the model statements are weak and have to be redefined. We choose water use efficiency (*WUE*) as an appropriate variable to evaluate model sensitivity because it is the most important input for plant species group net primary production (*NPP*).

The input variable *WUE* is computed per plant species group (Table 4). The output variable *NPP* is computed as a function of actual water uptake per plant species *Atrans* (Eq. 5), and *Awpet* (Eq 24). *Awpet* is a function of stomatal conductance (*Cs*) (Eq. 2). Therefore, the variation (±15%) of *Cs* minimum-maximum ranges should affect *Awtrans* and *NPP* of any species group. *Cs* per plant species is estimated as a fixed minimum and maximum value as at the Ball & Berry equation (Ball *et al.* 1987). The model commonly computes for C_3 plants a value ranging between 0.05 (minimum) and 9.0 mol m^{-2} s^{-1} (maximum). Both values have been changed in the same direction once positively +15% of the initial value and once negatively respectively. Often a sensitivity index (S) is taken to identify the range of model sensitivity (Giertz 2004). This index is calculated by

$$S_{15} = \frac{M_{15} - P_{15}}{Bs} \qquad \text{(Eq. 53)}$$

S_{15} = sensitivity index for 15% change

P_{15} = result of the simulation with variable 15% increase

M_{15} = result of the simulation with variable 15% decrease

Bs = result of the base-line simulation

The calculated S_{15} for *NPP* "sage shrub" ($S_{15}NPP_{sage}$) is the average monthly *NPP* for the plant species group over a 20 year simulation period. The result is

$$S_{15}NPP_{sage} = 0.02$$

To evaluate the S_{15} value obtained, Giertz (2004) introduced threshold levels of sensitivity. Zero values indicate low parameter sensitivity; model outcomes influenced by this parameter are not altered considerably. However parameter sensitivity and model uncertainty is not directly intercorrelated. At a threshold level of 0.0 to 0.05, parameter sensitivity criteria are negligible. This analysis indicates a light sensitivity of shrub sage *Cs*. Thus, the chosen values are sufficiently accurate for simulation.

Because the input parameter of monthly *Cs* varies throughout the year and strongly depends on given rainfall levels, we decided to account for that variation by splitting up total 20 years S_{15} values, into four time slices S_1, S_2, S_3 and S_4 with five years each. The results are

$$S_1 NPP = 0.05$$
$$S_2 NPP = -0.02$$
$$S_3 NPP = 0.03$$
$$S_4 NPP = 0.04$$

According to the given threshold level slices show a low sensitivity level which confirms the S_{15} sensitivity level before. Negative values are explained by the correlation of mainly the minimum *Cs* value to available water for *trans*. The variation of the initial minimum value (Ball *et al.* 1987) to 0.0425 mol $m^{-2}s^{-1}$ and maximum to 10.35 mol $m^{-2}s^{-1}$ respectively reduces available water and thus decreases *NPP*. Whereas the variation of the minimum value to 0.0575 mol $m^{-2}s^{-1}$ increases water availability and *NPP* whilst the maximum value is probably of lower importance (Table 28).

NPP is a collective expression for the entire vegetative growth of a plant. Table 28 shows the changes observed for “sage shrub” plant growth parameters (kg ha^{-1}) such as roots, leaves and current annual growth, shifting towards a change of minimum and maximum values of *Cs* by +15% and -15% during this analysis.

Table 28: *NPP* changes (%) for sage shrub leaves, roots and current annual growth due to stomatal conductance *Cs* values (%) relative to the base-line simulation during sensitivity analysis.

***Cs* changes to (Ball *et al.* 1987) values (%)**	***NPP* changes (%)**		
	leaves	**roots**	**current annual growth**
- 15	+5	+7	+3
+ 15	-4	-5	-4

Calibration with constant PFT vegetation patterns and fixed grazing livestock numbers was in good agreement with observed data.

4 Results

In this chapter, the different results obtained during this study are reported. The first part (sections 4.1 and 4.2) shows the outcomes of field studies of transpiration in March-April and August 2005. The next section (4.3) depicts the nutrient constraints of investigated plants in the study area. Section 4.4 reports the results of simulations for the Taoujgalt area, followed by two base-line scenarios for the Ouarzazate basin (section 4.5) and different stocking rates and climate scenarios modelled for different sub-catchments (sections 4.6 to 4.8).

4.1 Transpiration measurements

Figure 28 portrays an all-day transpiration experiment (August 24th, 2005) using the LICOR1600 steady state porometer (LI-COR 1999) on *Buxus balearicus* near Ameskar in the High Atlas Mountains. The figure also shows solar irradiance measurements from the neighbouring IMPETUS automatic climate station (Schulz 2007). The solar irradiance measurements are taken every ten minutes at two metres above the ground at the Imeskar IMPETUS station and are here presented as hourly sums of irradiance (W m^{-2}).

Generally, an increasing trend in solar irradiance is seen, from 53 W m^{-2} at 7:00 am to 824 W m^{-2} at noon, and a decreasing curve is observed in the afternoon. The diurnal transpiration of *Buxus balearicus* is described in the next paragraph.

Transpiration measurements were accompanied by relevant measurements of leaf temperature (T_{leaf}), air temperature (T_{atm}), average relative humidity (*Relh)* and maximum vapour pressure deficit (VPD_{max}) for a leaf area of 1 cm^2. These descriptive measurements are shown in Table 29.

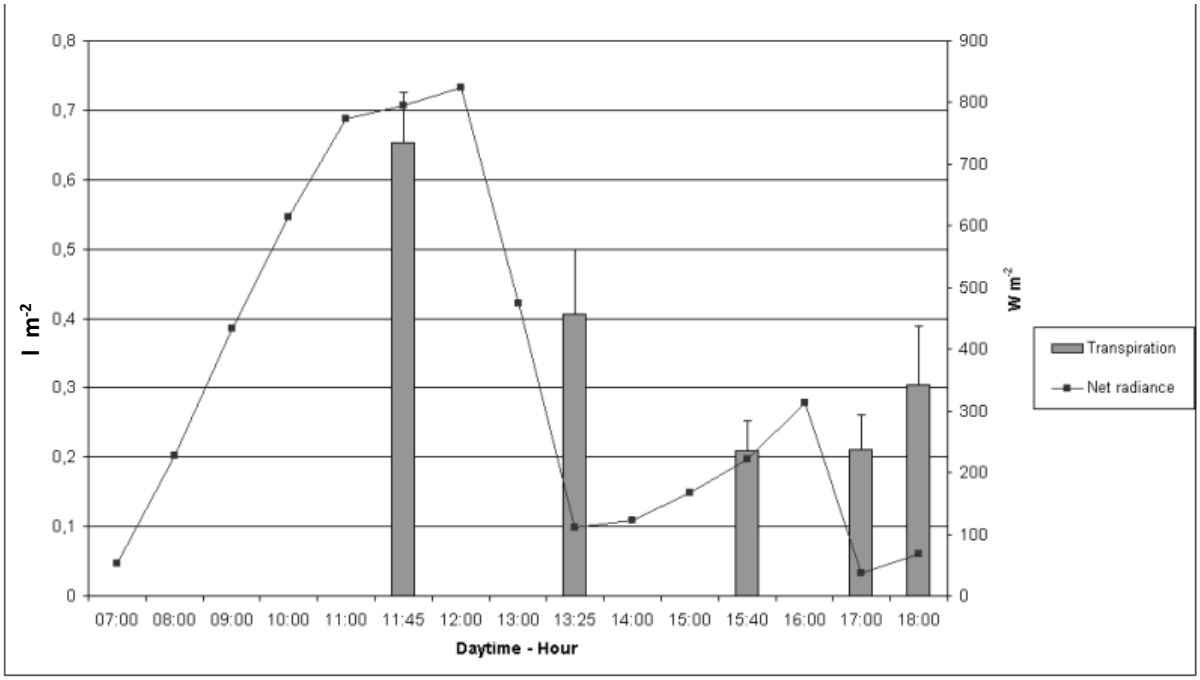

Figure 28: Diurnal patterns of transpiration (l m^{-2} leaf area) and net radiance (W m^{-2}). Transpiration values shown are averages of measurements taken on three different unshaded leaves of three different plants of *Buxus balearicus* for August 24th, 2005.

Table 29: Imeskar IMPETUS Climate Station (2300 m a.s.l.) measurement of VPD_{max} (Maximum Vapour Pressure Deficit, kPa) and T_{leaf} maximum (°C), T_{atm} maximum (°C) and avg. *Relh* (%) measurements from LI-1600M apparature.

Date	T_{leaf} max (°C)	T_{atm} max (°C)	avg. *Relh* (%)	VPD_{max} (kPa)
24.08.2005	36.4	35.0	6.0	2.5

The transpiration of *Buxus balearicus* paralleled the diurnal trend in irradiance. Transpiration measurements began at 11:45 am and ended at 6:45 pm. The values shown are averages of three transpiration measurements for each of three plants. Transpiration increased throughout the morning, reaching a maximum value of 0.7 l m^{-2} (liter per leaf area) near midday. A weakening trend occurred during the early afternoon, reaching a minimum value of 0.2 l m^{-2} at 3:40 pm. The total amount of diurnal transpiration of *Buxus balearicus* was 1.8 l m^{-2}. Meteorological measurements from the same day indicated high temperatures and low relative humidity, common conditions during the summer. The overall fit between daily transpiration of biomass and daily variation in irradiance is moderate. The measurements are consistent with those obtained in other studies in the same area and are used to evaluate modelled plant water use in the discussion (chapter 6).

4.2 Aspen experiments

4.2.1 Ameskar

Sap flow measurements on Aspen trees (*Populus canescens*) were conducted over multiple weeks in the Ameskar and Tichki Oases in the High Atlas Mountains (chapter 2.1). Selected daily results are presented in this section. Figure 29 shows diurnal measurements on Aspen trees at Ameskar from April 5th to 9th, 2005, with a ten-minute measurement interval. The measurements were taken automatically and the results were calculated by the integrated program PROSALog (UP-GmbH 2000). Channels one to three in the following correspond to the experimental data from aspen trees that were numbered one to three. The averaged leaf size (cm^2) for all trees was estimated manually and was then input to PROSALog (Table 1, Table 2). The results of an identical field study on Aspen trees (*Populus canescens*) at Tichki are given in section 4.2.2. Note that channel (tree) three is not represented due to a permanent failure of the experimental equipment.

Three riparian Aspen trees were chosen within a radius of about five metres. In the Ameskar experiment, the trees were not as close to the water channel (Assif Ait Achmed) as in the Tichki experiment (next section). The distance to the perennial stream was about 50 m. Due to a bug in the system functioning that was not noticed until afterward, diurnal measurements in each channel stopped at 6 pm and reset at midnight the next day. This explains the apparently sharp decline in sap flow seen in the figure. The sap flow values (l m^{-2} leaf area) of channels (trees) one and two showed similar changes over the period of measurement.

A sharp increase in sap flow was observed during the morning. Sap flow declined around midday and increased again during the afternoon. Channel two showed higher sap flow relative to channel one. Initially, channel two reported sap flow intensities at peak of approximately 100 l m^{-2}, whereas channel one reported about 50 l m^{-2} during the same time period. The differences between the channels were substantially smaller on the second day. This was mainly due to a decrease in channel two to a maximum sap flow of 75 l m^{-2}, while channel one maintained a maximum of 50 l m^{-2}. The period from April 7th to 8th, 2005 was characterised by a more erratic measurement due to the system error mentioned above. In general, measurements were slightly lower for both channels compared to the previous days. Finally, on April 9th, sap flow increased for both channels compared to the previous day. Values for channel one increased to about 50 l m^{-2}, while values for channel two increased to 90 l m^{-2}, potentially due to greater growth.

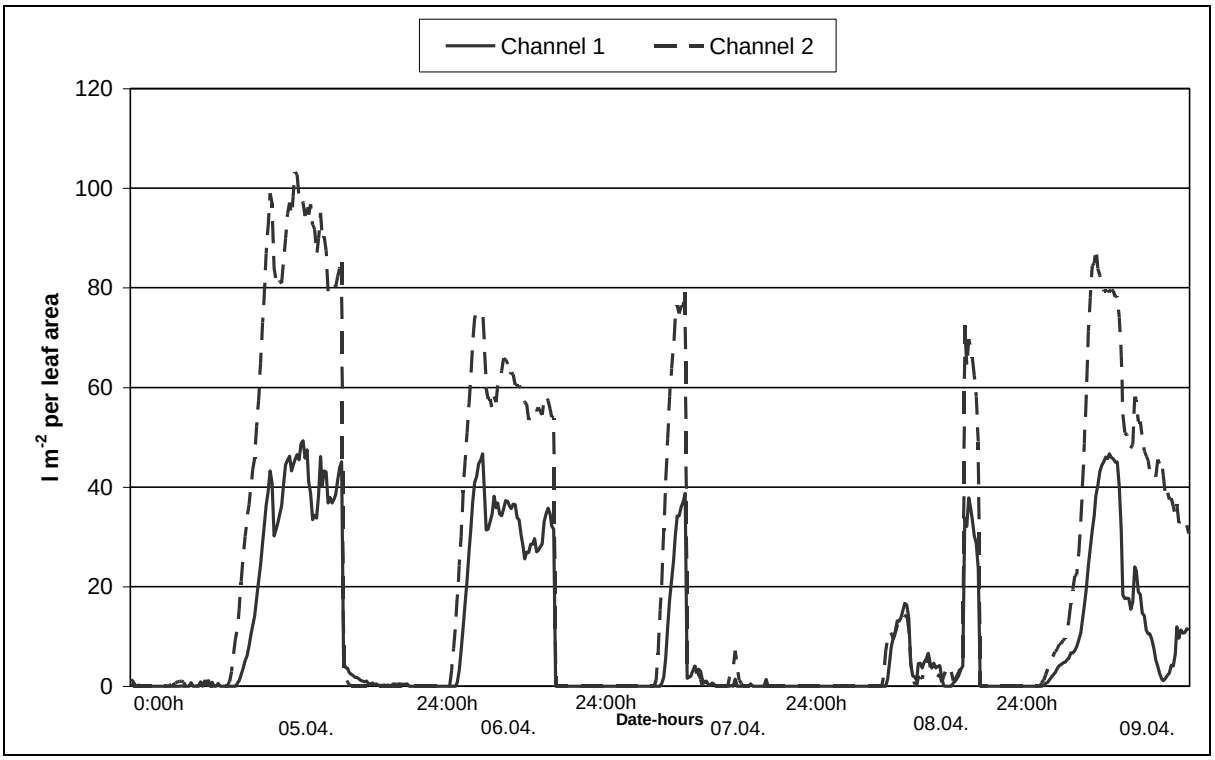

Figure 29: Sap flow measurements (l m^{-2} leaf area) on Aspen at Ameskar from April 5th-9th, 2005. Measurements were taken every ten minutes. Channel one and two correspond to individual trees: Aspen one and Aspen two.

Climate parameters (source: IMPETUS Imeskar station) including maximum radiation (W m $^{-2}$), average relative humidity and average temperature are shown in Figure 30. The average relative humidity and the low temperature values both show moderate change over time. It should be noted that this climate station is located at 2300 m a.s.l., about 200 m higher than the experimental site. Thus, the lower temperature and relative humidity and the higher irradiance might be expected. These figures are provided to facilitate interpretation of the sap flow results, but are of limited application due to the altitudinal difference. Greater irradiance was observed on April 8th, 2005 than on the days before and after. Sap flow measurements depend mainly on trends in light availability, so sap flow values are expected to parallel highs and lows of irradiance. However, irradiance levels in the oases are lower than those shown in Figure 30 and are more similar to the measurements from Tichki (Figure 32). However, relative humidity values are lower at Tichki station, so those data are also less useful due to the altitudinal difference. Precipitation did not occur during the time span of the experiment.

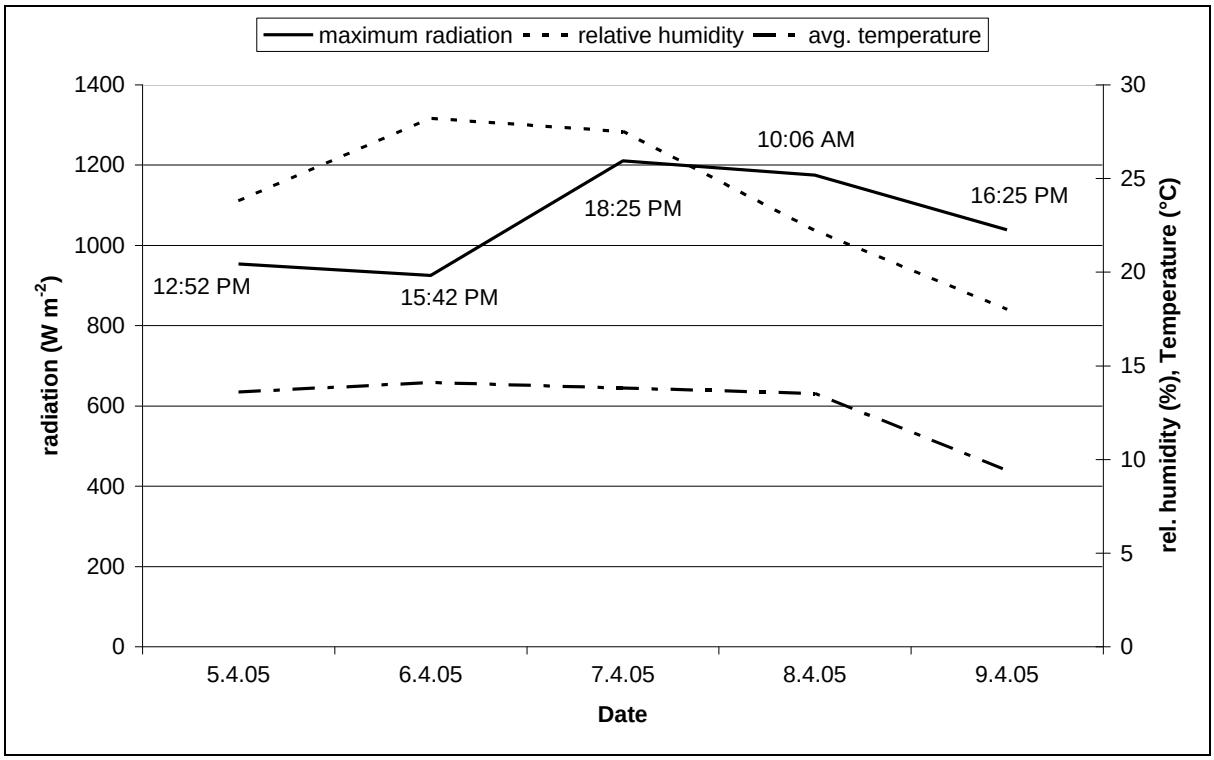

Figure 30: Automatic climate station measurements at Imeskar from April 5th-9th, 2005; daily averages of maximum radiation (W m^{-2}) with the corresponding times of day, relative humidity (%) and average temperature (°C) are shown.

4.2.2 Tichki

Figure 31 shows diurnal measurements on Aspen trees at Tichki from June 21st to 25th, 2005, with a 10-minute measurment intervall. The entire experiment lasted from June 18th to August 25th, 2005. The peaks seen in all three channels at noon on June 24th and 25th were caused by a measurement error from 10 am to 2 pm. All three channels were blocked because the recording apparatus had failed.

Important features here are the distinct midday depressions from 12 pm to 3 pm following the noon peak for every experimental aspen. The consistent changes in amplitudes of all channels are also remarkable. Channel one showed a minor daily fluctuation of 45 l m^{-2} amplitude, compared to channel two and three with fluctuations of about 110 l m^{-2} and about 300.0 l m^{-2}, respectively.

Channel three consistently showed higher sap flow than the other two. This may be due to the position of Aspen three at about one metre from the perennial stream; the other trees were located five metres and ten metres from the stream, respectively. Another possible cause is flooding that produced a permanent oversupply of water. All three trees reduced sap flow to low levels during the night, but a continuous increase occurred after daybreak. Values

for channel two steadily increased up to June 25th, 2005. From June 21st to 24th, channel two reached maximum sap flow values of about 117 l m^{-2}. Sap flow then increased rapidly to a maximum of approximately 272 l m^{-2} on the afternoon of June 25th. Initially, maximum sap flow rate of channel three was 293 l m^{-2} on June 21st. Subsequently, sap flow increased to a peak of 325 l m^{-2} at noon on June 23rd. Initial amplitudes showed a clear midday depression with a subsequent afternoon increase. The midday depression can be ignored due to the errors mentioned above.

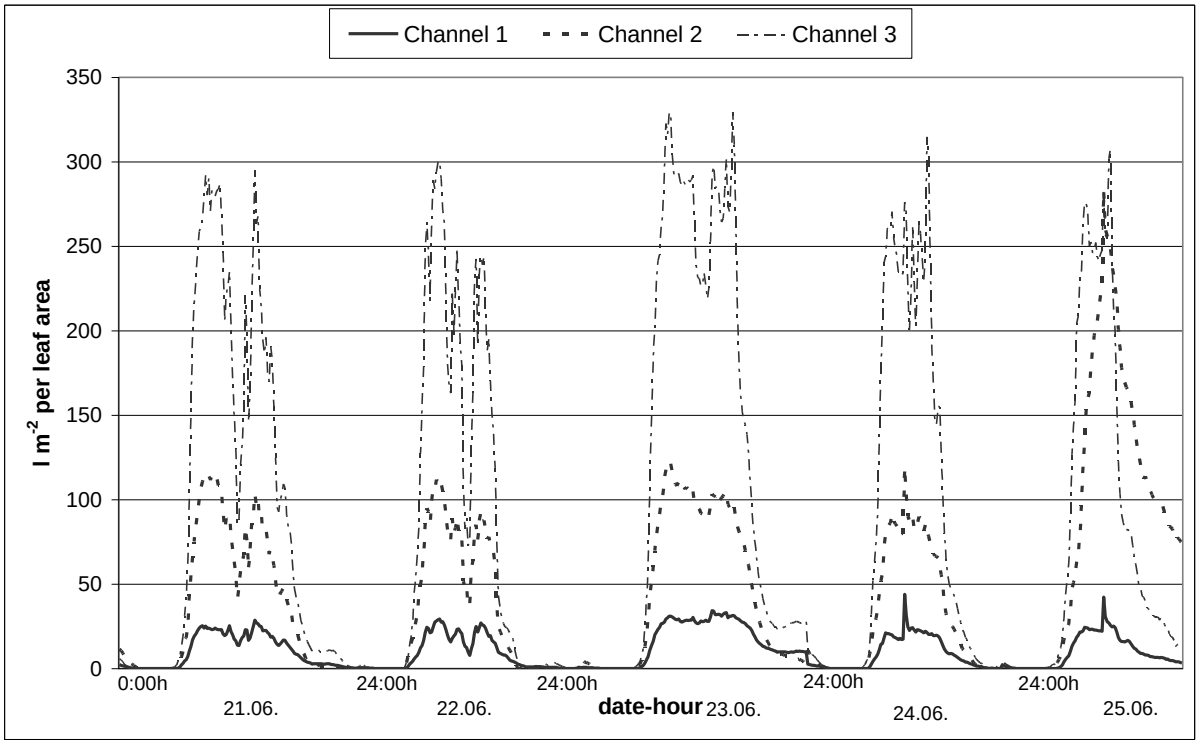

Figure 31 Sap flow measurements (l m^{-2} leaf area) on Aspen at Tichki from June 21st-25th, 2005. Measurements were taken every ten minutes. Channels one, two and three correspond to individual trees: Aspen one, Aspen two and Aspen three.

These data can be compared to solar radiation (W m^{-2}) and relative humidity (%) measurements from the automatic climatic station (Campbell Ltd.) (Figure 32) at Tichki village. This climate station is the nearest available, located about 100 m from the sap flow experimental site.

The relatively high night-time humidity between June 21st and 23rd, 2005 suggests a high precipitation potential. The climate station recorded 15 mm and 48 mm of precipitation for June 21st and 22nd, respectively. The differences between night-time and day-time sap flow measurements indicate the individual water status of the trees. Hence, we assume that the water status of each aspen tree measured is relatively high. The observed meteorological data for June 24th and 25th show consistently high irradiance with fewer declines in irradiance and lower humidity levels. Hence, the increased sap flow on those days may reflect the high irradiance. The relatively low humidity also promotes leaf-atmosphere exchange of water

vapour. Thus, climatic conditions induce aspen trees to increase their sap flow in order to adapt their water consumption to changing atmospheric vapour pressure.

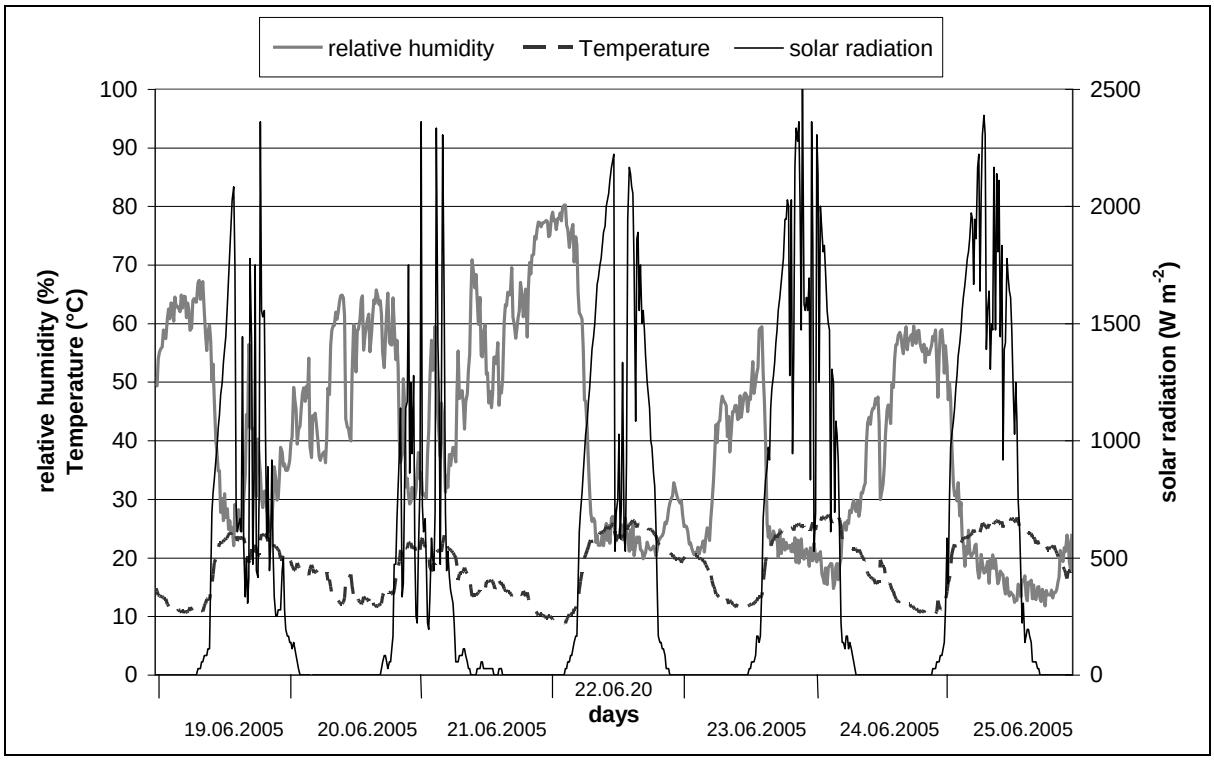

Figure 32: Automatic climate station measurements of relative humidity (%), solar radiation (W m^{-2}) and temperature (°C) from June 21st-25th, 2005 at Tichki Oasis.

4.2.3 Comparison of the sap flow experiments at Tichki and Ameskar

Diurnal patterns observed in the Ameskar experiment were comparable to those observed in the Tichki experiment, except for the range of sap flow values, which were about twofold higher in Tichki than in Ameskar. One reason for this may be the relative proximity of the experimental trees to the perennial stream. The experimental trees at Tichki were located at about one to ten metres from the perennial stream. The slope of this stream is relatively high, and flooding after heavy rainfall at higher altitudes is common. This may explain the higher sap flow measurements. A second explanation is the seasonal difference between the two experiments. The Ameskar experiment was conducted during the spring, with relatively low temperatures and higher rainfall compared to summer conditions. The Ameskar oasis is located in a narrow part of Assif valley and thus shaded, which may influence sap flow. Alternatively, the Ameskar experiment may have been influenced by surrounding Aspen trees, as it was conducted in a small forest. At Tichki, in contrast, the experiment was conducted on an open hillside with little surrounding vegetation. The Tichki oasis is also

located in a broader valley structure at the junction of multiple valleys (Figure 1). However, heavy rainfall at higher altitudes is not unusual during the summer and may contribute to increased water consumption by trees. Moreover, the Tichki experiment took place in June with relatively high irradiance on cloud-free days, together with high relative humidity and temperatures. The relatively high humidity, together with the high water vapour deficit, creates a greater demand for water and thus increase sap flow. Both experiments showed low evaporative demand at night and high water consumption during the day.

4.2.4 Comparison of simulated versus measured stomatal conductance rates

Figure 33 shows a comparison between simulated values of actual stomatal conductance (*Cs-act*) per km^2 for the “deciduous tree” plant group type in the High Atlas Mountains and the results of the Tichki and Ameskar Aspen experiments. Simulated values are based on climate station data. Simulated *Cs-act* shows a strict annual cycle with a minimum in summer and a maximum in winter. Due to the experimental design, which covered only a few months, we cannot show sap flow measurements for the full year. For April and June 2005, simulated *Cs-act* overestimates the measured amounts. For August, the measured values are underestimated. Only few measurements are available for March, so no reliable comparison can be made. One potential error is due to the aggregation of the measured data to a monthly scale. The upscaling of diurnal stomatal conductance values of single trees to monthly figures is critical, because individual values largely depend upon site-specific recent meteorological conditions. Moreover, due to the spatial heterogeneity of trees, planted as narrow bands in mountain valleys (oases), comparisons to point data are difficult. A simulated 1-km^2 cell located at the geographic position 31.315°N and -6.429°E may not correctly match the geographic position of the field experiment. Therefore, the stomatal conductance values are only a rough fingerprint of mountain plant's water usage.

The simulated actual stomatal conductance (*Cs-act*) monthly values are probably overestimated due to overestimated tree biomass amounts (see section 2.5.1.4) during model parameterisation. Thus, the model simulates stomatal conductance values incorrectly on an annual basis for the mountainous region. Exceptional levels of stomatal conductance (e.g., for April 2005) are not reproduced by any model. These values result from the high amplitude of measured sap flow in April. However, a more important feature of the model is its reflection of the annual frequency of high stomatal activities in winter compared to summer. The model plausibly simulates these figures.

In the High Atlas Mountains, however, water is not the limiting resource; streams are continuously supplied by wells, snow and rainfall (Schulz 2007).

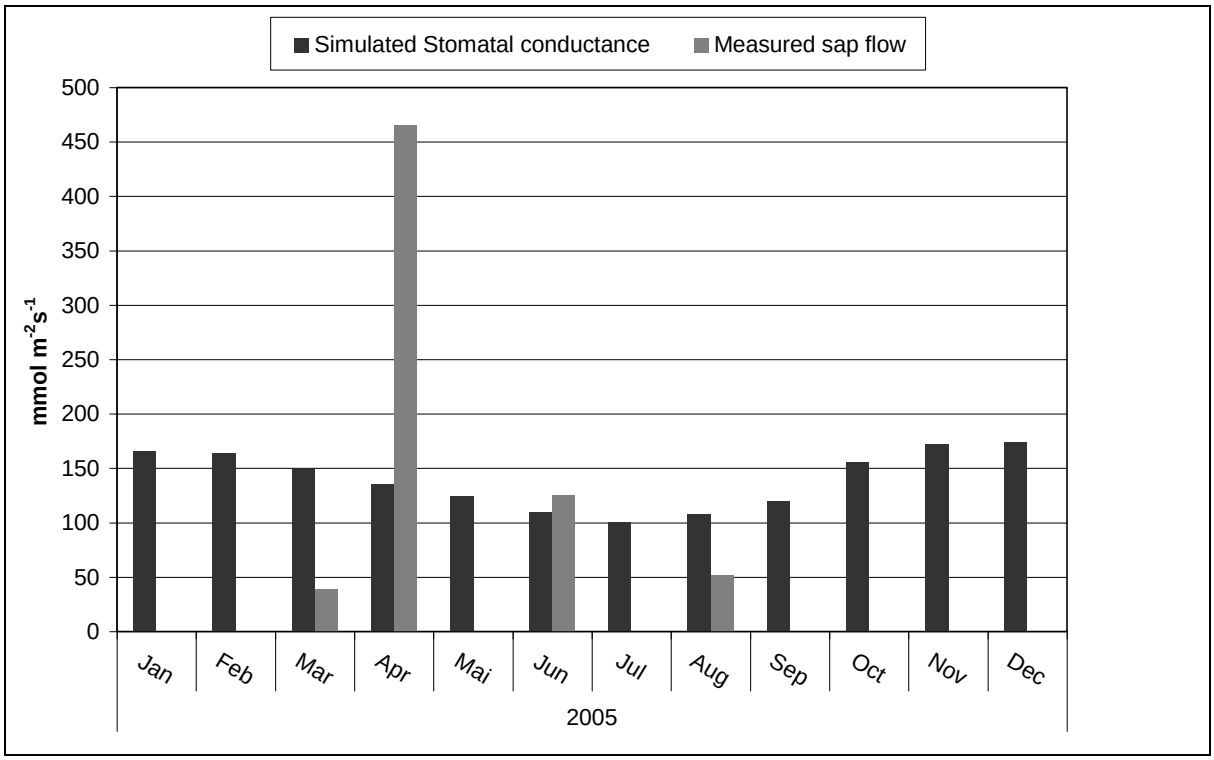

Figure 33: Simulated monthly actual stomatal conductance *Cs-act* (mmol m^{-2} s^{-1}) of the "deciduous tree" PFT group in the High Atlas Mountains compared to aggregated measurements from aspen trees at Tichki and Ameskar in 2005.

4.3 Plant nutrients

Plant nutrient content in selected rangeland vegetation plots are described next. These plots are the IMPETUS vegetation test sites Trab Labied, El Miyit and Taoujgalt. Nutrient content was measured separately for leaf and stem components (Table 30), mainly because of model parameterisation constraints. Therefore, the average nutrient content is given here. Leaf N content ranges from a maximum of 3.8% (*Hammada scoparia*) to a minimum of 1.6% (*Farsetia occidentalis*) and is higher than stem N content in all species. As with leaves, *Farsetia occidentalis* shows the lowest (0.7%) and *Hammada scoparia* shows the highest (2.1%) stem N content.

Carbon (C) content of leaves is lower than C content of stems in all species. Phosphorus (P) content shows larger differences between leaves and stems than calcium (Ca) content does. Generally, both P and Ca contents are higher in leaves than in stems.

The above figures provide a useful summary of major leaf and stem nutrient contents of predominant species at the selected test sites. These measurements can be compared to

the results of plant nutrient simulations described in the following chapters, but they are not at a useful scale for either spatial or temporal explanation of nutrient distribution.

Table 30: Plant nutrient content (C, N, Ca, P (%)) in selected rangeland plants at different IMPETUS test sites: El Miyit, Taoujgalt and Trab Labied, Plant species n=5.

Test site					
El Miyit	Averages	C (%) ±SD	N (%) ±SD	Ca (%)	P (%)
Acacia raddiana	leaf	45.1±0.5	2.4±0.2	1.6	1.1
	stem	46.7±2.4	0.9±0.2	1.5	0.6
Ziziphus lotus	leaf	44.3±2.0	3.1±0.5	0.9	1.7
	stem	46.0±1.1	0.7±0.1	0.8	0.4
Taoujgalt					
Artemisia herba-alba	leaf	42.7±1.5	2.2±0.1	1.3	1.5
	stem	43.6±1.7	0.8±0.1	0.7	0.6
Teucrium mideltense	leaf	42.0±2.0	1.8±0.2	1.5	1.3
	stem	42.8±1.7	0.8±0.3	0.9	0.4
Trab Labied					
Farsetia occidentalis	leaf	39.7±0.8	1.6±0.6	5.1	0.7
	stem	41.2±0.8	0.7±0.5	3.3	0.3
Hammada scoparia	leaf	39.4±0.2	3.8±0.1	3.0	0.8
	stem	41.9±1.6	2.1±0.3	1.5	0.8

4.4 Modelling results

For the concerted evaluation of results, the IMPETUS research team agreed to divide the study region into three different compartments. This is mainly due to the heterogeneity of research focuses for each discipline, including the evolution of soils, climate, vegetation and human activities in different landscapes. Therefore, the study region was divided into the High Atlas region (grey), the basin of Ouarzazate (dark grey) and the southern Drâa valley (black) (Figure 34). The focus of this study is on the rangelands within these divisions.

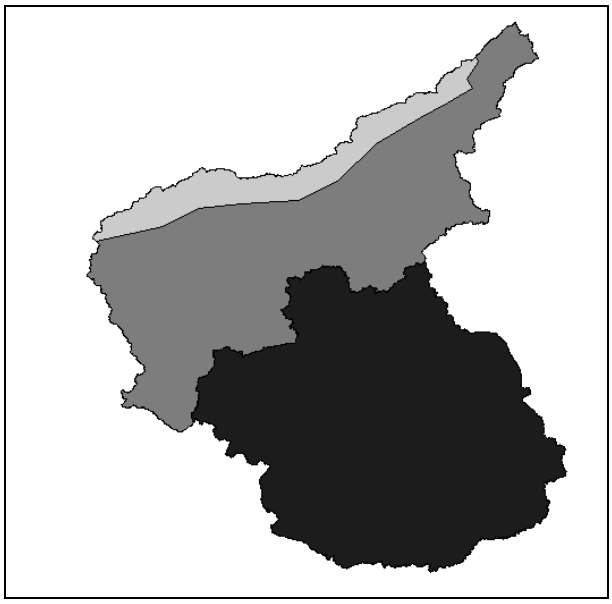

Figure 34: Division of the study area into research parts: the High Atlas region (grey), the basin of Ouarzazate (dark grey) and the southern Drâa catchment and their rangelands (black).

These divisions were used to determine regional changes in vegetation dynamics and thus hydrologic modifications in response to system disturbances. Diagnostic cells located in the research zone were used in this approach as identifiers corresponding to the regions shown in Figure 34. Note that this figure differs from the SAVANNA© simulated area (see Figure 11) as it illustrates the administrative borders of the Drâa basin. To investigate system disturbances, three key factors were introduced. The first factor was livestock number, which was assumed to be anthropogenic. The additional factors actual stomatal conductance (*Cs-act*) and transpiration (*trans*) were assumed to be determined by climate. Following this concept, system disturbances were grouped as either anthropogenic or climate-driven. Different scenarios were used in the model simulation (see below). First, a base-line scenario was simulated using historic and recent livestock and climate data as driving variables. Second, this base-line scenario was calculated with simulated REMO[12] climate data. Alternative livestock and REMO IPCC A1B and B1 scenarios (IPCC 2007a) were then investigated to distinguish between anthropogenic and climate-driven changes. In addition, human management scenarios for permanent grazed areas were compared to non-grazed areas.

The SAVANNA© model provides outputs as either temporal plots or spatial maps of simulated areas. Temporal plots, e.g., of aboveground net primary production (*ANPP*), belowground net primary production (*BNPP*), leaf and root biomass production per species

[12] REMO is a regional climate model developed at the Max Planck Institute for Meteorology in Hamburg, described in Jakob (2001).

and animal distribution or diets are obtained for the **entire** simulation area. High-resolution parameters such as nutrient cycling (C:N, N content, etc.), soil organic matter (SOM), photosynthesis (*Ps*) and stomatal conductance (*Cs*) obtained in **one** grid-cell (the diagnostic cell) in proxy for the entire simulation area, **must** be chosen by the user (see section 4.5). This cell, with the compiled simulation extent of 125 m^2 for model adaption to Taoujgalt (chapter 4.4.1) and 1 km^2 for the Drâa catchment simulations (chapters 4.5-4.7) reflects the parameterised herbaceous, shrub or woody/tree PFT's in the specified area (see section 2.5.1.1) in addition to specific soil type(s), geographic location and altitude. The aims of this procedure are to evaluate the temporal behaviour of vegetation patches for calibration and to interpret their responses to management alternatives and climate change. This is a practical approach, as simulations are far to complex to provide model results for each cell in the system.

The spatial outcomes for the entire simulated area are provided by separate spatial maps (see section 4.6.5). Here, results are presented across time and space for herbaceous cover (%), herbaceous green leaf biomass (kg ha^{-1}), shrub cover (%), shrub green leaf biomass (kg ha^{-1}) and tree cover (%) for the entire Drâa catchment simulation area.

Results of model adaption runs (section 3.1) are shown below. They are divided into two scenarios: "no-grazing" (NG) and "grazing" (G) (c.p. Figure 22 etc.), in order to evaluate and to improve the results based on the parameterisation database (section 2.4.6). Temporal plots of model runs are mainly shown below.

4.4.1 Model adaption results for the Taoujgalt plain-Basin of Ouarzazate

The temporal plots in this and the following chapters show month per years on the x-axis and specific units on the y-axis. The plotted lines (*ANPPHrb, ANPPShb*) exhibit the continuous annual increase in plant growth to the maximum flowering peak (here, in autumn). *ANNP* was similar across years for the "grazing" (G) 2002-2012 simulation. This was due to the constant number of sheep and goats present in the simulations for all years. Both *ANPP* was lower in the "no-grazing" (NG) than under G simulation (Figure 35 and Figure 36). *ANPP* predicted less PFT biomass production in g dry matter m^{-2} in the NG scenario (shrub PFT *ANPPShb*: 45-110 g m^{-2}, herbaceous PFT *ANPPHrb*: 20-35 g m^{-2}) than in the G scenario (shrub PFT *ANPPShb*: 60-110 g m^{-2}, herbaceous PFT *ANPPHrb*: 45-75 g m^{-2}), except in the later time periods of the simulation. The model predicted greater *ANPPHrb* production under G than under NG. *ANPPShb* development exhibited equal annual variability as compared to *ANPPHrb*. This suggests that grazing stimulated vegetative growth rates in this environment under the given climate. *ANPP* for the tree PFT was not represented in these simulations,

because this PFT is lacking in the modelled calibration area. These outcomes demonstrate the high potential for plant re-growth after grazing, even under current climatic conditions at an average precipitation of about 250 mm a^{-1}.

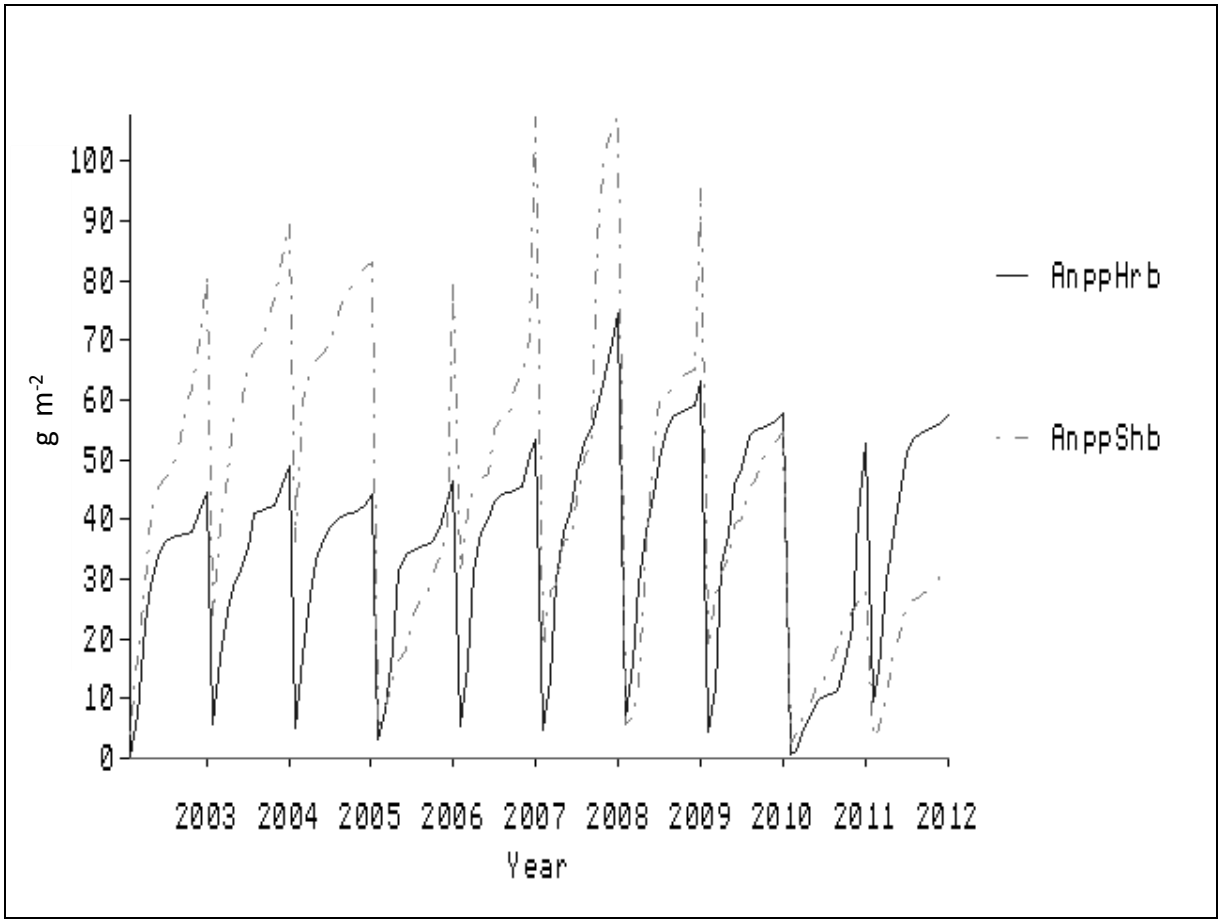

Figure 35: Aboveground net primary production (*ANPP*) of shrubs *ANPPShb* (dashed line) and herbaceous plants *ANPPHrb* (black line) (g m^{-2}) under the "grazing" (G) 2002-2012 scenario.

Simulated standing total (leaf, stem and dead) biomass for herbaceous plants (*TotHrb*) and shrubs (*TotShb*) (Figure 37 and Figure 38) corresponded to the *ANPP* results. Results for total herbaceous, shrub and woody biomass are presented. *TotHrb* remained constant across years, even in dry years, under both G and NG conditions. However, the G simulations showed larger intra-annual fluxes of *TotHrb* due to grazing removal, whereas *TotHrb* accumulated from year to year (Figure 38) under NG conditions. *TotShb* showed higher variability in response to climate under G than under NG conditions. *TotShb* declined in 2005, probably due to low rainfall amounts (precipitation <180 mm a^{-1}) but recovered, then declining again in years of similarly low rainfall.

The NG simulations (Figure 38) predicted *TotShb* to decline in 2005 to below its initial value and to recover in 2012 to the initial level of 70 g m^{-2}. The trend for *Artemisia herba-alba* (the dominant species in the "sage shrub" group) for G during the last years of the simulation (years 2010-2012) was remarkable. It approached levels (27 g m^{-2}) equal to those of the

herbaceous “fine grass“ group constituted by *Stipa cf. parviflora*. Herbaceous PFT biomass, however, increased under NG conditions. This is consistent with results from fenced ungrazed plots, where similar trends in growth have been observed (Puigdefabregas and Mendizabal 1998; Staudinger and Finckh 2005).

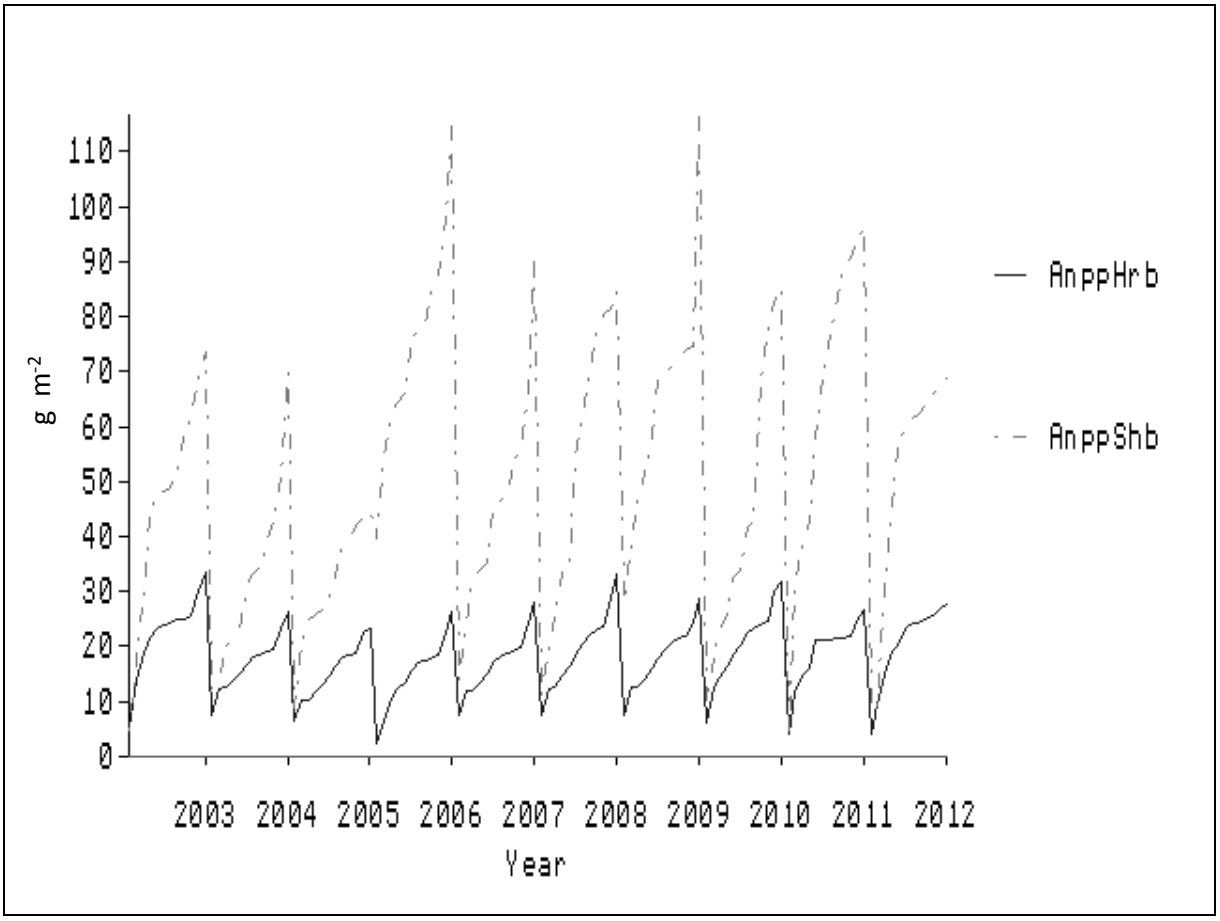

Figure 36: Aboveground net primary production (*ANPP*) of shrubs *ANPPShb* (dashed line) and herbaceous plants *ANPPHrb* (black line) (g m^{-2}) under the “no grazing“ (NG) 2002-2012 scenario.

More detailed examination of the leaf, root and dead biomass of the herbaceous “fine grass” indicated greater quantities and variability of herbaceous leaves under G conditions (<1 to 15 g m^{-2}) than under NG (<1 to 6 g m^{-2}) conditions. Herbaceous root dynamics were similar under G and NG conditions.

Dead herbaceous biomass, which is probably responsible for the continuous increasing trend of the herbaceous layer (*TotHrb*), is predicted to be carried over from year to year under NG conditions (Figure 38). However, dead herbaceous biomass is probably carried over in smaller quantities (14-20 g m^{-2}) under G conditions (Figure 37), as it declined to low amounts (<5 g m^{-2}) at the end of the growing seasons due to grazing.

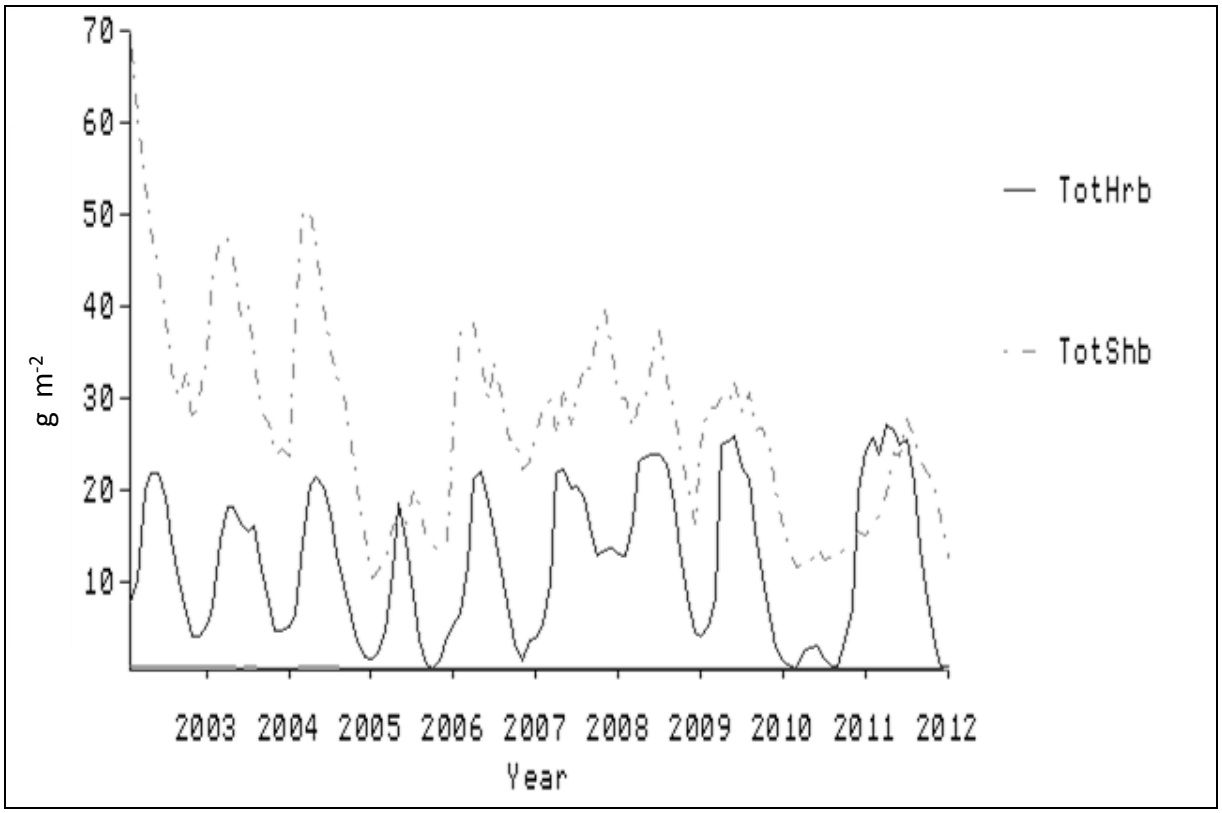

Figure 37: Total biomass (leaf, stem and dead) of herbaceous *TotHrb* (black line) and shrub *TotShb* (dashed line) PFT's for the Taoujgalt simulation over the years 2002-2012 under "grazing" (G) conditions.

Animal grazing probably stimulated growth during some time periods and reduced transfer to standing dead biomass during the dry season. After constant biomass dynamics were determined from the adaption results, parameters for the Drâa catchment were selected.

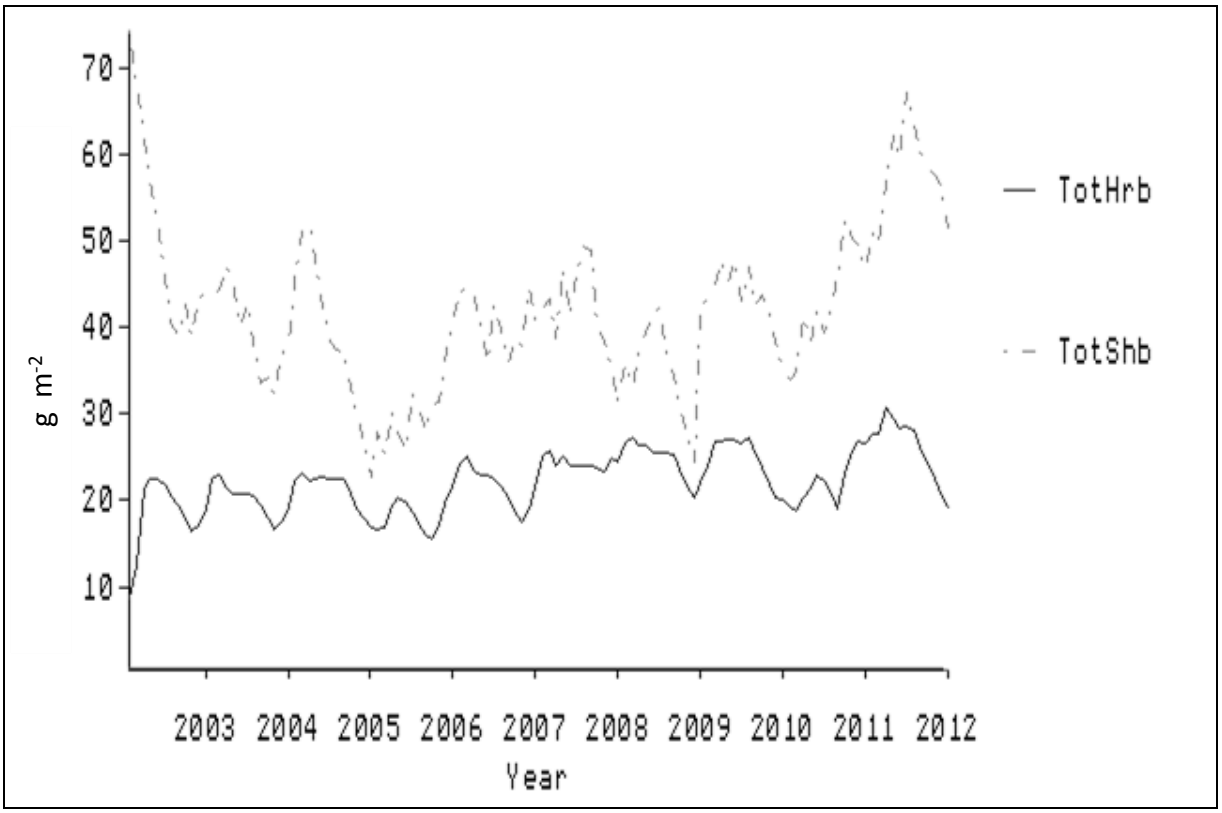

Figure 38: Total biomass (leaf, stems and dead) of herbaceous *TotHrb* (black line) and shrub *TotShb* (dashed line) PFT's for the Taoujgalt simulation over the years 2002-2012 under "no grazing" (NG) conditions.

4.5 Drâa catchment simulations and scenarios

In this and the following sections, the results of simulations for the Drâa catchment under alternative livestock number scenarios (heavy, medium and light grazing rates) are shown. Simulations were driven by different climate scenarios, which including atmospheric CO_2 enrichment.

This study was designed to determine whether the research hypothesises (see section 1.5) were induced by an anthropogenic factor (livestock number) or by a climatic factor (observed via the ranges of *trans*, *Ps* and C*s-act* and *Cs-pot*).

Two base-line scenarios, 1a and b, were examined first (Table 31). Next, alternative livestock numbers and climate scenarios were examined to reflect specific regional factors, temporal heterogeneity and elevated CO_2. The outcomes of these alternative scenarios were then compared to the base-line scenarios to distinguish the impact of the two research factors.

Table 31 Scenario design and descriptions.

Scenario		Climate source	Stocking rate and Management	Region	Location (Lat/Lon) of diagnostic cell
1 Base-line	a	DRH /IMPETUS 1979-2000	census animal data	Dades valley, Basin of Ouarzazate	31.508°N -5.91°E
	b	REMO 1979-2000	census animal data	Dades valley, Basin of Ouarzazate	as above
2	a	IPCC A1B scenario 2001-2050	moderate grazing intensity, *with range exclusion area*	Basin of Ouarzazate	31.279°N -6.434°E
	b	IPCC B1 scenario	moderate grazing intensity, *with range exclusion area*	Basin of Ouarzazate	as above
	c	IPCC A1B scenario	high grazing intensity, *No range exclusion area*	Basin of Ouarzazate	as above
	d SPATIAL	IPCC A1B	Range exclusion (Scenario 2a) versus No range exclusion area (Scenario 2c)	Basin of Ouarzazate	
3		DRH /IMPETUS 1975-2050 and elevated CO_2 (700ppm)	alternative stocking rates: light, heavy and moderate	Southern Drâa catchment zone	30.117°N -5.443°E

Each model run must relate to one diagnostic cell identified by the upper left corner geographic coordinates. Results in the diagnostic cell (e.g., N content, C*s-act* and *Cs-pot* etc.) refer to the smallest model scale, unique cells (here, 1 km^2). Results at the scale of

PFT's, such as ANPP and BNPP, PFT-separated leaf and root biomass, and intra-PFT change, are instead calculated for the entire Drâa simulation area.

First, we evaluate the base-line simulations (1a and b) with regard to observed numbers of sheep, goats and dromedaries. Figure 39 shows the temporal changes in animal numbers in the province of Ouarzazate from 1979 to 2000 according to ORMVAO (Service d´elevage/ Bureau of animal breeding) census data (ORMVAO 2005) introduced to the model as driving force (besides climate). These simulations were conducted to distinguish historic and recent changes in known stocking rates from 1979 to 2000 due to anthropogenic impacts from those induced by climate differences. The number of dromedaries was fixed at 10,000. Human population size increased from 5,000 to 8,200. The temporal range was fixed by the dataset, since data could be obtained for all animals only for the period 1979 to 2000.

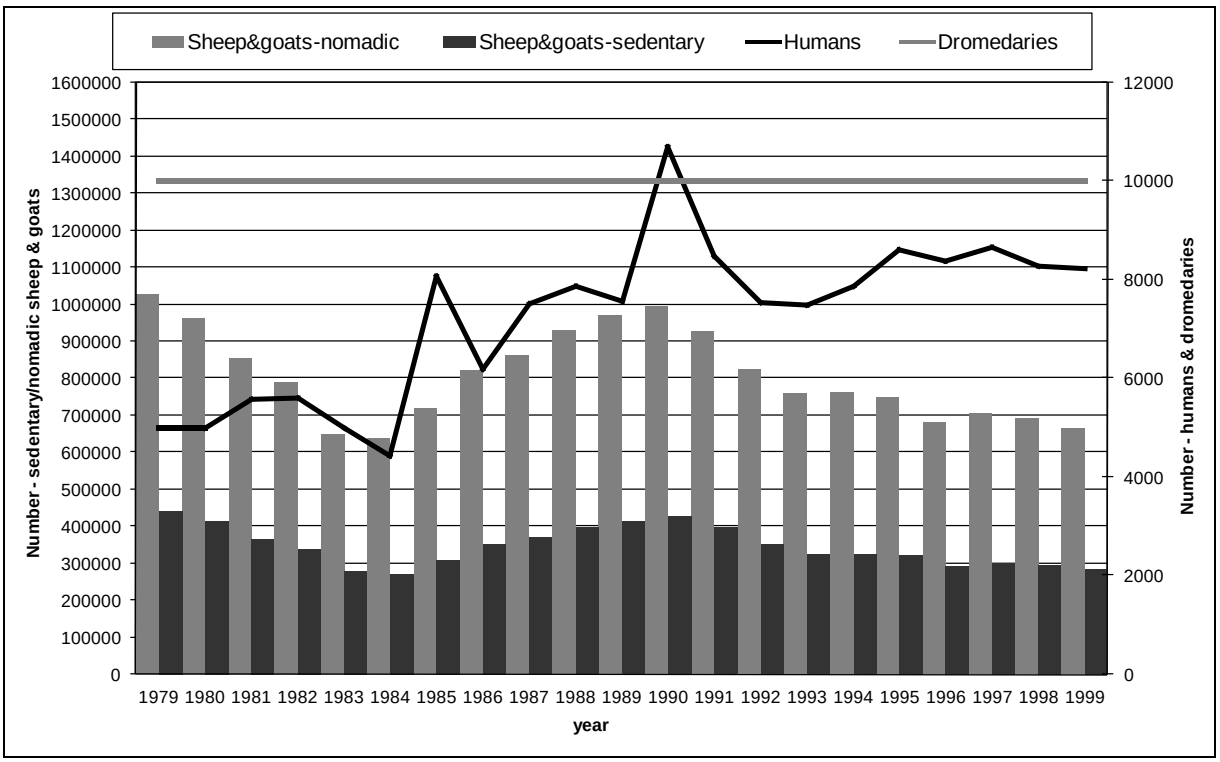

Figure 39: Annual observed numbers of sheep and goats (left axis) in the Drâa catchment from 1979-2000 (ORMVAO 2003) introduced to the model as driving forces and simulated numbers of humans and dromedaries (right axis).

The climate data sets used here originated from a downscaled non-linear Regional REMO Model from the Institute of Meteorology of the University of Bonn. These datasets were formatted to match the SAVANNA© meteorological data format to fully include them in the simulations. Observed twenty year data sets 1979 - 2000 from the DRH and IMPETUS climate stations were next used to simulate a comparison base-line run. The base-line diagnostic cell was characterised by soil type no. 24 (see Appendix, Table 35) and vegetation type no. 9 (Figure 11), at 683 m a.s.l. in the upper Dades valley of the basin of Ouarzazate in the northeastern Drâa catchment.

4.5.1 Base-line scenarios: Plant growth

Predicted results of the REMO simulation runs are described first. *ANPP* is presented in Figure 40. *ANPP* is then compared to belowground figures (*BNPP*) from the same simulation. The partitioning of biomass into *ANPP* and *BNPP* is useful to determine the re-growth potential of plants, especially in arid environments. In times of drought, *BNPP* serves as a nutrient pool for the aboveground parts of the plants. For example, *BNPP* figures for *Hammada scoparia* are estimated by Nording (2008) to account for 90% of total biomass at Bou Skour in the Anti-Atlas region of the basin of Ouarzazate. This indicates that *BNPP* plays an important role as a resource pool for plant growth.

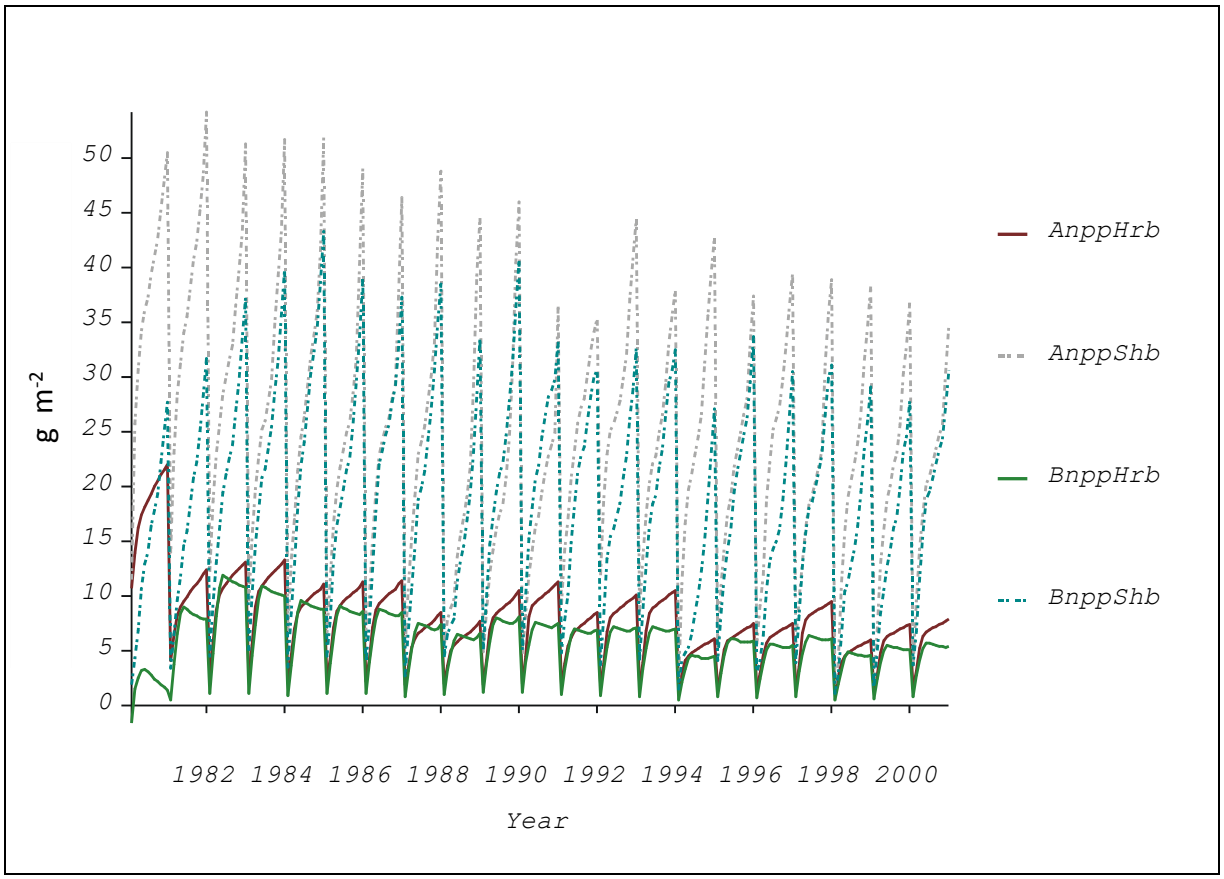

Figure 40: Monthly accumulated *ANPP* and *BNPP* (g m^{-2}) from 1980-2000 in REMO simulations with observed animal census data (model drivers): herbaceous *AnppHrb* (red line) and shrub ANPP *AnppShb* (dashed grey line), herbaceous *BnpppHrb* (green line) and shrub BNPP *BnppShb* (dashed blue line).

At the start of the simulation, the amounts of both herbaceous and shrub *BNPP* were small compared to the amounts of *ANPP* (Figure 40). Subsequently, the amount of *BNPP* for both PFT's increased continuously to a stable level of about ¾ of *ANPP* throughout the remainder of the simulation. The amounts of herbaceous and shrub *ANPP* and *BNPP* reflected precipitation levels and tended to decrease throughout the simulation.

An explanation for this pattern of growth is given by the average annual precipitation (Figure 41). Values from the REMO simulations are predicted to be greater than the measured rainfall at the DRH and IMPETUS climate stations.

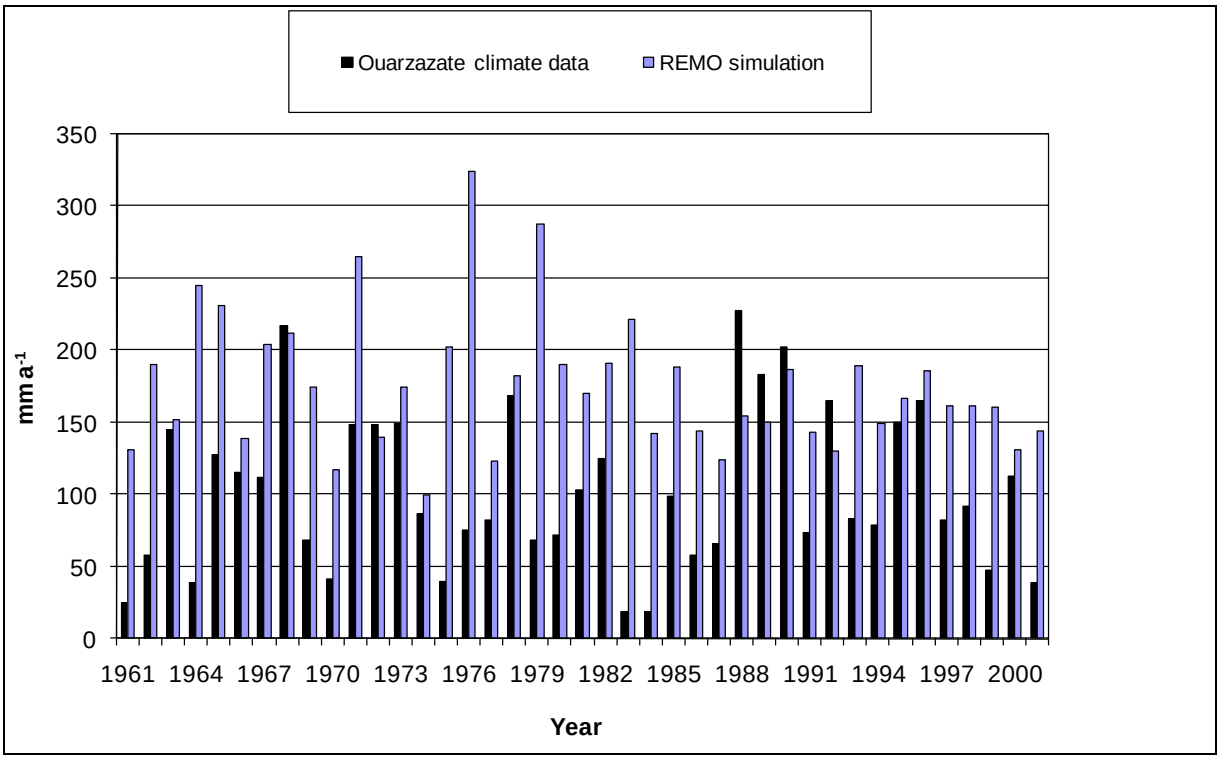

Figure 41: Comparison of total annual precipitation (mm a^{-1}) from REMO simulations (blue) with measured data from 1961-2001 from the Ouarzazate climate station (black).

The herbaceous (*AnppHrb and BnppHrb*) and shrub (*AnppShb* and *BnppShb)* simulations based on Ouarzazate climate data produced a different picture (Figure 42). *ANPP* amounts were within a lower range, probably due to the lower rainfall amounts from the climate station data. If rainfall is absent, a decrease in *ANPP* and *BNPP* was predicted for all PFT's, but *ANPP* and *BNPP* are predicted to increase as rainfall permits.

Although *ANPP* and *BNPP* amounts decreased somewhat, they did not decrease strongly from the beginning of the simulation, as they did in the REMO scenario. This suggests that the higher rainfall in the REMO scenario may lead to higher production but also to continuous decline if precipitation amounts decrease over a long time span.

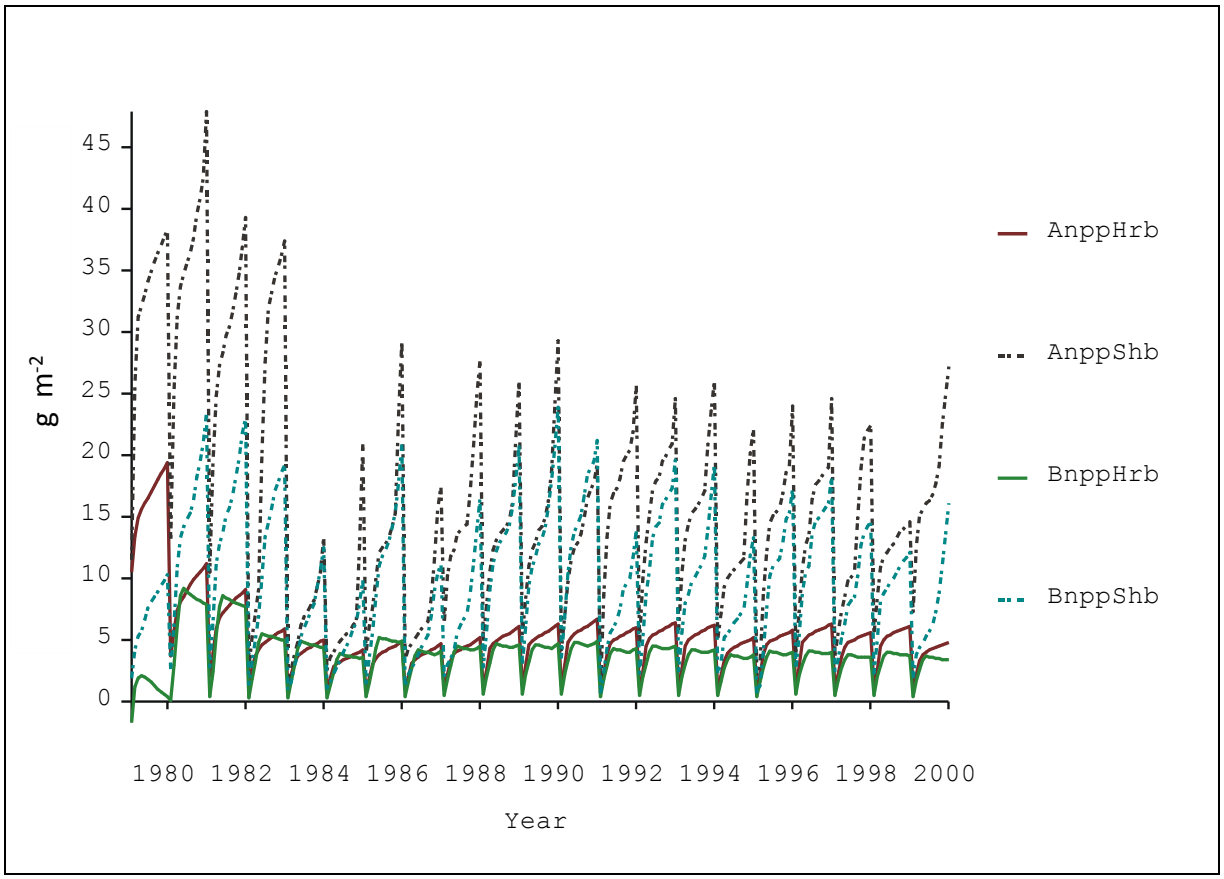

Figure 42 Monthly accumulated *ANPP* and *BNPP* (g m^{-2}) from 1980-2000 in simulations with observed animal census data and measured climatic data from the Ouarzazate climate station (model drivers): herbaceous *AnppHrb* (red line) and shrub *AnppShb* (dashed black line), herbaceous *BnppHrb* (green line) and shrub *BnppShb* (dashed blue line).

Figure 43 shows the limitation of vegetation growth by N (*Eff-N*), temperature (*Eff-T*), water (*Eff-W*) and light (*Eff-L*) in the REMO simulations (see section 3.3). An interesting point here is the low limitation of *Eff-W*, in other words, the high availability of water in the system. This is explained by the high levels of precipitation seen in the REMO data (Figure 41). *Eff-W* is predicted to be 2.0, which is twice the model inherent index of “no limitation“ (indicated by 1.0). This means that there is more than enough plant available water in the system to maintain plant growth. Other limitations are offset by the high *Eff-W*; e.g., *Eff-N* tends to low (1.0) levels, as explained in section 3.3. The variability of *Eff-T* is the only factor considerably limiting vegetation growth.

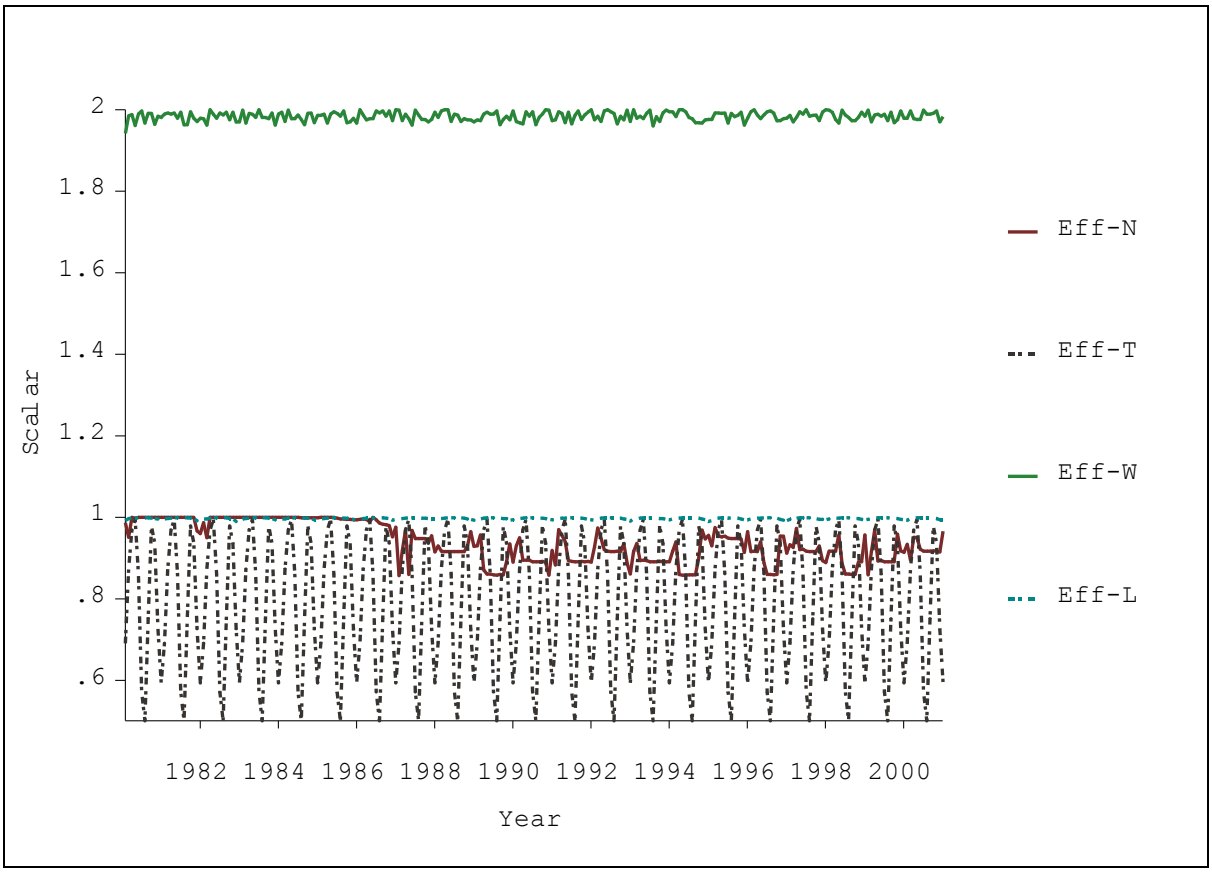

Figure 43: Monthly limiting effects of nitrogen *Eff-N*, temperature *Eff-T*, water *Eff-W* and light *Eff-L* from 1980-2000 on vegetative growth in the REMO simulation; scalar units from 0.0 (high limitation) to 1.0 (low limitation) (see Figure 22).

The Ouarzazate simulations depicted in Figure 44 provide a more reliable picture than those shown above of water, N, light and temperature limitation of vegetation growth. *Eff-W* was constant at 0.4 as in the model adaption simulation; see section 3.3. However, *Eff-T* was also a limiting factor, and *Eff-N* was strongly limiting during certain time steps (e.g., 1985). During 1985, practically all plant available N pools were exploited (indicated by high *Eff-N* (0.0)), but N pools recovered the next year. Due to the controlling role of water indicated above, the Ouarzazate scenario is probably more reliable than the REMO scenario. Because herbaceous and shrub green leaves are highly palatable to animals (Table 22 and Table 23), their variability over time is described next.

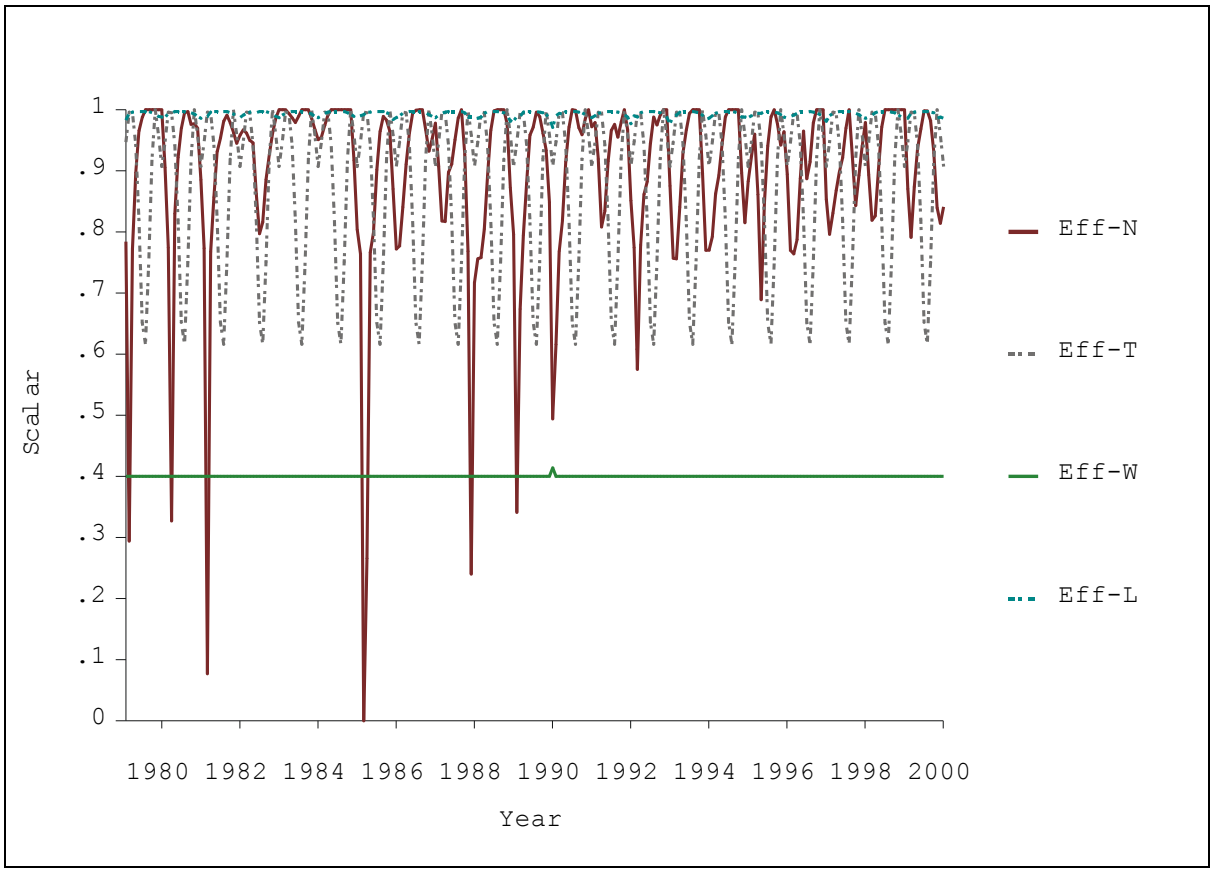

Figure 44: Monthly limiting effects of nitrogen *Eff-N*, temperature *Eff-T*, water *Eff-W* and light *Eff-L* from 1980-2000 on vegetative growth in the Ouarzazate climate station data simulation; scalar units from 0.0 (high limitation) to 1.0 (low limitation) (see Figure 22).

The change over time in green leaf biomass for different grass species modelled in the herbaceous PFT is shown in Figure 45. Curves indicate annual development to the flowering peak and subsequent decline of the plant group due to animal consumption. The grass species are grouped into “fine-”, ”coarse-” and “alpine” grass categories in all simulation results described in this section in order to provide comparability. Starting with the REMO run, (Figure 45) the most remarkable result was the decline in “coarse grass” biomass, together with an increase in “fine grass”. All grasses remained in a more or less constant equilibrium after 1990.

The “alpine grass” PFT declined sharply by about one quarter to 0.5 g m $^{-2}$ DWT over the 20 years of the simulation. Coarse grass declined by about one eighth to about 1.0 g m^{-2} DWT.

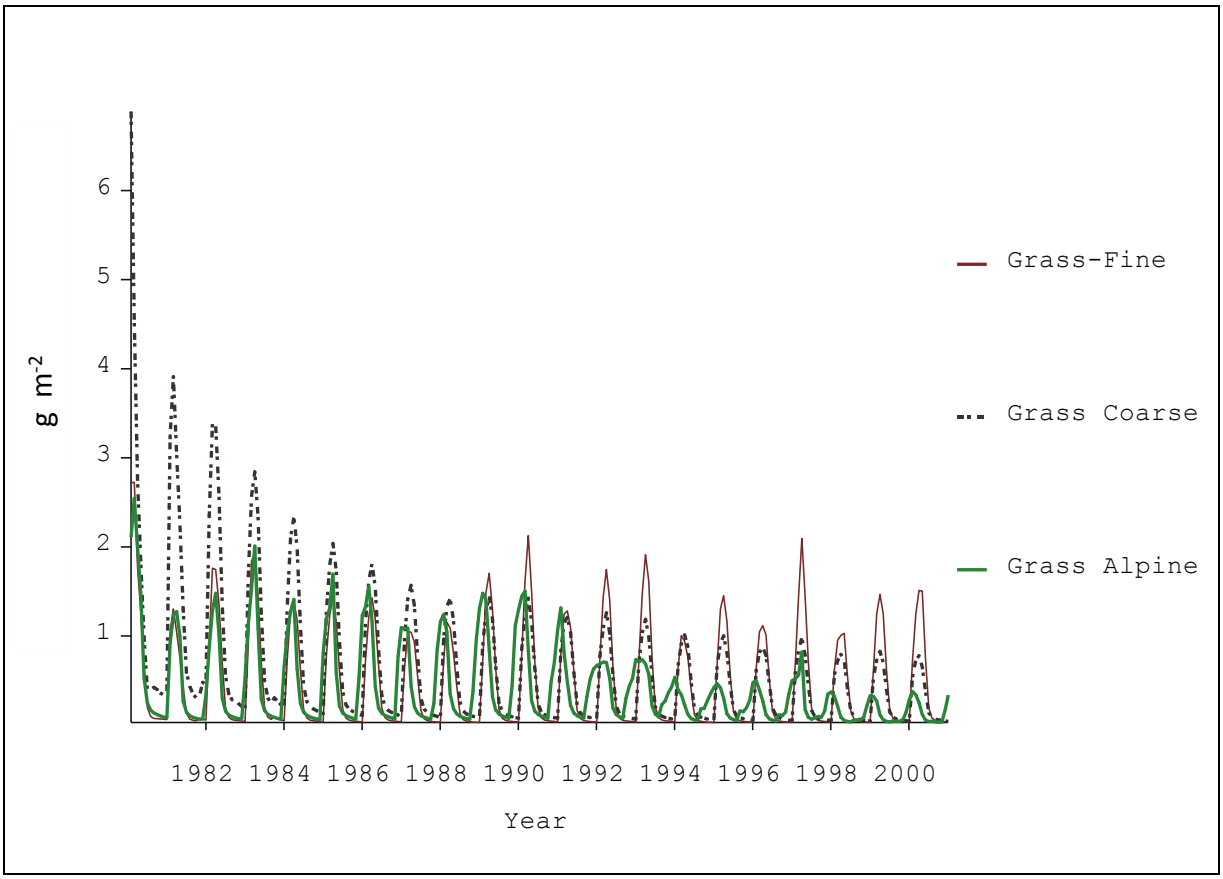

Figure 45: Monthly changes in green leaf biomass of grasses (g m^{-2}) from 1980-2000 under the REMO scenario: "fine grass" (red line), "coarse grass" (dashed black line) and "alpine grass" (green line).

In contrast, "fine grass" maintained a level of about 1.5 g m^{-2} DWT across years. This very low amount was even further reduced under the Ouarzazate scenario (Figure 46), due to the precipitation regime. The proportion of "coarse grass" was probably overestimated at the beginning of both simulations due to the "warm-up" phase of the model. The same observation is true for all outcomes described in this section. These values declined to lower equilibria as the model fitted all grass groups to climatic and animal consumption constraints. The "fine grass" and "alpine grass" groups also declined, but the first was able to increase its proportion again, perhaps because of animal dietary preferences. Otherwise, "alpine grass" parameterisation may have been insufficient in terms of ground cover and/or climatic adaptiveness. At the end of both 20-year simulations, the proportion of "coarse grass" was three times higher (REMO) and that of "fine grass" was ten times higher than that of "alpine grass" (Ouarzazate). Growth of the shrub PFT for the REMO and Ouarzazate simulations is discussed below.

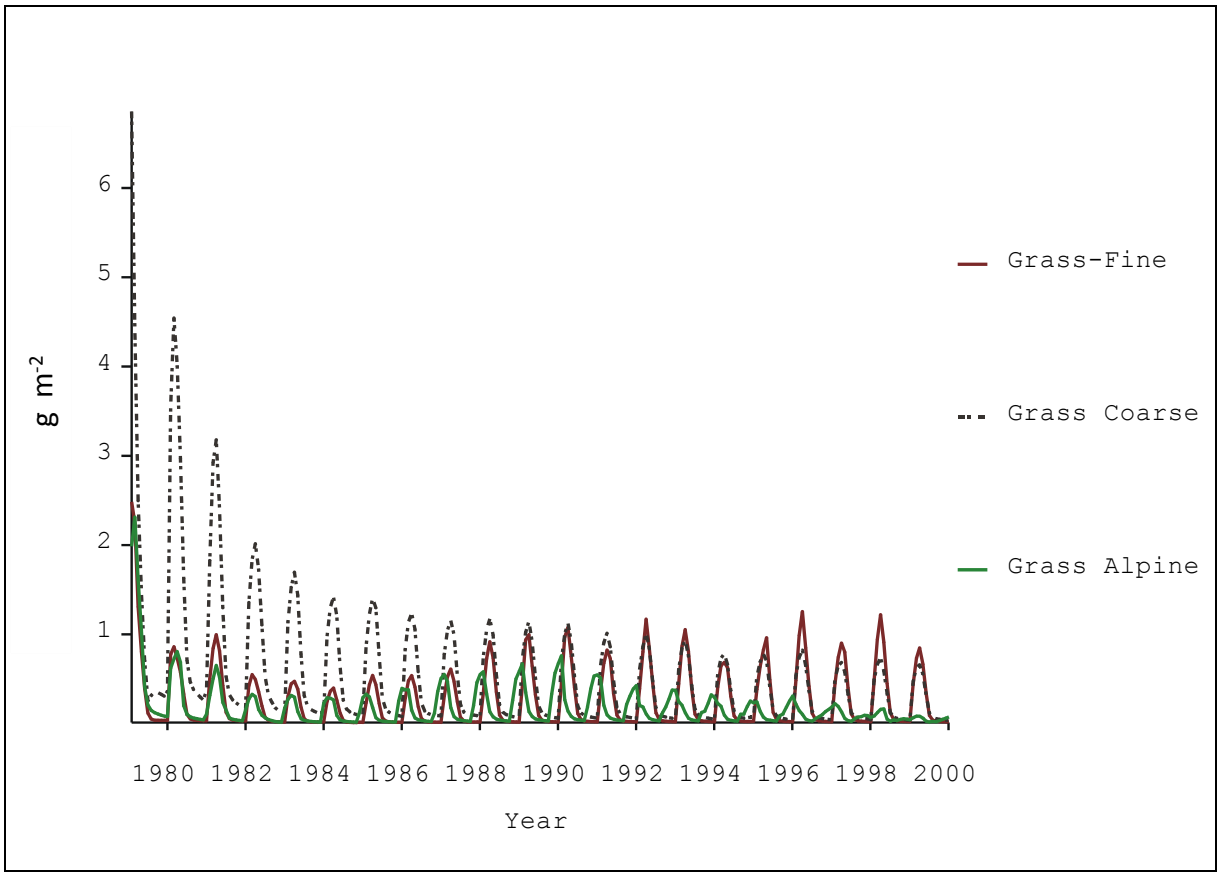

Figure 46: Monthly changes in green leaf biomass of grasses (g m^{-2}) from 1980-2000 under the Ouarzazate scenario: "fine grass" (red line), "coarse grass" (dashed black line) and "alpine grass" (green line).

A decline in shrub PFT green leaf biomass was predicted (Figure 47), as previously indicated by the shrub *ANPP* results for the REMO scenario (Figure 40). The shrub PFT included "evergreen", "low DMD" and "sage" species. The change over time in "alpine forbs" was also incorporated. Figures showed that the "alpine forb" species rapidly became extinct after the start of the simulations. This was due to the inappropriate parameterisation used for this PFT. Therefore, this category is excluded from the discussions in the following sections. "Evergreen shrub" green leaf biomass showed the strongest decline, probably due to animal's high preference for this type of plant (Table 22, Table 23). Animal preferences are probably also responsible for the declines in green leaf biomass of "sage-" and "low DMD shrubs". However, both shrub types were able to recover on an annual basis and stabilised at certain levels of growth in spite of the animal preferences.

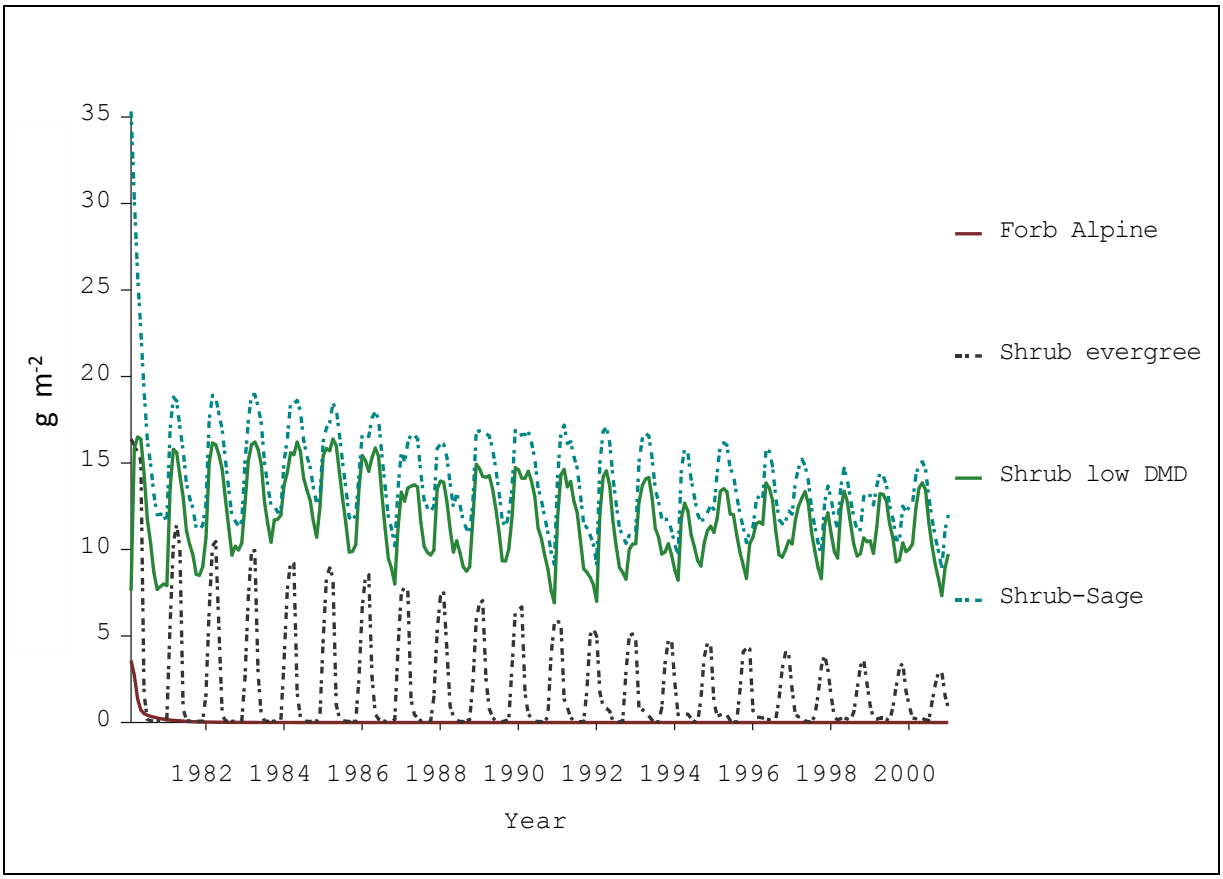

Figure 47: Monthly changes in green leaf biomass (g m^{-2}) of shrub PFT groups from 1980-2000 under the REMO scenario: "alpine forb" (red line), "evergreen-" (dashed black line), "low DMD-" (green line) and "sage shrub" (dashed blue line).

The change over time in green leaf biomass of shrub PFT species differed in the Ouarzazate simulation (Figure 48). So was the decline in "evergreen shrub" green leaf biomass, probably for the same reasons discussed above. "Sage-" and "low DMD shrub" green leaf biomass continuously increased until an equilibrium was reached. This constant level was based on lower DWT amounts compared to the REMO scenario, probably because of lower rainfall. The "sage-" and "low DMD shrubs" were clearly affected by rainfall input (e.g., from 1983-1985), whereas "evergreen shrubs" were less affected. This difference is probably due to the vast ground cover of "sage shrubs" and to the unpalatability of "low DMD" and high palatability of "sage shrub" green leaves, respectively.

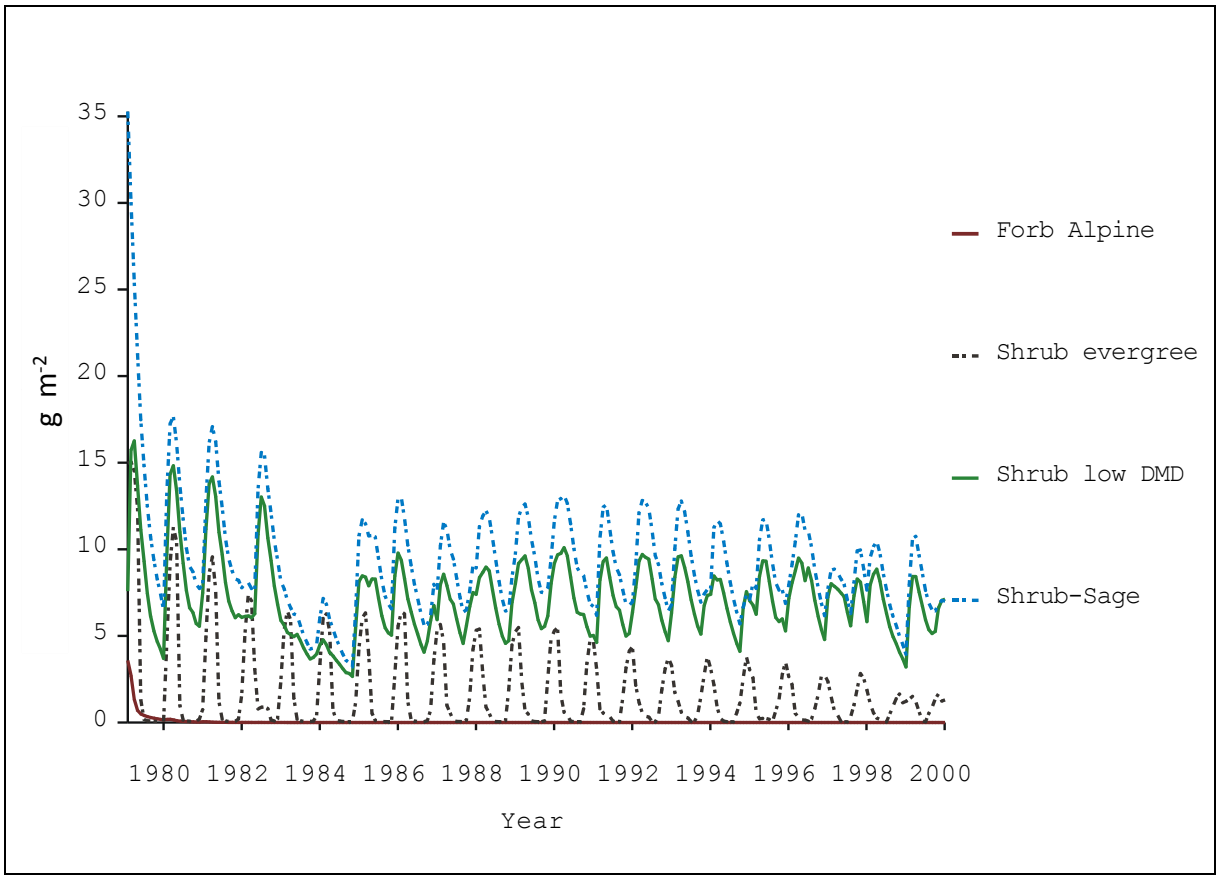

Figure 48: Monthly changes in green leaf biomass (g m^{-2}) of shrub PFT groups from 1980-2000 under the Ouarzazate scenario: ”alpine forbs” (red line), ”evergreen-” (dashed black line), “low DMD-” (green line) and ”sage shrub” (dashed blue line).

A completely different pattern was seen for the green leaf growth of tree PFT’s (“deciduous-” and “aspen trees”) in both the REMO and Ouarzazate simulations (Figure 49 and Figure 50). The “deciduous tree” group declined sharply during the simulation from >1100 g m^{-2} DWT to about 250 g m^{-2} DWT. The “aspen tree” group also declined by about half, from 400 to 200 g m^{-2} DWT. This trend halted once, during the exceptional precipitation amounts of the early 1990s.

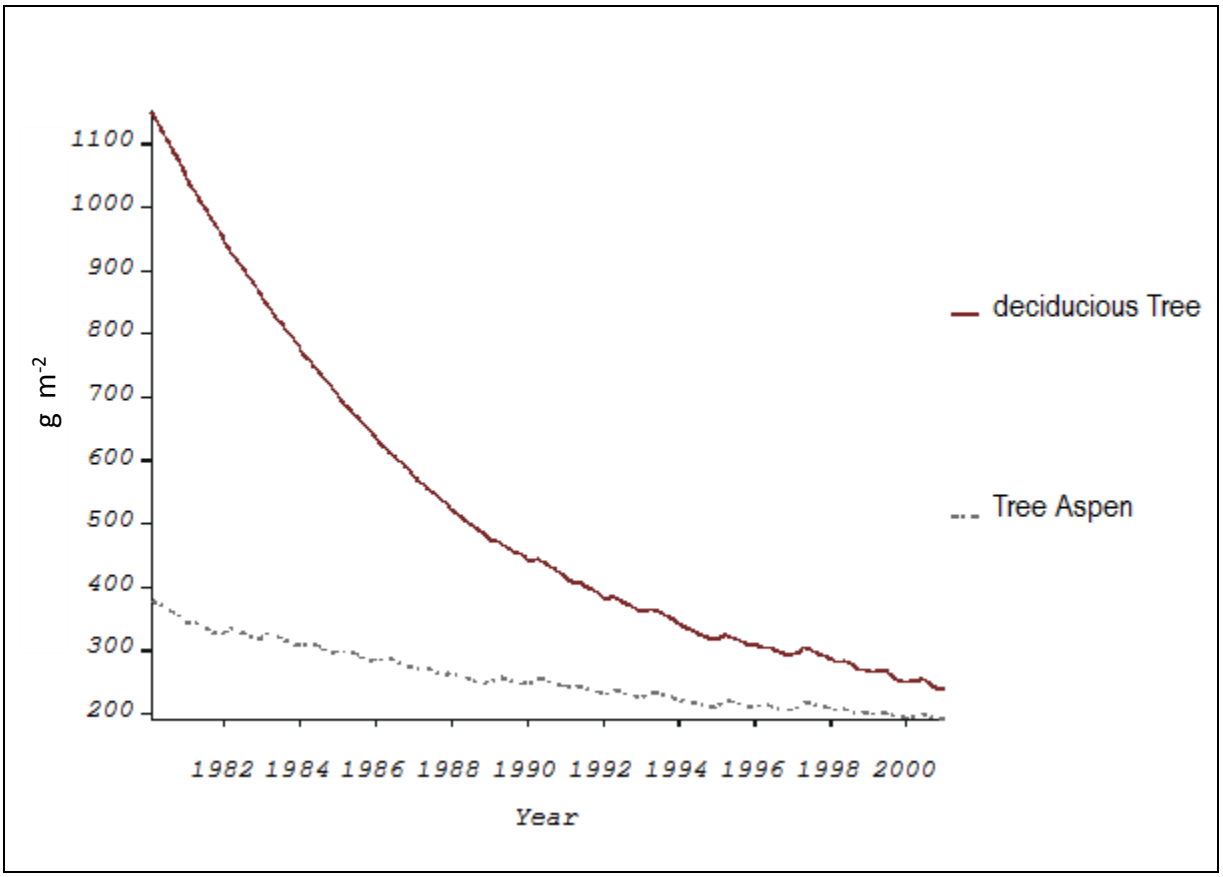

Figure 49: Monthly changes in green leaf biomass (g m^{-2}) of tree PFT groups from 1980-2000 under the REMO scenario: ”aspen-” (dashed grey line) and “deciduous trees” (red line).

The strong decline in green leaf biomass of trees (especially “deciduous trees”) highlights the overestimation of leaf DWT in the parameterisation procedure. Leaf DWT was „normalised“ during the simulation. This normalisation toward climatic and environmental conditions occupied most of the simulation period. However, the normalised equilibrium level seems to be about 200-300 g m^{-2} tree leaf DWT. Both tree types possess extremely low ground cover (<1%) in all rangelands except for the Middle Drâa oases and the oases in the High Atlas Mountains (see section 1.4.3). Because tree cover is so low, we dispense with tree biomass and nutrient descriptions in the following sections and refer instead to section 4.2 for characteristic descriptions of patches with high ground cover of trees.

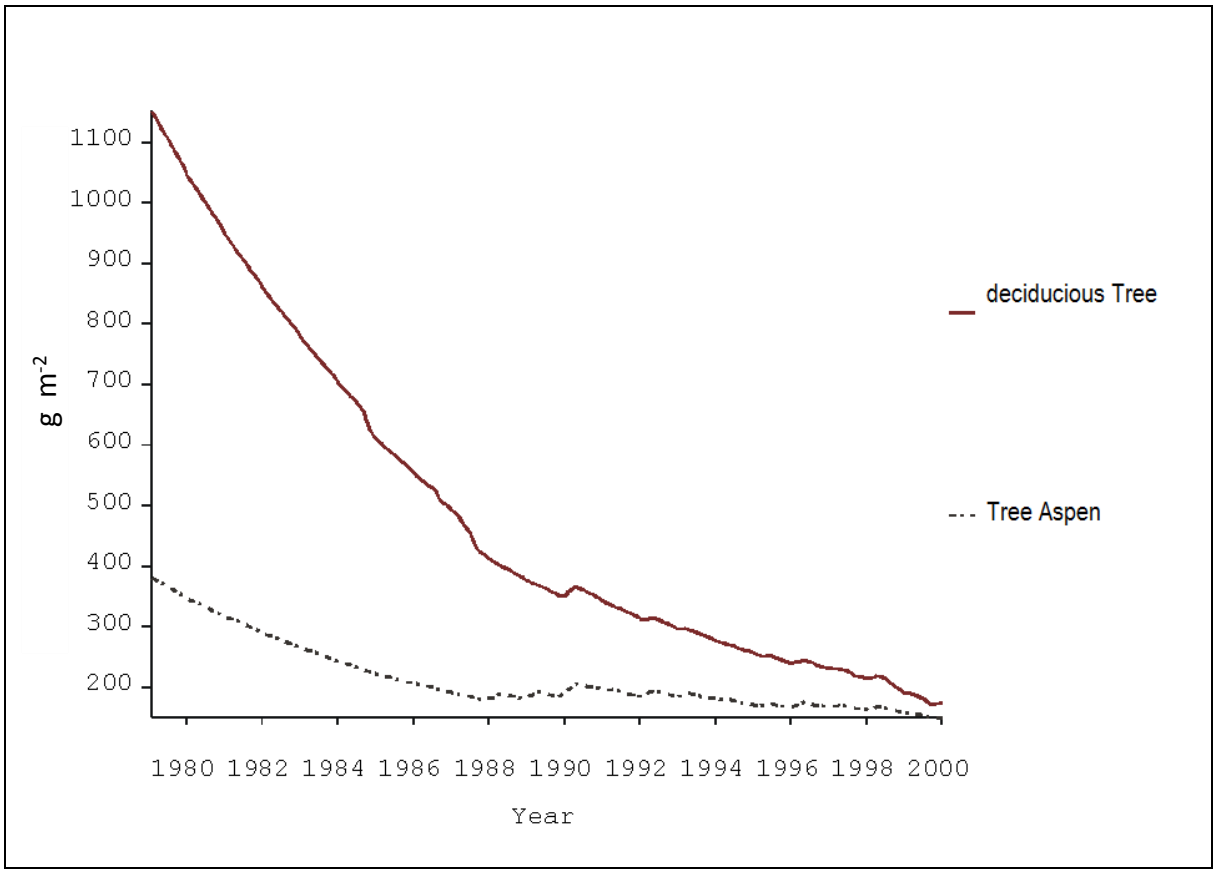

Figure 50: Monthly changes in green leaf biomass (g m^{-2}) of tree PFT groups from 1980-2000 under the Ouarzazate scenario: "aspen-" (dashed grey line) and "deciduous trees" (red line).

The predicted photosynthetic (*Ps*) features of all three *ANPP*s (Figure 51) during the REMO and Ouarzazate simulations are described next. *Ps* levels strongly depend on changes in temperature and light, which vary in an annual cycle. Moreover *Ps* depends on rainfall and thus falls to minimum levels when precipitation is lacking. Because *Ps* activity and *Cs* are important indicators of plant *ANPP* productivity, they are used here as a direct link to the different climatological inputs assumed in the working hypothesises (see section 1.5).

As expected from the results described previously, predicted monthly *Ps* levels under the REMO scenario exceeded those of the Ouarzazate simulation. Both scenarios showed a more or less constant *Ps* activity rate after the "warm-up" phase. The REMO simulation showed higher average *Ps* activity levels of 4-6 µmol m^{-2} s^{-1} than the avg. of 2 µmol m^{-2} s^{-1} in the Ouarzazate simulation. In the REMO simulation, *Ps* activity rarely declined below 1 µmol m^{-2} s^{-1}. In the Ouarzazate simulation, on the other hand, *Ps* rates decreased to a minimum level of <0.01 µmol m^{-2} s^{-1} for several months, probably because of the low *ANPP* of all PFT's predicted for the diagnostic cell.

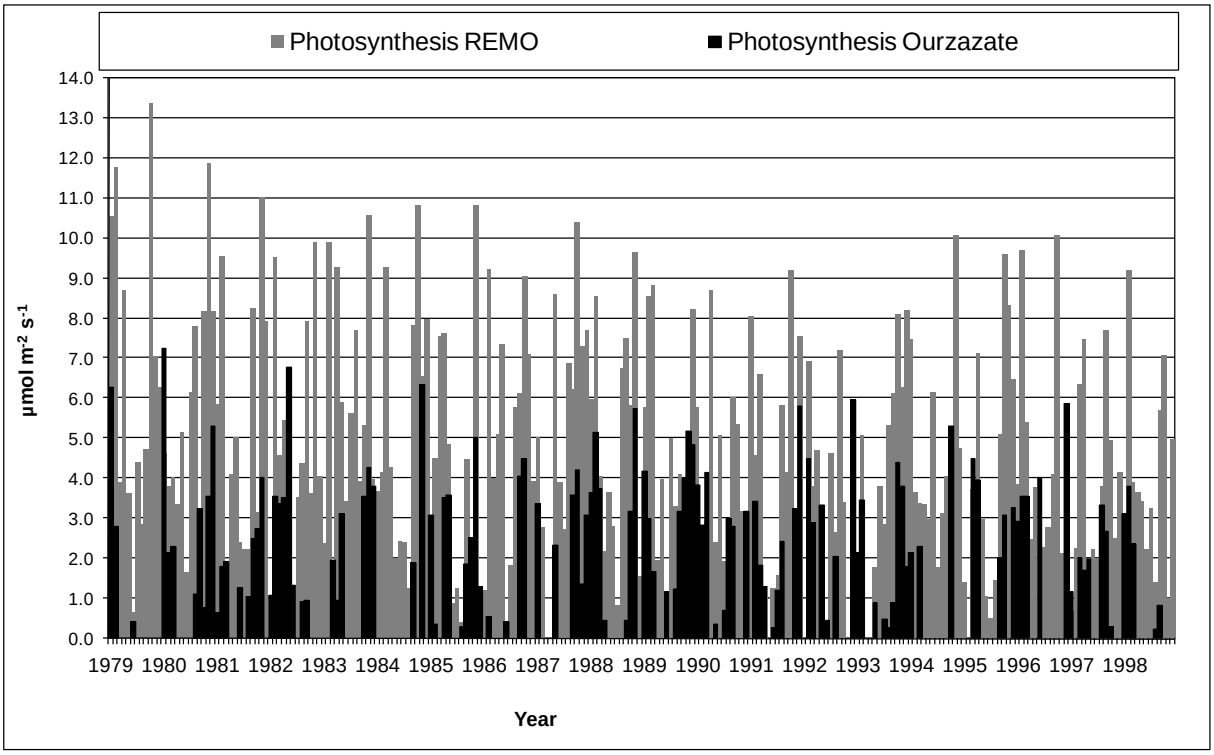

Figure 51: Comparison of predicted monthly photosynthesis *Ps* rates (µmol m^{-2} s^{-1}) of herbaceous, shrub and tree PFT's under the Ouarzazate scenario (black area) and under the REMO simulation (grey area) for the period 1979-2000.

Predicted actual stomatal conductance[13] (*Cs-act*) and potential stomatal conductance[14] (*Cs-pot*) results are shown in Figure 52 (REMO) and Figure 53 (Ouarzazate) for all three PFT's. *Cs-pot* levels in the Ouarzazate simulation exceeded those of the REMO simulation. While the REMO simulation produced maximum values of 170 mmol m^{-2} s^{-1}, the Ouarzazate simulation produced peak values of 190 mmol $m^{-2}s^{-1}$. The *Cs-pot* values from the Ouarzazate simulation showed a large range of variation, whereas values from the REMO simulation showed less variability, suggesting the availability of sufficient and equally exploited water resources. Surprisingly, despite the difference in *Cs-pot* values, both scenarios showed equal ranges for predicted *Cs-act*. Considering (for example) the higher herbaceous and shrub green leaf biomass predicted by the REMO simulation (see Figures 45-48) higher *Cs-act* levels were expected for the REMO simulation, as seen for *Ps* rates. One assumption for this difference may be that PFT's in the Ouarzazate scenario are probably forced to use water resources efficiently due to water-limited (*Eff-W*) conditions (Figure 44), whereas in the REMO scenario, water limitation does not occur.

[13] the amount of water used by all three PFT's based on predicted plant available water
[14] the level of water that plants in the system could use if water was not a limiting factor

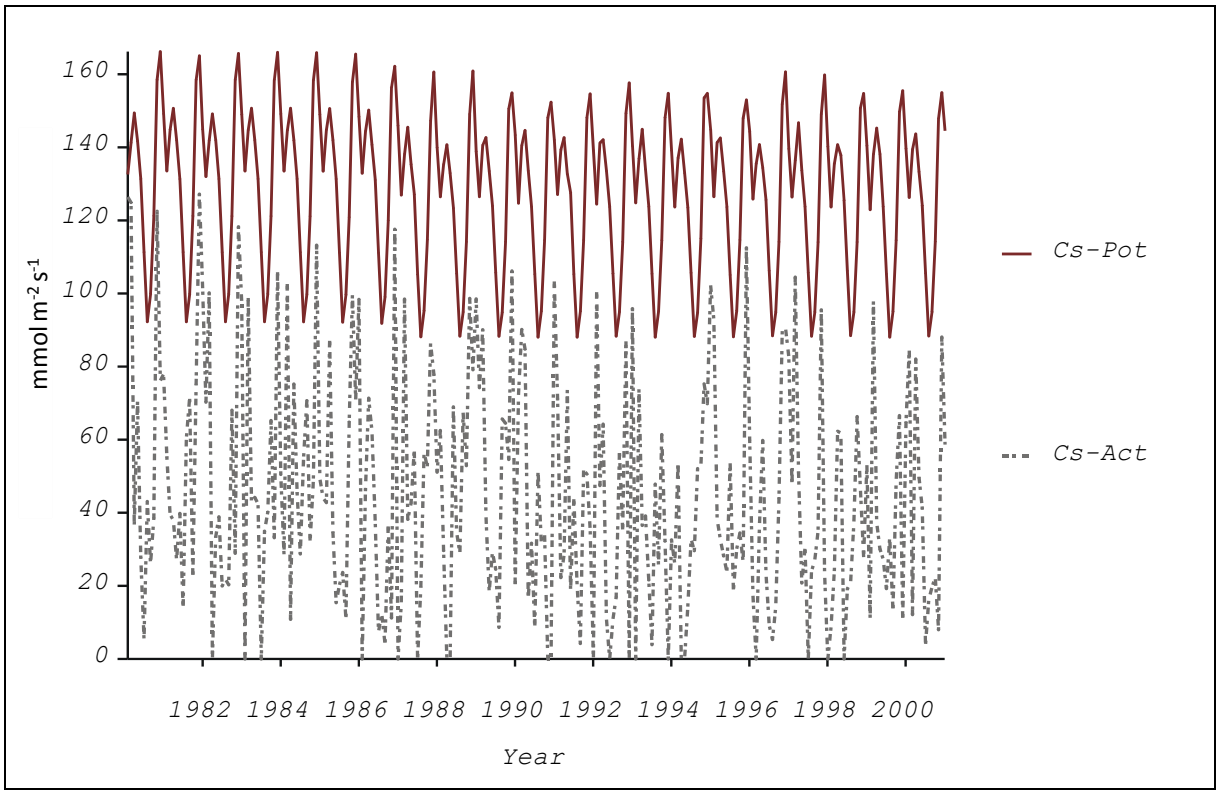

Figure 52: Simulated annual sum of potential stomatal conductance *Cs-pot* (red line) versus sum of actual stomatal conductance *Cs-act* (dashed blue line) (mmol m^{-2} s^{-1}) for all three PFT's from 1980-2000 under the REMO scenario.

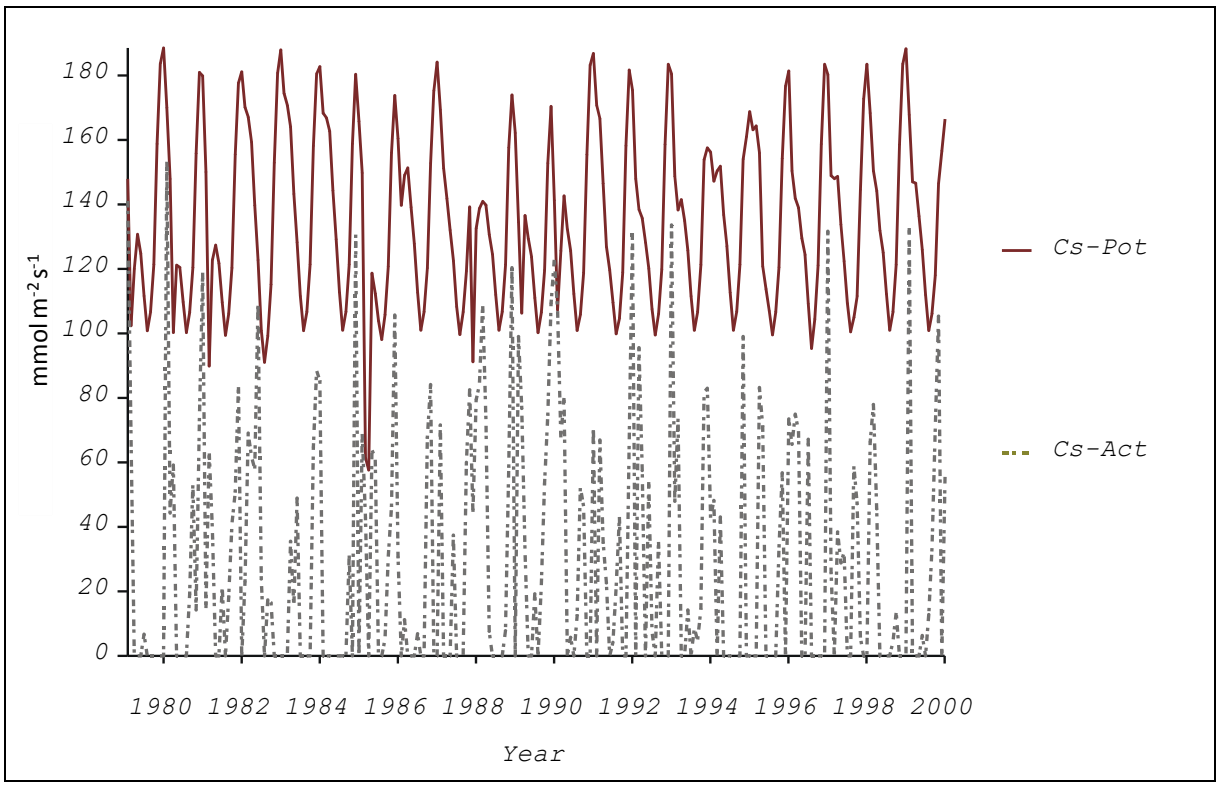

Figure 53: Simulated annual sum of potential stomatal conductance *Cs-pot* (red line) versus sum of actual stomatal conductance *Cs-act* (dashed blue line) (mmol m^{-2} s^{-1}) for all three PFT's from 1980-2000 under the Ouarzazate scenario.

Both runs periodically indicated very low monthly levels (<5 mmol $m^{-2} s^{-1}$) of *Cs-act*. Figure 53 describes declines in *Cs-act* lasting several months under the Ouarzazate scenario. Plants are thought to reduce *Cs-act* activity due to higher temperatures or unavailability of water.

4.5.2 Base-line scenarios: Nitrogen cycle and Nitrogen budgets

An effective measurement of plant growth performance is the simulated nitrogen (N) to biomass (B) *N:B* ratio for herbaceous, shrub and tree PFT's. Figure 54 and Figure 55 indicate *N:B* ratios for the plant (*Pl-N:B*), active (*Act-N:B*)[15] and leaf (*Lf-N:B*) compartments. We performed two identical simulations in spatial and temporal terms, and the evolution of the *N:B* parameter differed considerably in both. In both runs, however, the first five years behaved as a model "warm-up" phase. The *Lf-N:B* ratio, which is an indicator of shoot growth, is described in detail. In the REMO simulation (Figure 54), *Lf-N:B* initially showed a continuously high monthly ratio of 0.026 for a long period, but showed short-phase oscillations later in the run. The cause for this change was probably the allocation of N from to shoots via active translocation as long as sufficient plant N resources were available. The temporal change in the *Pl-N:B* ratio also showed a continuous decrease from spring to autumn.

As plants allocate N to shoot growth and flowering, the soil N pool is probably depleted. Hence, in the spring, more N is distributed throughout less biomass whereas, in the summer and autumn, more biomass must be sustained by smaller pools of plant available N.

[15] This term describes the allocation mechanism transferring N from plant to shoot growth.

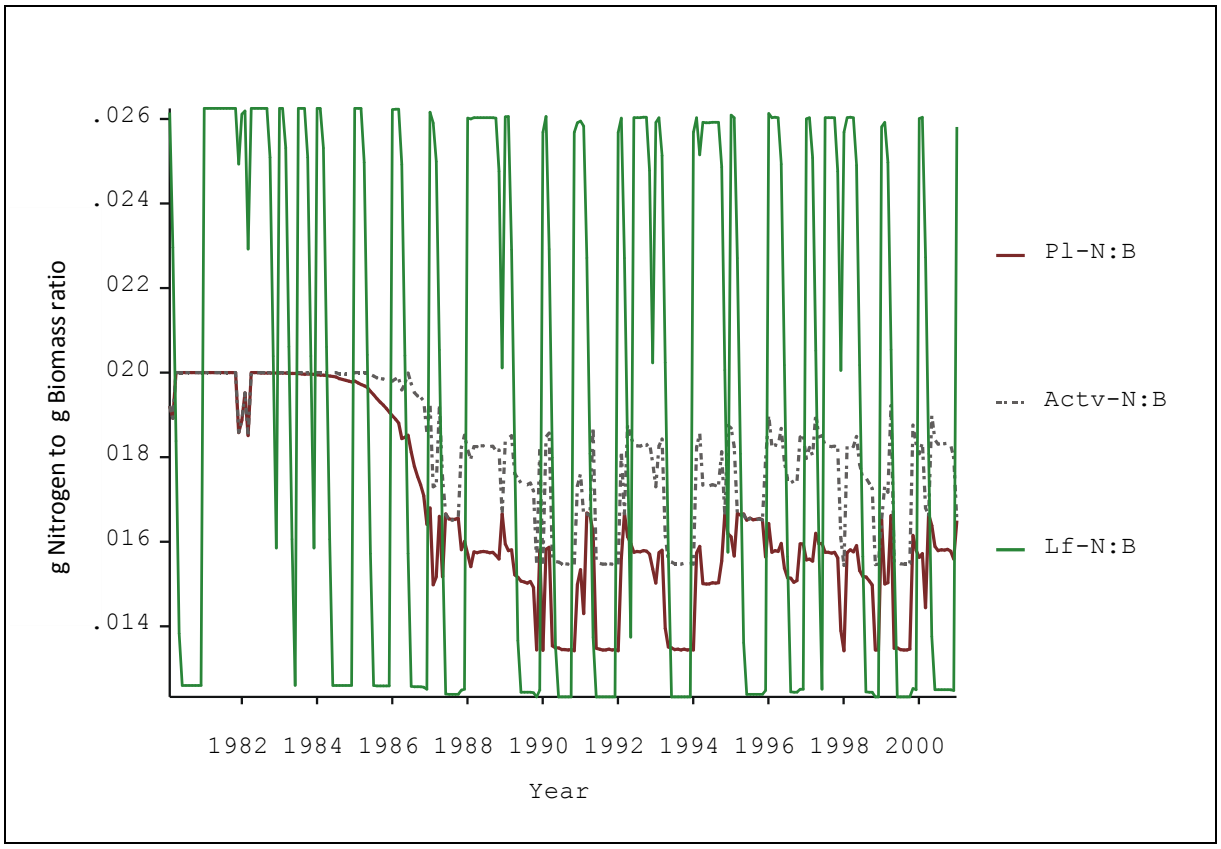

Figure 54: Monthly changes in *N:B* ratio for herbaceous, shrub and tree PFT's in whole plant *Pl-* (red line), active *Actv-* (dashed blue line) and leaf *Lf-* (green line) levels under the 1980-2000 REMO scenario.

However, in the Ouarzazate simulation (Figure 55) after the "warm-up" phase, these three ratios showed more constant individual levels, and the *Lf N:B* ratio did not decline by half, as in Figure 54. Instead, *Lf N:B* decreased temporarily to a minimum threshold ratio determined by the processes described for the REMO simulation. *Pl-N:B* was able to maintain a certain minimum ratio and was probably favourable for leaf N allocation for shoot growth.

Pl-N:B reached higher ratios in the REMO simulation than in the Ouarzazate simulation, but fluctuated considerably. The Ouarzazate simulation produced *Pl-N:B* ratios about half those of the REMO simulation, but the Ouarzazate simulation showed that a certain ratio of *Pl-N:B* could be consistently maintained and allocated to shoot growth in the range of 0.016 to 0.21. The range of variation in the *Act-N:B* ratio was equal in both simulations.

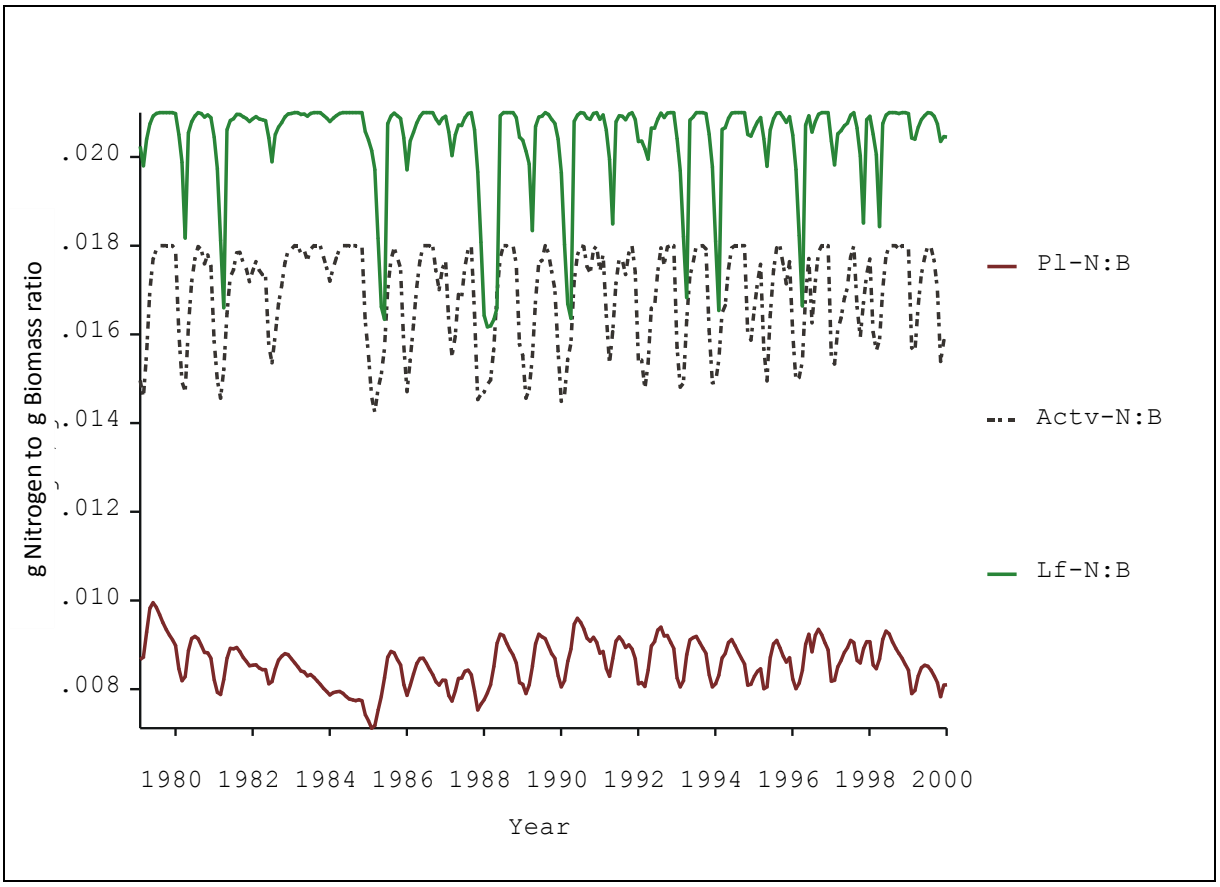

Figure 55: Monthly changes in *N:B* ratio for herbaceous, shrub and tree PFT's in whole plants *Pl-* (red line), active *Actv-* (dashed blue line) and leaf *Lf-* (green line) levels under the 1980-2000 Ouarzazate scenario.

The differences between the REMO and Ouarzazate simulations in *N:B* ratio were probably due to the various limitations to plant growth. Whereas little N limitation (*Eff-N*) was predicted for the REMO scenario (Figure 43), the predicted N limitation for the Ouarzazate scenario (Figure 44) was somewhat greater. However, this does not sufficiently explain the wide range of *Lf-N:B* ratios found in the REMO simulation. Instead, the greater predicted *ANPP* growth under the REMO scenario (Figure 40) forces plants to place excessive demands on the small predicted N pools, resulting in large variation in the *Lf-N:B* ratio.

Upscaling the previous description of plant *N:B* ratio to the N budget of herbaceous (*Tfac1N*) and shrub (*Tfac3N*) PFT's produced the results shown in Figure 56 (REMO) and Figure 57 (Ouarzazate). Both simulations performed similarly, with *Tfac1N* increasing and *Tfac3N* decreasing during the simulation. *Tfac1N* reached up to 5 kg of N per m^2 (in the diagnostic cell). Conditions implemented for the base-line scenarios favoured the allocation of N to the herbaceous PFT, and therefore an increase in N content was predicted. On the other hand, the *Tfac3N* showed a decline in N content during the simulation. Multiple causes might be responsible for these shifts from shrub to herbaceous N allocation.

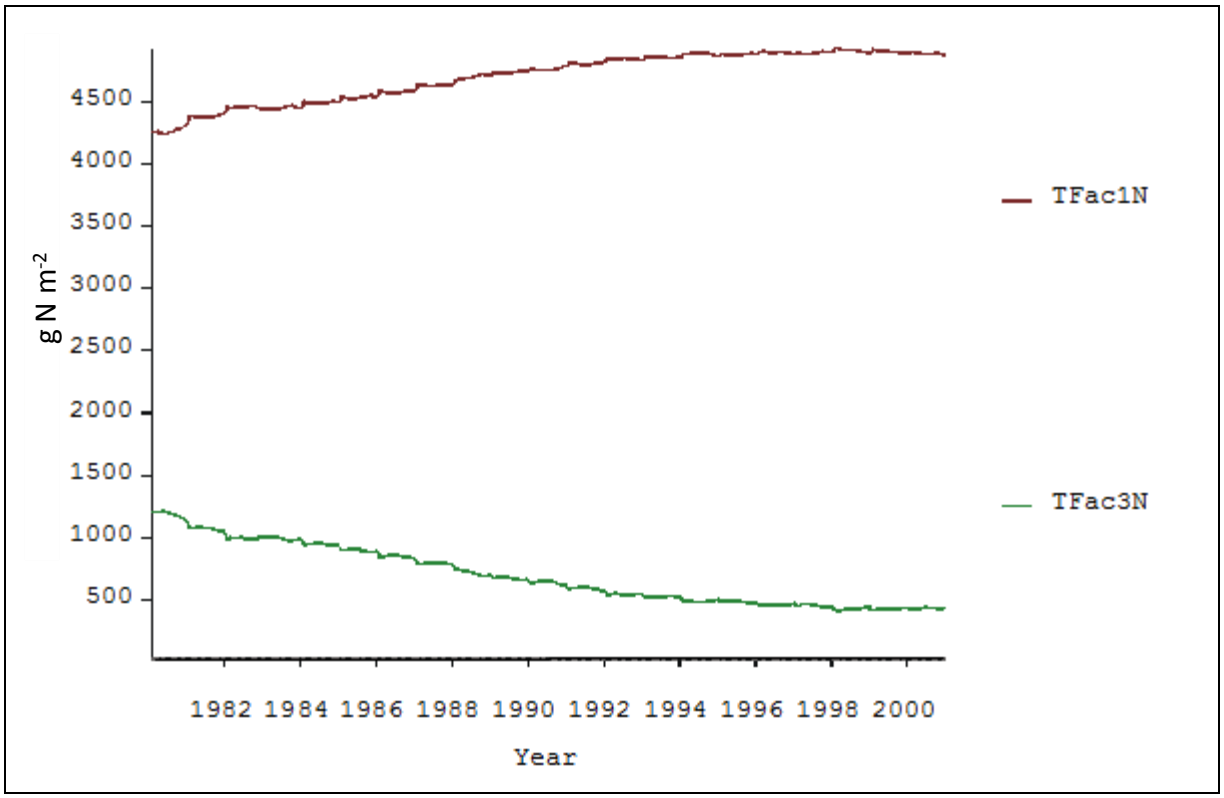

Figure 56: Changes in total N budgets (g m^{-2}) for herbaceous *Tfac1N* (red line) and shrub *Tfac3N* (green line) PFT's under the 1980-2000 REMO scenario (*in the diagnostic cell*).

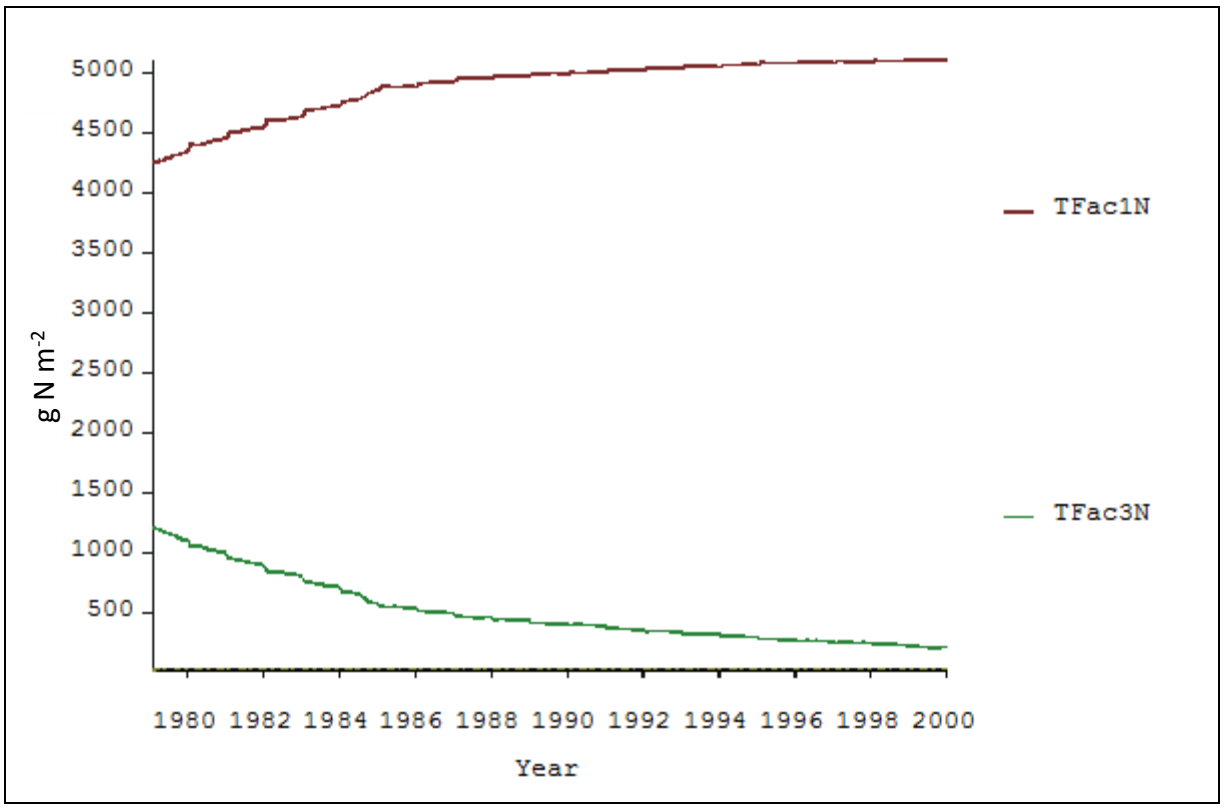

Figure 57: Changes in total N budgets (g m^{-2}) for herbaceous *Tfac1N* (red line) and shrub *Tfac3N* (green line) PFT's under the 1980-2000 Ouarzazate scenario (*in the diagnostic cell*).

Most likely, precipitation levels and temperatures favoured annual development instead of the growth of perennial shrubs, and animal preferences depleted shrub biomass. However, the differences between the two simulations were negligible.

Figure 58 (REMO) and Figure 59 (Ouarzazate) report average and maximum root water content (*rwc*) values over time. The input of higher rainfall in the REMO simulation was directly reflected by high average and maximum *rwc* values (about 0.02 and 0.10 mm per month, respectively). In the Ouarzazate simulation, rwc was probably more rainfall-driven, as indicated (for example) by the high rainfall in 1990. Whereas plants may be continuously supported by sufficient *rwc* levels under the REMO scenario, the Ouarzazate simulation predicts multiple years of very low *rwc* levels.

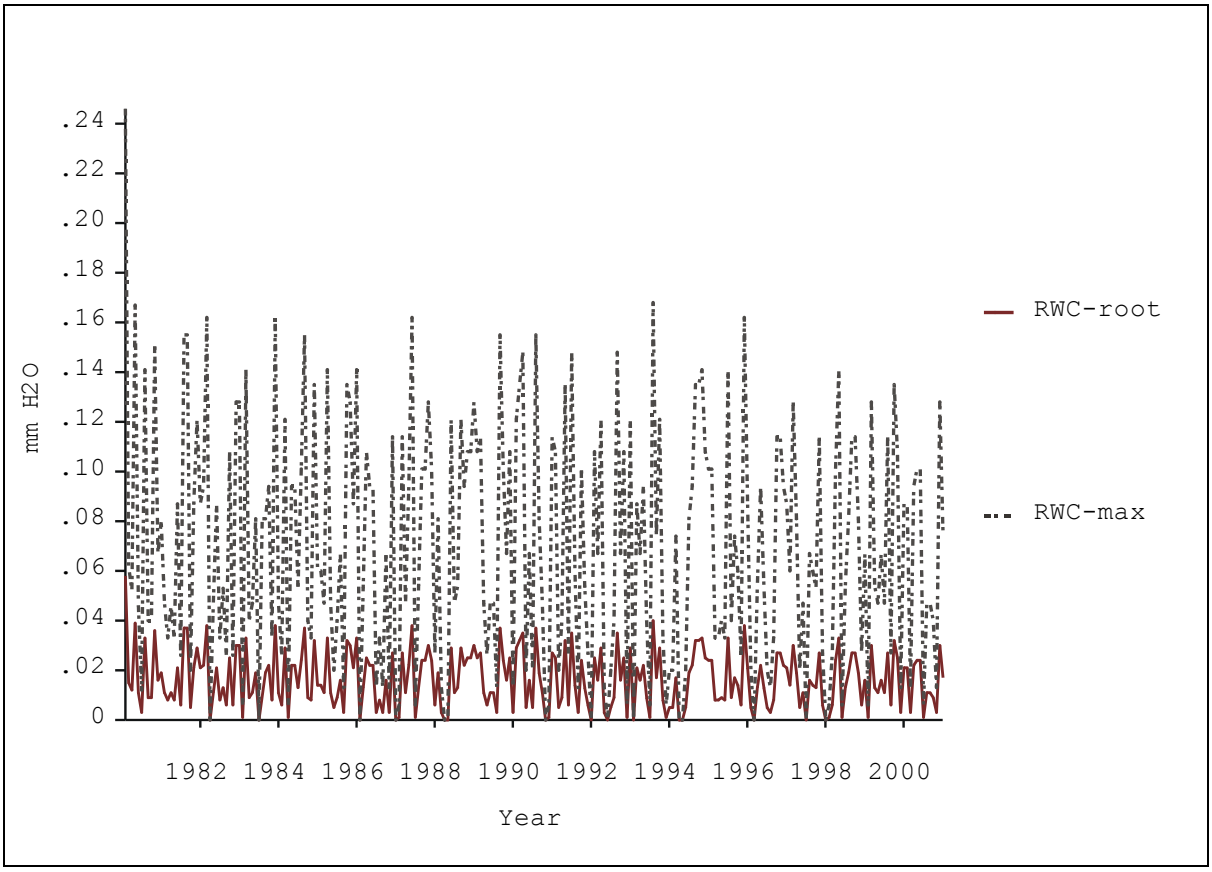

Figure 58: Simulated cumulative annual average *–root* (red line) and maximum *–max* (dashed blue line) root water content *rwc* (mm H_2O) under the 1980-2000 REMO scenario (*in the diagnostic cell*).

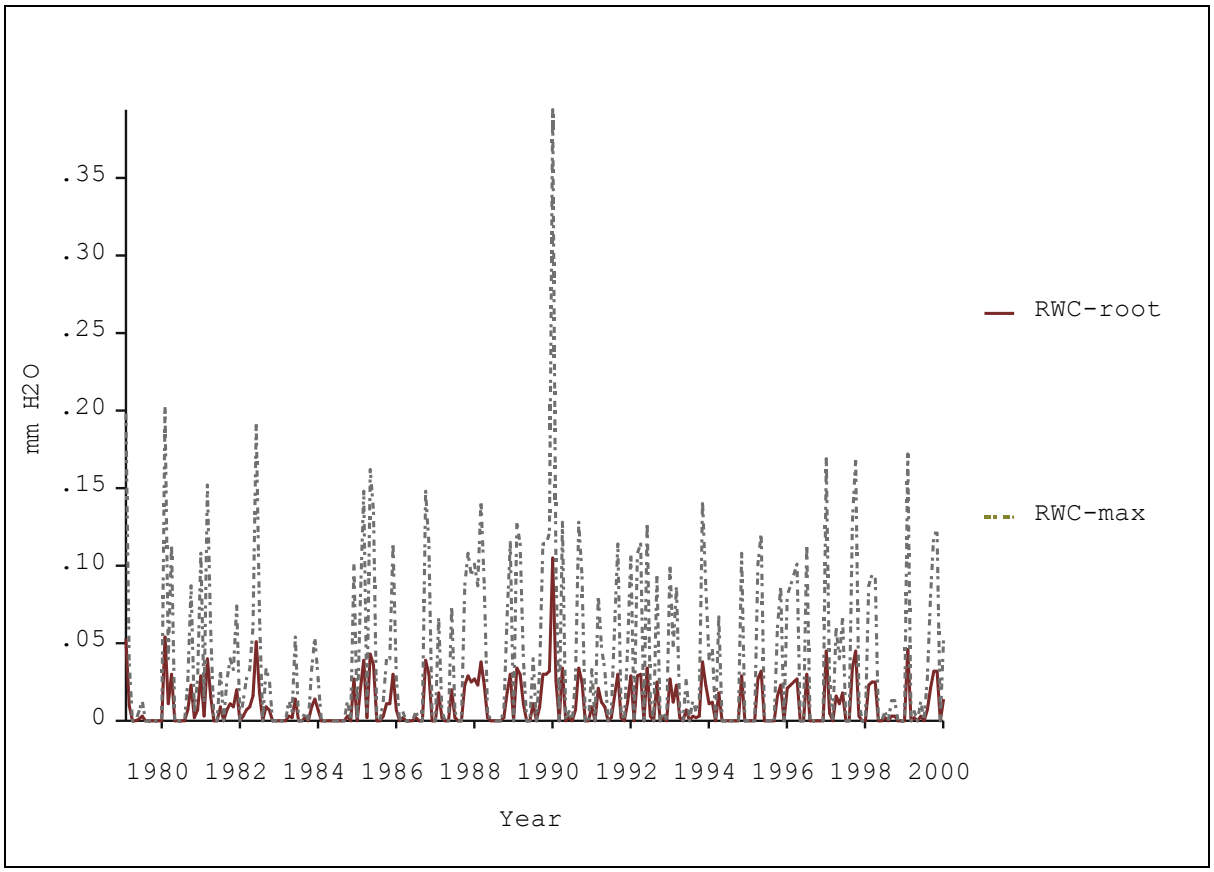

Figure 59: Simulated cumulative annual average *–root* **(red line) and maximum *–max*** **(dashed blue line) root water content *rwc*** **(mm H_2O) under the 1980-2000 Ouarzazate scenario (*in the diagnostic cell*).**

4.5.3 Base-line scenarios: Animal diets

In this section, the performance of grass, shrub and tree PFT's under grazing conditions is reported. First, we describe the change over time under the REMO scenario in the proportional amount of each PFT in the diets of sedentary sheep and goats in the summer range (May) (Figure 60). Next, we describe the same results for nomadic animals in the winter ranges (November) (Figure 61). The weighting factor indicates the proportion of energy intake needed to satisfy animal's daily energy requirements that is provided by each PFT (MJ $kg^{-1}d^{-1}$) (see section 2.5.2.4). These results are followed by a description of the summer and winter diets of nomadic and sedentary herds in the Ouarzazate simulations. To correctly evaluate the data on dietary proportions of herbaceous, shrub and tree PFT's, it is important to recall that there are twice as many nomadic animals as sedentary animals (Figure 39).

The REMO simulation (Figure 60) for the sedentary summer range started with a high weighting factor for the dietary proportions of all PFT's for sedentary sheep and goats. This

led to a sharp decline during the “warm-up“ phase of the model. A more equilibrium level was seen during the subsequent years of low rainfall in the mid-eighties. These conditions favoured the tree PFT (e.g., caused it to have a higher dietary factor) as a dietary alternative to grasses and shrubs, whose availability in the summer ranges was reduced.

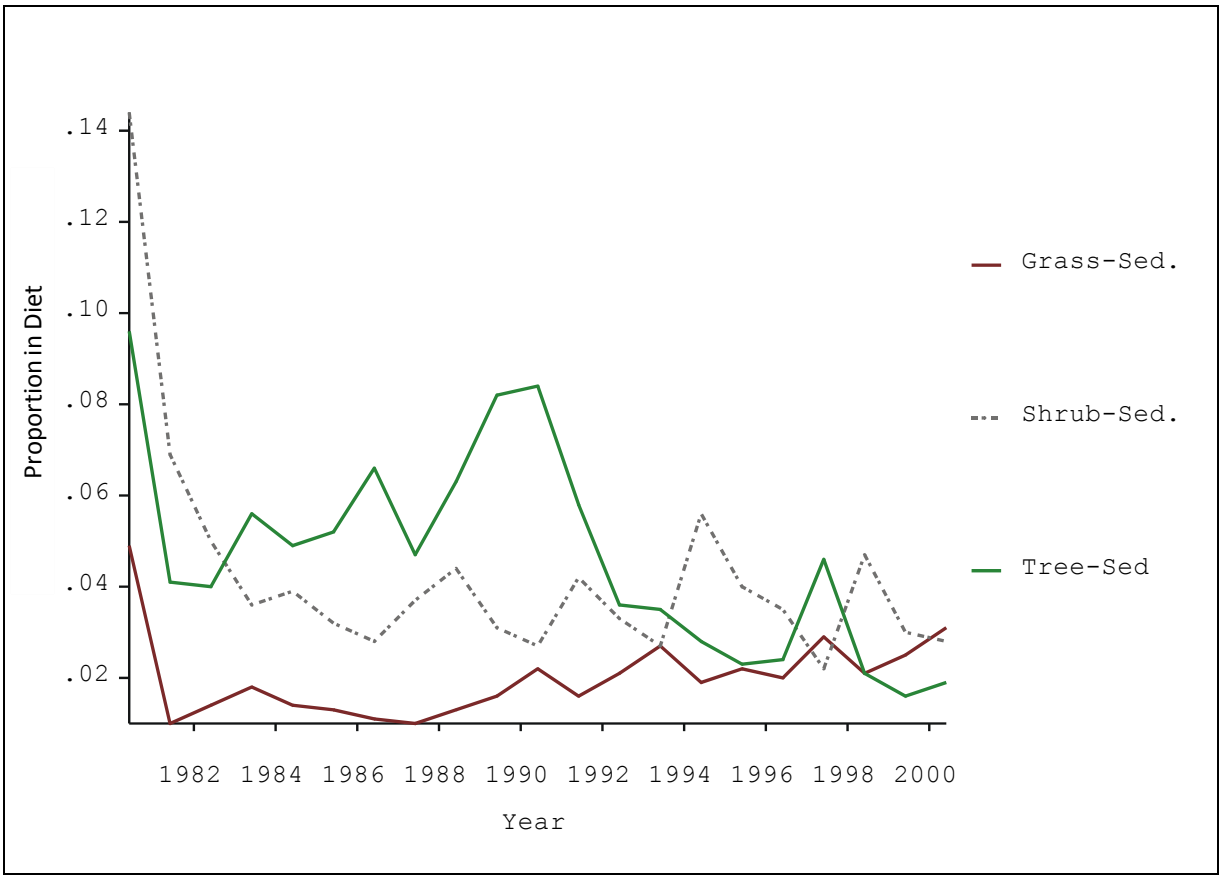

Figure 60: Monthly dietary proportions of grass (red line), shrub (dashed blue line) and tree (green line) PFT’s during the summer (May) for sedentary –*Sed.* sheep and goats under the 1980-2000 REMO scenario.

At the end of the simulation, all three PFT’s reached similarly low levels (shrub and grass dietary proportions of 0.03, tree dietary proportion of 0.02). The initial decline followed by a continuous increase of grasses in animal summer diets was remarkable.

A description of REMO plant PFT proportions in nomadic winter (November) diets follows (Figure 61). Due to their greater numbers and the availability of shrubs (flowering peak), nomadic animals showed higher preferences for shrubs than for the other two vegetation types. Shrub PFT varied within a consistent range during the model “warm-up“ phase but increased considerably during the final years of the simulation. Compared to the dietary proportion of shrubs, the dietary proportions of trees and grasses were negligible.

Figure 61: Monthly dietary proportions of grass (red line), shrub (dashed blue line) and tree (green line) PFT's during the winter (November) for nomadic *–Nom* sheep and goats under the 1980-2000 REMO scenario.

In the Ouarzazate simulation, nomadic summer diets were comparable to the nomadic winter diets described above. Figure 62 (May) show that the shrub PFT initially had a weighting factor of 0.10. Subsequently, the dietary proportion of the shrub PFT increased sharply to 0.35, resulting from the rains of 1990. In contrast, grass and trees composed about 0.05 of the diet of nomadic animals during the "warm-up" phase and then declined sharply, reaching a near-zero dietary proportion, as in the REMO simulation.

Next, we describe the proportions of each plant PFT in sedentary winter (November) diets (Figure 63). Initially, the shrub PFT because of its flowering peak composed the largest proportion of the diet (0.05), followed by the tree PFT (0.03). The grass PFT had a weighting factor of only 0.02. Following the "warm-up" phase of the model, the dietary proportion of the shrub PFT increased (largely due to the 1990 rainfall), reaching a final level 0.09. The dietary proportions of the grass and tree PFT's also increased due to rainfall, but their values were about 0.03 and 0.01, respectively. Grasses, however, showed a slight continuous increase in sedentary diets, whereas trees declined.

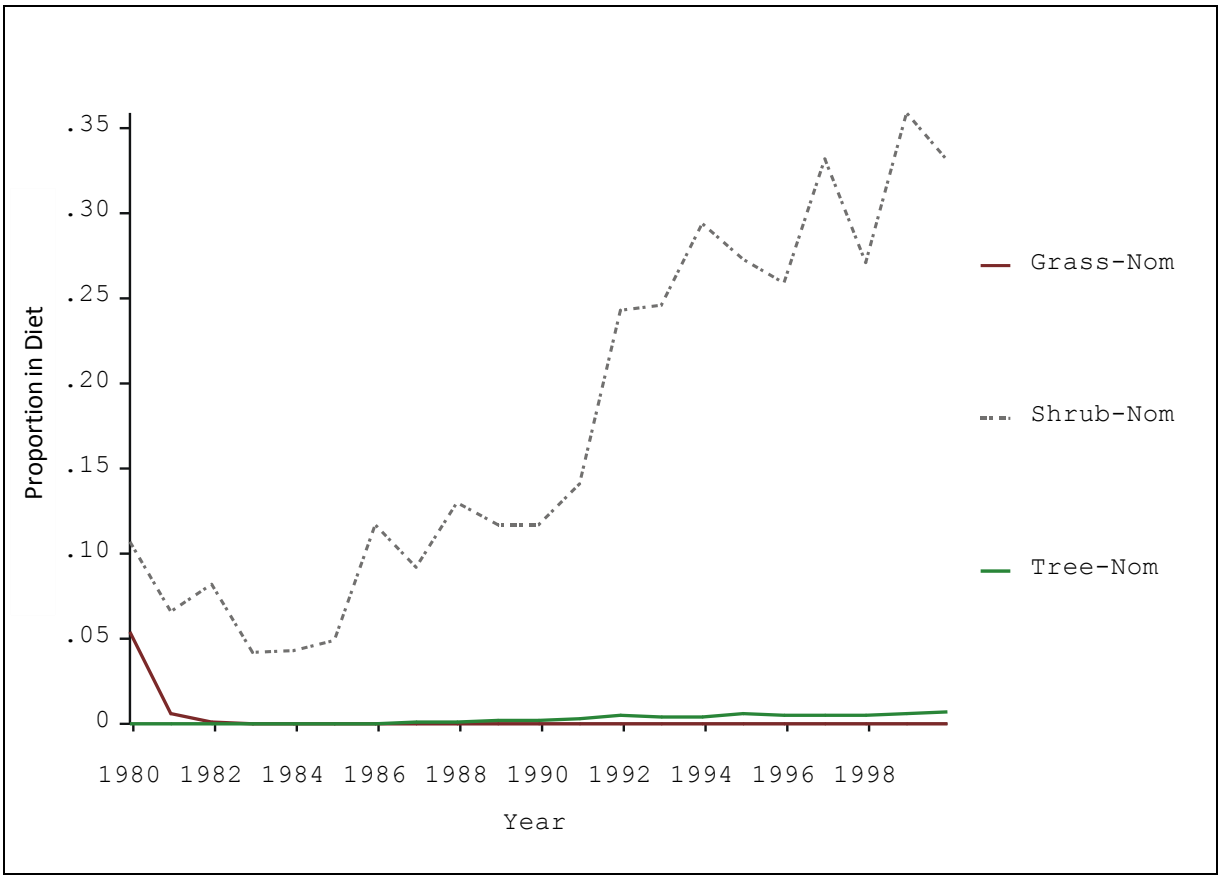

Figure 62: Monthly dietary proportions of grass (red line), shrub (dashed blue line) and tree (green line) PFT's during the summer (May) for nomadic *–Nom* sheep and goats under the 1980-2000 Ouarzazate scenario.

The aim of this section was to portray the selective character of nomadic diets, regardless of whether summer or winter diets were simulated. The high preference of nomadic animals for the shrub PFT was clearly seen in the simulations and is due primarily to the greater numbers and expanded ranges of nomadic animals. These preferences led to a decline of trees and grasses in the nomadic diet in both simulations, but also are thought to stimulated shrub growth. The proportion of shrubs in the diet was further affected by rainfall events in both runs. Sedentary diets (due in part to the much smaller number of animals) were more heterogeneous, but were also dominated by the shrub PFT during the winter. Winter is the peak of flowering for the shrub species simulated here, but the number of sedentary animals permits tree and herbaceous PFT's to also produce sufficient biomass during the winter to support sedentary diets. In sedentary summer diets, the tree PFT must satisfy animal needs if herbaceous and shrub biomass does not supply the necessary amount of energy due to low rainfall. This situation is inverted when rainfall permits the growth of more preferred shrubs and grasses in sedentary diets.

Figure 63: Monthly dietary proportions of grass (red line), shrub (dashed blue line) and tree (green line) PFT's during the winter (November) for sedentary –*Sed.* sheep and goats under the 1980-2000 Ouarzazate scenario.

These observations are supported by field observations, in which nomadic animals are forced to graze on shrubs, while trees and grasses are abandoned mainly because of total animal numbers. On the other hand, the number of sedentary animals probably permits a heterogeneous diet composed of grasses and trees in addition to shrubs.

4.5.4 Base-line scenarios: Water status

Water balance parameters reflecting system precipitation (*SysPpt*) and system potential evaporation (*SysPet*) (Figure 64 REMO, Figure 65 Ouarzazate) are discussed below.

SysPpt values (mm) are monthly sums, whereas SysPet is a cumulative monthly total in order to track the annual amount. The fact that the REMO simulation tended to show more homogenous annual rainfall amounts than the Ouarzazate simulation (discussed above; see Figure 41) was also reflected in the SysPpt values.

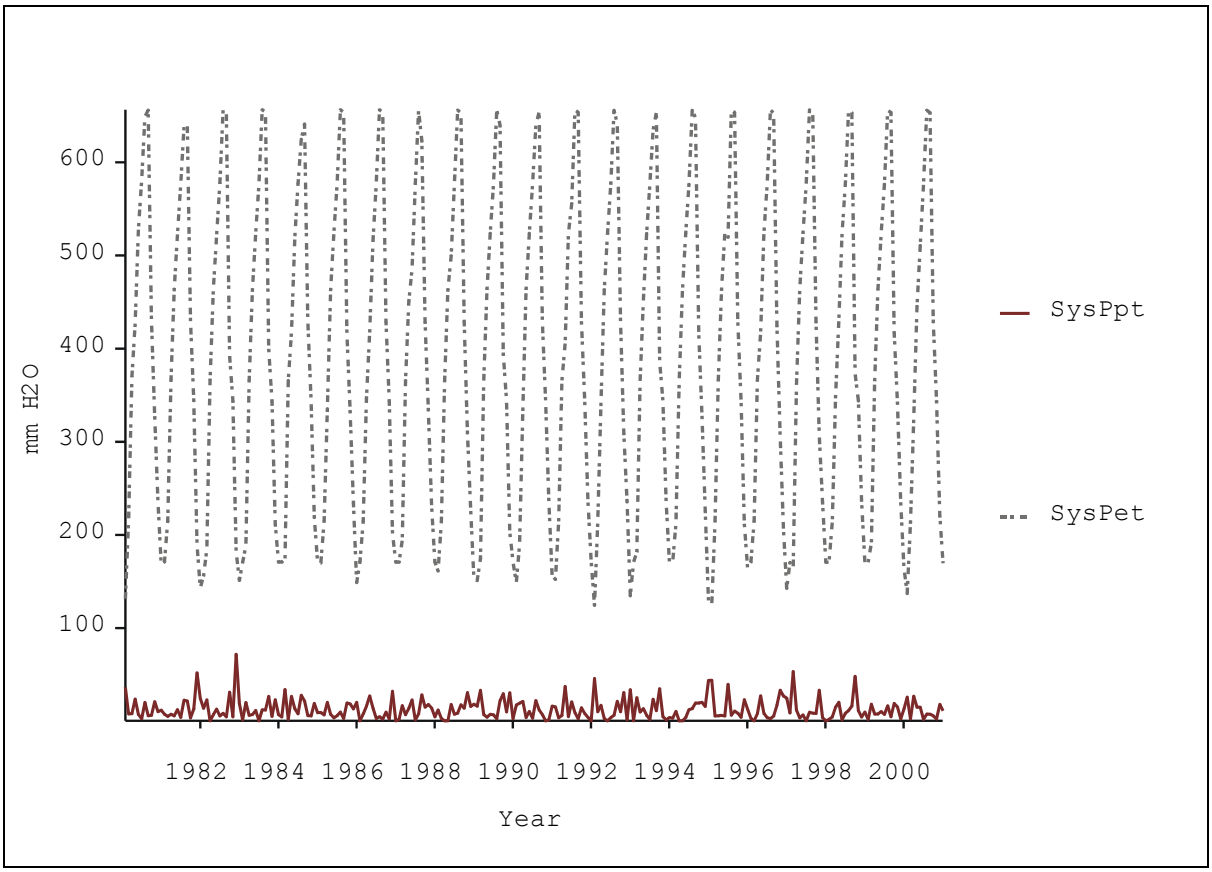

Figure 64: Simulated monthly precipitation *SysPpt* (mm H_2O, red line) and cumulative annual predicted potential evapotranspiration *SysPet* (mm H_2O, dashed blue line) under the 1980-2000 REMO scenario.

The monthly *SysPet* rates varied between 150 and 650 mm in the REMO simulation and between 200 and 800 mm in the Ouarzazate simulation. The range of *SysPet* rates in the Ouarzazate simulation was greater than that in the REMO simulation, even with smaller *ANPP* amounts for each PFT. This may reflect greater water limitation but more efficient plant water consumption performance under the Ouarzazate scenario.

The above assumptions were evaluated using the performance of predicted monthly transpiration (*trans*) by all three PFT's (Figure 66) during February, May, August and November of each year from 1979-2000.

The *trans* and bare soil evaporation (*Bsev*, Eq. 27), values at the cell level (see section 2.4.2) are a result of monthly incoming rainfall amounts. In the REMO simulation the t*rans* was constant and greater than in the Ouarzazate scenario. The amounts showed a continuously increasing trend in the Ouarzazate simulation whereas the *trans* patterns in the REMO simulation may be explained by the wide monthly distribution of rainfall (c.p. Figure 41). These may enable plants to maintain a continuous level of *trans*. In contrast, for the Ouarzazate run *trans* levels were highly variable but were able to increase. In these simulations, 90-100% of incoming *SysPpt* evaporated and transpired from ground layer to the atmosphere due to the above mentioned water balance equation.

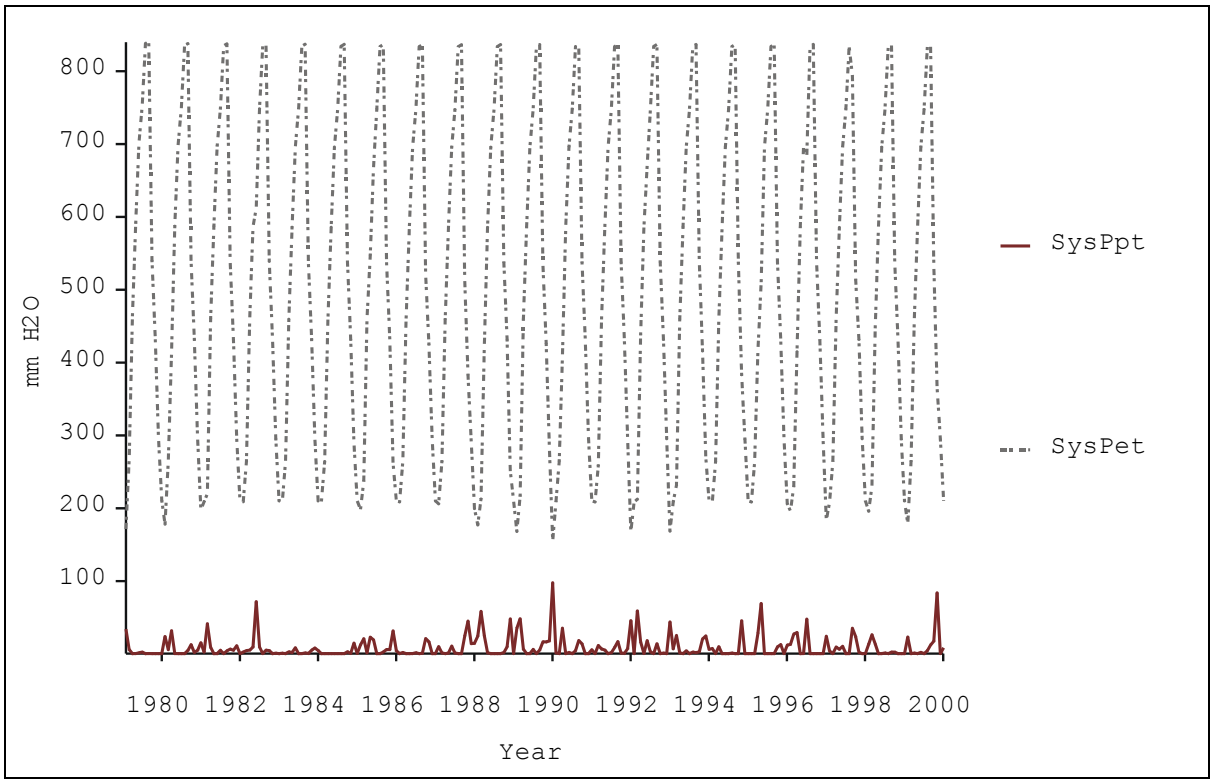

Figure 65 Simulated monthly precipitation *SysPpt* (mm H_2O, red line) and cumulative annual predicted potential evapotranspiration *SysPet* (mm H_2O, dashed blue line) under the 1980-2000 Ouarzazate scenario.

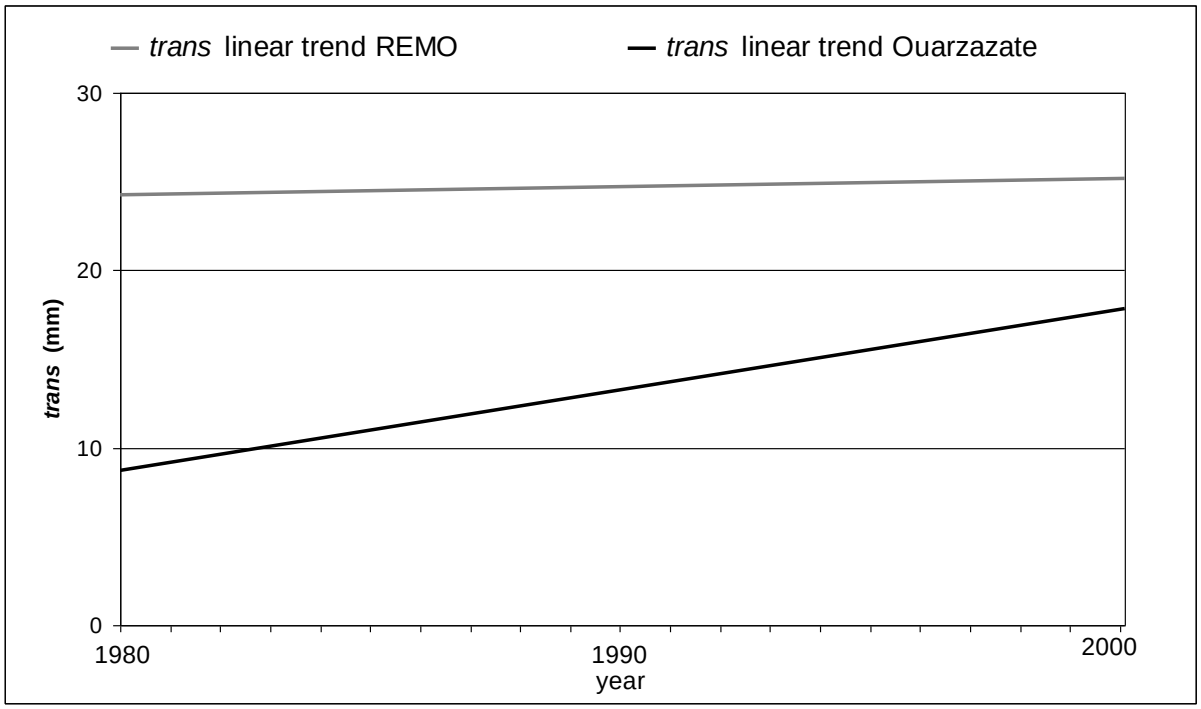

Figure 66 Monthly (February, May, August and November) predicted linear trend of transpiration *trans* (mm) for the Ouarzazate (black line) and REMO 1980-2000 simulations (grey line).

The next section compares four scenarios driven by IPCC A1B and B1 with various fixed livestock numbers for heavy, medium and light stocking rate in the Basin of Ouarzazate.

4.6 Scenarios for the Basin of Ouarzazate

Based on evaluation of historic and recent patterns of vegetative cover and growth under the base-line scenarios, we now present simulations of the impacts of livestock number, climate and range exclusion on vegetative growth and cover patterns under future scenarios. We used the IPCC A1B and B1 scenarios for 2001-2051 (IPCC 2007a) with regional meteorological characteristics (REMO) included as climatic driver variables.

This section first presents three scenarios (2a, 2b and 2c,) simulated for the Basin of Ouarzazate (Table 31). Here, temporal outcomes are described without the effect of range exclusion. The spatial impact of one “range exclusion“ plot compare to “no range exclusion“ is characterised in section 4.6.5. The diagnostic cell as characterised by soil type no. 24 (see Appendix, Tables 35 and 36) and vegetation type no. 9 (Figure 11) at an elevation of 1397 m a.s.l. Our objective was to determine the temporal variation in vegetative performance responses to constant livestock numbers, range exclusion and climate scenarios and to compare these to the base-line scenario.
These three scenarios differ by the climatic input parameters from IPCC A1B (scenario 2a) and B1 (scenario 2b) as well as by heavy stocking rates of 350,000 sedentary and 550,000 nomadic sheep and goats for scenario 2c (which assumed IPCC A1B climate parameters). Stocking rates of 200,000 sedentary and 400,000 nomadic sheep and goats were assumed instead for scenarios 2a and 2b. These different grazing intensities and climatic conditions are evaluated in the following sections.

4.6.1 Plant growth

As above (section 4.5.1), the change over time in *ANPP* is shown first to ensure comparability to the base-line and other scenarios. *ANPP* is divided among herbaceous, shrub and tree (woody) PFT’s (Table 32).
Like those described in the previous sections, the simulations described in this section showed a “warm-up“ phase during the first ten years. After this phase, the IPCC A1B (2a) scenario showed a continuous increase in *ANPP* (g m^{-2}) for all PFT’s, followed by a break, and then an increasing tendency again. Scenario 2b showed a decreasing trend in *ANPP* for shrub and woody PFT’s, but the herbaceous PFT maintained constant at *ANPP*. For scenario 2c, *ANPP* of the shrub PFT was predicted to decrease strongly, while herbaceous and woody PFT’s maintained constant low *ANPP* levels of 3 g m^{-2} and <1 g m^{-2}, respectively.

Under the B1 (2b) scenario, the herbaceous PFT reached only approximately half of the final predicted *ANPP* of A1B (2a). Scenario 2c showed only one third of the final herbaceous *ANPP* of scenario 2a. Whereas *ANPP* of the shrub PFT held constant level at about 25 g m^{-2} under scenario 2a (Table 32), shrub *ANPP* decreased by 10 g m^{-2} under scenario 2b and strongly declined under scenario 2c from 25 g m^{-2} to 10 g m^{-2}.

Scenario 2a yielded a final *ANPP* of 2 g m^{-2} for the woody PFT, while scenario 2b yielded a final woody *ANPP* of about 1 g m^{-2}. Woody *ANPP* was < 1 g m^{-2} during the entire simulation period under scenario 2c.

The tendency of simulated PFT's to reach a constant level either by climatic impact or due to animal dietary preferences was remarkable. In addition, a large intra-annual fluctuation was observed for the *ANPP* of all three PFT's. Different stocking rates were responsible for the large differences in *ANPP* between the two IPCC A1B scenarios (2a and 2c).

Figure 67 summarises the total cumulative *ANPP* of herbaceous and shrub PFT's during the 50-year simulations. All three scenarios produced a large decline in total *ANPP*. As expected, the greatest decline was predicted for the A1B scenario (2c). The smallest decline was predicted for the A1B scenario (2a). Total *ANPP* was lower under the scenario 2b than under scenario 2a. This may be explainable by different climate constraints included in this scenario.

Table 32: Comparison of initial and final ANPP (g m^{-2}) levels for the Basin of Ouarzazate under scenarios 2a-2c.

Scenario / **avg. ANPP (g m^{-2})**		**2a**	**2b**	**2c**
herbaceous	initial	8	8	8
	final	10	5	3
shrub	initial	25	25	25
	final	20	18	8
woody	initial	3	3	3
	final	2	1	<1

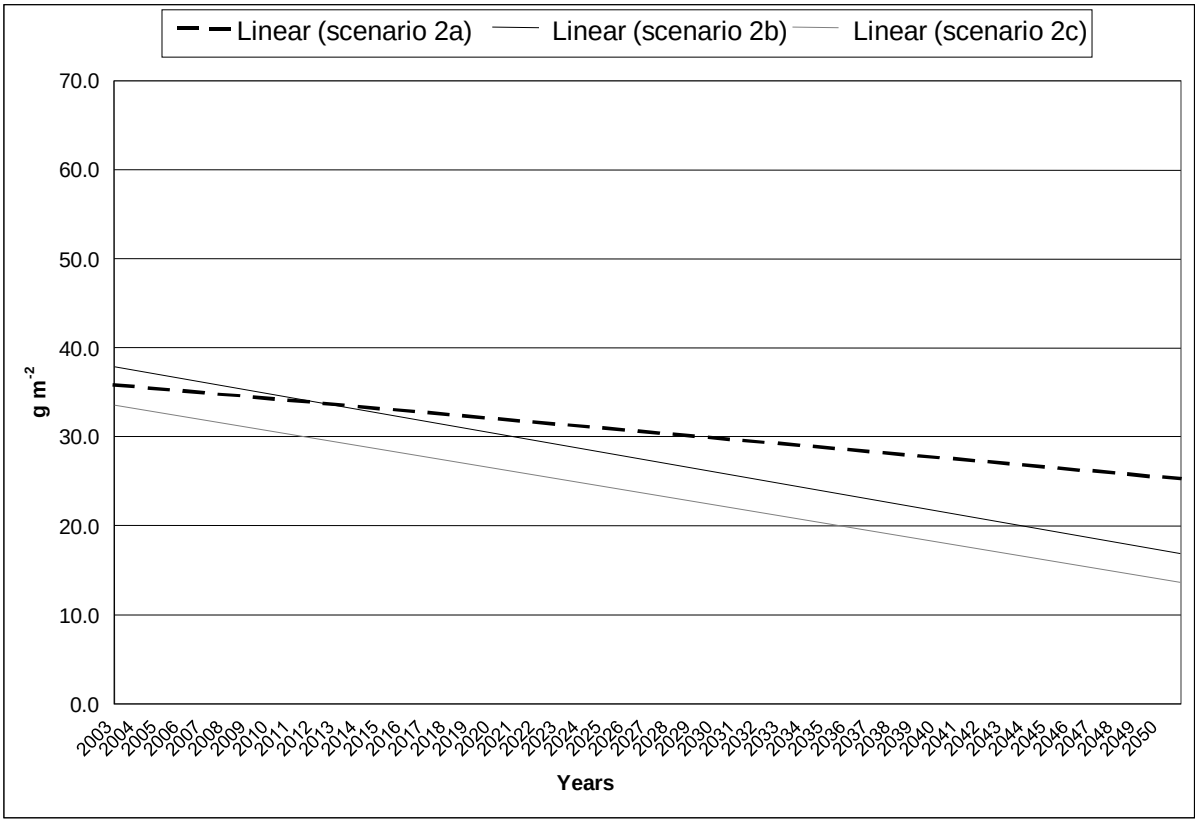

Figure 67: Linear trends in Annual Total *ANPP* (herbaceous and shrub PFT's, g m^{-2}) under scenarios 2a-2c.

The large variation in *ANPP* of herbaceous and shrub PFT's was also seen in the changes over time in *BNPP* (see section 4.5.1). Interestingly, shrub *BNPP* was equal to or greater than *ANPP* at certain time steps under both climate scenarios. This may indicate either continuous overgrazing or water and nutrient limitations. *BNPP* of the herbaceous PFT is constant at about two thirds of herbaceous *ANPP* under scenarios 2b and 2c and remains constant even when *ANPP* increases under scenario 2a.

Generally, herbaceous leaf production differed between scenarios 2a and 2b (data not shown). This was mainly due to the outstanding leaf growth of the "fine grass" (Table 9) PFT species that seems to be favoured under A1B climate constraints. The B1 scenario (2b) and scenario 2c showed slightly lower levels of herbaceous leaf production. However, the two A1B scenarios (2a and 2c) showed large differences in herbaceous leaf production. Herbaceous leaf biomass was reduced in scenario 2c because of the increased livestock numbers. All simulations showed a serious decrease in "coarse grass" leaf production from 5.0 g m^{-2} to 0.25 g m^{-2} by 2050. Again, "coarse grass" leaf biomass was overestimated in the parameterisation process, which was justified by the environmental constraints in the simulation. The "fine grass" leaf biomass was also subject to large inter-annual variations. Under scenario 2a, it fluctuated between 1.5 g m^{-2} and 3.0 g m^{-2} whereas scenarios 2b and 2c showed no similar increase, but "fine grass" leaf production varied between 0.5 g m^{-2} and

2.0 g m^{-2}. The ”alpine grass” leaf biomass amounts decreased greatly in the beginning of the simulation and then remained constant at about 0.5 g m^{-2} showing no striking differences between scenarios. The ”alpine grass” productivity is probably limited by its restricted growth area at higher altitudes. Again, ”fine grass” leaf biomass, which occupies the largest (parameterised) ground cover area, showed the best adaptability to both grazing and climatic constraints.

Herbaceous root production of ”fine-”, ”alpine-” and ”coarse grass” is described next (Figure 68). After the “warm-up“ phase, all grasses showed a tremendous decrease in root biomass (g m^{-2}) under all scenarios. Differences in these declines occurred only at the scale of 1.0 g m^{-2}. However, the largest decrease was found for ”coarse grass”, from about 80.0 g m^{-2} initially (in all three scenarios) to a stable level of about 3.0 g m^{-2} at the end of run. The ”fine grass” root biomass also declined by about one quarter of its initial value, to about 5.0 g m^{-2} for scenarios 2b and 2c. Under scenario 2a, ”fine grass” root production increased and then remained constant at a level of about 10.0 g m^{-2}. The ”alpine grass” root production decreased under all scenarios to about 0.5 g m^{-2}. Except for the A1B exclusion scenario (2a), a level of 0.5-2.0 g m^{-2} was predicted.

Figure 69 shows predicted leaf production (g m^{-2}) for the shrub PFT’s ”evergreen”, ”low DMD-” and ”sage shrub”.

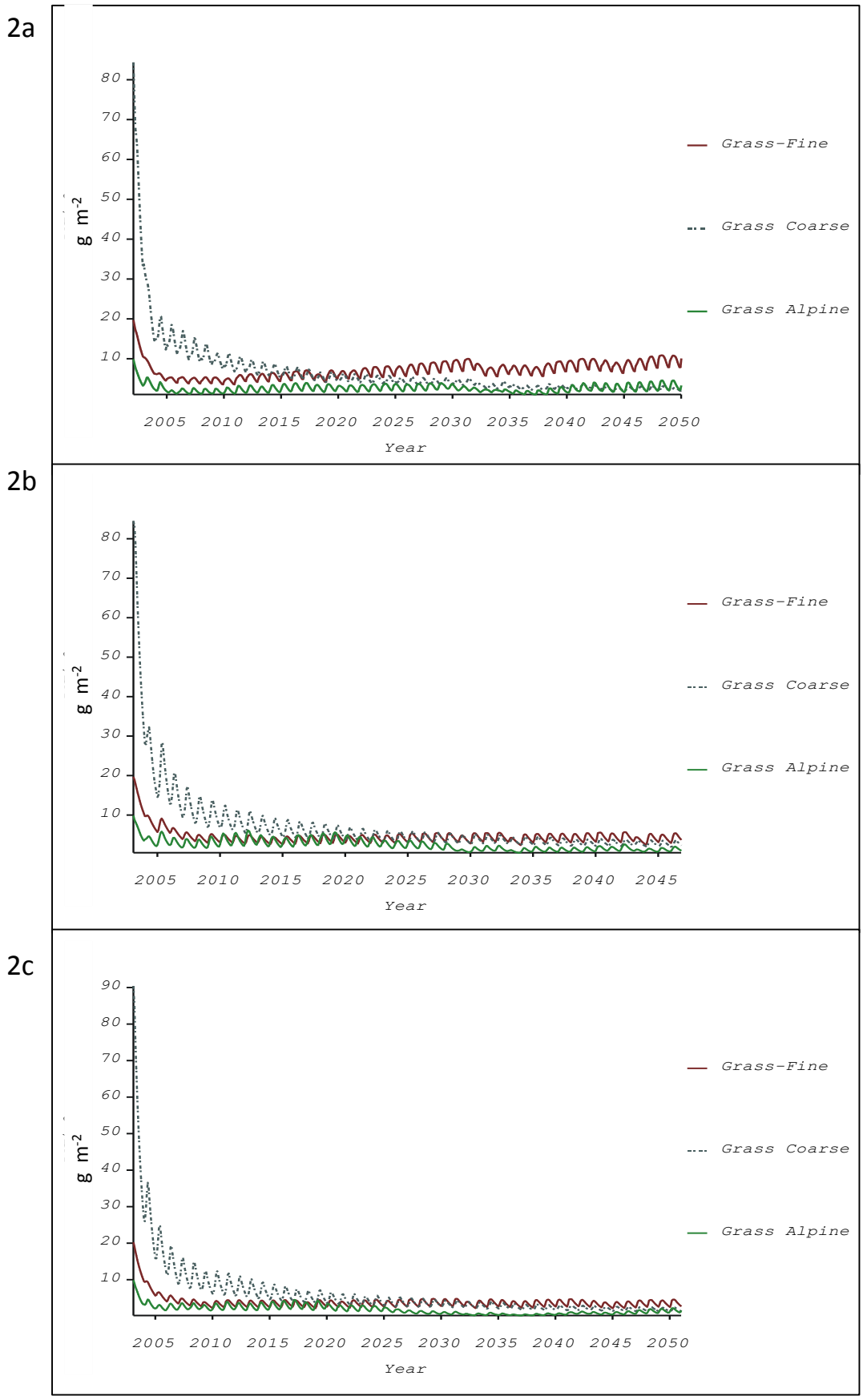

Figure 68: Monthly cumulative and annual growth of roots (g m^{-2}) of "fine grass" (red line), "coarse grass" (dashed blue line) and "alpine grass" (green line) for scenarios 2a (A1B climate scenario, 2001-2050), 2b (B1 climate scenario, 2001-2048) and 2c (A1B, heavy stocking rate scenario).

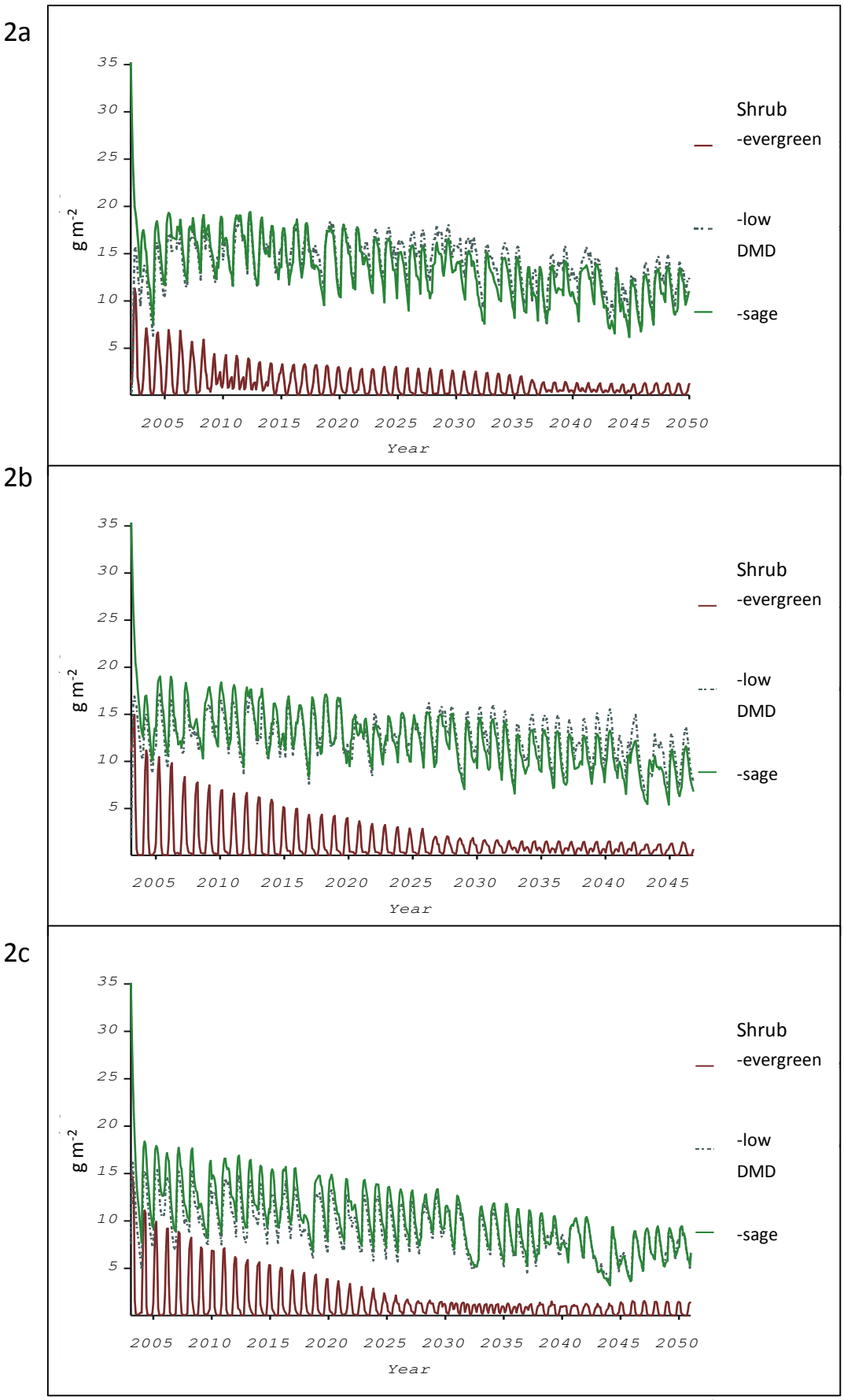

Figure 69: Monthly cumulative and annual growth of leaf biomass (g m^{-2}) of "evergreen-" (red line), "low DMD-" (dashed blue line) and "sage shrub" (green line) under scenarios 2a (A1B climate scenario, 2001-2050), 2b (B1 climate scenario, 2001-2048) and 2c (A1B heavy stocking scenario).

The ”evergreen shrub” leaf production showed the strongest decrease, from 10.0 g m^{-2} to 1.0 g m^{-2} or less under all scenarios. The ”low DMD shrub” leaf production declined to half its initial value under scenario 2c. The other scenarios (2b and 2d) showed a moderate decline in “low DMD shrub” leaf biomass, from 15.0 g m^{-2} to about 12.0 g m^{-2}. Scenario 2a showed the smallest decline in “low DMD shrub” leaf from 15.0 g m^{-2} to about 13.0-14.0 g m^{-2}.
The ”low DMD shrub” leaf production was equal to or ultimately greater than “sage shrub” leaf production, except under scenario 2c. Nevertheless, the similarity between “low DMD-” and ”sage shrub” leaf production is obvious. Similar adaptation strategies of both shrub classes probably facilitate continuous leaf production under these climatic and environmental conditions. The higher digestibility of “sage shrub” leaves in comparison to ”low DMD shrub” leaves may explain the slight difference observed between these two PFT’s.
The patterns described above were paralleled by the development of ”evergreen-”, ”low DMD-” and ”sage shrub” root biomass (data not shown). Under the simulated climatic conditions, “evergreen-” and “sage shrub” root biomass declined to stable levels after 50 years of simulation. The ”evergreen shrub” root biomass declined considerably, to <1.0 g m^{-2}. The ”low DMD shrubs” were able to increase their root biomass at first, but they too declined after 50 years of simulation, except under scenario 2c, in which “low DMD shrubs” increased their root biomass by one third of the original value. The root biomass production of “sage-” and ”low DMD shrubs” was similar (as for leaf production). However, different levels of biomass production were predicted for these two shrub PFT’s. The ”low DMD shrub” root biomass was greater by 5.0 g m^{-2} to 15.0 g m^{-2}. Under the B1 scenario (2b), this difference was even greater. Under the A1B scenario (2a), in contrast, the difference between these two shrub PFT’s was smaller. However, scenario 2c predicted a consistent difference between the root biomass production of ”sage-” and ”low DMD shrubs”.

4.6.2 Nitrogen cycle and Nitrogen budget

The *N:B* ratio is an indicator of the conversion of nutrients to biomass (see section 4.5.2). Here, it was observed at the level of PFT’s for ”fine-”, ”coarse-” and ”alpine grasses” (data not shown). During the model “warm-up“ a considerable decline in the *N:B* ratio was observed for all three grass PFT’s under all three scenarios, from 1.8 initially to a stable level of 0.1 to 0.3. This was consistent with the decreasing trend in herbaceous *ANPP* during the same period (see previous section). Because of the discrepancy between grass biomass production parameters in the simulation, N content probably also had to undergo a regulation during this phase. The *N:B* ratio of “coarse grass” reached amounts <0.05 under all three scenarios. The *N:B* ratios of ”alpine grass” and ”fine grass” were fixed at 0.1 under scenarios

2b and 2c. Under scenario 2a (A1B climate scenario), the *N:B* ratio of ”fine grass” increased steadily reaching a final fixed value of 0.3. Lower *N:B* ratios may indicate an adaption of biomass production in the presence of low N pools. An *N:B* ratio of 0.01 to 0.3 seems to be the adaptive level for the simulated grasses.

The *N:B* ratios for the ”evergreen-”, ”low DMD-” and ”sage shrub” PFT’s under the three scenarios are described next (data not shown). The highest *N:B* ratios were predicted for “sage shrub” species, as this group probably benefits most from the climatic conditions of IPCC B1 (scenario 2b). This PFT maintained a constant *N:B* ratio of 1.6. This seems to indicate a supply of N compared to biomass that is sufficient for shoot growth. In contrast, the A1B scenario (2a) caused the *N:B* ratio of “sage shrub” to decrease slightly, to 1.4. Under the A1B scenario with heavy grazing (2c), the *N:B* ratio of “sage shrubs” declined by half its initial value, to 0.8. Most remarkable, however, was the strong decline in *N:B* ratio of ”low DMD shrubs”, from an initial value of 1.2 to a final value of 0.3 under all three scenarios. The magnitude of this decline was similar under all three scenarios. The *N:B* ratio of “evergreen shrubs” was fixed at 0.2 under scenarios 2b and 2c. In the A1B scenario (2a), the *N:B* ratio continuously increased to double its initial value (0.4). “Sage shrubs” showed high competitive ability in consuming predicted N pools, probably due to their dominance in the simulated community. This was similar to the results found for “sage shrub” leaf production (Figure 69). “Low DMD-” and ”evergreen shrubs”, in contrast, may be forced to consume less N. Nevertheless, “low DMD shrubs” may be able to maintain constant biomass comparable to that of “sage shrubs”, regardless of low *N:B* ratio. “Evergreen shrubs” may be forced to reduce their biomass. The performance of “low DMD shrubs” may be explained by their unpalatability, while the high palatability of “evergreen shrubs” exacerbates the effects of low *N:B* ratios, resulting in low productivity.

Figure 70 shows the change over time in *N:B* ratios at the plant (*Pl-N:B*), active biomass (*Act-N:B*) and leaf (*Lf-N:B*) levels. Differences between scenarios 2a and 2b in *N:B* ratios at *Pl-N:B*, *Act-N:B* and *Lf-N:B* levels were negligible. The strong inter-annual variations under scenarios 2a and 2b, up to a ratio of 0.014 for *Lf-N:B*, were remarkable. *Pl-N:B* and *Act-N:B* ratios were within ranges of 0.01 to 0.016 and 0.014 to 0.020 for scenarios 2a and 2b, respectively. Ratios between 0.013 and 0.026 represent an equilibrium range within which plants can maintain a constant leaf N allocation and transmission to biomass.

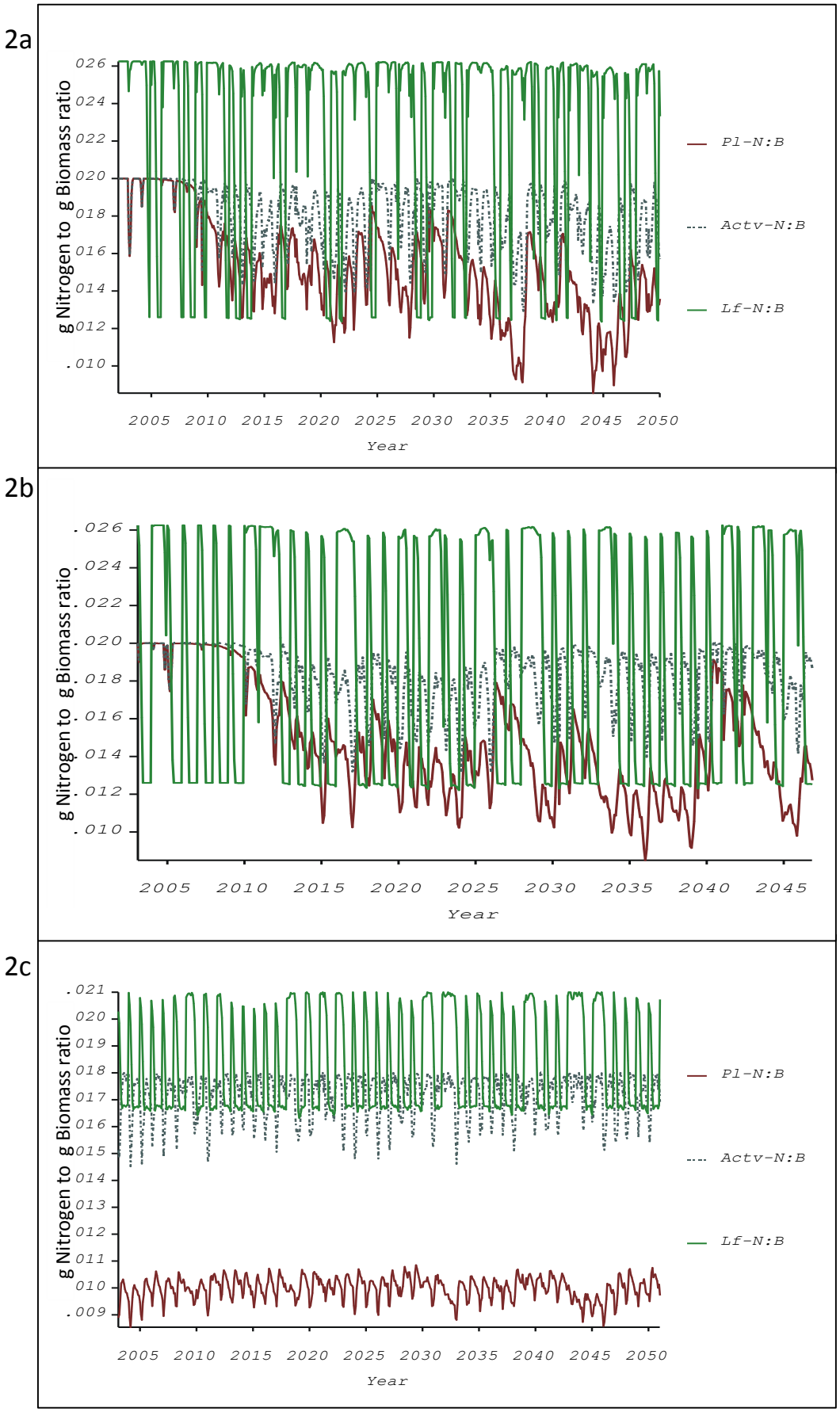

Figure 70: Monthly cumulative changes in nitrogen to biomass ratio (*N:B*) for plant *Pl-N:B* (red line), leaf *Lf-N:B* (green line) and active *Actv-N:B* (dashed blue line) levels for scenario 2a (A1B climate scenario, 2001-2051), 2b (B1 climate scenario, 2001-2048) and 2c (A1B, heavy stocking rate).

A different picture was shown by scenario 2c, under which the *Pl-N:B* ratio was about 0.010 less than that given above. The *Lf-N:B* ratio ranged between 0.021 and 0.017. These narrow ranges compared to scenarios 2a and 2b indicate possible difficulties of plants under scenario 2c in satisfying their demand for N during growth periods. This was probably due mostly to excessive depletion of biomass because of the high animal stocking rates. Alternatively, the large ranges found under scenarios 2a and 2b may indicate the ability of plants to maintain an *N:B* ratio sufficient for plant growth. These ranges indicate the sensitivity of plants to local N budgets and the allocation of N, which is subject to large temporal fluctuations.

4.6.3 Animal condition

The following section describes the predicted animal-specific outcomes of the simulations. Animal condition index (*CI*) values (see section 2.4.4) for sedentary and nomadic sheep and goats under all three scenarios are shown in Figure 71. A constant *CI* was reached after the ten years of model “warm-up“ under scenario 2a. Under this scenario, nomadic and sedentary sheep and goats were found to be at approximately the balanced normal index of 1.0, but *CI* varied considerably within years (as in all three scenarios). Hence, animal condition was determined to be good in terms of diet composition and water availability during the simulation. *CI* declined after 40 years to 0.95 under scenario 2a; under scenario 2b, it declined to a more critical level of 0.85, especially for sedentary sheep and goats. These levels characterise time steps at which animals did not meet their energy requirements due to water and diet restrictions. An even more critical situation was found under the heavy stocking rate scenario (2c). Under those conditions, the *CI* of both nomadic and sedentary sheep and goats declined considerably during the “warm-up“ phase. At a stocking rate of 900,000 animals, a *CI* of 0.0 was reached. This means that the number of animals was normalised to a lower level due to water and diet constraints. However, this number is no longer indicated by a *CI* (see section 2.4.4). The results indicate, first, that a stocking rate of total 600,000 animals is a good assumption for the area based on climatic scenarios, water availability and dietary composition. Second, a heavy stocking rate of 900,000 animals is not supported by edible biomass and water availability under IPCC climate scenario A1B.

Next, we describe the patterns of consumption of herbaceous biomass by sedentary and nomadic sheep and goats (data not shown). These figures determine the conversion of the *CI* to the biomass needs of animals. Under scenario 2a, herbaceous biomass increased, so that nomadic sheep and goats could meet their requirements by the consumption of

herbaceous biomass alone. Nevertheless, herbaceous biomass decreased if the needs of sedentary sheep and goats were also considered. Scenario 2a showed a severe reduction of both sedentary and nomadic sheep and goat numbers, together with a sharp decline in edible biomass. For scenario 2b, edible biomass decreased but is reached a constant level. Because of the constant animal numbers in scenarios 2a and 2b scenarios, herbaceous biomass consumed by sheep and goats was stable. Under the heavy stocking rate scenario (2c), animal consumption greatly exceeded herbaceous production. Here, nomadic sheep and goats consumed the largest amounts of herbaceous biomass due to their heavy stocking rate of 900,000 animals. Thus, shrubs had to provide the additional forage for nomadic sheep and goats.

These outcomes underline the severe forage situation for grazers in terms of herbaceous biomass availability, consistent with the *CI* results.

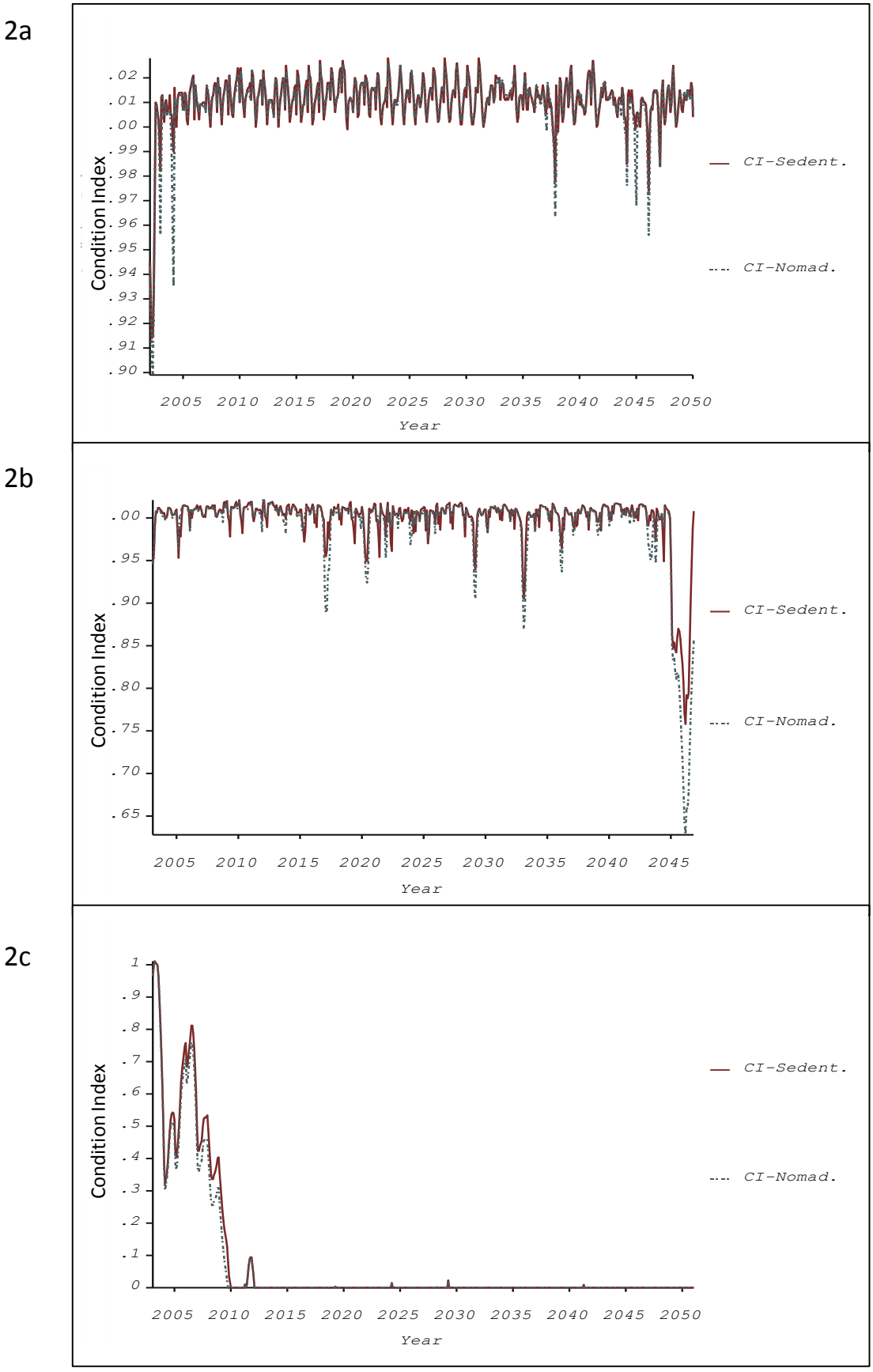

Figure 71: Condition Indeces (*CI's*) for nomadic *Nomad.* (dashed blue line) and sedentary *Sedent.* (red line) sheep and goats for scenarios 2a (A1B climate scenario, 2001-2051), 2b (B1 climate scenario, 2001-2048) and 2c (A1B heavy stocking rate).

The dietary proportions of grasses and shrubs (formulated as weighting factors) during the summer (May) for sedentary and nomadic sheep and goats are described next (Figure 72). The weighting factor indicates the proportion of energy intake via shrubs and grasses to satisfy daily animal energy requirements (MJ kg^{-1} d^{-1}) (see section 2.4.4). Shrubs provided the largest proportion of the nomadic diet in all three scenarios. However, shrub consumption by nomadic sheep and goats had a weighting factor of 0.60 (out of 1.0) under scenario 2a and only 0.24 under scenario 2c. Shrub growth is subject to large inter-annual fluctuations, which is reflected by the variation in the proportion of shrubs in the diet. Shrub species tend to recover even after periods of heavy decline, e.g., due to lack of rainfall. The weighting factor of shrubs for sedentary sheep and goats declined from an initial value of 0.16 for scenario 2a and 0.06 for scenario 2c to a final value of 0.03 for both scenarios. This was probably due mostly to the greater consumption of edible shrubs by nomadic sheep and goats. Under the B1 scenario (2b), the weighting factor for shrubs remained constant at an average of about 0.10. In the sedentary diet under scenario 2b, grasses maintained a constant low proportion of approximately 0.02. The proportion of grasses in nomadic diets during the summer (and winter) was close to zero (see section 4.5.4). The weighting factor of shrubs in the sedentary diet declined from an initial value of 0.12 to a final value of 0.02. The change in weighting factors in nomadic diets was probably caused by the heavy stocking rate of 900,000 sheep and goats and their impact on grasses (section 4.5.3) and shrubs in the simulated rangelands. Due to the lower numbers of sedentary sheep and goats, less edible biomass was found. Biomass availability may also have been limited by aestival restrictions.

In the following paragraph, the weighting factors of shrubs and grasses as proportions of animal diets during the winter (November) are presented (Figure 73). During the winter, a higher weighting factor (0.60) was observed for shrubs in the nomadic diet (see section 4.5.3) under scenario 2a, together with an increasing trend for shrubs in the nomadic diet from an initial value of 0.35 to a final value of 0.60 under scenario 2c and 0.45 under scenario 2b conditions. This reflects the higher groundcover amounts of the grass and shrub PFT's, possibly due to higher rainfall during the winter (see section 1.4.1). As in the summer, grasses played practically no role in nomadic sheep and goat winter diets. Sedentary sheep and goat shrub consumption, however, declined considerably, from initial weighting factors of 0.25 to final weighting factors of about 0.05 (for scenario 2a) and <0.05 (for scenarios 2b and 2c). Grasses and shrubs in sedentary diets converged upon similar proportions by the end of simulation, to a factor of approximately 0.05 for each. The simulated dietary proportions of grasses and shrubs were equal under scenario 2b. The animal dietary situation is probably not as severe in terms of edible biomass during the winter as during the summer. During the winter, nomadic sheep and goats were able to increase the proportion of shrubs in their diet, although high shrub ground cover variation was predicted in the later years of the simulation.

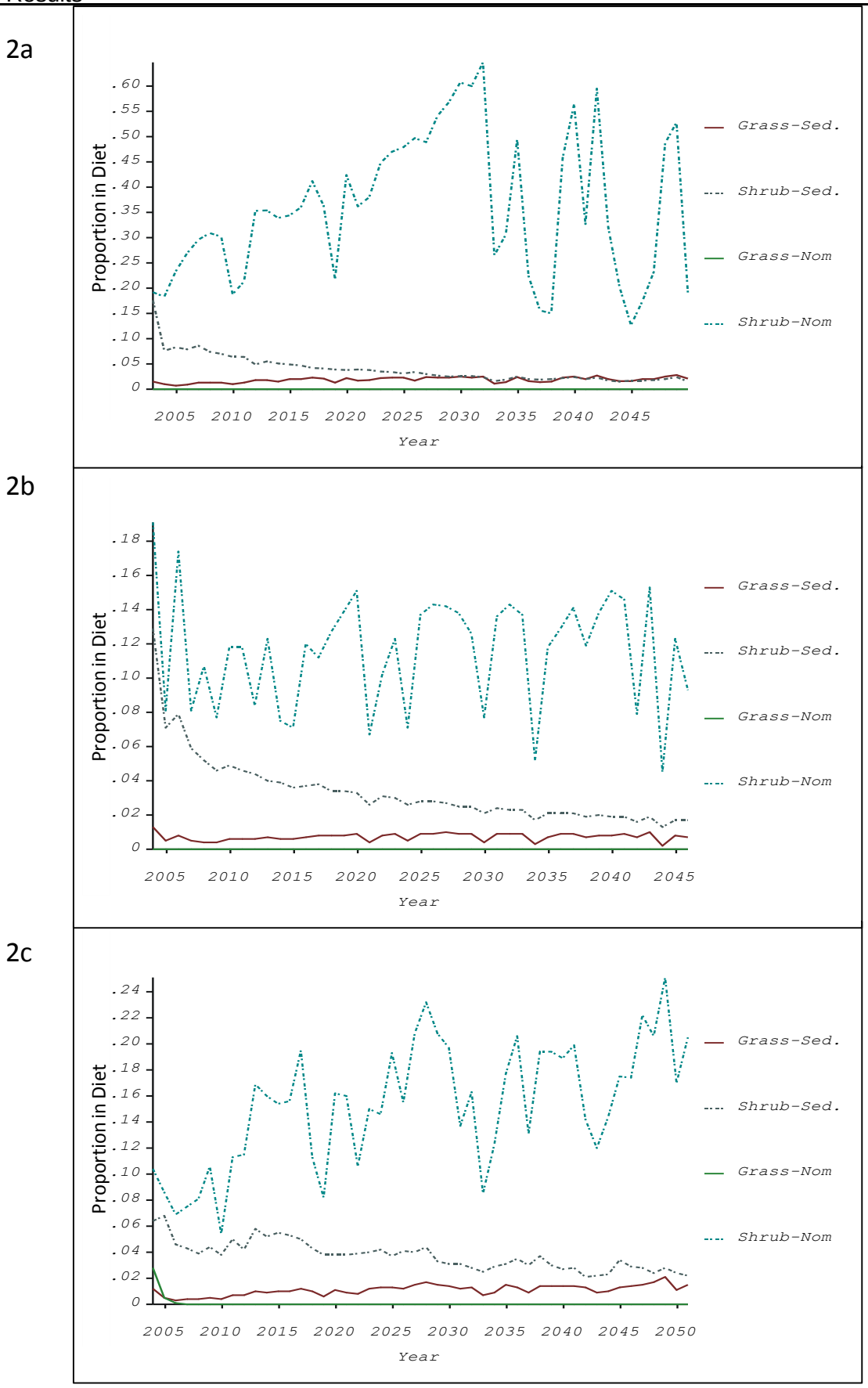

Figure 72: Monthly weighting factors for the proportions of grasses (solid lines) and shrubs (dashed lines) in summer (May) diets of nomadic *–Nom* (green/blue lines) and sedentary *–Sed.* (red/black lines) sheep and goats under scenarios 2a (A1B climate scenario, 2001-2051), 2b (B1 climate scenario, 2001-2048) and 2c (A1B, heavy stocking rate).

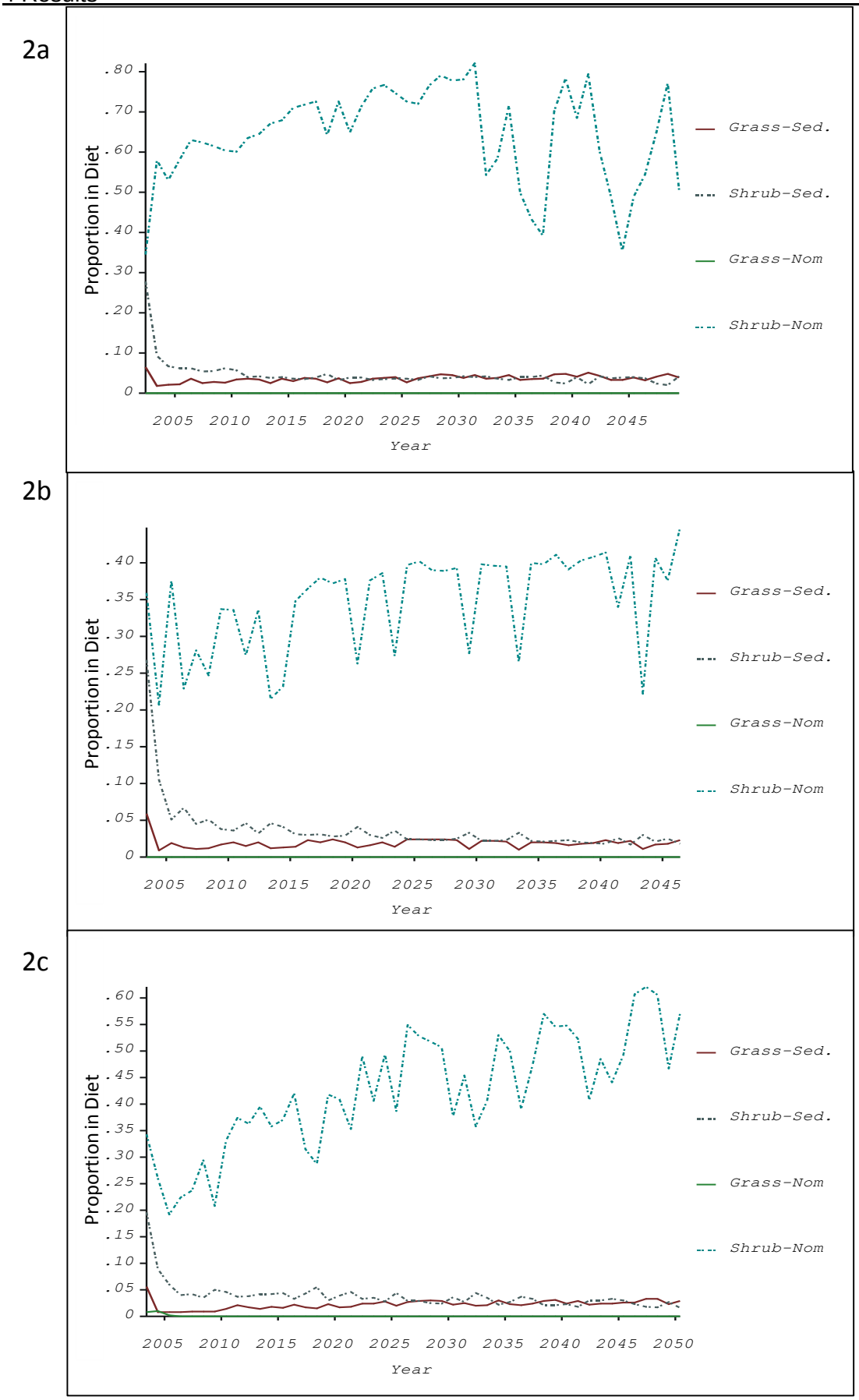

Figure 73: Monthly weighting factors for the proportions of grasses (solid lines) and shrubs (dashed lines) in winter (November) diets of nomadic *–Nom* (green/blue lines) and sedentary *–Sed.* (red/black lines) sheep and goats under scenarios 2a (A1B climate scenario, 2001-2051), 2b (B1 climate scenario, 2001-2048) and 2c (A1B, heavy stocking rate).

4.6.4 Water budget

This section describes simulated regional water budget characteristics (mm) including monthly precipitation (*SysPpt*) and monthly accumulated potential evaporation (*SysPet*) (Figure 74). Monthly accumulated *SysPet* was highest during the summer and decreased toward winter, while *SysPpt* was highly variable among months and years. The following descriptions are of monthly peak values of both parameters. The IPCC A1B scenarios differed in pattern (2a) and amount (2c) of precipitation. Under scenario 2a, the maximum *SysPet* rate was rather low with 550 mm per year wherein the minimum was 190 mm a^{-1}. Scenario 2c produced the highest *SysPet* values of all three runs, ranging from 160 mm a^{-1} to 820 mm a^{-1}. The *SysPe*t ranges of the 2c scenario showed high inter-annual variability, probably caused by excessive vegetation cover losses due to the heavy stocking rate. Vegetation cover losses led to high bare soil evaporation and displaced transpiration in this simulation (see section 4.5.4). Scenario 2a, with its narrow annual range of 360 mm a^{-1}, showed less water losses due to bare soil evaporation. On the other hand, this scenario also showed a restricted *trans* range related to *SysPpt*. Monthly *SysPet* under scenario 2b ranged between 130 mm a^{-1} and 650 mm a^{-1}. Scenario 2b, due to the similar number of animals simulated, produced a SysPet range equal to that of scenario 2a. Monthly precipitation under both the A1B and B1 scenarios rarely exceeded 100 mm.

Monthly levels of simulated stomatal conductance (*Cs*) (Figure 75) indicate the volume of water used by vegetation to maintain plant growth. The aim of this section is to compare predicted potential stomatal conductance (*Cs-pot*) (mmol m^{-2} s^{-1}) (see section 4.5.4) to predicted actual stomatal conductance (*Cs-act*). The following description is based on the annual peak amounts predicted for each run. Scenario 2a showed monthly variation in *Cs-pot* between a minimum of 100 mmol m^{-2} s^{-1} and a maximum of 400 mmol m^{-2} s^{-1}, while *Cs-act* ranged between a minimum of 0.0 mmol m^{-2} s^{-1} and a maximum of 400 mmol m^{-2} s^{-1}. Scenario 2b produced a minimum *Cs-pot* of 80 mmol m^{-2} s^{-1} and a maximum of 450 mmol m^{-2} s^{-1}, while *Cs-act* was predicted to vary from a minimum of 0.0 mmol m^{-2} s^{-1} to a maximum of 450 mmol m^{-2} s^{-1}. *Cs-act* declined under all three scenarios to less than 10 mmol m^{-2} s^{-1} monthly. Under scenario 2c, *Cs-pot* varied between a minimum of 100 mmol m^{-2} $s^{-1}$and a maximum of 180 mmol m^{-2} s^{-1}, while *Cs-act* ranged from 0.0 mmol m^{-2} s^{-1} to only 170 mmol m^{-2} s^{-1}. Very low *Cs-act* values were reached temporarily under all three scenarios. Since both *Cs-act* and *Cs-pot* are dependent on precipitation, a reduced maximum *Cs-pot* value (as in 2c) together with a small range in *Cs-pot* values could be used as an indicator for plant available water limitation (see section 6.2).

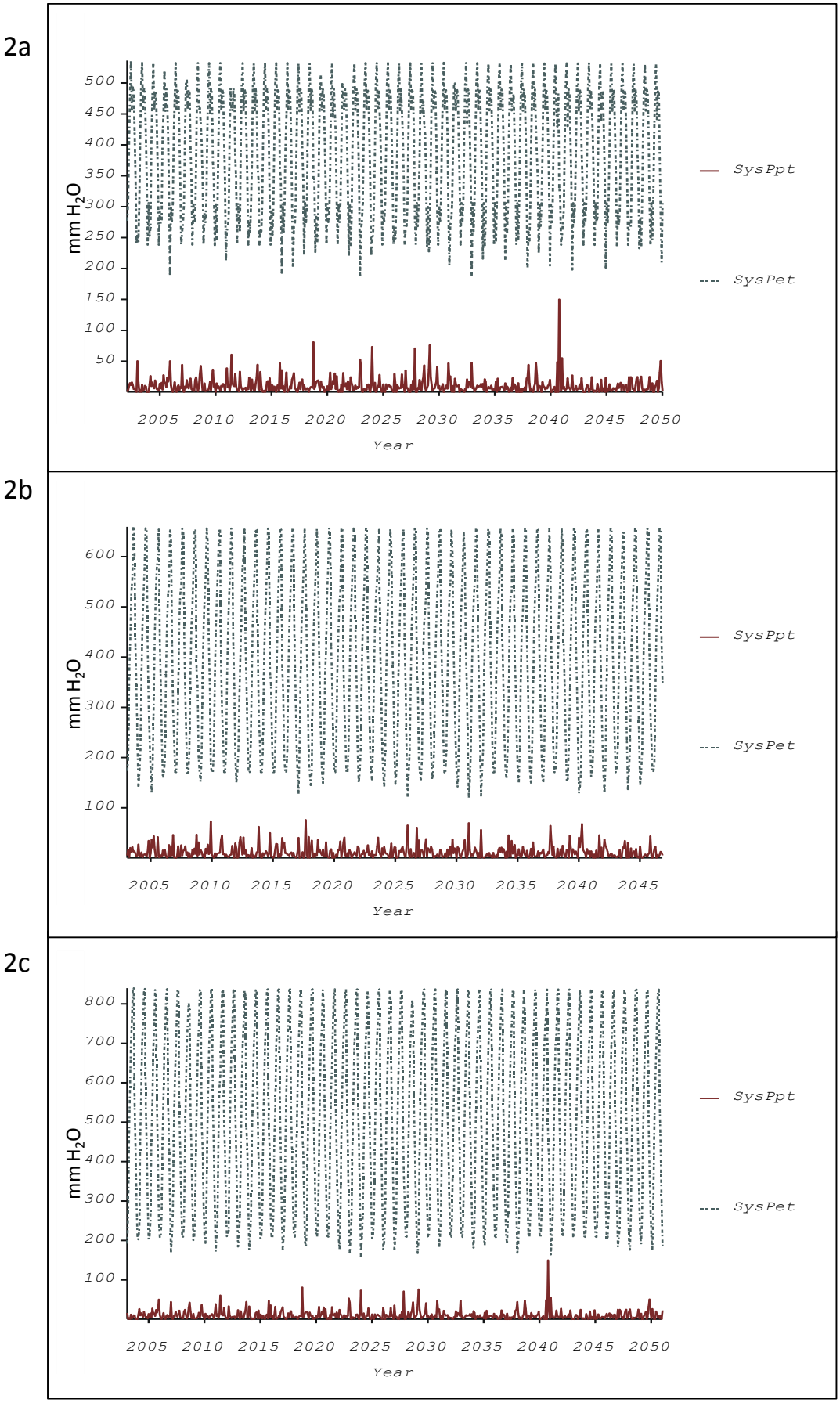

Figure 74: Monthly predicted precipitation *SysPpt* (red line) and cumulative annual predicted evapotranspiration *SysPet* (dashed blue line) (both mm H_2O) for scenarios 2a (A1B climate scenario, 2001-2051) 2b (B1 climate scenario, 2001-2048) and 2c (A1B, heavy stocking rate).

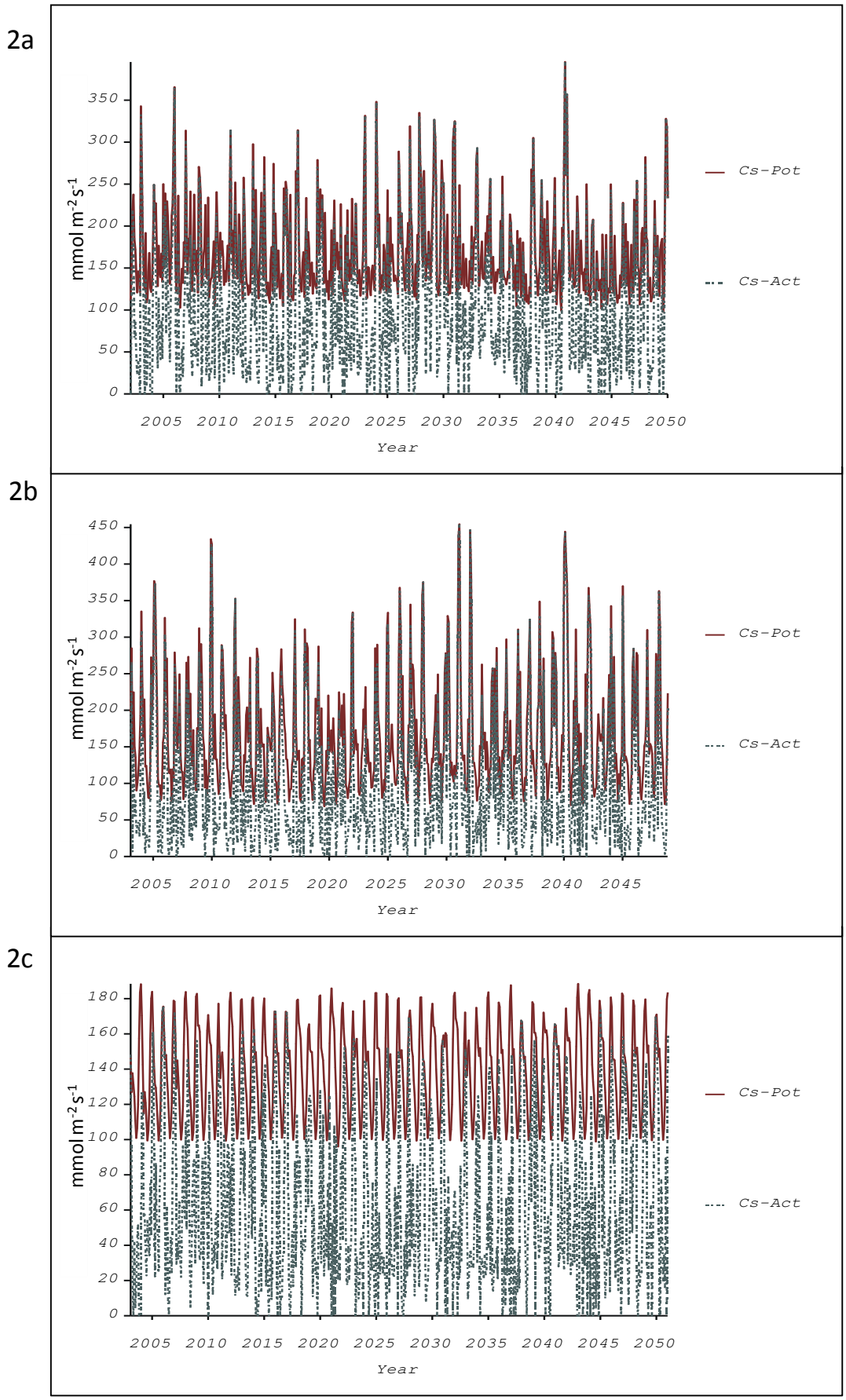

Figure 75: Annual sum of predicted potential stomatal conductance *Cs-pot* (mmol m^{-2} s^{-1}, red line) and actual stomatal conductance *Cs-act* (mmol m^{-2} s^{-1}, dashed blue line) under scenarios 2a (A1B climate scenario, 2001-2051), 2b (B1 climate scenario, 2001-2048) and 2c (A1B, heavy stocking rate).

Predicted monthly (February, May, August and November) actual bare soil evaporation (*Bsev*) and actual predicted transpiration (*trans*) values (mm) were clustered around 90 to 100% of the predicted *SysPpt* values (see section 4.5.4). This was probably caused mostly to high evaporative losses from bare soil, especially during the summer months, due to the dominant patterns of vegetation in the research area (see Figure 74). This statement is supported by the patterns of monthly *trans* calculated for all PFT's (Figure 76). Initial values of predicted actual *trans* under scenario 2a were greater than those under scenario 2c, and values declined as both simulations progressed. This is consistent with the decline in *SysPpt* predicted for the A1B climate scenarios. In contrast, *trans* values under scenario 2b were initially equal in range to those under scenario 2c, but were able to continuously increase with *SysPpt* and finally exceed the actual *trans* amounts found under scenario 2a.

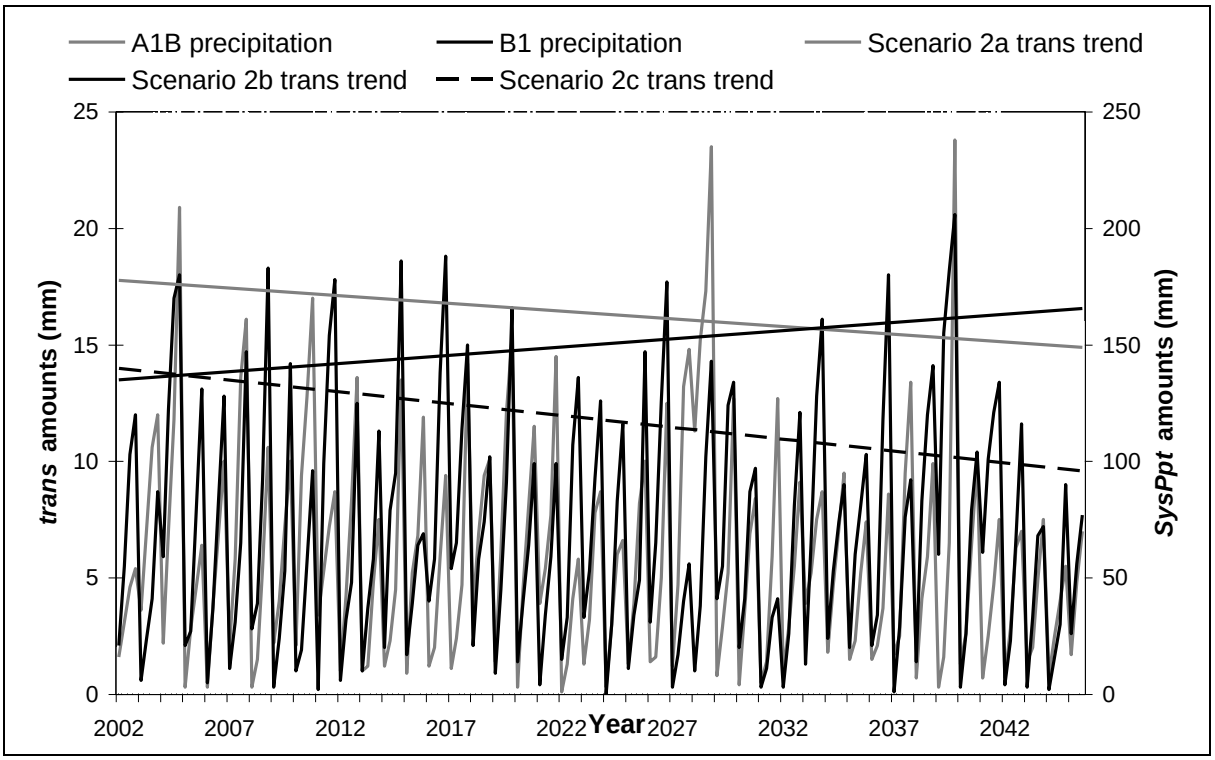

Figure 76: Monthly (February, May, August and November) accumulated annual predicted precipitation *SysPpt* (mm) and predicted linear trends in transpiration *trans* (mm) of all three PFT's under the A1B (2a-dark grey line, 2c dotted black line) and B1 (2b-black line) scenarios.

4.6.5 Spatial distribution patterns of animal comsumption and forage - scenario 2d

The above described vegetation patterns are now set in a spatial context (see Table 31). In the following section, the annual patterns of herbaceous green leaf growth and cumulative consumption by animals under scenario 2a (IPCC A1B climate parameters with a "range

exclusion area“) are compared to those under scenario 2c (IPCC A1B climate parameters with “no range exclusion“). Figure 77 shows the location of the hypothetical range exclusion area. For this purpose, one particular year (2025) was chosen after the model “warm-up“ phase and halfway through the fifty-year simulation. Spatial resolution is 1 km^2 simulating the entire Wadi Drâa catchment study area. Cell values are predicted average amounts of herbaceous green biomass and cumulative animal consumption. In order to evaluate green biomass production, the pattern of precipitation for 2025 was needed. Figure 78 portrays predicted monthly *SysPpt* in 2025 under the IPCC A1B climate scenario. This figure shows the highest *SysPpt* (up to 33.33 mm) occurring in December 2025; less than 15 mm is predicted to occur in all other months. Differences in *SysPpt* are due to topographic differentiation.

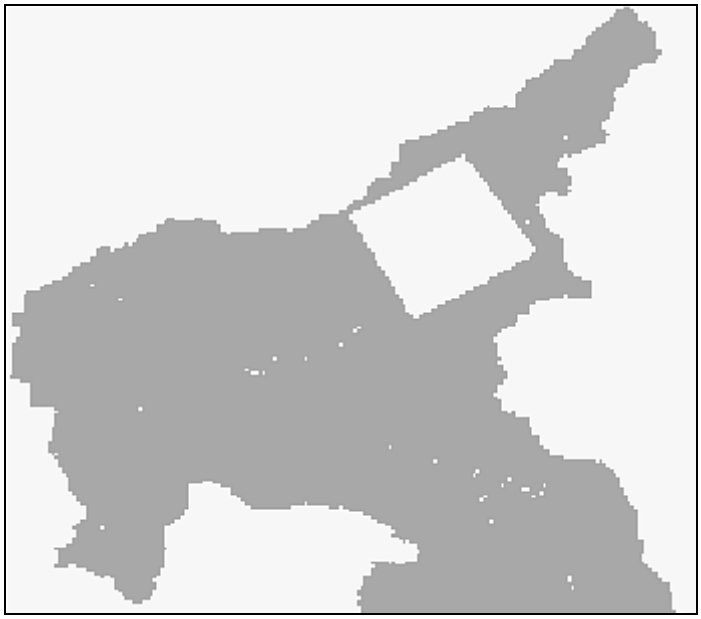

Figure 77: Hypothesised computed range exclusion area (as used in scenario 2a) in the northeastern part of the Drâa catchment (basin of Ouarzazate).

Figure 79 displays monthly amounts and distribution of herbaceous green leaf biomass during 2025 under the scenario with “no range exclusion“ (2c). Herbaceous green leaf biomass production was examined to obtain comprehensive insights on spatial dependencies of animal food resources. During the first four months, herbaceous green leaf biomass quantities were mostly between 1.0 g m^{-2} and 7.0 g m^{-2} per grid cell.

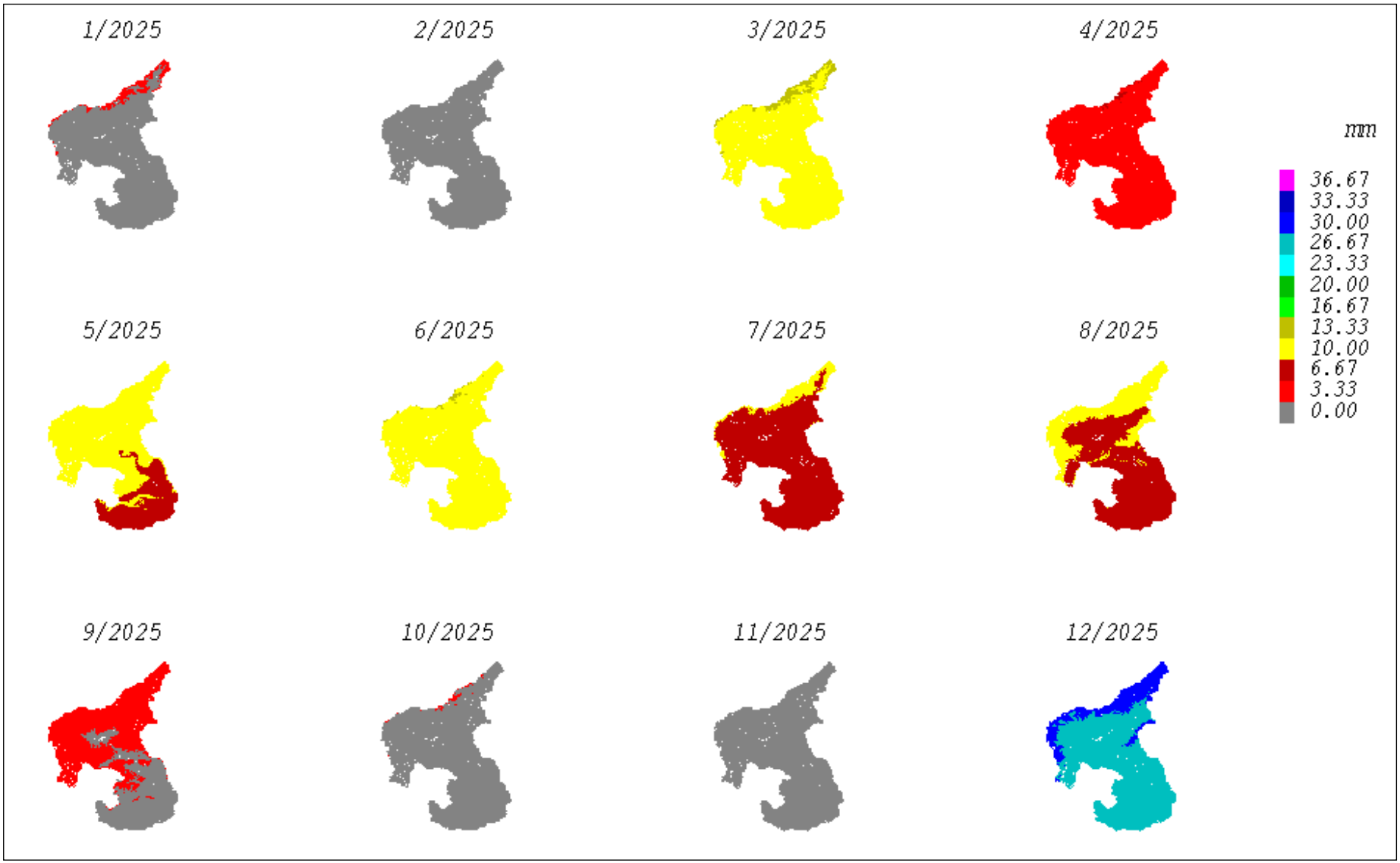

Figure 78: Monthly predicted precipiatation *SysPpt* (mm) for January-December 2025 for the Drâa catchment area under IPCC A1B climatic conditions.

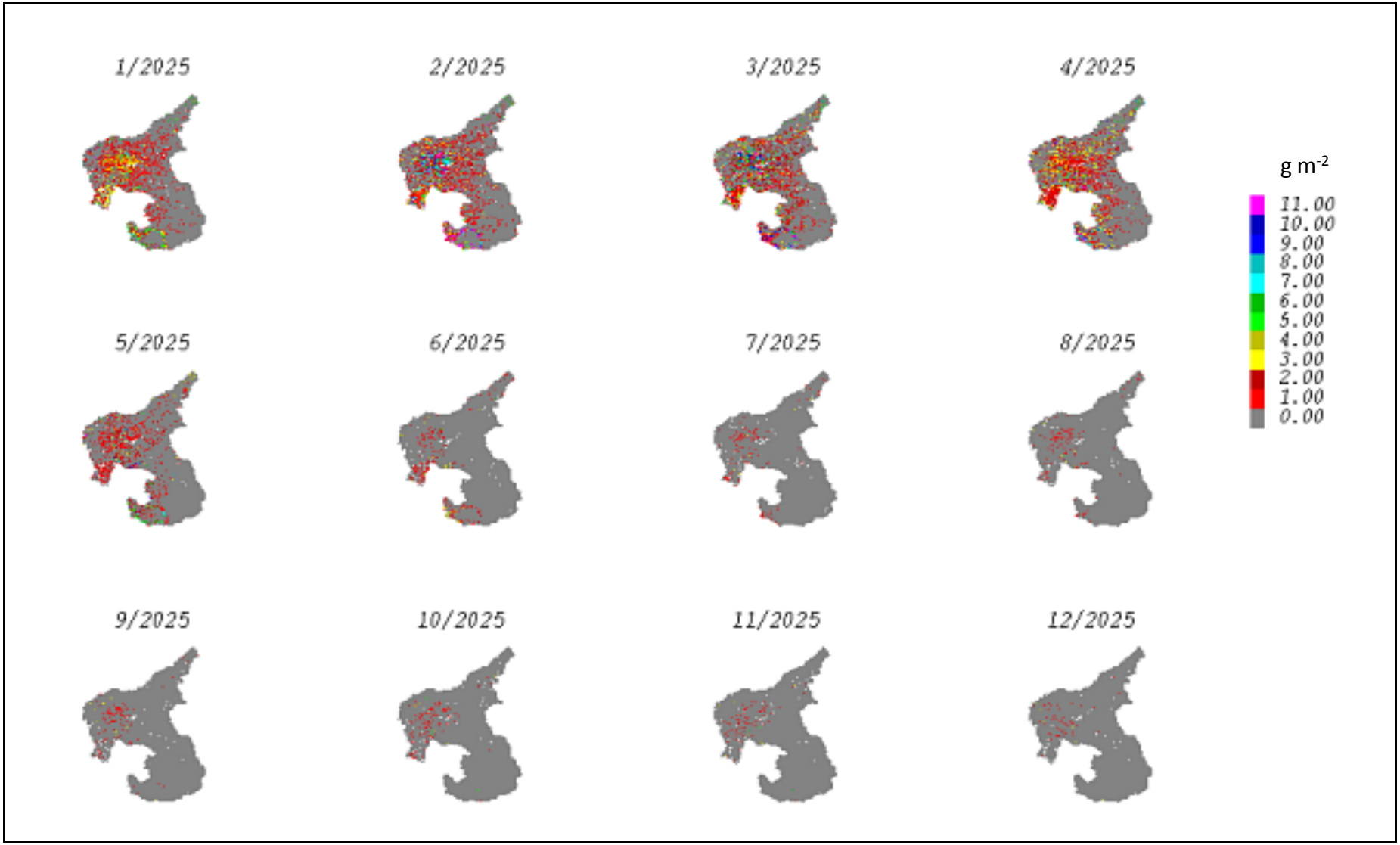

Figure 79: Predicted monthly herbaceous green leaf biomass (g m^{-2}) during January-December 2025 for the Drâa catchment area under scenario 2c.

Herbaceous green leaf biomass figures were close to the average quantities found in the longer-term A1B simulations (Table 32) and reflect the given rainfall regime. The western part of the basin of Ouarzazate showed the highest production indices. Herbaceous leaf biomass declined throughout the remainder of the year, mainly due to lack of precipitation (Figure 78). In the second half of the year, the basin maintained high productivity compared to its surroundings, even with only 1.0 g m^{-2} of herbaceous green leaf biomass production. In vast parts of the research area, herbaceous green leaf biomass production declined to 0.0 g m^{-2} to 0.25 g m^{-2}. Greater production was found only in small, isolated patches.

Figure 80 portray the change over time in herbaceous green leaf biomass under the IPCC A1B scenario 2a with a northern range-exclusion area (Figure 77). Again, the highest production occurred in the western part of the basin of Ouarzazate. High biomass production extended through the first six months of the year, and the subsequent decrease was not as severe as under the “no range exclusion“ scenario (2c) (Figure 79).

Herbaceous green leaf production reached > 9.0 g m^{-2} per grid cell in the western part of the basin (Figure 80). Broader areas of the region were predicted to produce >1.5 g m^{-2}. The range exclusion area in the western part of the basin produced up to 5.5 g m^{-2} of herbaceous green leaf biomass. During the summer (from July to October until November) only the western part of the basin exhibited recordable biomass production of 1.0 to 2.0 g m^{-2}. Seasonal green leaf biomass production patterns were apparently unaffected by the exclusion of grazing. From November to December, green leaf biomass production began, with up to 5.5 g m^{-2} or more. Until December, the southern catchment area reached amounts of about 1.0 g m^{-2} of green leaf biomass in isolated productive areas.

Figure 81 shows the pattern of cumulative consumption (kg ha^{-1}) by sedentary and nomadic sheep and goats, dromedaries and humans in the Wadi Drâa catchment during 2025 under scenario 2c (A1B climate scenario, heavy stocking rate of 900,000 head) with “no range exclusion“. Under this scenario, biomass consumption was notably concentrated in the basin of Ourzazate (see Figure 79). Consumption in other areas was less than 25 kg ha^{-1} (grey cells).

Consumption was moderate during the first two months. During March, a threefold increase (to 175 kg ha^{-1}) occurred in the western basin. This was mainly due to increased animal forage needs, probably induced by the simulated birth rate for sedentary and nomadic herds. Consumption increased to a maximum of 275 kg ha^{-1} by June 2025. This consumption was concentrated in the basin, but moderate consumption levels of about 50 kg ha^{-1} were also observed in southern parts of the catchment. These southern areas showed similar levels of productivity to those of the basin of Ouarzazate.

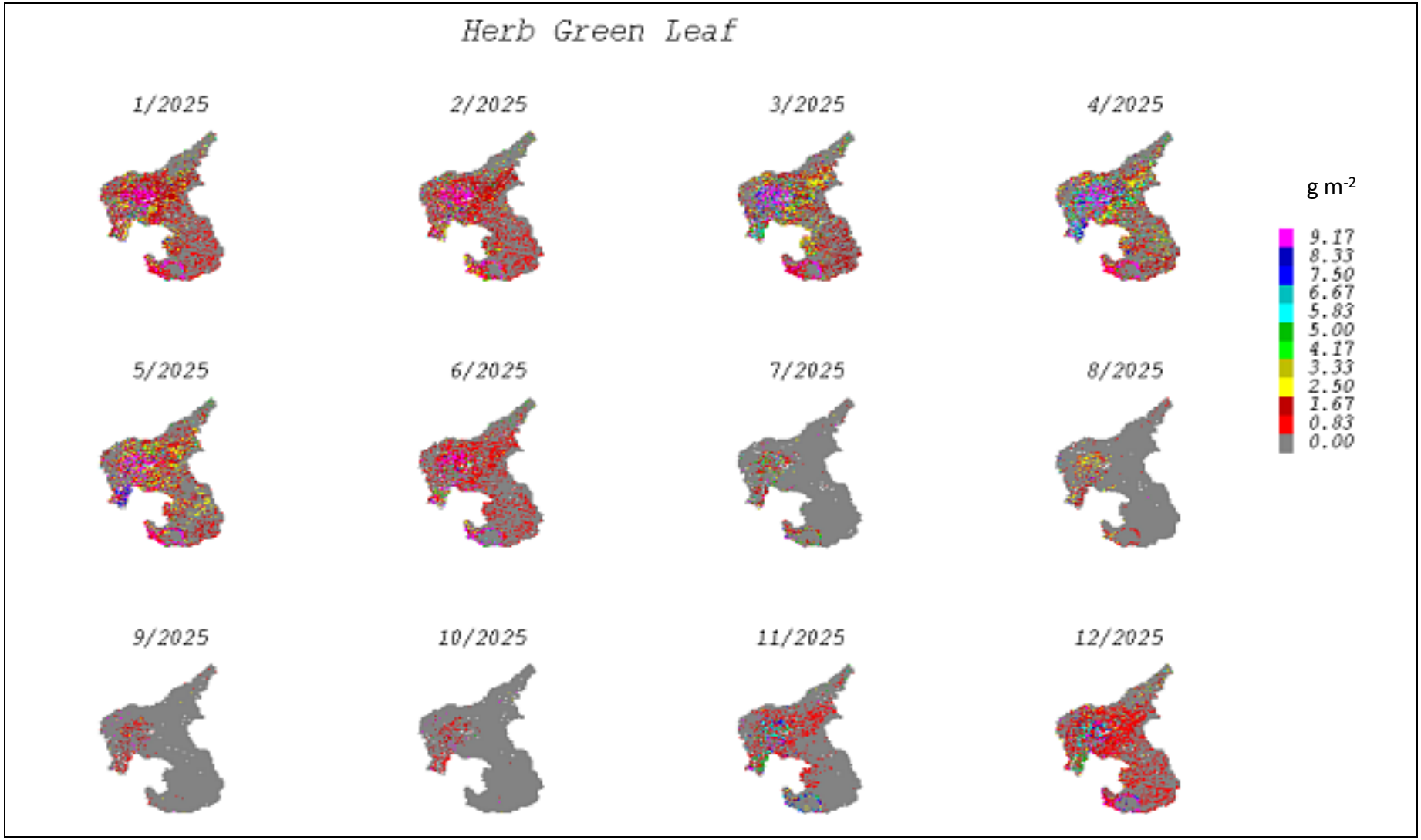

Figure 80: Predicted monthly herbaceous green leaf biomass (g m^{-2}) during January to December of 2025 for the Drâa catchment area under scenario 2a.

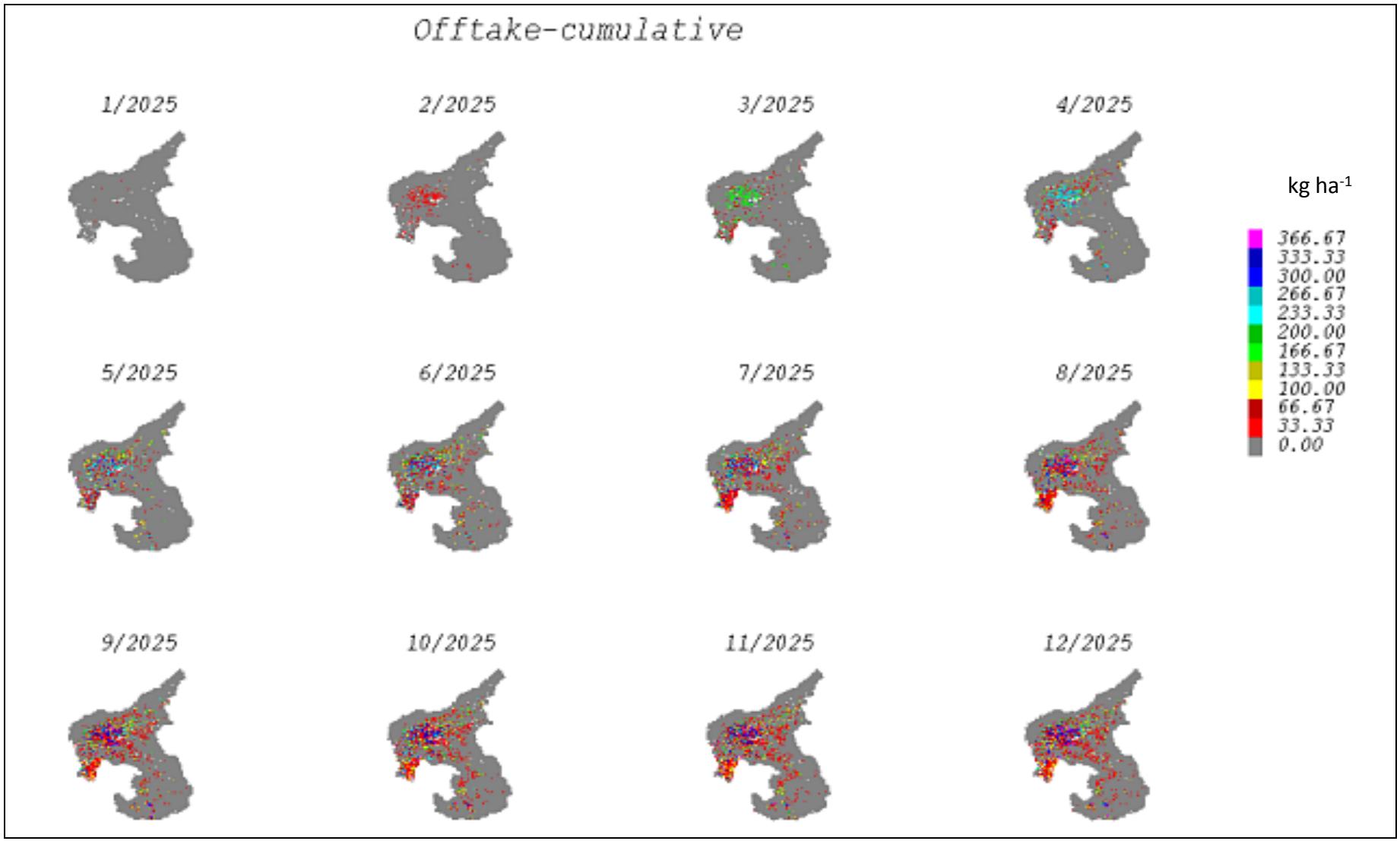

Figure 81: *Cumulative offtake* (kg ha^{-1}) by all animal herds during 2025 for the Drâa catchment area under scenario 2c with "no range exclusion".

However, the basin of Ouarzazate (especially its western part) continued to be the most productive area in terms of herbaceous biomass and continued to have the highest consumption. A southward trend in biomass consumption was predicted on an annual basis. The large number of nomadic sheep and goats was responsible for this pronounced intensification of biomass consumption and production in the basin of Ouarzazate. The high availability of water wells in this region promotes its utilisation by animals.

Animal stocking rates (see section 2.4.4) were balanced in January 2025 at about 220 nomadic sheep and goats per km^2. In February and March, herds moved to the highly productive areas of the western basin of Ouarzazate (data not shown). During this period, animal numbers temporarily reached levels of about 2,000 sheep and goats per km^2. Due to the expansion of available edible biomass throughout the catchment, the basin declined in importance compared to the southern parts of the study area during the later part of the year. Due to the large numbers of nomadic sheep and goats (550,000), high and homogeneous grazing intensities (an average of about 200-400 sheep and goats per km^2) were reached throughout the Wadi Drâa catchment in this simulation.

Sedentary sheep and goats reached maximum numbers of about 1,000 per km^2 in the western basin of Ouarzazate from February to April 2025. In the later months of 2025, a lower-level homogenous distribution of about 200 animals per km^2 was achieved, similar to the numbers of nomadic sheep and goats. These numbers indicate the high capacity of the biomass to provide the basic forage needed to sustain these animal numbers.

Figure 82 shows the cumulative animal consumption (kg ha^{-1}) by all herds under scenario 2a with a “range exclusion area“. Cumulative consumption reached its maximum value (in February) and was twice the value found for the “no exclusion area“ scenario in the western basin of Ouarzazate. These high levels of consumption continued to the end of the year.

The numbers of nomadic sheep and goats per km^2 outside of the range exclusion area was nearly identical under the two scenarios. Differences occurred in the intensity of grazing (number of animals per km^2), since scenario 2c (“no range exclusion area“) had higher total livestock numbers (900,000) compared scenario 2a (600,000). During the first half of the year under scenario 2a, nomadic sheep and goats were concentrated in the most productive area, the western basin of Ouarzazate, with 700 head per km^2. Until June, 130 to 330 head per km^2 of nomadic sheep and goats were found in isolated patches within a short distance of water wells in the southern part of the study area. This changed completely in the second half of the year. As biomass productivity increased, animal numbers and distribution patterns also increased.

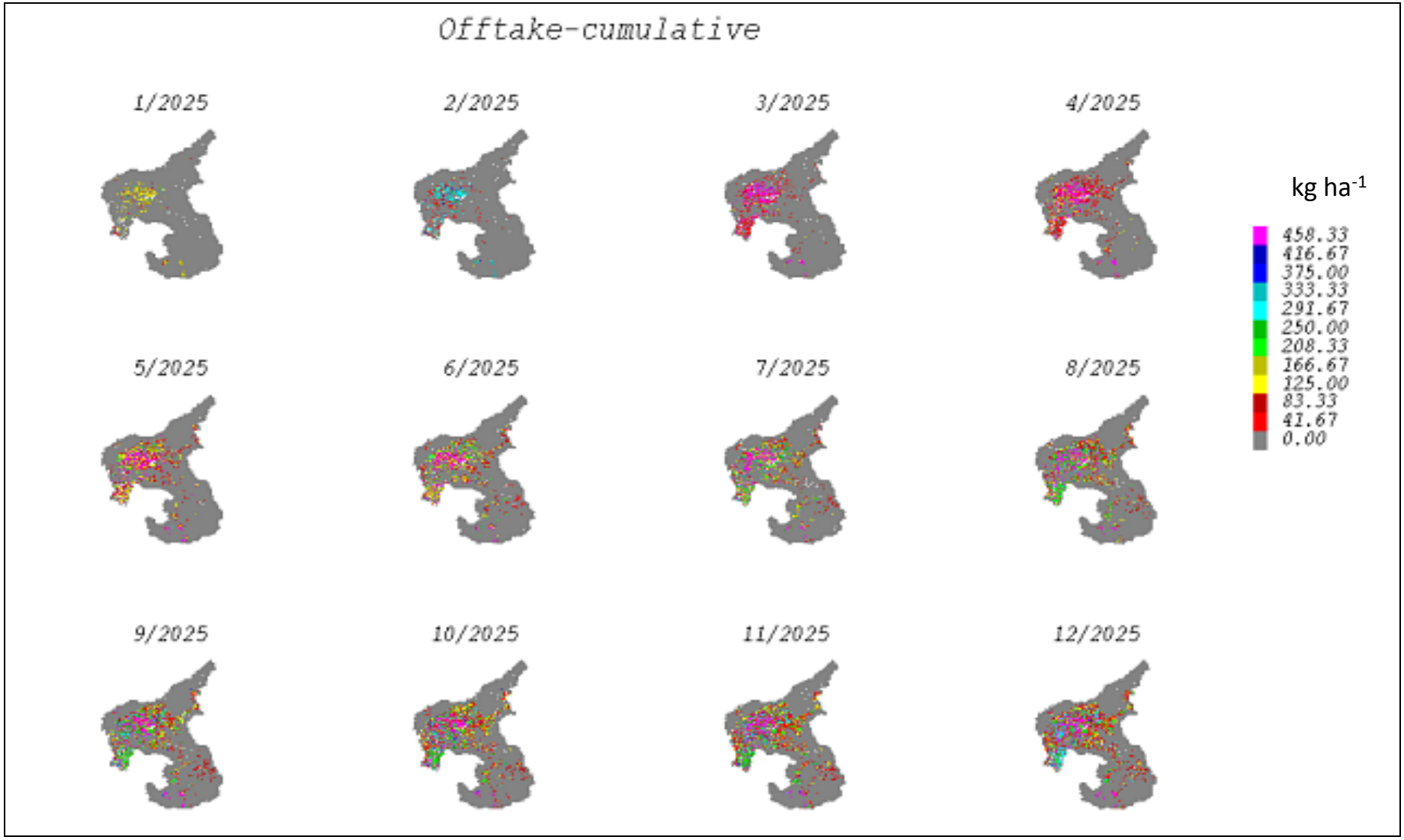

Figure 82: *Cumulative offtake* (kg ha^{-1}) by all animal herds during 2025 for the Drâa catchment under scenario 2a with "range exclusion" area.

Moderate animal numbers, such as those in scenario 2a (600,000), seem to permit higher grazing intensities of more than 400 head per km^2. However, these values were also reached on grid cells containing water well plots under both scenarios. The numbers of dromedaries (10,000) and humans (5,000) were negligible. Significant numbers of dromedaries (about 100 head per km^2) occurred only in small, isolated patches.

The aim of this section was to identify spatial-temporal dependencies and interactions between green leaf biomass production and animal consumption and distribution. The herbaceous PFT was selected for evaluation because of the seasonally abundant green leaf biomass produced by this PFT. The ability to predict growth patterns of this PFT is important because it is highly sensitive to animal grazing. The temporal contribution of herbaceous biomass to animal diet is highlighted by the predicted levels of consumption. Figure 81 and Figure 82 show that cumulative consumption is temporally and spatially haphazard, except in the western basin of Ouarzazate. This highly productive area appears to function as the key resource for newly generated herbaceous biomass. Thus, this area is heavily utilised by animals, intensified by the high concentration of water wells in this region. Biomass production attracts animals to move to more productive areas, in turn inducing growth of certain plants. This leads to heavy grazing in the proximity of water wells within degraded, unfertile areas with little vegetative cover. The results of these scenarios will be discussed in section 6.2.

4.7 Southern ranges CO_2 variation from 1975 to 2051

The results presented in this section are based on a 75-year simulation (1975-2051) designed to compare recent CO_2 rates (350 ppm) with doubled CO_2 enrichment (700 ppm) under different animal stocking rates in the southern ranges of the Drâa catchment (Figure 34). These experiments were not driven by the IPCC A1B or B1 climate scenarios. Instead, 1975-2006 data from the DRH and IMPETUS (Zagora) climate stations, in addition to the main climate station (Ouarzazate) (see section 2.7), were used. Based on local meteorological expert knowledge (Born, 2007, personal communication), temperatures after 2006 were projected to the year 2050 with winter temperatures increasing by +0.6°C (SD ± 0.5°C) and summer temperatures increasing by +1.1°C (SD ±0.3°C). The aim of this study was to determine the impact of anthropogenic livestock numbers and climate-induced changes to PFT's. The diagnostic cell (Table 31) was characterised by soil type no. 31 (see Appendix, Table 35) and vegetation type group no. 10 (see Table 5) and is located at an

elevation of 816 m a.s.l. To achieve the experimental goals stocking rates were modified twice. From 1975-2004, we simulated light grazing (50,000 sedentary and 100,000 nomadic sheep and goats, 10,000 dromedaries and 5,000 humans). From 2004-3024, we simulated heavy grazing (350,000 sedentary and 550,000 nomadic sheep and goats, 20,000 dromedaries and 20,000 humans). Finally, from 2034-2051 we simulated moderate grazing (200,000 sedentary and 400,000 nomadic sheep and goats, 10,000 dromedaries and 10,000 humans). Results based on CO_2 enrichment to 700 ppm are presented in the following section. Section 4.7.5 then presents *Cs*, *Ps* and water use efficiency (*WUE*) results from the simulations based on recent (350 ppm) atmospheric CO_2 levels in comparison to doubled CO_2 levels.

4.7.1 Plant growth

Figure 83 shows the change over time in simulated total biomass of herbaceous (*TotHrb*), woody (*TotWdy)* and shrub (*TotShb)* PFT's (live+dead leaves, stems and roots) from 1975-2050 under various stocking rates. The figure displays annual plant growth to the maximum flowering period in autumn each year. Values given in the following descriptions are maximum or minimum values.

During the "warm-up" phase and thereafter, *TotWdy* showed a continuous decline in peak values but stabilised after approximately 15 years of simulation at about 9.0 g m^{-2}. It then declined again due to the introduction of heavy stocking rates until it stabilised at about 5.0 g m^{-2} during the last 40 years of the simulation. This pattern, except for the level of adaption, is consistent with the patterns observed for aspen and deciduous trees in the Ouarzazate base-line scenario (Figure 50). *TotHrb* declined during the model "warm-up" and stabilised at annual peak values of 6.0 g m^{-2}. It declined following the introduction of heavy stocking rates in 2004 but then increased to annual peaks of about 8 g m^{-2} during the last 40 years of the simulation. *TotShb* varied considerably in maximum total annual biomass. Even after the "warm-up" phase, *TotShb* declined continuously and broke down after the introduction of heavy stocking rates in 2004. Thereafter, it increased to stabilise at an annual peak of about 18.0 g m^{-2}. Stocking rates produced large effects on *Tothrb*, *Totwdy* and *Totshb* production. *TotWdy* stabilised after the change in stocking rates, probably due to the number of dromedaries. *TotHrb* and *TotShb* experienced a break-in period but stabilised subsequently. *TotHrb* eventually reached greater average total biomass under heavy grazing than under light stocking rates.

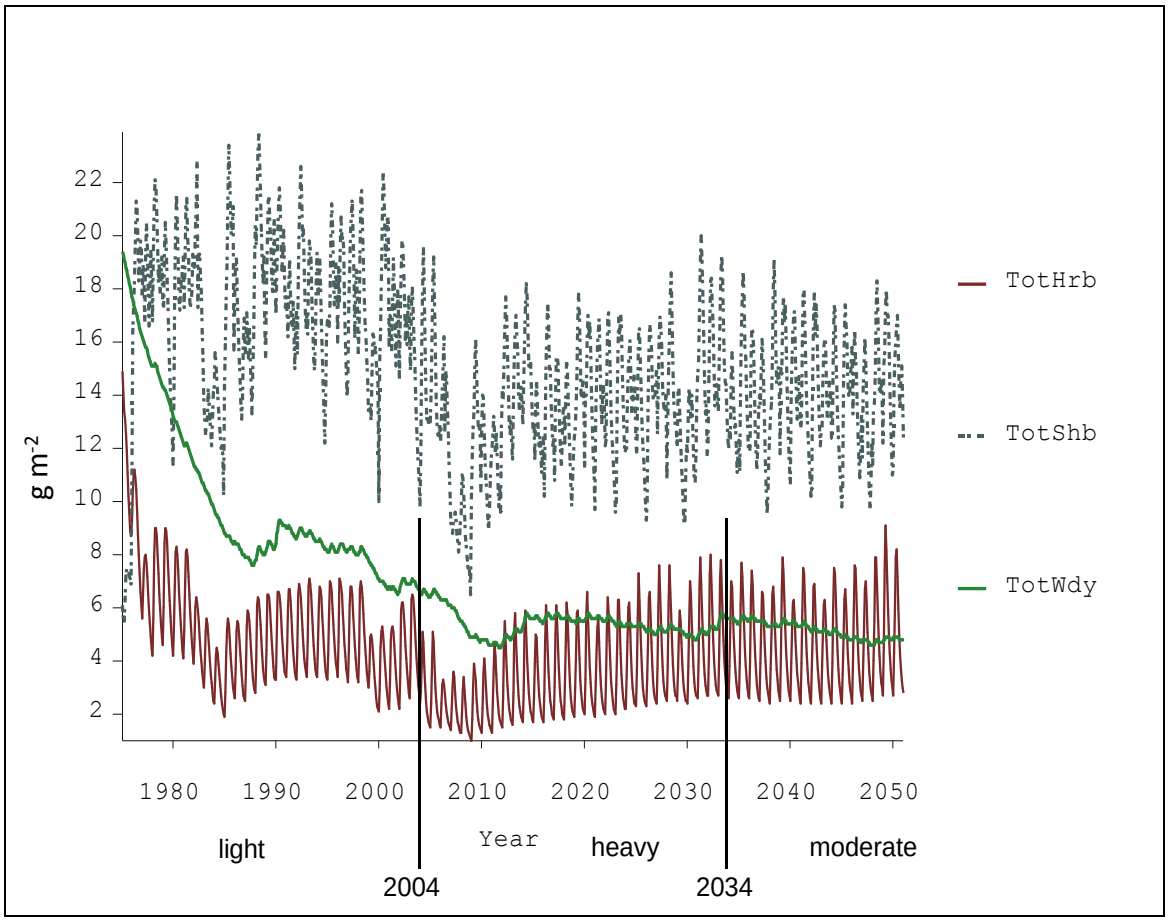

Figure 83: Annual sum of Total (live+dead) biomass (g m^{-2}) for the entire Drâa zone from 1975-2051 under elevated CO_2: total herbaceous *TotHrb* (red line), total shrub *TotShb* (dashed blue line) and total woody (tree) *TotWdy* (green line) biomass.

Figure 84 shows the results described above in detail. Stocking rates, especially heavy grazing, had substantial effects on herbaceous and shrub *ANPP,* even though the effects were delayed for some years (2004-2007). The effects of livestock on woody *ANPP* were negligible, within ≤ 2.0 g m^{-2} of the peak amounts (see section 4.6.1). After 30 years of the simulation, however, herbaceous *ANPP* showed an increasing trend and finally stabilised at a peak of approximately 10 g m^{-2}. After the transition to heavy grazing, shrub *ANPP* re-stabilised at a peak of approximately 20 g m^{-2}. These maximum levels were similar to those observed during the light grazing period from 1975-2004. As seen before, (see sections 4.5.4 and 4.6.4) *SysPpt* was the main reason for the inter-annual fluctuations of *ANPP*.

Turning from PFT descriptions to more detailed descriptions of plant groups, primarily the herbaceous grass types, we now present leaf growth. Figure 85 shows the herbaceous leaf production of ”fine-”, ”coarse-” and ”alpine grass” for the period 1975-2051. The “coarse grass” leaf production, even after the “warm-up“ phase, strongly declined to an annual sum of only 2 g m^{-2} after 75 years of simulation. The ”fine grass” leaf production increased continuously, interrupted only by the change to heavy grazing, to approximately 12 g m^{-2} at the end of the simulation. This amount made ”fine grass” the single greatest leaf biomass

producer in the southern ranges. This was probably due to animal dietary preferences for ”fine grass” leaves (see Table 22), which stimulated new shoot growth from year to year at high stocking rates more than for other grass types.

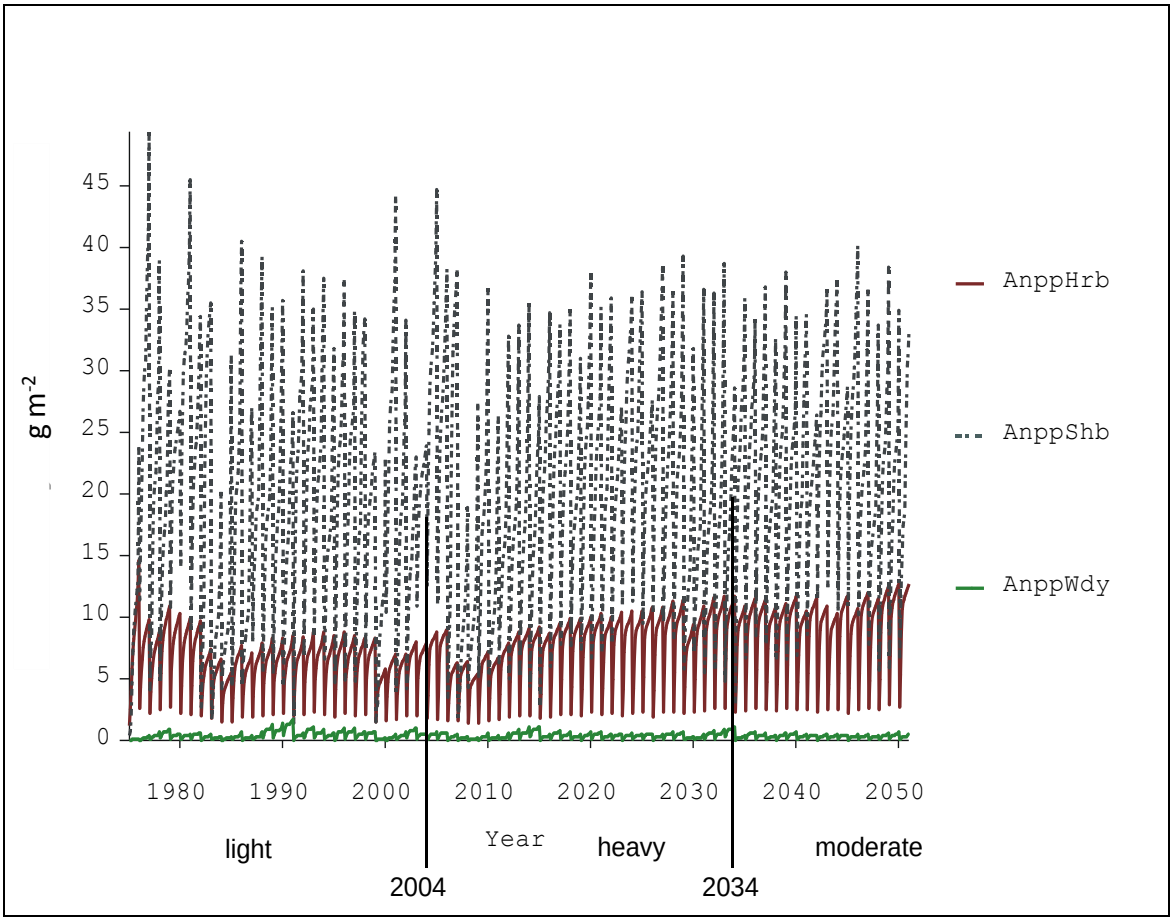

Figure 84: Annual sum of *ANPP* (g m^{-2}) for the entire Drâa catchment zone from 1975-2051 under elevated CO_2: herbaceous *AnppHrb* (red line), shrub *AnppShb* (dashed blue line) and woody *AnppWdy* (green line).

The “alpine-” and ”fine grass” may both have benefited from the humidity and light grazing intensities of the early 1990s to increase their leaf biomass production and ground cover. But due to the lesser spatial coverage and greater animal dietary preference of ”alpine grass” (compared to ”fine grass”), it declined strongly in dry years, e.g., after 1995. Increased stocking rates probably had the same induction effects on ”alpine grass” leaf biomass as on ”fine grass”.

We conclude that ”fine grass” leaf growth shows the greatest increase in relationship both stocking rates and precipitation thresholds, indicating that this group of grasses may perform best in spatial and environmental reclamations. This is probably due to animal dietary preferences for ”fine-” and ”alpine grass” leaves instead of ”coarse grass” leaves. These grass PFT’s are thought to benefit in terms of pollination from animal feeding and trampling.

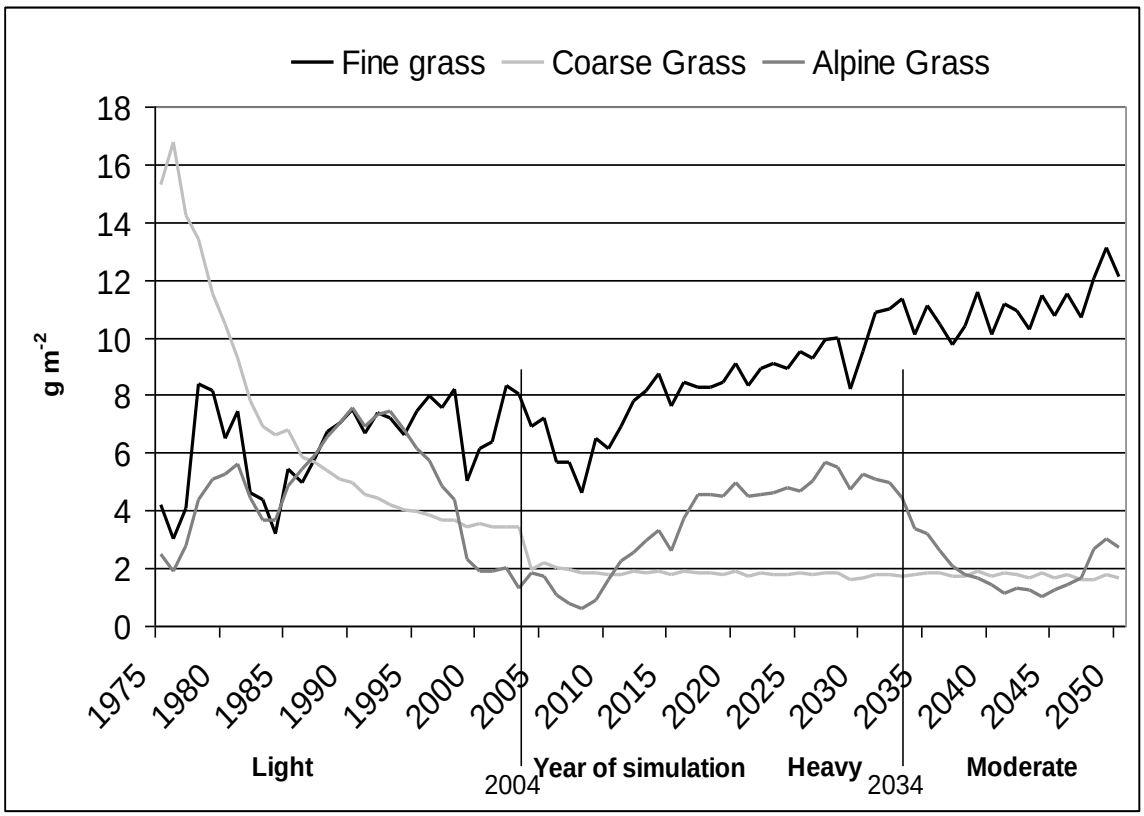

Figure 85: Simulated annual sums of "fine-" (black line), "coarse-" (light grey line) and "alpine grass" (grey line) leaf production (g m^{-2}) for the entire Drâa zone from 1975-2051 under elevated CO_2.

Figure 86 shows the pattern of total annual leaf biomass for "evergreen-", "low DMD-" and "sage shrubs" under this scenario. "Evergreen shrubs" showed a continuous decreasing trend throughout whole simulation period, as seen in previous simulations. Again, the curves discussed indicate leaf biomass increasing to its peak in autumn. Next, the maximum and minimum values are discusses. Leaf biomass decreased by half at the end of the 20th century and again when the heavy stocking rate was introduced. Shortly after this transition, leaf biomass increased. Leaf biomass again declined under the moderate grazing regime, to ≤ 1 g m^{-2} by the end of the simulation. Neither "low DMD-" nor "sage shrubs" showed an equal decreasing trend for leaf biomass production. Otherwise, both shrub PFT's showed equal levels of leaf production. Growth was strongly influenced by precipitation rates, e.g., in the early 1980s (see Ouarzazate precipitation data, Figure 41), during the light grazing period. The introduction of heavy grazing apparently forced both "low DMD-" and "sage shrubs" leaf biomass to decrease, but only after a delay of four to five years, as already observed for shrub *ANPP* (Figure 84). Subsequently, leaf growth was probably induced by grazing, reaching constant maximum levels of about 14.0 g m^{-2}. By contrast, "evergreen shrub" leaf production declined rapidly, probably because of its high animal dietary preference. The "sage shrubs" and "low DMD shrubs" seem to be more adapted to animal

feeding and trampling, perhaps even benefitting from these conditions to increase leaf development.

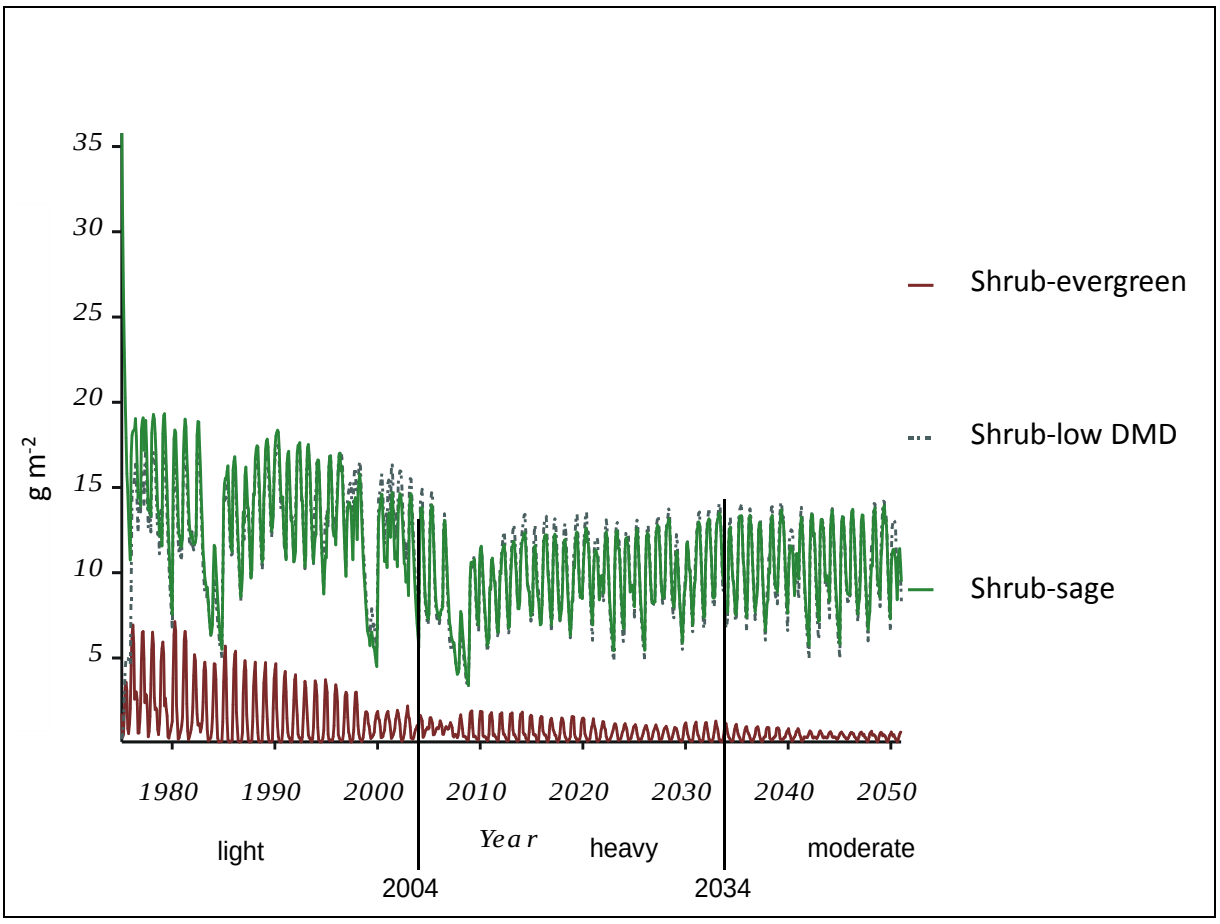

Figure 86: Simulated annual sum of ”evergreen-” (red line), ”low DMD-” (dashed blue line) and ”sage shrub” (green line) leaf biomass (g m^{-2}) for the entire Drâa zone from 1975-2051 under elevated CO_2.

Simulated root growth of shrubs is discussed next (data not shown). Roots of “evergreen shrubs” declined from 30.0 g m^{-2} to <1.0 g m^{-2} by the end of the simulation, paralleling the trend described above (Figure 86) and demonstrating that these shrubs are not adapted to the predicted environment and stocking rates and are thus vulnerable to extinction.

The ”low DMD-” and ”sage shrubs” increased their root biomass to a maximum of 55.0 g m^{-2} during the first 30 years of the simulation. However, these values were strongly influenced by low precipitation. This and the heavy stocking rate together reduced shrub root biomass to 30.0 g m^{-2}. The “sage shrub” root biomass finally stabilised at about 40.0 g m^{-2}, whereas ”low DMD shrub” root biomass continually exceeded ”sage shrub” root biomass by about 10.0 g m^{-2}.

Figure 87 exhibits the annual pattern of green leaf area index (*Glai*) for all three PFT’s in the simulated diagnostic cell. *Glai* represents all green parts of plants, including stem and leaves, and increases annually up to the point of flowering. Apart from a few interruptions during years with low rainfall (early 1980s and late 1990s), *Glai* increased and stabilised at a

maximum of about 45 m^2 m^{-2} until about 2034. With the introduction of moderate stocking rates, however, the maximum *Glai* value declined. This trend in *Glai* was interrupted only by considerably drier years and moderate grazing. The figure shows a reliable increase in biomass, probably produced mostly by “sage-” and ”low DMD shrubs”, as indicated by Figure 86.

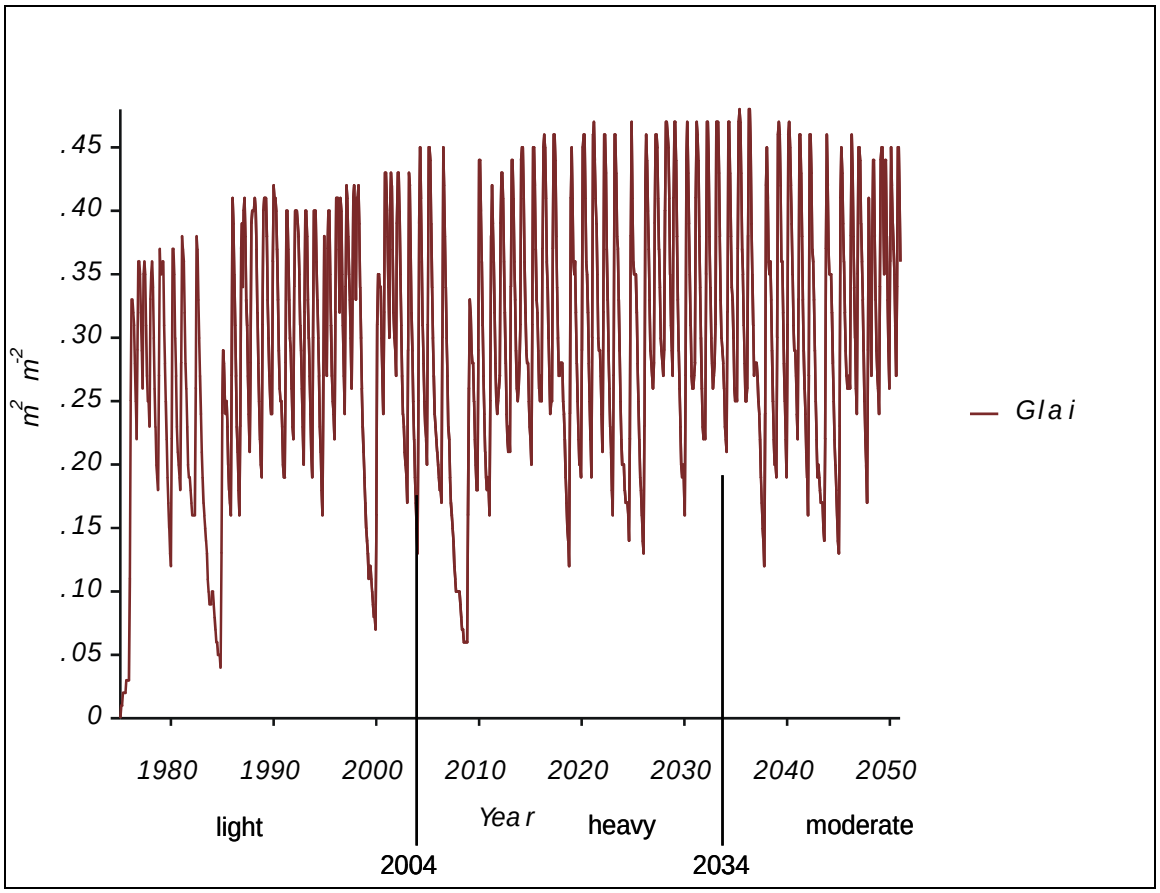

Figure 87: Simulated annual sum of green leaf area index *Glai* (m^2 m^{-2}) for all three PFT’s in the southern ranges (based on the diagnostic cell) from 1975-2051.

4.7.2 Nitrogen cycle and Nitrogen budget

Figure 88 displays the limitations to plant growth by nitrogen (*Eff-N*) and water (*Eff-W*) in the diagnostic cell of the modelled system. Values above 0.2 indicate limitation of plant growth by the factor in question; a value of 1.0 indicates low limitation. *Eff-W* held constant at 0.4 (see section 4.5.2, Figure 54 and Figure 55). This was due to the parameterised soil properties and climate constraints used here (see section 3.1). However, *Eff-N* was highly variable during the 75 years of the simulation. The values for N mainly fell between 1.0 and 0.80, indicating highly variable conditions with respect to N limitation in the system.

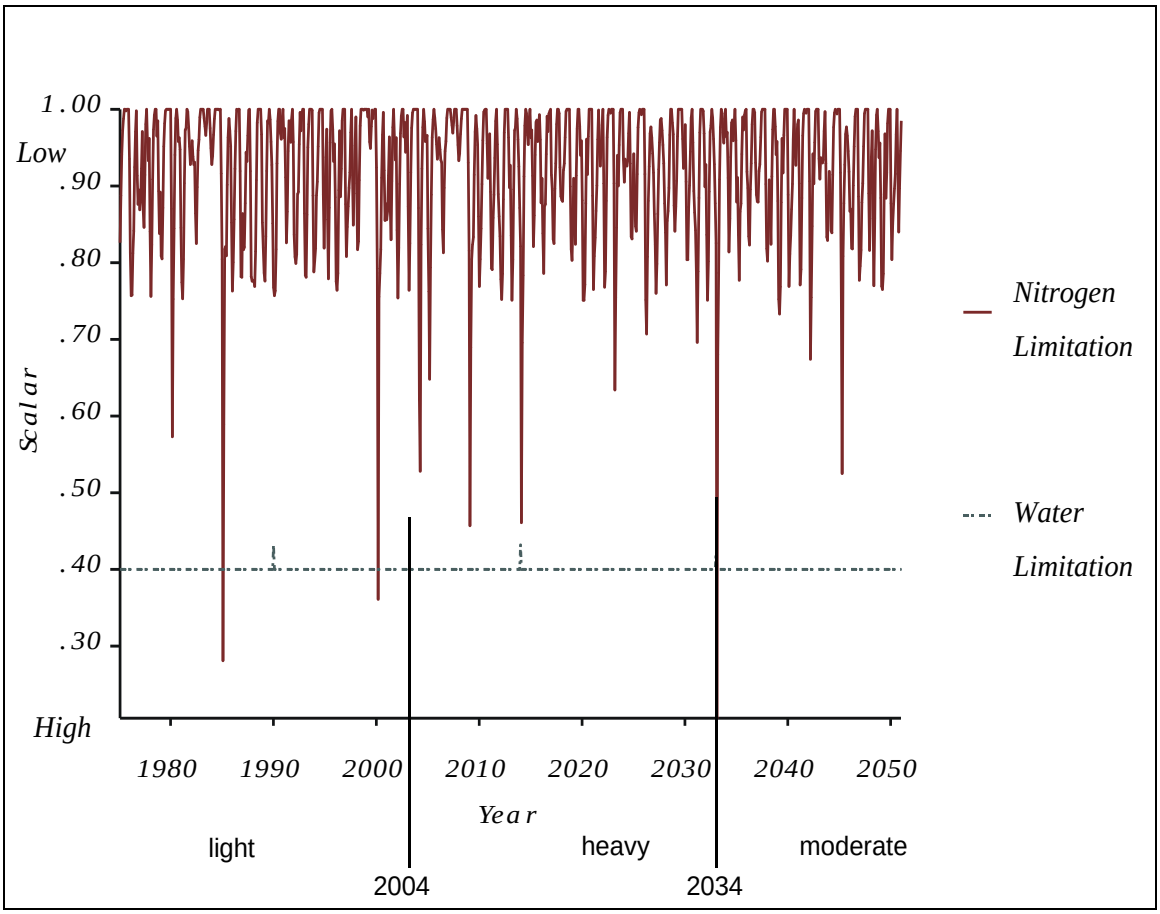

Figure 88: Annual sum of scalar unit changes in nitrogen (red line) and water (dashed blue line) limitation (ranging from 0.2 to 1.0) for the southern ranges (diagnostic cell) from 1975-2051.

Nevertheless, N content is variable, probably due to the variation in stocking rate (e.g., in 2034) and lack of rainfall (e.g., in the early 1980s and late 1990s). Generally, the N situation was adequate for plant growth (0.8 to 1.0), as sufficient resources were probably stored and provided by soil litter. Another source for plant available N might be animal urea. However, N limitation increased after the transition to heavy grazing, making it unclear whether plant N is discharged by animals.

Figure 89 illustrates *N:B* ratios at the plant (*Pl-N:B*), active biomass (*Act-N:B*) and leaf (*Lf-N:B*) levels (see section 4.6.2) in the diagnostic cell. *Pl-N:B* ratios were mostly less than 0.010 for the entire simulation. This ratio fell to even less than 0.007 during time periods with very low rainfall (e.g., the early 1980s). The transition to heavy stocking rates induced a decline in *Pl-N:B*, but an increasing trend was observed thereafter until the transition to moderate grazing, when *Pl-N:B* decreased slightly again.

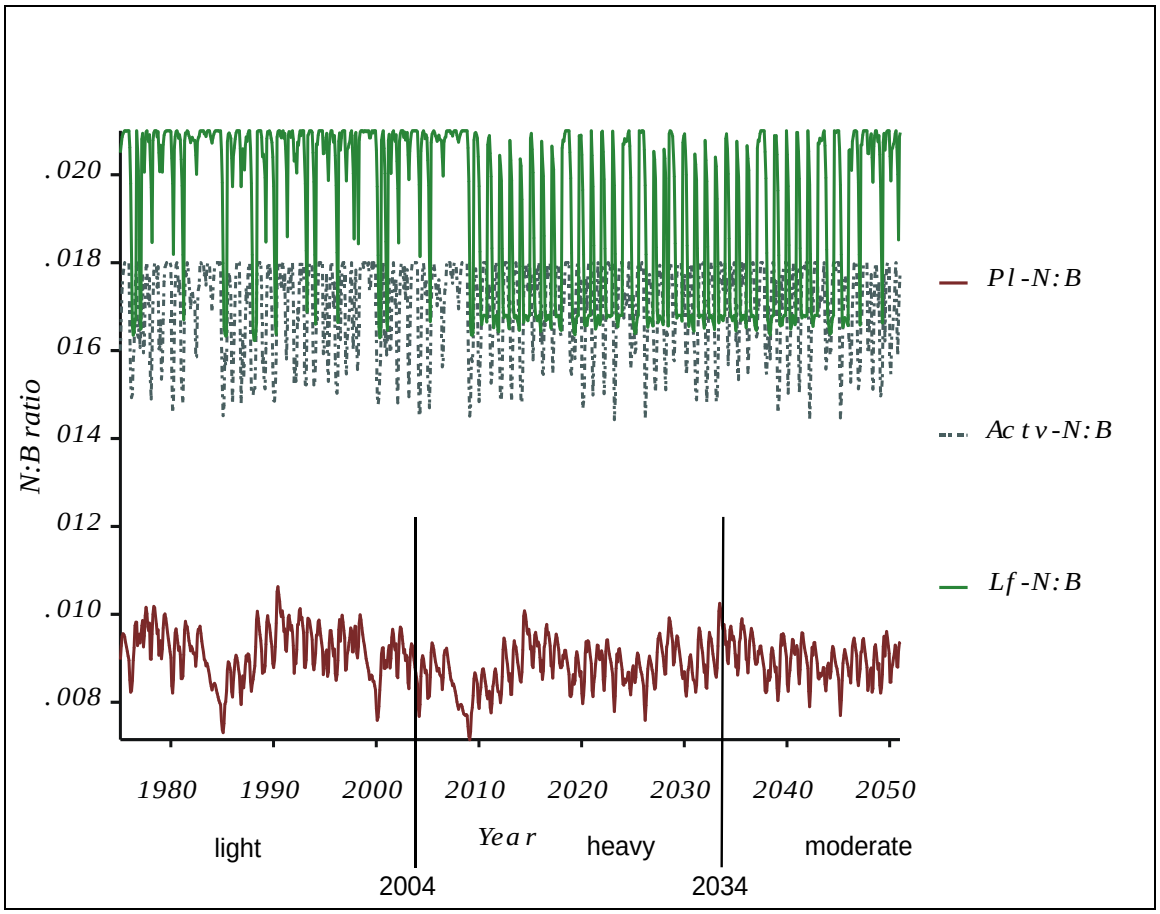

Figure 89: Simulated annual sum of monthly *N:B* ratios for plant *Pl-N:B* (red line), active *Act-N:B* (dashed blue line) and leaf *Lf-N:B* (green line) levels for the southern ranges (diagnostic cell) from 1975-2051.

Lf-N:B ratios ranged between 0.021 and 0.016 during the simulation. Notably, *Lf-N:B* values tended to remain close to the upper value (0.02) until the introduction of heavy stocking rates. Under heavy grazing, the range of *Lf-N:B* values remained the same, but the values tended to remain close to the lower value for longer periods, indicated by the narrow peaks at 0.02 (see section 4.6.2). A possible explanation might be that before 2004 there was enough N to hold the level of biomass production. This relationship broke down as N decreased after the introduction of heavy stocking rates. The *Act-N:B* ratio, used to transfer *Pl-N:B* to leaves and to maintain shoot growth, stabilised in a range of 0.015 to 0.018.

Figure 90 shows N content (g m^{-2}) of “evergreen-”, “low DMD-” and “sage shrubs” for the entire Drâa zone. Maximum values for “low DMD shrubs” declined continuously throughout the simulation, from 1.1 g m^{-2} to about 0.2 g m^{-2}, while “evergreen-” and “sage shrubs” were subject to large variations in N. Primarily induced by climate, N content stabilised at about 0.3 g m^{-2} and 2.0 g m^{-2} for “evergreen-” and “sage shrubs”, respectively, until the introduction of heavy stocking rates. However, “sage shrubs” had the largest quantity of N. Maximum values for this group of shrubs declined only once, to 0.8 g m^{-2}, a few years after (see section

4.7.1) the introduction of heavy grazing. N content then stabilised at about 1.6 g m^{-2} with large inter-annual variations.

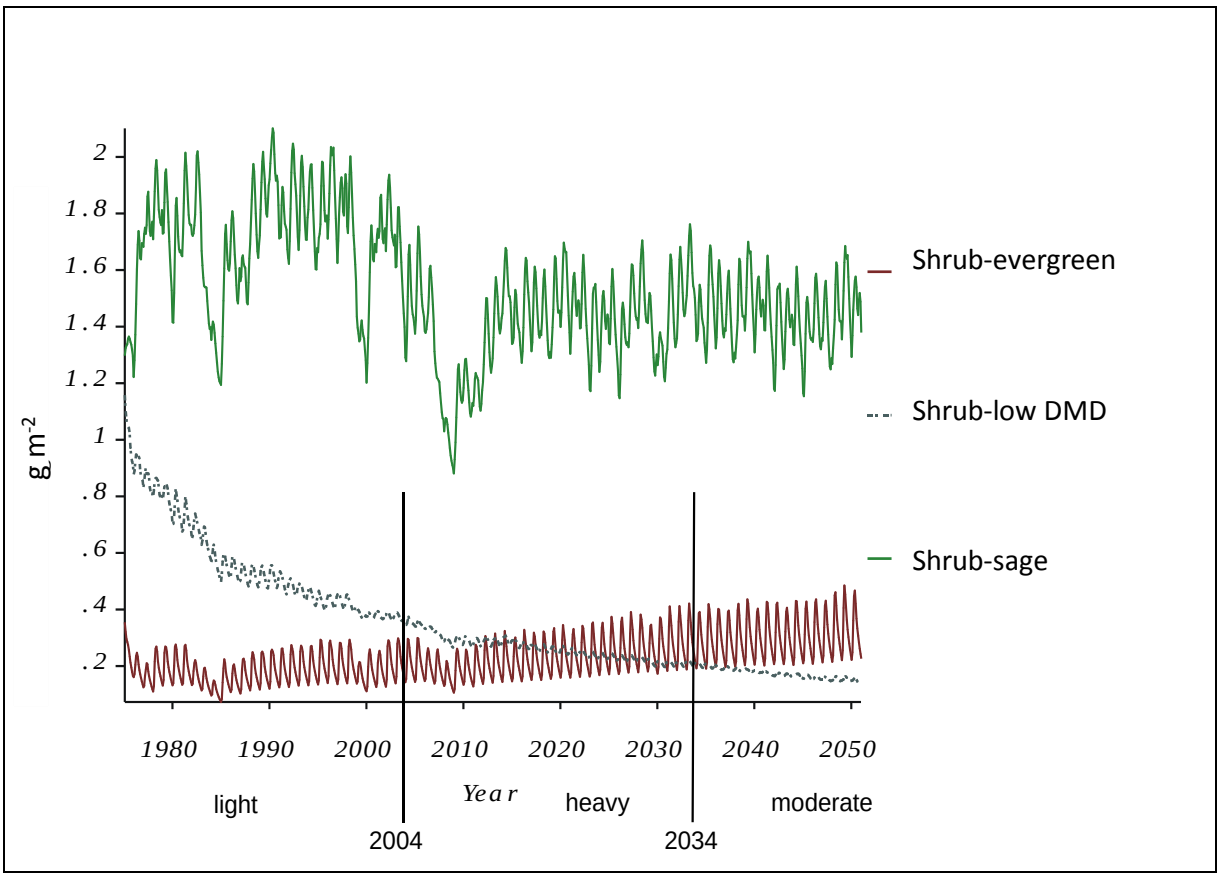

Figure 90: Simulated annual sum of N content (g m^{-2}) for "evergreen-" (red line), "low DMD-" (dashed blue line) and "sage shrub" (green line) for the entire Drâa zone from 1975-2051.

The trend for "evergreen shrubs" before the heavy grazing period is notable. Values for this group of shrubs stabilised at about 0.3 g m^{-2}, with inter-annual variation. After the introduction of heavy stocking, values for "evergreen shrubs" continuously increased to about 0.4 g m^{-2} and even exceeded the N content of "low DMD shrubs". After the introduction of moderate grazing, "evergreen shrub" N values increased to about 4.5 g m^{-2}. Here, it is necessary to distinguish between the effects of herd numbers and climatic effects for each type of shrub. Heavy grazing led to a decline in N content and stabilisation at a lower level for "sage shrubs". The "sage shrubs" are probably affected strongly by variation in animal number due to their high spatial ground cover and animal dietary preference. Nevertheless, climate also had a strong effect on N content. The "evergreen shrub" N content was less affected by variation in animal numbers, as this group of shrubs has less ground cover. Changes in stocking rates are second in importance to lack of rainfall in explaining the continuous decline of "low DMD shrubs".

4.7.3 Animal condition

Figure 91 characterises the predicted energy balance (*Ebal*) according to condition index (*CI*) throughout the simulation for nomadic sheep and goats in the entire Drâa zone. Note that the *CI* of nomadic sheep and goats is identical to that of sedentary sheep and goats. As described in section 4.6.3, *CI* for sheep and goats was initially 1.0, indicating a balance between energy used by animals, e.g., for travelling, and the energy intake rate, e.g., from edible biomass. This ratio was set based on observations from the model adaption procedures. This index was subject to small variances around a value of ± 1.0 during the first 30 years of the simulation (with light stocking intensities), indicating good animal condition. The introduction of heavy grazing in 2004, with (nearly) doubled numbers of animals, prompted a decline in *CI* during the following years to 0.65. The *CI* values increased subsequently, but showed large inter-annual fluctuation. This indicates a dramatic imbalance in animal energy budgets, mainly due to the lower availability (see Figure 92) and greater spatial variation in abundance of edible biomass (see Figure 93) and the intensive resource usage by the larger herds.

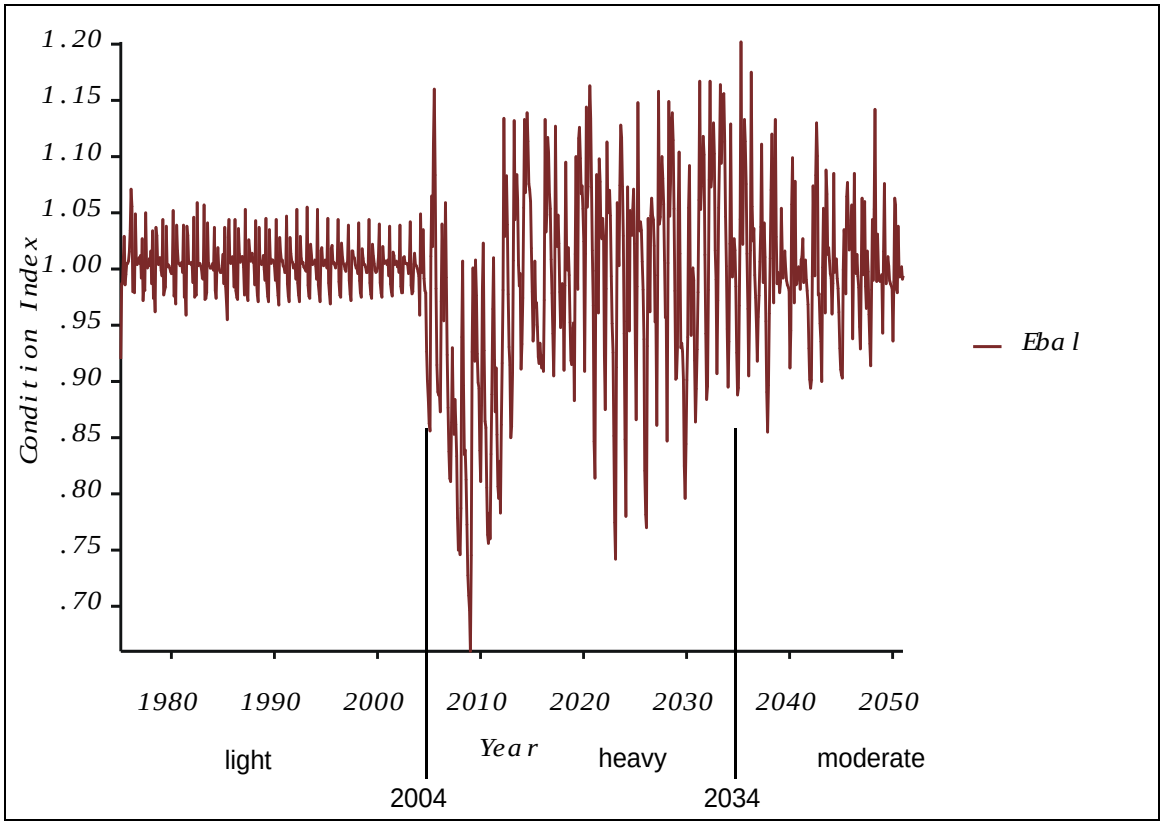

Figure 91: Simulated annual sum of the animal condition index (*CI*) formulated as energy balance *Ebal* (values range from 0.65 to 1.0) for sheep and goats in the Drâa catchment area from 1975-2051.

Reducing animal numbers to moderate stocking intensities after 2034 caused *CI* values to normalise, but *CI* continued to fluctuate. Energy balance thus provides insight into appropriate feeds for animals and the availability of biomass in space.

Figure 92 shows the consumption of herbaceous biomass by sedentary (*Hrbspp1*) and nomadic (*Hrbspp2*) sheep and goats (g m^{-2}) and compares this to the total biomass (*Biomtot*) predicted for the entire Drâa zone. *Biomtot* is the sum of herbaceous and shrub biomass available for animal consumption. Hence, the amount of herbaceous biomass should normally be subtracted from *Biomtot*. The light stocking intensities in 1975 to 2004 offered enough palatable *Biomtot* to animals in the system, as demonstrated by the relatively low but constant *Hrbspp1* and *Hrbspp2* values. Nevertheless, *Biomtot* decreased due to animal feed requirements and the periodic absence of rainfall during this period. The heavy stocking rate from 2004 to 2034 tended to further reduce *Biomtot* while increasing *Hrbspp1 and Hrbspp2*. This is consistent with the description of energy balance above. Thereafter, *Biomtot* increased again, but was not able to fully satisfy the dietary requirements of the animals; both *Biomtot* and *Hrbspp1* and *2* showed constant rates. This pattern did not change substantially after the introduction of moderate stocking rates.

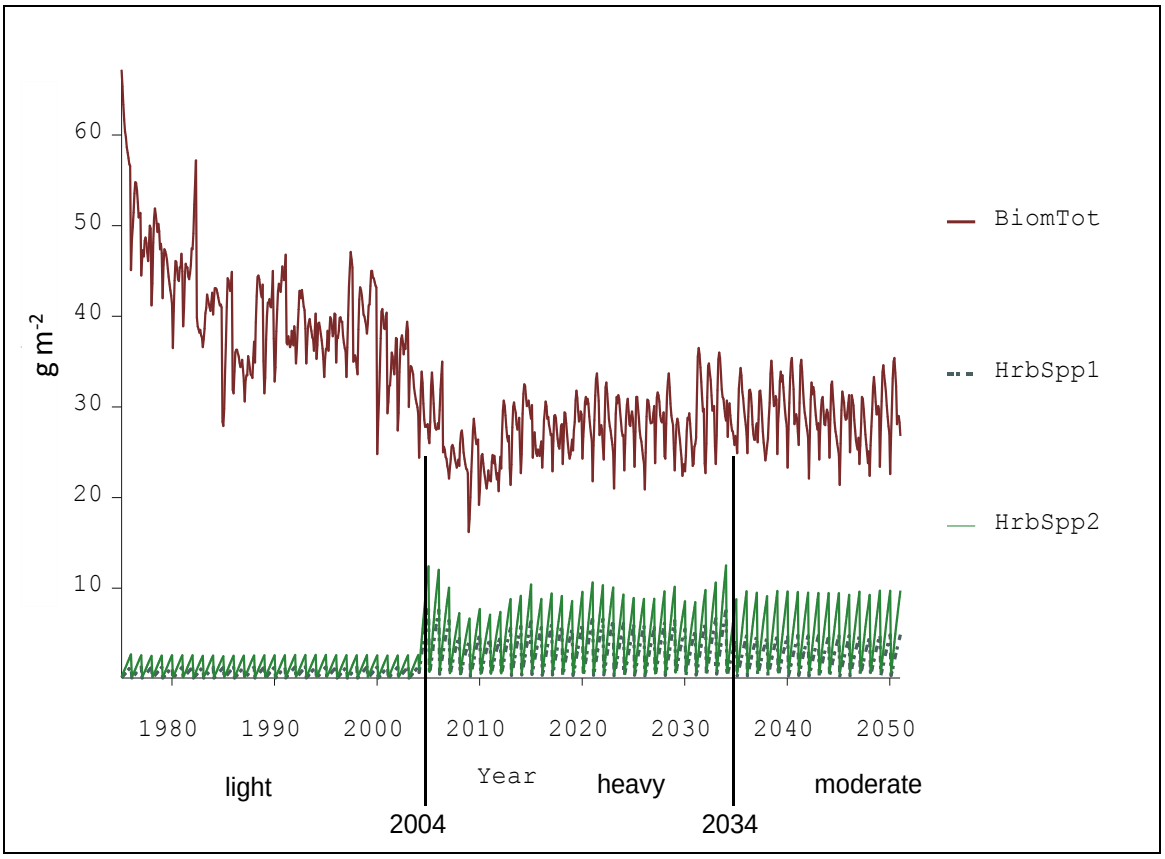

Figure 92: Annual sum of herbaceous consumption (g m^{-2}) by sedentary *Hrbspp1* (dashed blue line) and nomadic *Hrbspp2* (green line) sheep and goats and total (live+dead) biomass *Biomtot* (red line) production for the entire Drâa zone from 1975-2051.

Figure 93 shows the predicted weighting factors of shrubs and grass in the summer (May) diet of both types of sheep and goat herds. The proportion of shrubs in the diet of nomadic sheep and goats increased continuously from 0.34 to >0.60 during the first 30 years. With the introduction of heavy grazing, the percentage of shrubs in the nomadic diet declined to only 0.10, then increased again to 0.25. Under moderate stocking rates, the proportion of shrubs in the nomadic diet further increased to 0.30.

Under the light stocking rate, the proportion of shrubs was greater than the proportion of grasses in sedentary diets, but decreased from 0.25 to 0.05. However, the constant increase of shrubs in nomadic summer diets under heavy and moderate stocking rates inhibited sedentary shrub consumption, thus reducing the proportion to <0.05. The variation in grass usage between nomadic and sedentary herds (solid red and green line) was notable. Grass consumption by sedentary herds exceeds that of nomadic herds. This is probably due to the large numbers of nomadic animals, which primarily focus on shrubs; sedentary herds must use the proportion left over by nomadic herds. Finally, nomadic herds may be able (due to their numbers) to fully satisfy their energy requirements by consuming shrubs; thus, grasses are negligible in nomadic diets. In contrast, sedentary herds probably must consume both shrubs and grass to satisfy their energy requirements (see Figure 91).

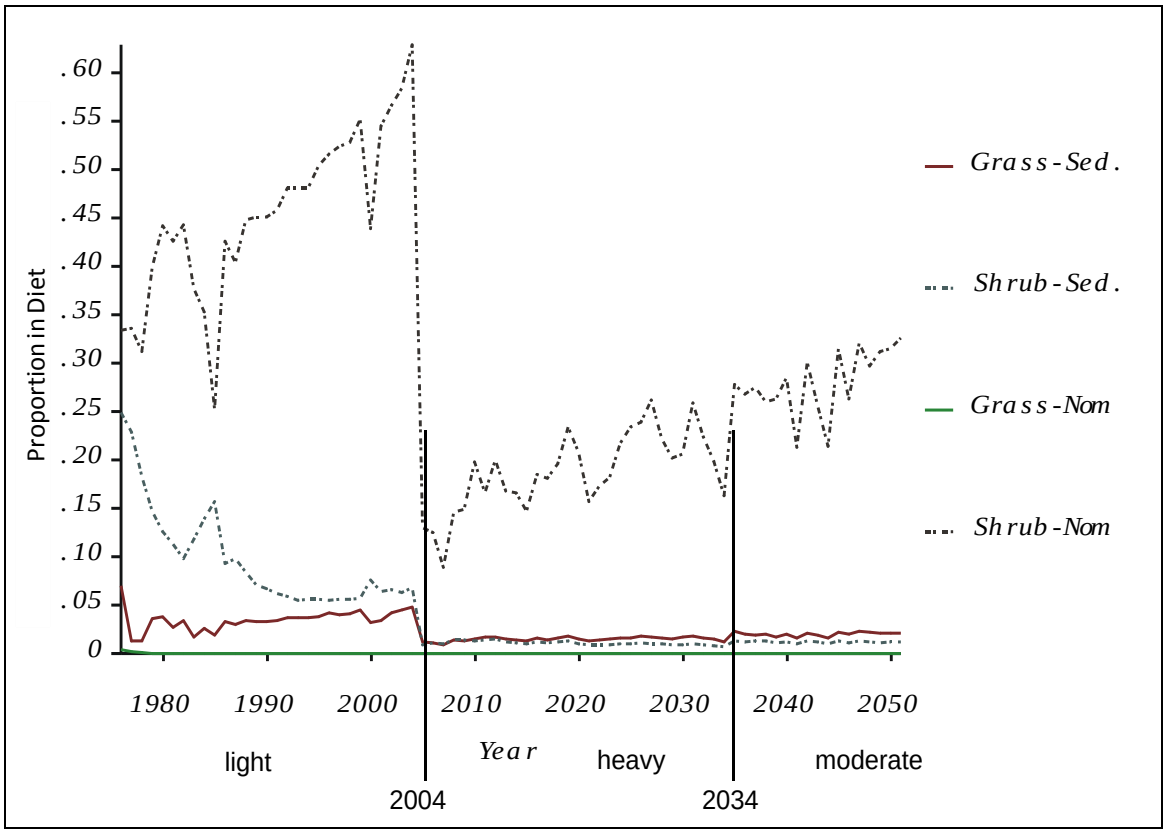

Figure 93: Proportions of shrubs (dotted lines) and grasses (solid lines) in the diets of nomadic *–Nom* (green/black line) and sedentary *–Sed.* (red/blue line) sheep and goats (as weighting factors) during the summer (May) for the entire Drâa zone from 1975-2051.

The sharp decline in the proportion of shrubs in nomadic and for shrubs and grasses in sedentary diets was due to the change in herd numbers as more animals competed for about the same amount of biomass. Furthermore, after the switch to heavy stocking intensities, both nomadic and sedentary herds tended to change their diets in response to the new conditions. While the weighting factor of shrubs in the nomadic diet continuously increased, the weighting factor of shrubs in the sedentary diet reached the same value (0.02) as that of grasses. With the introduction of moderate stocking intensities, the consumption of shrubs by nomadic herds increased further, while the weighting factor of shrubs in the sedentary diet was lower than that of grasses.

Similar trends were observed in winter (November) when comparing sedentary and nomadic grass and shrub dietary weighting factors (Figure 94). However, winter biomass figures were generally higher in terms of g m^{-2} (see Figure 73), and this was reflected by the dietary weighting factors for shrubs and grasses in the nomadic and sedentary diets. The results for light stocking intensities (1975-2004) were similar between May and November, as the weighting factor for shrubs in the nomadic diet continuously increased and that in the sedentary diet continuously decreased. However, both factors were initially higher and the gradient for nomadic diets and slope for sedentary diets were steeper under these conditions. In addition, the proportion of grasses in the sedentary diet was considerably greater (>0.05) during this period than in the summer. In contrast, the weighting factor for grasses in the nomadic diet was again 0.0 for the entire simulation period. The break after the transition to heavy grazing in 2004 was not as crucial for nomadic shrub diets but was even stronger for sedentary diets in the winter than in the summer. This was probably due primarily to aestival biomass availability (see Figure 73) and secondarily to nomadic herd numbers. Moreover, the immediate increasing trend in weighting factors of shrubs in the nomadic diet indicates that high biomass availability in November continued after the transition to moderate stocking rate.

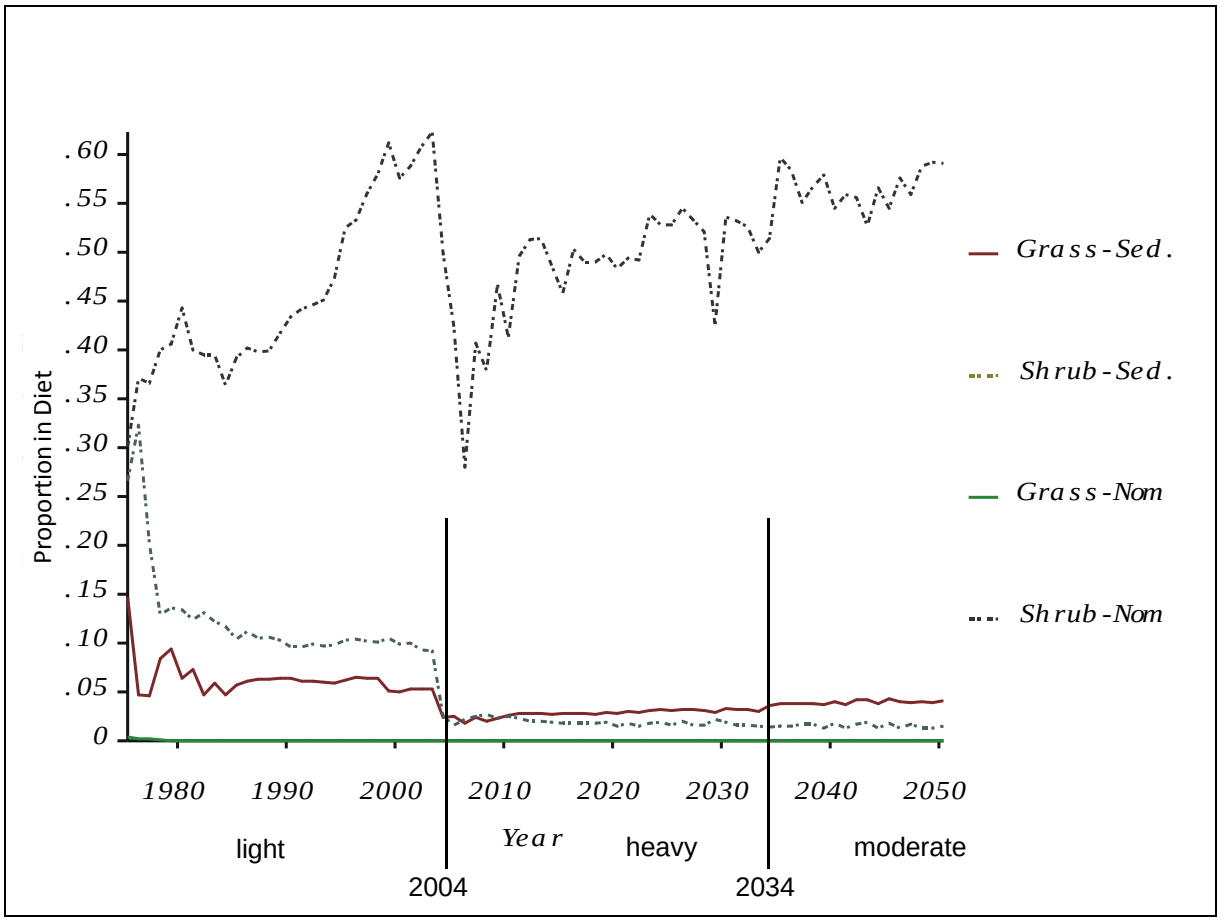

Figure 94: Proportions of shrubs (dotted lines) and grasses (solid lines) in the diets of nomadic *–Nom* (green/black line) and sedentary *–Sed.* (red/blue line) sheep and goats during the winter (November) for the entire Drâa zone from 1975-2051.

In contrast, the weighting factor of shrubs in the sedentary diet declined considerably (to 0.02) due to nomadic shrub consumption, as in the summer. Sedentary diets probably must be satisfied by increased consumption of grass. This again shows the overall dominance of shrubs in nomadic diets, which makes shrubs unavailable to sedentary herds as indicated by the weighting factor.

4.7.4 Water budget

Figure 95 illustrates the change over time in plant available soil water content (*Swatr 1*) for the diagnostic cell. The soil type was No. 31 (see Appendix, Table 35). *Swatr 1* is calculated based on field capacity (*Swatr 2*, at about 10 mm) and wilting point (*Swatr 3*, at about 14.5 mm).

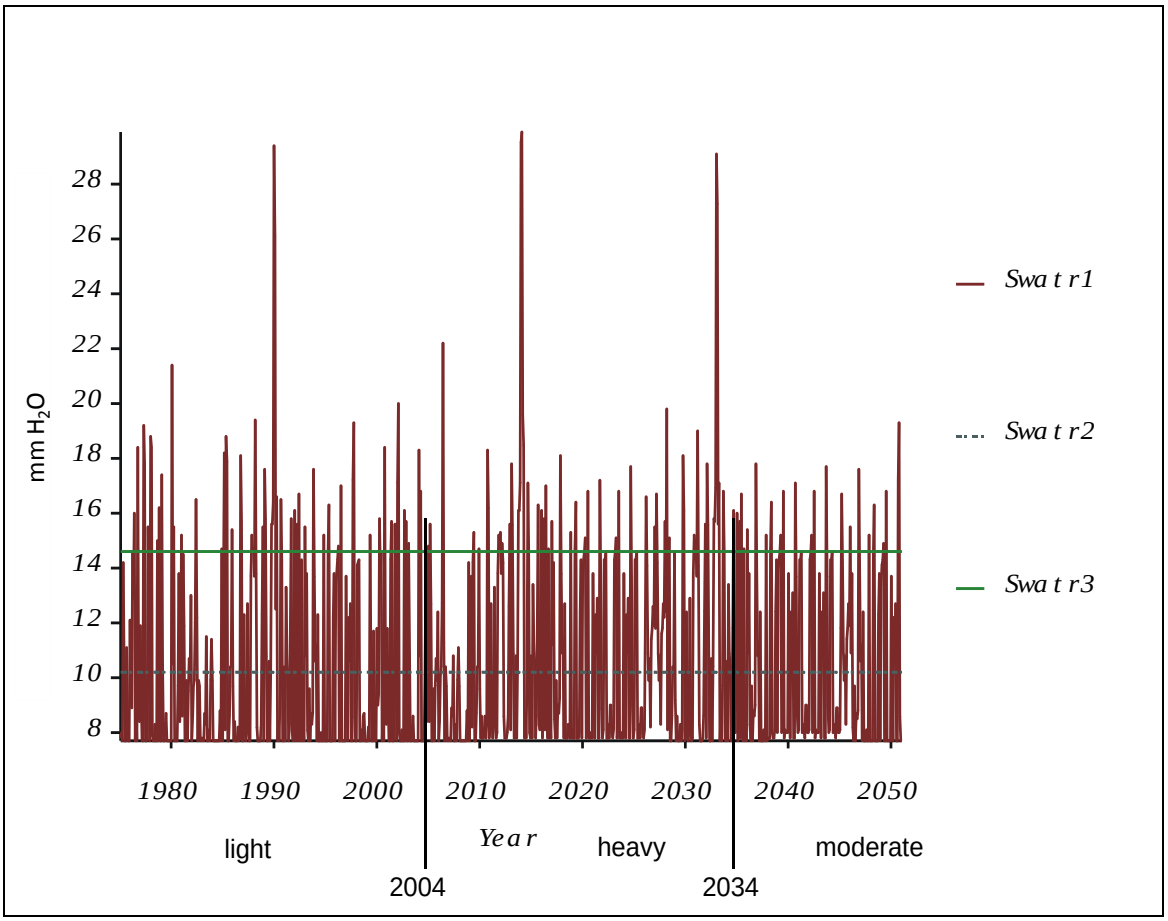

Figure 95: Total annual plant available soil water *Swatr 1* (red line), field capacity *Swatr 2* (dashed blue line) and wilting point S*watr 3* (green line) (mm H_2O) for the diagnostic cell from 1975-2051.

These low *Swat1* values compared to northern ranges are remarkable, but are probably related to the low rainfall in the southern ranges (see section 1.4.1).

A low difference between *Swatr2* and *Swatr3* is a necessary condition for plant access to the available water resources. In addition, *Swatr1* is strongly dependent on *SysPpt* and highly variable among years. Annual peak *Swatr1* values ranged between about >28 mm (maximum) and about 9 mm (minimum). For this scenario, the low level and high inter-annual variation of *Swatr1* and its strong relationship to *SysPpt* (see Figure 96) are of great importance for plant growth. Stocking rates and their variation probably did not have an effect on *Swatr1*.

Figure 96 shows predicted *SysPpt* and *SysPet* (mm) values for the entire Drâa simulation zone. The following paragraph describes annual cumulative maximum and minimum values of *SysPpt* and *SysPet*. *SysPet* ranged between an annual upper limit of >800 mm in summer to a lower limit of about <200 mm in winter. Annual *SysPpt* was predicted to be mostly <100 mm in this simulation. Probably *Bsev* contributed greatly to *SysPet* for the southern ranges of the Drâa catchment (see Figure 74). The variation in stocking rates did not have a considerable effect on either *SysPpt* or *SysPet*.

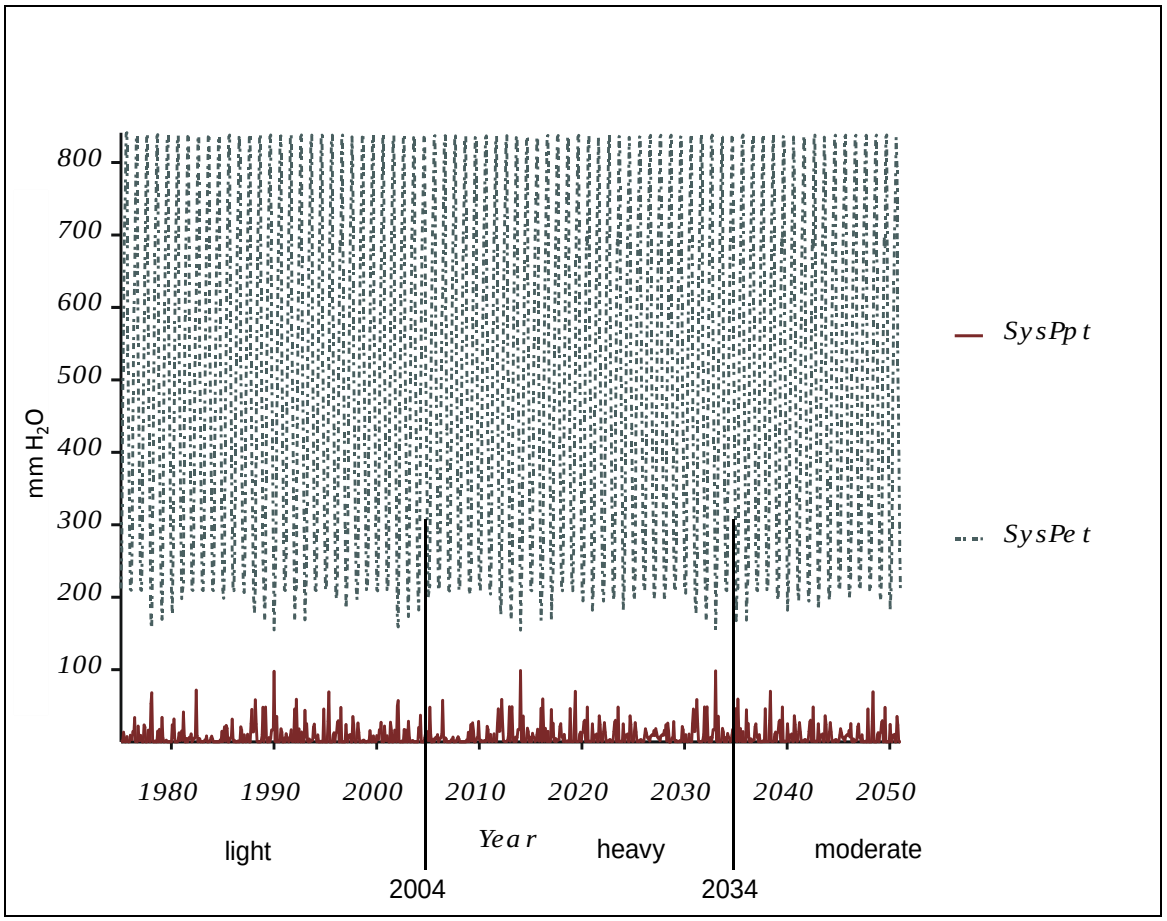

Figure 96: Monthly predicted precipitation *SysPpt* (red line, mm H_2O) and cumulative predicted annual evapotranspiration *SysPet* (dashed blue line, mm H_2O) for the entire Drâa zone from 1975-2051.

Figure 97 displays plant water consumption in terms of annual sum of actual (*Cs-act*) and potential (*Cs-pot*) stomatal conductance in the diagnostic cell. The following paragraph describes summer maximum and winter minimum peaks of annual *Cs-act* and *Cs-pot*. Predicted *Cs-pot* ranged between an annual minimum of about 70 mmol m^{-2} s^{-1} and maximum of approximately 110 mmol m^{-2} s^{-1}, while predicted *Cs-act* ranged between an annual minimum of <10 mmol m^{-2} s^{-1} and maximum of about 90 mmol m^{-2} s^{-1}. These figures indicate the huge inter-annual variability of *Cs-act*, reflecting actual regional (diagnostic cell) plant water availability. On the other hand, the narrow range of *Cs-pot* may indicate the annual limit of plant water resources for the southern ranges of the Drâa catchment. The variation in stocking rates had no effect on these figures.

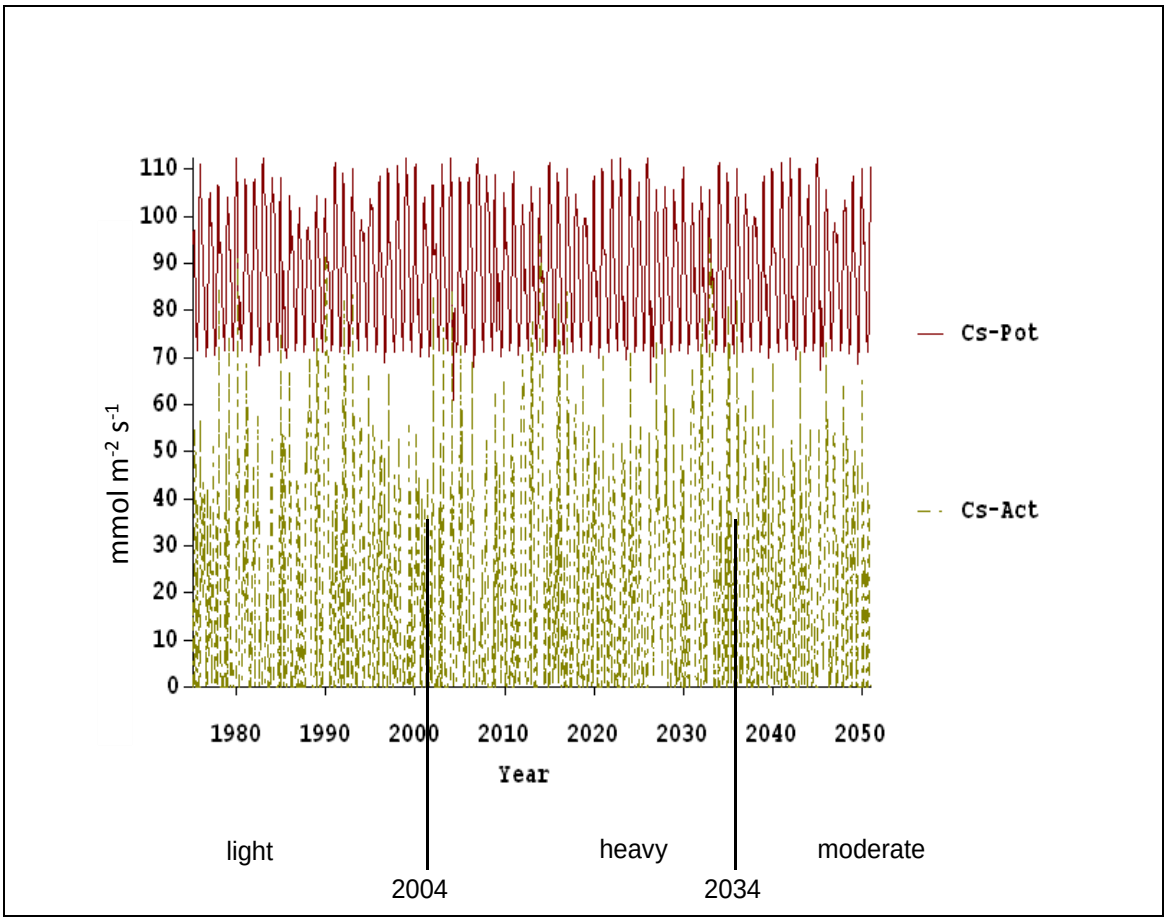

Figure 97: Total annual simulated sum of potential stomatal conductance *Cs-pot* (red line) and actual stomatal conductance *Cs-act* (dashed green line) (mmol m^{-2} s^{-1}) for the diagnostic cell from 1975-2051.

The predicted *trans* values (data not shown) as sum of the shrub, herbaceous and tree PFT's are reported for the diagnostic cell under CO_2 levels of 700 ppm and 350 ppm (for February, May, August and November). Differences in *trans* values between these two scenarios were in the range of approximately 1 mm to 10 mm per month. The doubled CO_2 scenario showed higher *trans* amounts then the recent (350 ppm) scenario throughout the simulation. Increased *trans* levels, together with higher temperatures, were observed during this model run.

However, *trans* amounts represented only a small part of the regional water budget compared to *Bsev*, as already shown for other scenarios. The results of these scenarios are discussed in section 6.2.

4.7.5 Plant water budget consequences of atmospheric CO_2 scenarios

In this section, the results described in the previous section are compared to contemporary CO_2 concentrations (350 ppm). Except for the CO_2 level, all other climate parameters were identical between simulations. Hence, differences resulted from increased CO_2 levels only. Due to the fact that increased CO_2 concentrations mainly affect the metabolism of plants and thus plant growth, the plant' s *Ps, WUE* and *Cs-act* are highlighted in the following paragraph. For the elevated CO_2 scenario, average monthly *Cs-act* values were reduced by approximately 35%, whereas monthly average *Ps* rates were increased by approximately 16%. However, stomatal conductance is driven by temperature and humidity. The same is true for *trans* rates, for which water vapour deficit plays a key role. Monthly average *WUE* values increased at approximately 37% on average. No differences in *Swatr 1* were found between these two scenarios, because *SysPpt* amounts were equal. The increase of *WUE* and *Ps* in a water-limited system, indicated by the constant *Swatr 1* value, nevertheless greatly affected plant growth. *ANPP* under the doubled CO_2 content scenario showed a significant increase for all PFT's. In contrast, the recent CO_2 scenario showed a decline in *ANPP* for the shrub PFT and constant values of *ANPP* for the herbaceous PFT. The large increase in *ANPP* of the shrub PFT under doubled CO_2 was thus mainly physiologically driven by the increased *Ps* and *WUE*, as other parameters (such as *Swatr 1*) are climate-driven.

Table 33 is used to summarize scenario outcomes concerning vegetative growth parameters of different PFT groups in order to transfer this knowledge to dicussion in chapters 6.1 and 6.2.

Table 33: Summary of annual *ANPP* (kg ha^{-1}) amounts and monthly average herbaceous and shrub PFT group leaf and root (kg ha^{-1}) amounts for all scenarios.

annual *ANNP* sum* (kg ha^{-1}) ± (SD)		**base-line scenarios (1985-1999)**		**scenario (2a) IPCC A1B (2010-2050)**	**scenario (2b) IPCC B1 (2010-2050)**	**scenario (2c) IPCC A1B heavy (2010-2050)**	**scenario (3a) 700ppm (1985-2050)**	**scenario (3b) 350ppm (1985-2050)**
		Ouar-zazate (1a)	**REMO (1b)**					
herbaceous "fine grass" PFT		58 ± 6	89 ± 19	143 ± 30	69 ± 10	61 ± 10	96 ± 18	52 ± 8
diagnostic shrub PFT		"sage shrub" (plant group no. 8)					"low DMD shrub"	
		1222 ± 520	1491 ± 185	1293 ± 458	1413 ± 411	1290 ± 452	339 ± 52	257 ± 48
avg.monthly *ANPP* (kg ha^{-1}) *plant group no.* (Table 4)		**1a**	**1b**	**2a**	**2b**	**2c**	**3a**	**3b**
(1)	leaf	2.8 ±0.6	4.8 ±0.8	10.0 ± 2.1	4.1 ± 0.8	2.6 ± 0.5	7.2 ±1.7	3.6 ±0.9
	root	27 ±3	52 ±4	74 ±14	41 ±3	35 ±2	61 ±14	33 ±6
(2)	leaf	3.7 ±0.9	4.6 ±1.4	3.5 ±1.5	2.7 ±1.1	2.0 ±0.8	2.1 ±1.1	1.6 ±1.0
	root	60 ±13	75 ±21	43 ±18	46 ±17	39 ±19	39 ±17	28 ±16
(3)	leaf	1.6 ±0.6	3.8 ±1.8	2.6 ±0.6	2.1 ±1.0	1.4 ±0.8	3.0 ±1.7	1.2 ±1.1
	root	19 ±6	44 ±18	26 ±5	23 ±11	15 ±9	29 ±15	13 ±11
(8)	leaf	90 ±8	133 ±11	130 ±21	118 ±19	97 ±23	108 ±21	71 ±20
	root	368 ±34	562 ±53	535 ±87	486 ±75	404 ±88	463 ±66	287 ±63
(7)	leaf	70 ±5	116 ±9	141 ±19	124 ±12	89 ±17	109 ±21	83 ±20
	root	356 ±37	607 ±63	695 ±93	621 ±52	467 ±91	547 ±66	398 ±58
(6)	leaf	15 ±4	18 ±6	10 ±4	11 ±5	10 ±5	8 ±4	7 ±4
	root	140 ±27	165 ±37	100 ±33	111 ±38	103 ±40	78 ±35	68 ±33

*Model ´warm-up phase have not been considered for calculation

In the same tenor, Table 34 serves as basis on water budget parameters derived during simulations for dicussion chapters 6.1 and 6.2.

Table 34: Summary of annual predicted *SysPpt*, *SysPet* and average *trans* (mm of 4 months) amounts for all scenarios-a comparism of diagnostic cells.

annual (mm a^{-1})	base-line		scenario 2a	scenario 2b	scenario 2c	scenario 3a			scenario 3b		
	1a	1b				light	heavy	moderate	light	heavy	moderate
SysPpt	122	154	241	280	241	128			128		
SysPet (accumu-lated) maximum peak	800	600	550	650	800	850			850		
SysPet (accumu-lated) minimum peak	200	200	250	150	200	150			150		
Average *trans* (4 months)	40	74	66	60	47	54	62	59	64	73	64

5 Modelling uncertainties

The modelling results presented here are subject to various kinds of uncertainties. This section aims to highlight the most significant sources of these uncertainties occurring in the modelling process. The sources are as follows: the model structure, the model input data and the data used for model adaption and plausibility test.

5.1 Model structure

A weakness in this modelling approach occurs primarily in the discrepancy between the temporal resolution of the input data and the variable calculations. For example, climate data, such as precipitation for each month, is broken down by the model into weekly data to consider environmental processes (e.g, to calculate evapotranspiration rates; see chapter 2.4.2). The input data based on spatial characteristics (e.g., vegetation and soil maps) created a second set of uncertainties. These are based on the sub-model internal re-calculation of the basic input maps into the derive parameter values, such as hight points from the digital elevation model. Another example is the precipitation against slope regression curve routine which can not be altered by the user.

5.2 Model input data

5.2.1 Relief

The spatial resolution of the digital elevation model, the slope and the aspects of maps at a resolution of approximately 30 x 30 m (Drey 2004) provide an ample amount of information. Considering the large catchment extent, and thus the huge amounts of data, this information had to be aggregated to a resolution of 125 x 125 m for the first model application and then further to a 1 x 1 km resolution for catchment simulation purposes. During these processes an information loss occurs, which we believe will effect the calculation of certain variables, such as the precipitation to the slope of the regression curve that was described in the

previous section. While a higher resolution would be very useful for model applications this would require powerful computers and a need to focus the research approach on the numerous SAVANNA© outcomes (see Chapter 7).

5.2.2 Vegetation

In this modelling approach, the environmental landscape characterisation is achieved only using a vegetation cover map as this is considered to be the most important part of a grazed ecosystem simulation. Information on landcover that is derived from remote sensing images and GIS in developing countries is scarce. Therefore, the elaboration of a vegetation map for this approach was of tremendous importance. The vegetation map by default is based on the spatial resolution given by the digital elevation model. The aggregation of maps to the chosen resolution is followed by a considerable loss of spatial vegetation pattern information. However, the basic vegetation map was elaborated by Finckh and Poete (2008). The vegetation classification was worked out by Finckh (2006), including habitat simulation results by Oldeland (2006). The vegetation data are derived from iterative field studies, the analysis of the spatial distribution of plants, and the physiology and emergence of these plants in both fenced and unfenced observation plots in typical rangelands. Finally, the raster resampling was elaborated by Poete (Table 3, see Figure 11) based on an in-field land-use classification. However, the vegetation cover and the vegetation dynamics in semi-arid to arid landscapes are subject to huge inner- and inter-annual variability. Nevertheless, we had strong confidence in the vegetation cover classification as it represents the major predominant plant types and their abundances based on intensive field studies including Finckh and Staudinger (2002); Finckh (2006); Oldeland (2006) and Gresens (2006). The plant types in this approach are parameterised and classified according to their individual physiometric measurements with a subjective, author-based selection process and a snapshot of plant growth that is transferred into the model PFT database. Based on this information the *Lai* and ground cover information are computed by the model. Additional information on the individual PFT group growing seasons was parameterised by the author.

The representation of animal foraging on plants was of great importance and was included in the vegetation map in the model. On the other hand, this map contains the most detailed classification of plants with respect to resolution. We attempted to accommodate the intersection between both requests in our vegetation map. The advantage with this type of vegetation classification map is that no other map sources, such as the occurrence of herbaceous plants, etc., are needed. However, validation data, especially on the bases of the PFT's, are hard to achieve in this highly variable environment. Other SAVANNA© ecosystem

applications (Coughenour and Chen 1997; Coughenour 2005) used carrying capacity outcomes, such as the species numbers of animals, to validate the vegetation quantities and their dynamics. A detailed description of the temporal development of the animal species numbers at the provincial level was only available for the period from 1980-2000. Species numbers and conditions as a result of the simulations indicated that, nevertheless, the carrying capacity was not changed (despite the heavy stocking rate scenario). Otherwise, the animals would have died and their numbers would seriously decrease. On the other hand, the uncertainties for the upper level of biomass production at Wadi Drâa must be considered. These weaknesses could only be verified by further detailed plant/biomass evaluation studies.

5.2.3 Soil data

Since soil profile maps were not available the Continental Hydrosphere project group B2 were relied for the elaboration of a soil map. Uncertainties in the soil data are based on the resolution of the soil map used (Klose 2009), primarily due to the aggregation of the soil map to match the model resolution (1 km^2). One of the weaknesses of soil data is the difficulty of asssigning reprensentative soil profiles for a specific area. Representative soil profiles were derived using topographic transect sequences. The physical and chemical properties of each horizon identified were analysed and transferred into a soil database (Klose 2009). Due to model restrictions (see chapter 2.4.2) only two soil horizons are simulated here. Specific soil properties needed for this research approach, such as the permanent wilting point and the field capacity (see Appendix, Table 35), were statistically analysed and then broken down and plotted in a soil map with a grid-cell size of 1 km^2. The alignment of the soil property information in the regional maps during these statistical procedures is critical and thus another source of uncertainty. As the model resolution was chosen to be 1 km^2, the loss of information from the regional level must be taken into account. Simulations have shown that the soil drainage functions have also been underrated during this approach and therefore further investigations at this site might be useful.

5.2.4 Climate data

A factor responsible for model weaknesses relating to climate is the need to personally pre-processing any data used in order to fulfil the specific model format restrictions. The input datasets were obtained from IMPETUS stations and used for the Taoujgalt model application

(see chapter 3.1). Historical data (1980-2000) for the base-line scenarios were provided by DRH stations. In general, the upscaling of automatic weather station data to the level of the entire catchment area implicates spatial uncertainties (e.g., on rainfall patterns). Furthermore, automatic weather stations data records suffer from data loss due to instrumental errors and local restricted rainfall events that were not recorded by instruments, especially in the southern Drâa catchment. In general, the high variability of rainfall is not well recorded by any of these weather stations. Continuous climate station data was a must in this study and therefore the climate data were supplemented with DRH data. In total, eight weather stations throughout the catchment have been considered for base-line runs.

Weather input data for the model came from monthly measures of the amounts of precipitation and maximum and minimum temperature. Spatially interpolated rainfall values for each grid cell were computed as the simulation progressed. Regressions of rainfall on elevation (calculated from the base of each station) were performed for each month. Coughenour (1993) constated that generating monthly precipitation data by dynamic spatial interpolation accounts for the effects of elevation and the topographic induced rainfall that is common in this region. Since this approach is time-intensive, we recommend the usage of monthly precipitation maps that would decrease rainfall pattern uncertainties in this region.

The availability of continuous REMO scenarios (2001-2050) using the ASCII standard reduces the uncertainties form data formatting processes and enables this approach to study the influence of different scenarios, notably IPCC A1B and B1. The main uncertainties during the adaptive phase of the IPCC scenarios came from weaknesses in the rainfall patterns in the regional downscaled model of the REMO. With respect to rainfall trends in Western Africa, using different global circulation models (GCM's) might cause different trends to be observed (IPCC 2007a). Here, the REMO is based on the physical parameterisation of GCM ECHAM4. If the REMO would be nested into another GCM or into other IPCC SRES[16] scenarios, different outcomes concerning the *ANPP* and the Drâa catchment carrying capacity might result. This underlines the key role of climate scenarios within this modelling approach.

5.3 Model sensitivity

A set of uncertainties arises regarding the behaviour of the model while alternating certain input parameters. A weakness of the model used in this approach, in terms of the sensitivity

[16] SRES – acronym for Special Report on Emissions Scenarios

analysis, is the high module complexity of interfering parameters. Furthermore, a specific single input parameter could not be extracted and observed exclusively as in other modelling approaches. Moreover, in our case, the sensitivity analysis is identical to any other ordinary simulation run. This means that all of the input parameters are considered and the changes to the sensitive parameter in the output must be excluded and evaluated. These facts complicate the determination of the effects caused by one certain parameter to another.

Sensitivity analysis is a quality criterion of model applicability and we have decided to observe the effects of various *WUE* values towards the *NPP* for "sage shrub" in the sensitive study. This parameter decision was based on the first SAVANNA© modelling approaches, for which similar sensitivity analyses have been conducted (Coughenour, 2008, personal communication). Our previously mentioned approach is different to that of Hiepe (2008) who conducted a sensitivity analysis in order to evaluate the calibration parameters. The proposition by Giertz (2004) to alternate variables by ±10% was increased here to 15% in order to observe changes in the output parameters. The -15% variation of *Cs* minimum/maximum values affected leaf *NPP* at +5%, which we distinguish to be a considerable increase. A +15% variation provoked a decrease of 4% of leaf *NPP*. Sensitivity values that range from 0.02 to 0.05 are in the low to medium range (with <0.05 considered as low and >1.0 considered as high in the sensitivity evaluation scheme (Giertz 2004)). These changes indicate that the expected positive alternation (a constraint of the minimum/maximum range) of *Cs* led to a reduction in biomass as the *WUE* decreased and vice versa.

5.4 Model adaption and plausibility test data

The major uncertainties in the model adaption data occurred in the plant type group data, as these datasets required a large amount of data for parameterisation. The specific subjective view of the modeller is needed to classify plant compartments to fit into the model. However, the plant biomass of the predominant species and its phenology fit the observations from plots throughout the catchment. Permanent observation plots for biomass development on rangelands and the transectional and topographic depended observations would decrease model uncertainties.

The data availability for model plausibility test was limited. For a few years only seasonal aggregated plant numbers and *Lai* calculations are available for the Taoujgalt sub-catchment. Model uncertainties also occur with aggregated data. Uncertainties arise as *Lai* estimations display huge inter-annual variability, similar to those of the aggregated plant

numbers. The test of plausibility in the comparison of the NDVI derived from remote sensing images with the simulated green shrub *Lai* indicated a moderate fit (see chapter 3.4). The onset of vegetative growth is replicated in the simulated green *Lai*, but it is overestimated. The weakness of the NDVI estimations derived from remote sensing images is due to the general reception of ground signals. A differentiation between soil and vegetation signals, especially in arid and semi-arid areas, is difficult (Fritzsche, 2008, personal communication). Moreover, the derived simulated SAVANNA© vegetation signal is a result of the induced IPCC *ANPP* growth and this might explain the overestimation compared to the NDVI signal (see Chapter 6.1).

5.5 Evaluation of modelling uncertainties

As with most modelling approaches, a broad range of uncertainties must be considered when interpreting the model results. In this case, the majority of the uncertainties are related to the model input and the plausibility of the data, as these are the most important sources of model weakness. The first as it defines the starting point of the modelling approach. Second as it evaluates the model's plausibility and applicability. It is also important to mention the input of both the vegetation database and the rainfall data, as uncertainties within these datasets occur in the extrapolation from the point scale to the mapping data (see previous chapters). Further ecosystem research in the area should focus on the importance of the vegetation database. Continuing to capture grazed plant parts and their spatial occurrences will aid in carrying forward this approach. A key point for future scientific research should be the improvement of high-resolutional spatial rainfall patterns in semi-arid landscapes.

Uncertainties in the model structure are difficult to specify. Nevertheless, as ecosystem modelling expert knowledge continuously increases so does the accomplishment of models, such as SAVANNA© in semi-arid to arid research areas. Future research must increase and broaden the understanding of plant water circulation for more plant species in this environment, as well as for the physical soil parameters used to reduce the uncertainties regarding climate impact. Modelling soil moisture and its impacts on runoff, for example, could not be investigated in detail during this approach, but was subject of investigations by Klose 2009.

The uncertainties regarding the outcomes of the individual scenarios (2001-2050) are higher than the base-line run results (1980-2000). This is primarily due to the uncertainties in climate data pertaining to the extremely difficult reception of rainfall patterns in an arid environment and significant topographic relief. Future computational development will likely

enable scientific research to enhance the spatio-temporal resolution of climate models. Further research concerning the downscaling of mechanisms in the REMO model to regional level of the Drâa catchment is in progress. Moreover, this development will probably include coupling between the atmosphere and the ground in greater detail.

The databases used for model adaption and plausibility test primarily enable this approach to accurately model the semi-arid to arid grazed ecosystem. A further discussion of the research hypothesises and the fit of the simulation results into our scientific knowledge of the subject will be given in Chapters 6.1 to 6.2.

6 Discussion

6.1 Spatio-temporal development of PFT's

A fundamental aspect of ecosystem functioning in grazed ecosystems is the *ANPP*, as it determines the amount of energy that is available for higher trophic levels (McNaughton *et al.* 1989). In order to predict the *ANPP*, it is necessary to understand and correctly represent the factors that control phytomass production (Wiegand *et al.* 2008). Regarding the annual temporal development of the *ANPP* for herbaceous and shrub PFT we must assume a decline concerning the annual averages of the *ANPP* contents for most scenarios. The exception to this tendency can be found in scenarios 2b and in both of the CO_2 scenarios (3a and 3b) for the Southern ranges, in which the annual *ANPP* is constant (3b) or increases (3a). The annual rainfall amount is primarily responsible for the temporal development of *ANPP* as outlined by Paruelo *et al.* (1999). This argument is supported in Figure 5, which shows the coincidence of the *ANPP* with rainfall amounts. As the rainfall regime in the study area is highly variable (c.p. chapter 1.4.1) we must differentiate *ANPP* amounts in their regional context and in the respective scenario. Meanwhile, the base-line run of Ouarzazate (1a) shows a decline in rainfall, which can also be seen in the IPCC scenarios 2a and 2b. The base-line scenario (1b) indicates a slight increase and the CO_2 scenarios (3a and 3b) have constant rainfall regime. The base-line simulation for Ouarzazate "sage shrub" PFT *ANPP* (the diagnostic shrub for the northern catchment, see chapters 4.5.1-4.7.4) has outcomes that might serve as references for discussing simulation results (see Table 27) as its inherent rainfall level and temperature drivers are based on climate station measurements. The simulation resolution (month) is probably temporaly closest to the *ANPP* reference estimations in other studies. The Ouarzazate run (after model "warm-up" valid for all following model output descriptions), exhibits the monthly average "sage shrub" PFT *ANPP* amounts of 640 kg ha^{-1}, but shows an annual average sum of 1222 kg ha^{-1} in the basin of Ouarzazate for the 1985 to 1999 run (see Table 33). Even if the amounts are calculated at a diagnostic cell in the central basin we can consider this as an overestimation if we compare these to the regional biomass assumptions at predominantly *Artemisia herba-alba* that are 156 to 324 kg ha^{-1} by ROSELT (2004) and 1 to 250 kg ha^{-1} in the Anti Atlas Ridge, estimated by Nording (2008). However, the predicted inter-annual "sage shrub" *ANPP* variability of 520 kg ha^{-1} for the Ouarzazate run and the study of the biomass ranges for *Artemisia herba-alba* indicate that the high intra- and inter-annual variability related to soil and rainfall amounts are representative of the difficulties of semi-arid *ANPP* estimations.

Moreover, the *ANPP* contents are temporal assumptions and are valid in a small regional context only as outlined by Gresens (2006). Floret *et al.* (1982); Le Houérou (1995) and Gresens (2006) pointed out the pre-dominant character of the perennial *Artemisia* and *Hamada* steppes as well, and their high variability in this region supports the assumptions of this study.

An explanation for the "sage shrub" *ANPP* overestimations compared to those of ROSELT (2004) and Nording (2008), which are particularly noticeable in scenarios 1b, 2a to 2c, can be delivered by scenario specific rainfall level, water and temperature parameters. These considerably affect "sage shrub" PFT development along with nutrient availability and the particular animal stocking rates that are discussed in the next chapter. The base-line 1a run calculated annual averages of 122 mm *SysPpt* for 1985 to 1999 (see Table 34). Thus only slightly overcomes the long-time annual average of 104 mm (at "Mansour Eddahbi" reservoir (DRH 2004)). The "sage shrub" *ANPP* contents decrease continuously in the late 1990´s, similar to the *SysPpt* for the amounts that decrease at approximately 20 mm in the simulation. Alternatively, scenario 1b (1985-1999 run) calculated annual *SysPpt* averages of 154 mm and the amounts increase at approximately 7 mm during simulation. The IPCC (2010-2050) runs 2a and 2c report 241 mm and scenario 2b 280 mm; a considerable *SysPpt* overestimation for this region compared to DRH (2004) estimations. Both scenarios, however, predict a decline of approximately 30 mm (2a) and 14 mm (2b) of *SysPpt* amounts, respectively. We assume that in these scenarios particularly higher *SysPpt* levels induced higher average annual "sage shrub" *ANPP* contents compared to the Ouarzazate scenario 1a and literary references. For scenario 1b, an annual average sum of "sage shrub" *ANPP* of 1491 kg ha^{-1} (SD 185 kg ha^{-1}) was estimated (see Table 33). Comparing the two base-line runs, the average sum of the "sage shrub" *ANPP* amounts is added from 1a to 1b but the SD is lower. This is probably a clue that the continuous higher *SysPpt* amounts mentioned before have some effect. Scenario 2a reported 1293 kg ha^{-1} of shrub *ANPP* (SD 458 kg ha^{-1}); 2b calculated 1413 kg ha^{-1} (SD 411 kg ha^{-1}) and 2c reported 1290 kg ha^{-1} (SD 452 kg ha^{-1}) in the basin of Ouarzazate. The reasons for these considerable predicted *ANPP* differences compared to the measured amounts beside *SysPpt* might be multiple.

In addition to the *SysPpt* amounts, temperature (*T*) plays a key role for the "sage shrub" PFT growth because it affects photosynthesis (*Ps*) rates. Hence, the variation of the monthly T_{min} and T_{max} considered in this approach is crucial. The long-term difference of minus 11.0°C in the T_{max} comparing between base-line scenario 1a (32.7°C) and 1b (21.7°C), together with the increased T_{min} of +0.6°C at scenario 1b, might be responsible for the predicted increase of "sage shrub" *ANPP* contents in the 1b run. Moreover, the reduction of T_{max} reduces temperature stresses and together with the described rainfall patterns might induce shoot growth. These assumptions are in line with Gresens (2006) who reported an induced shoot

growth for *Artemisia herba-alba* at a monthly precipitation of approximately 10 mm and daily average Temperature of >15°C. From the 15-year simulation average, only two months (April and May) report rainfall amounts <10 mm for 1b run compared to five months (April to August) at scenario 1a, which may support an increased "sage shrub" *ANPP* at sufficient water supply for 1b run.

In addition to rainfall, the *Avlwat* plays a key role for PFT *ANPP* growth. *Avlwat* is given in a monthly average for scenario 1a (1985-1999) as 10.9 mm and for 1b (1985-2000) as 12.4 mm. These amounts neglect the seasonal *Avlwat* limitations described by Gresens (2006) for the Taoujgalt plain and support an overestimation of the "sage shrub" *ANPP* contents. This assumption is reasonable, especially regarding the water contents for scenarios 2a and 2b, as these scenarios are again at the onset of monthly averages of approximately 30 mm. These increased monthly *SysPpt* amounts are probably once again responsible for the increased "sage shrub" *ANPP* growth. Weber (2004) reported a strong relationship between soil water contents and precipitations in this region. Moreover, he predicted that apart from rainfall heightening for different test sites, a base water content in deeper soil horizons of approximately 15% Vol. for Taoujgalt and of about 10% Vol. for Bou Skour. Hence, it is assumed that in the here presented study the predicted *Avlwat* contents are to high. In our study it is likely that we paid less attention to the water drainage to deeper soil layers. High solar irridiance are common for this study region and are similar among all runs. If water is not limited it probably induces PFT growth and the result can be seen as *ANPP* overestimations in accordance to Gresens (2006).

The southern range CO_2 scenarios are different as we used climate station parameters and forwarded rainfall and temperature patterns (Born, 2007, personal communication). The average *SysPpt* for both CO_2 runs is 128 mm. Which is an overestimation compared to the long-time measurements of an average of 80 mm (DRH 2004) at the Zagora station (Figure 1) and thus *Avlwat* was again overestimated. These water settings probably led to the overestimated *ANPP* amounts comparable to the northern range scenarios. In scenario 3b the CO_2 (350ppm) may serve as reference for *ANPP* estimation in the literature in order to evaluate the model outcomes. Increased average summer temperatures of +1.1 C (for both scenarios throughout the simulation) from 2005 onward resulted in 257 kg ha^{-1} (SD, 48 kg ha^{-1}) (see Table 33) at the 3b scenario, with an annual average sum of "low DMD shrub" (diagnostic shrub for southern ranges) PFT *ANPP*. These model estimations are below the amounts from the northern ranges but at the upper level of shrub PFT patterns measured on the southern ranges compared to single point or transect measurements of 3 to 541 kg ha^{-1} by Yessef (1996) or 7 to 26 kg ha^{-1} by ROSELT (2004). Herbaceous "fine grass" (diagnostic herbaceous PFT) leaf *ANPP*, as an important animal feed factor (see chapter 1.4.4), had predicted outcomes for the 3b scenario (CO_2 350ppm) that are of a monthly

average at 3.6 kg ha^{-1} (SD 0.9 kg ha^{-1}) (see Table 33) and at an annual sum of approximately 43 kg ha^{-1}. In contrast to these amounts Yessef (1996) estimated 270 kg ha^{-1} for the perennial grass *Panicum turgidum* at Fezouata range near Zagora. Comparing the amounts of the total palatable biomass for southern ranges by Yessef (1996) at 5 to 287 kg ha^{-1} with the amount predicted here, again these numbers show the high spatio-temporal variability of biomass and low replicability due to high dependence on rainfall. Nevertheless, the lower *ANPP* productivity in southern ranges compare to the northern is modeled correctly. In scenario 3a (CO_2 at 700ppm) this overcomes previous amounts at an annual average sum of "low DMD shrub" *ANPP* of 339 kg ha^{-1} (SD 52 kg ha^{-1}). The reasons for the higher "low DMD shrub" *ANPP* contents at doubled CO_2 might be due to increased *Ps* and higher *WUE* rates (c.p. chapter 6.2) brought in by partial stomata closure in accordance to Coughenour and Chen (1997).

In order to appropriately describe the temporal PFT development, a sub-differentiation of shrub and herbaceous PFT must be considered to fully include resource use and *ANPP* outcomes. In the basin of Ouarzazate herbaceous PFT plays an important but minor role in *ANPP* contents compared to shrub PFT (see Table 33). Both the shrub and herbaceous PFT, as well as their sub groups ("fine grass" etc.), compete for nutrients, light, water and are considered as animal feed in all scenarios. For the shrub-herbaceous PFT relation it is imperative that the higher the shrub plant size the higher its resource competitiveness and advantages (Owens and Norton 1990). During this study we observed a similar trend for the "sage shrub" number per hectare where large sized shrubs dominated smaller size classes (see chapter 2.5.1.3). Herbaceous "fine grass" *ANPP* decreases for northern range scenarios 1a, 1b, 2a and 2b scenarios for the same reasons as described for shrub *ANPP* above. The decreasing rate is probably due to lower herbaceous *ANPP* contents (kg ha^{-1}) as well as ground-cover. The relatively high proportion of shrub *BNPP* observed during model runs (Table 33) compared to herbaceous *BNPP* might explain the high competitiveness of the shrubs as assumed by Tielborger and Kadmon (2000). Herbaceous PFT's have shallow roots and in this approach probably use soil water resource and nutrients more effectively. Instead, shrub PFT´s may use soil water but additionally because of higher ground-cover and *Lai* benefit from inducing rainfall as assumed by Bates *et al.* (2006).

N and water uptake by the roots and their usage must be observed at not only the herbaceous and shrub inter-PFT level, but the PFT level as well. In this study this was achieved through the observation of the temporal development of "sage"-, "low DMD"- and "evergreen shrubs" as well as "fine"-, "coarse"- and "alpine grass" root and leaf content development (Table 33). According to this list, the individual PFT group development is considerably different although all groups are confronted by low N availability in this region as documented by El Moudden (2005) and Nording (2008). During this study, the *N:B* ratio

provides information on the temporal availability of N for plant shoot growth. The flowering period for most shrub PFT's is autumn, here we observed that during the simulation period, and especially during the end of each year (e.g., at "sage" and "Low DMD" in the shrub PFT group), the temporal N availability becomes weaker. Our assumption is that the N resource pool was exploited by PFT's and probably not sufficiently refilled, for example, by PFT litter. As water during simulations is sufficient an increased shrub *ANPP* production is facing limited N pools. The wetter than usual rainfall amounts create a qualitative response from herbage production which is dependent on the added N as reported by Henkin *et al.* (2007). Animals might be an additional N source (Coughenour 2005) but we assume that they might evoke N leaching through surface clearing followed by surface runoff. Nevertheless, in this approach grazing animals did not improve N conditions. In this study the temporal development of leaves in the PFT groups is mainly caused by leaf palatability and delicateness in accordance to Christensen *et al.* (2003). Animals grazing the terrain are searching primarily for very delicate and palatable to low palatable and unpalatable PFT group leaves. Moreover, this study showed that low palatable PFT groups, such as "sage-" and "low DMD shrubs", have a higher tolerance rate against, or are more resistant (in chemical or physical terms) towards grazing. Retzer *et al.* (2006) found adaptive levels against grazing stresses and towards maintaining growth, whereas in this study highly palatable PFT leaves, such as "evergreen shrubs" or "coarse grasses", are heavily grazed and reduced in *ANPP* amounts. Other scenarios (Table 33), for example, the scenario 3a run (CO_2 700ppm), showed that PFT groups such as "alpine grass" (in *ANPP* terms) are able to adapt to heavy stocking rates and even increase shoot growth.

The monthly average herbaceous "fine grass" PFT leaf *ANPP* ranges are from 2.6 kg ha $^{-1}$ in scenario 2c to approximately 10 kg ha^{-1} in scenario 2a. The "sage shrub" PFT leaf *ANPP* showed amounts from 71 kg ha^{-1} in scenario 3b up to 133 kg ha^{-1} (scenario 1b) for the respective regional study area. These amounts are important in animal diets but they are difficult to compare as they are highly variable and until now range research did not differentiated the palatability of plant parts in this area (Table 33). A primary assumption under the realistic conditions of the herbaceous and shrub leaf *ANPP* monthly averages is likely portrayed by scenario 1a. This scenario shows "fine grass" leaf *ANPP* amounts of 2.8 kg ha^{-1} (SD 0.6 kg ha^{-1}) and "sage shrub" of 90 kg ha^{-1} (SD 0.6 kg ha^{-1}). Herbaceous and shrub PFT roots are forced to provide resources for PFT group re-growth at these adaptive levels. In semi-arid to arid environments, the amount of *BNPP* greatly overcomes *ANPP* amounts (see Table 33) and is crucial as it serves as a nutrient and water resource pool as indicated in Tielborger and Kadmon (2000) and ROSELT (2004).

The spatial distribution and development of PFT's based on their pre-dominant character and ground-cover in the study region is mainly caused by the palatability fractions of the PFT

groups, as is also described in Coughenour (2005). For example, the spatial distribution of herbaceous leaves is highly rainfall dependent and above what is commonly found in the vicinity of water wells with high animal number grazing (see Chapter 4.6.5). The impacts of grazing are further discussed in the next chapter. Summarising this chapter we can confirm the first research hypothesis – The spatio-temporal structure of the herbaceous and shrub PFT groups is highly variable under the assumptions of different climate and stocking rate scenarios. The impact of stocking rates in this approach affected the temporal structure of PFT's more profoundly, whereas the spatial structure of PFT's is assessed by both stocking and climate change as reported by Oldeland (2006).

6.2 Carrying capacity and its impacts to the regional water cycle

As denoted in the previous chapter, grazing affected the spatio-temporal PFT structure in all scenarios. In the same context in this chapter the research question that will be discussed is to what degree do stocking rates affect the specific rangeland carrying capacity. Additionally, as both factors are close and interrelated the question of how this carrying capacity affects the regional water cycle will be a subject of the discussion as well.

In this study animal stocking rates and their varied affects on the PFT structure and *ANPP* was assessed. Grazing influenced PFT group ground-cover data and the spatial patterns. Additionally these patterns appeared aggregated by the climatic changes as seen in rainfall patterns. Thus, the second research hypothesis stating that the impacts of either stocking rates or climate will permit a continuous vegetation growth and meet the requirements of human needs can be confirmed.

Changing ground cover patterns in turn influenced bare soil evaporation (*Bsev*) figures and thus the regional water cycle. This study shows that ground cover is affected by stocking rates. Whereas the base-line scenario 1a shows an average monthly shrub cover data (for the diagnostic cell) of 16% per km^2 and a maximum of 18%, scenarios 1b, 2a and 2b recorded averages of 25%, 29% and 26% for shrub cover and corresponding maxima of 29%, 34% and 31%. The higher shrub cover data of IPCC scenarios is probably due to rainfall patterns and predicted constant stocking rates. However, scenario 2c shows reduced shrub cover at 20%, which is likely related to the heavy stocking rate in accordance with reports by Alrababah *et al.* (2007). Scenario 3a (CO_2 700 ppm) and 3b (CO_2 350 ppm) depict explicit shrub cover changes in relation to stocking rates. Light stocking rates in scenario 3a predicted a monthly average of 27% that decreases to 20% at heavy stocking rates, and further to 19% shrub cover at a moderate stocking rate. Scenario 3b exhibited 20% shrub

cover for the light stocking rate followed by decreasing cover to 14% and 15% at heavy and moderate stocking rates. The difference between scenarios 3a and b is explainable by increased *ANPP* due to doubled CO_2. According to the assumptions presented by Staudinger and Finckh (2005) for the Taoujgalt test site at which *Artemisia herba-alba* showed about 13% cover in relation to topographic position. Our assumptions, except for scenario 1a, overestimate cover data. For the southern ranges (scenario 3a and 3b) one must assume even lower shrub cover data as reported by Gresens (2006). As this study covers a limited number of grazed PFT's in simulations we were not able to confirm amounts presented by Zaady *et al.* (2001) who reported a decrease in plant species density of approximately 20% as well as soil surface exposure of approximately 50% due to long-term grazing in Israel.

The base-line scenario 1a showed that even stocking rates adapted to past rainfall patterns led to a small *ANPP* decrease, which likely referred to decreasing rainfall patterns outlined by climate measurements (DRH 2004). Otherwise, the assumption of an intra-annual constant stocking rate, as in scenario groups 2 and 3, contradicts PFT regeneration periods assumed by El Moudden (2005) as it performs continuous grazing stresses. This might be the source for the permanent *ANPP* decrease seen in scenarios 2a-2c even if sufficient plant available water is provided. Comparing the two base-line scenarios (1a, 1b) and three IPCC (2a-2c) scenarios *ANPP* development the 2b scenario illustrates smallest monthly reduction rate. On the other hand, heavy stocking rates (scenario 2c) had tremendous effects on vegetation ground cover patterns and led to the highest *ANPP* reduction when comparing all three IPCC 2 scenarios. However, we may confirm here that the variation of stocking rates affects shrub ground cover, as it is reported form many semi-arid landscapes as a result of long grazing histories (Christensen *et al.* 2003).

Herbaceous and shrub PFT leaves, stems and branches are classified according to their animal palatability and digestibility in this approach. Highly palatable and preferred "evergreen shrubs" nearly extinct in *ANPP* leaf terms (in scenarios 2a-2c) and were replaced by specialists, such as "sage shrub", primarily adapted to animal feed. The "low DMD shrub" is another specialist that was less palatable but adapted to animal feed and moreover water/temperature stress tolerant. Adaptive strategies to our understanding are indicated by the constant leaf production in many simulations for both shrubs. Finally, both the "sage-" and the "low DMD shrub" leaf *ANPP* is constant and at low levels in scenarios 2a-2c, probably due to the constant grazing pressure. For grass PFT the same was observed. Grass PFT's of preferred and highly digestible by animals, such as "fine grass", are adapted to grazing, indicated by the constant *ANPP* leaf production, whereas both "coarse grasses" and "alpine grasses" heavily reduce *ANPP* leaf production. In this study scenario a selective feed intake took place, which confirms the assumption by Jauffret and Lavorel (2003) who

predicts a decrease in perennial plants for a moderate grazing intensity in the Tunesian steppe and for heavy grazing a dominance of less to unpalatable plants.

Using the ratio of digestible material to total feedable biomass as a key factor in the IPCC A1B scenario 2a grazing plots are of 40.2%, compared to 30.1% digestible material at ungrazed plots for the same scenario. An explanation might be the high dead material content at ungrazed plots as outlined in Figure 38. This is contrary the study of Zaady *et al.* (2001) that assumes higher values of grazed plots at 63.7% compared to ungrazed plots of 57.4%, which might be a result of their palatability definition, the number of plants in that study expressed by density and bare soil exposure amounts. In this approach the state of the *Artemisia* and *Hamada* steppes in the northern basin seems to be tightened so that we were not able to determine the inter-PFT changes. This may be the result of parameterised grazing preferences and palatability for *Artemisia,* which consolidate the situation (see Figure 73 and Table 33). Another study of similar precipitation regimes by Noy-Meir *et al.* (1970) gives an outlook indicating that after a long grazing history in Israel with goats and sheep (30-100 years) vegetation composition changes markedly.

The annual varying stocking rates from census data included at base-line scenarios 1a and 1b (Figure 5) showed that herders use precipitation appropriate livestock number. On the other hand, as feedable *ANPP* decreases herds must decrease or expand ranges to meet the seasonal variation in annual *ANPP*. This strategy, we believe, will continue into the near future, as well as the local tradition of resource regeneration areas in the “Agdal”. The constant annual animal numbers that are assumed here neglect the variation of animal numbers due to variable *ANPP* yields and forced the predicted *ANPP* amounts into constant low or decreased means. Translating this to the future *ANPP* would not meet animal diet requirements and subsequently human needs. Future human biomass withdrawal if continued to the predicted extent will be in concurrent situation to grazing herds on available biomasses as outlined by El Moudden (2005). Scenario 2d was used to evaluate the spatial dependencies between local and seasonal availability of forage resources (e.g., herbaceous leaves) and animal consumption (offtake) patterns. The scenario showed that herds have to move to high herbaceous leaf production areas to achieve diet requirements if rainfall amounts provoke herbaceous plant growth. Additionally, herds must satisfy their water requirements, which affected vegetation plots by the physical breakdown in the vicinity of water wells. We were able to distinguish the transformation of the intake of herbivores into varying feed availability. The seasonal character of the feed accounted mainly for the daily digestive capacity and for the changing diet quality as seen by the *CI* development (see Figure 71). Animal condition was seriously affected, as seen in scenario 2c, if the feed resource in the research area was seasonally depleted. In this approach the number of animals allocated to sedentary or nomadic herds largely determines the feed selection

between grasses and shrubs. As both numbers are very different, the larger nomadic herds dominate and the shrub compare to grass consumption in the animal diets is overestimated during this study compared to other studies, e.g., by Weber *et al.* (2000).

The stabilisation of grazed ecosystems supposes an equal feed to consumer ratio as resulted when (biomass) resources are heterogeneous with respect to species composition and herbivores adjusted their resource selection adaptively over the course of the year, as explained by Smith *et al.* (2000). In terms of stability, we must assume that the simulated ecosystem was labile because plant growth for most areas in the Drâa catchment was highly dependent on variable rainfall amounts and because herds are restricted in PFT selection by either topographic or tribal limits. Additionally, constant herd numbers contradict the assumption of adaptive resource selection. The considerable instability and rainfall dependence of resources forced local breeders either to give-up or illegally enter resource areas as confirmed by CBTHA (2002). To overcome the considerable nutritional hollows in the animal diet most herders breed native Moroccan goat species, which, unlike sheep, possess additional fat reservoirs (CBTHA 2002). Nevertheless, the productivity of Moroccan sheep and goats must be determined as low compared to European species due to the variation in feed availability and the lack of water resources as well as the increasing land degradation as documented by Iniguez (2004). Thus, we may assume that moderate grazing intensities under extreme variable rainfall regimes are fairly productive under the viewpoint of animal weight gain, which is supported by Retzer *et al.* (2006).

Grazing activities in the study region must be determined at the threshold of animal production due to the nutritional quality of PFT's and the spatial limitation of productive areas. Herders must consider large areas in order to satisfy animal diet requirements. But ranges are administrative state property and distributed to different tribes, hence herders are allowed to graze in predefined areas only (Le Houérou 1995). Additionally, the growing concurrence of grazing activities on fertile land is evoked by the claim for arable land to meet the growing population demand on agricultural goods as documented by CBTHA (2002). This forces herders to move to less fertile grazing grounds that are less adequate in terms of dietary requirements. Hence, we may assume that the governmental regulation of herd sizes against the background of future increasing climate uncertainties must be considered as a management practice for future decades. Nevertheless, the intensification of biomass resource protection areas (the "Agdal"), rainfall expertises and short-term forecasts, plus adaptive herd numbers might provide the potential of *ANPP* in future to meet both animal and human needs.

The third research hypothesis, effects to the regional water budget, can be answered only indirectly. Sap flow measurements of Mountainous aspen tree *Populus canescens* are used

here to present the most important factor in the regional water cycle – the non-grazed oases tree populations. Selected results on *Populus canescens* water consumption showed maximum daily ranges for Tichki on June 25th 2005 of 42 l m^{-2} d^{-1} for tree (channel) one up to 307 l m^{-2} d^{-1} at tree (channel) three (Figure 31). The amount for the Tichki experiment may be due to large rainfall amounts reported in the direct vicinity at the Tichki field station of 48 mm in 24 hours on June 22nd 2005 (Figure 32) that may have yielded water saturated soils and thus sufficient tree water supply. Ameskar, in earlier spring on April 6th 2005, indicated 47 l m^{-2} d^{-1} for tree (channel) one and 72 l m^{-2} d^{-1} for tree (channel) two (Figure 29). These Ameskar experiment amounts indicate lower levels compare to the Tichki on the one hand due to smaller leaf area assumed. On the other hand probably because of the greater water stream distance (see chapter 4.2.1) and missing rainfall during the measurement period. For the Tichki and Ameskar experiment, sap flow ranges assume, nonetheless, a good riparian water supply situation. The presented values are in line with comparable rainfall regimes from *Populus* tree studies indicating 51 l m^{-2} d^{-1} maximum daily rates of *Populus trichocarpa x Populus deltoides* with 15 m height and a canopy diameter of 15 m (Hinckley *et al.* 1994) and 108 l m^{-2} d^{-1} an individual 4 m tall (Ansley *et al.* 1994). Measurements with a weighting lysimeter on *Populus x euamerica* with a 5 m height and a sap wood area of 133 cm^2 report a maximum water use of 109 l m^{-2} d^{-1} (Edwards *et al.* 1996). According to Nadezhdina (1999) we assume the curves of tree two at Ameskar and tree three at Tichki with high daily amplitudes and accelerated night sap flow to have a low evaporative demand and the trees are probably saturated by ground water. Although *Populus canescens* is exceptional in terms of plant available water and represents a narrow strip of vegetation cover in this mountainous area the measurements presented here portray the importance of trees as consumers (c.p. Figure 33) in water budget calculations. Contrary to this *Buxus balearicus* transpiration measurement on August 24th 2005 depicted daily averages of a sum of 1.8 l m^{-2} leaf area (Figure 28). *Buxus balearicus* transpiration rates might be limited by shadowing effects in the mountainous valley at Ameskar, which is supported by an increasing transpiration rate as insulation and net radiation increases. No comparable transpiration measurements for semi-arid *Buxus balearicus* could be found in the literature. Transpiration measurements of the predominant shrub species *Artemisia herba-alba* by Gresens (2006) might help to evaluate the local semi-arid ratio of shrub water consumption. Transpiration amounts in 24 hours by *Artemisia herba-alba* in the nearby *Artemisia* steppe (at Tauojgalt test site) at selected days ranges from 1.0 l m^{-2} leaf area (October 6th, 2003) to 4.2 l m^{-2} leaf area for October 13th 2002. Individual shrub PFT transpiration measurements carry important regional information through their spatially predominant occurrence as well. Thus, this study further outlines the regional aspects at shrub PFT group level water consumption in the actual model resolution. The water budget assumptions of the entire study area will be outlined later.

For the basin of Ouarzazate the predicted average actual *trans* sum of “sage shrub” PFT for four months (February, May, August and November) for the IPCC A1B scenarios 2a and 2c are 66 mm and 47 mm, respectively (Table 34). Scenario B1 (2b) portrayed an average sum of the actual *trans* amounts of 60 mm. The maximum predicted sum of actual *trans* for scenario 2a is 122 mm, for scenario 2b it is 100 mm and for scenario 2c it is 77 mm. We assume that the difference among the IPPC scenarios is mainly due to *SysPpt* patterns that affected the annual *trans* sum. Moreover, a reduction of the sum and the maximum *trans* was observed between the two A1B scenarios (2a and 2c). This might be related to heavy stocking rates reducing the actual *trans* amounts by reduced *ANPP* as it performs constant grazing stresses. The predicted annual average *SysPpt* for A1B scenarios 2a-2c in the northern basin of Ouarzazate is a good approximation to the annual precipitation measured at the Taoujgalt climate station of an average of 250 mm. Compared to these base-line scenario 1a indicates average sums of the actual *trans* of 40 mm and the maximum *trans* of 74 mm (Table 34) with increasing *trans* trend during simulation. Scenario 1b shows an average sum of the actual *trans* of 74 mm and maximum 122 mm. Similar to the other IPCC scenarios, scenario 1b *trans* is characterised by a constant trend and compare to 1a approximated nearly doubled sum and maximum values. However, higher average *SysPpt* was assumed for scenario 1b, but this is probably due to the increase of *trans* caused by sufficient *Avlwat*. Scenario 1a supports the assumption that under census herd sizes *trans* increase potential is provided by climate station data drivers and thus vegetation possesses growth potential.

The model findings of the CO_2 scenarios 3a and 3b for “low DMD shrub” PFT in the southern ranges exhibited a *trans* sum for four months at 59 mm (CO_2 700 ppm) to 64 mm (CO_2 350 ppm) up to a maximum sum of 103 mm (CO_2 700 ppm) to 134 mm (CO_2 350 ppm) (Table 34). Different stocking rate periods showed an average sum of *trans* as follows: 54 mm, 62 mm and 59 mm (light, heavy and moderate stocking rate) at scenario 3a (Table 34), whereas scenario 3b forms the average sums of 64 mm, 73 mm and 64 mm of *trans*. The average inter-annual variation of the resulting *trans* might be informative as well, and these measures are 23 mm, 22 mm and 12 mm for scenario 3a and 25 mm, 24 mm to 12 mm at scenario 3b. The considerable differences of *trans* amounts are on the one hand dependent on CO_2 concentrations and on the other hand a considerable impact comparing stocking rate periods must be assumed. Increased CO_2 amounts led to a decrease of *trans* amounts as documented by Coughenour and Chen (1997). Furthermore, we may assume that “low DMD shrub” PFT of the southern ranges uses a higher ratio of incoming *SysPpt* for *trans* in relation to the northern range ratios and this is probably caused by the leaf cooling affects in accordance to Gresens (2006). As indicated in Chapter 6.1, the annual average sum of both southern scenarios *SysPpt* of 128 mm overrate the long-term (30 year)

measurements of the average of 80 mm at the climate station in Zagora (DRH 2004, Figure 1). Hence, the *trans* amounts for the southern ranges must be assumed as high and they might be induced by higher predicted biomass production. Gresens (2006) extrapolated daily transpiration amounts to the entire vegetation period, concluding an average amount of 4.5 mm a^{-1} and maximum 21 mm a^{-1} for the southern area underselling the amounts depicted here. However, as the *trans* amounts presented in this study represents the sum of two summer and two winter months these amounts might be too low at an annual perspective. For the northern ranges at the Taoujgalt area Gresens (2006) shows 60 to 360 mm a^{-1} of average transpiration for the entire vegetation period dependent on rainfall amounts. Predicted average *trans* amounts are probably only minor compared to these measurements because of the smaller *Lai* (see Figure 25) assumed. Constant stocking rates in scenario 2c probably led to the decrease of *ANPP* amounts followed by a reduction of actual predicted *trans*. During measurements Gresens (2006) evaluated amounts of 14% Vol. water content in the soil to be the minimum after which *Theucrium middeltense* (see chapter 2.5.1.2) is affected in transpiration capacity. However, as the ”sage shrub” PFT for the northern ranges in model is not water limited (as outlined in Chapter 6.1) this PFT might use full *trans* capacity in the model. Higher *trans* averages and maximum sums at scenario 3b (CO_2 350 ppm) compared to scenario 3a are reasonable as they are probably attributed to sufficient CO_2 amounts in atmosphere. Partial stomatal closure is a water deficit strategy of plants that encounter radiation or temperature stresses as documented by Noy-Meir *et al.* (1970); Christensen *et al.* (2003) and Chaves *et al.* (2003).

We assume water deficit, radiation and high temperatures to be the most limiting factors to plant growth agreeing with Gresens (2006). For example, *Artemisia herba-alba* uses a specific adaptation to drought; a reduction of stomatal conductance (*Cs*) to 0.5 mmol m^{-2} s^{-1} and a rapid decline in shoot-to-leaf hydraulic reductance as documented by Kolb and Sperry (1999). The “shrub PFT” *Cs* outcomes underline the *trans* results as they downscale plant water consumption to the individual diagnostic shrub PFT group level. For scenarios 2a and 2b the *Cs-act* rests constant at higher levels as indicated by base-line run 1a and is probably due to sufficient water supply as mentioned above. Instead, the base-line runs 1a and 1b illustrate a certain potential of augmenting *Cs-act* to higher levels permitted by incoming *SysPpt* and more adapted stocking rates as proposed by Schulze *et al.* (1980). Scenario 2c *Cs-act* predictions instead are constant but down-set to lower values compared to the 2a and 2b runs. This probably reflected the reduction of *ANPP* due to stocking rates, but sufficient water resources are available by predicted *SysPpt*.

In succession to the doubled CO_2 (700ppm) content, *Cs-act* was reduced by 30% comparing both section 3 scenarios. Scenario 3a called for the increase of *Cs-pot* if rainfall amounts permitted. These results agree with the assumptions of *Cs-act* decrease of 20% in the

doubled CO_2 scenario in a modelling study of assimilable rainfall regimes in Inner Mongolia by Christensen *et al.* (2003). Doubled CO_2 conditions have induced *ANPP* growth in simulations due to increased photosynthesis (*Ps*) amounts (+16%) and higher water use efficiency (*WUE*) (+37%) in this study. *Ps* amounts depended on radiation amounts and light intensities are at monthly average for “low DMD shrub” PFT of 6.9 µmol m^{-2} s^{-1} (350ppm) and 7.4 µmol m^{-2} s^{-1} (700ppm). The ”low DMD shrub” PFT aggregated *Ps* amounts are limited mainly by water supply and light intensities. Schulze (1972) and Gresens (2006) showed that in daily photosynthesis values the actual water supply in deserts decreases on with light intensities followed by water reduction and increases as light intensities decrease. *WUE* in scenario 3b (CO_2 350ppm) is of a monthly average of 6 kg DWT ha^{-1} mm^{-1}, whereas scenario 3a (CO_2 700ppm) exhibits a 10 kg DWT ha^{-1} mm^{-1} in relation to *SysPpt* in the annual course. Monthly *WUE* declines continuously considering each stocking rate period. From 6.6 kg DWT ha^{-1} mm^{-1} (3b) and 10.2 kg DWT ha^{-1} mm^{-1}(3a) at a light stocking rate period to 6.0 kg DWT ha^{-1} mm^{-1} (3b) and 9.9 kg DWT ha^{-1} mm^{-1} (3a) at a moderate stocking rate period. Foetzky (2002) evaluates *WUE* during the vegetation period in desert plants in central Asia with an annual average rainfall amount of 33 mm recommending 0.6 kg DWT ha^{-1} mm^{-1} at *Alhagi sparsifolia* and 1.2 kg DWT ha^{-1} mm^{-1} at C_4 *Calligonum caput-medusae*. These values are exceeded by our results for two reasons: primarily the C_3 shrubs presented here (see Chapter 1.4.3) have a higher water demand and, secondly, they receive higher precipitation amounts and thus are less water limited.

Regional assumptions of the predicted annual accumulated sum of the potential evapotranspiration amounts (*SysPet*) depicted for the heavy stocking rate scenario (2c) in the basin of Ouarzazate show minimum peaks of approximately 200 mm in the winter period to maximum peaks of approximately 800 mm in summer months. These then decrease again to the minimum (see Figure 74, 2c). The other IPCC scenarios 2a and 2b (Figure 74) show the annual minimum (winter) -maximum (summer) peaks of 150 mm to 600 mm and 200 mm to 550 mm, respectively. The minimum value reflects approximately the monthly evaporative capacity in the perspective cell. The development of the heavy stocking rate scenario is likely induced by the physical breaking of vegetation cover by animals that then accelerate *Bsev*. On the other hand, the lower maximum values of *SysPet* might result from water amounts stored in soils as *Avlwat* and was not available to evaporation in scenarios 2a and 2b. However, these *Avlwat* amounts depend on the scenario *SysPpt* amounts as scenarios 2a and 2b showed differences. The *SysPet* amounts for the southern range scenarios 3a and 3b (see Figure 96) indicated both annual accumulated sums of minimum-maximum peaks of 150 to 850 mm. The maximum is likely resulting from higher annual *SysPet* amounts driven by *Bsev* probably caused by rare vegetation cover (see ground cover discussion above) and high temperatures. The base-line scenarios 1a and 1b indicated the annual minimum and

maximum assumptions of 200 to 800 mm (1a) and 200 to 600 mm (1b). The smaller range of scenario 1b is probably due to the higher water amounts that might be bounded as soil water (*Slwat*) compared to scenarios 2a to 2c with similar climate conditions. The outcomes of this study underline the assumptions that 90 to 100% of rainfall amounts in arid to semi-arid environments are re-distributed by actual evapotranspiration to the atmosphere (Huxman *et al.* 2005). Moreover, the assumption of Gresens (2006) that on average 9% of the potential evapotranspiration and up to a of maximum 28% is transpiration by plants in the northern catchment in the basin of Ouarzazate can be confirmed. Furthermore, he distinguishes that rangeland plants, for example, *Artemisia herba-alba* ("sage shrub" PFT group) and *Theucrium middeltanse,* at Taoujgalt may, under the assumption of a maximum of *Lai*, account for about 150% of the annual average precipitation as actual evapotranspiration, which would be reasonable regarding these study results. Other measurements assumes 1300 mm a^{-1} for the basin of Ouarzazate (Le Houérou 1995), which we distinguish as the upper level of the potential evapotranspiration. For the southern ranges Le Houérou (1995) estimated a potential evapotranspiration rate of approximately 1600 mm a^{-1}. This study agrees that the potential evapotranspiration of the southern ranges is influenced by a larger portion of *trans* and that *Bsev* is higher. The variance of these outcomes showed high variability of both the actual and the potential evapotranspiration calculations based on the rainfall amounts for the studied period. However, the amounts of plant available soil water and the scenario rainfall assumptions probably falsify the predicted potential evapotranspiration.

7 Synthesis and Conclusions

The findings of this study highlight the key processes of inter- and intra-PFT variations towards livestock numbers for this region in a spatial and temporal manner. The goal of this study was to understand the role of anthropogenic induced variation of livestock numbers on the resultant ecosystem processes as well as other climatic and landscape factors. According to this study, anthropogenic factors have more impact on the amounts on biomass and their spatial distribution than climatic factors, except for doubled CO_2 scenario. The presented scenarios, however, show that the vegetation composition will change to temperature tolerant and graze resistant vegetation types in the future due to higher temperatures. As vegetation is identified to be the major player in the view of the water balance prospective in this environment its dependencies and consequences are significant. These results are useful for the evaluation of vegetative water potentials under changing climatic conditions.

From the results of this study, the carrying capacity in relation to vegetation patterns in the future may be used for pasture managing operators on both local and administrative levels.

The future stocking rate scenario of 900,000 animals at Province level (assumed here to be the Drâa catchment) was estimated as high and it seriously affect PFT structure and animal condition. This study proposes a carrying capacity of approximately 600,000-700,000 animals to supply a constant future herbivore-human-biomass ecosystem. However, for an insight into the understanding of plant water usage further studies on range specific plants and on an annual scale are necessary. In this study we highlighted the different mechanisms of plant species and functional types within different grazing regimes and growth constraints in this particular environment.

An important issue for future studies will be the better and deeper understanding of PFT responses to grazing. This study uses literature and extern scientific expert knowledge to determine this important feature on simulation purposes; model adaption. Also the sheep, goats and dromedaries regional specific metabolisms, their life cycles and growth parameters are included but not evaluated in this study. These characteristics are highly desirable for more reliable scenarios of animal conditions and diet parameters in future approaches.

The SAVANNA© model used in this study is on the foresight of ecological modelling herbivore – vegetation dynamics under changing climatic parameters. However attention has to be payed on the determination of cross scale dynamics, e.g. the plant-to-plant competition and interferences of water related topics such as transpiration. Another models error pool is probably the impact to plant growth patterns resulting from past heavy grazing intensities included as input data. Many carrying capacity models, such as SAVANNA©, overrate the

role of palatable PFT's. In that way animals obviously graze on these biomasses first as seen here. These models are restricted in applications that simulate non-palatable or un-palatable PFT's, for example, ungrazed plots. These issues have to be kept in mind by the model user. Long-term biomass data in the research region for model plausibility analyses and validation purely exists. Hence the model sensitivity and predictability has to be refined particularly, e.g. on insolation and phenology characteristics. Due to the large temporal and spatial fluctuations of biomass production single point and/or period data is useful with limitations only.

The model predicts a vast number of outcomes related to biomass, animals, hydrology and the environment. Hence for a useful scientific approach in a given research area, large datasets have to be measured and transferred to the model formatted database to simulate herbivore-biomass ecosystems. This assumes that the user should have a profound herbivore-biomass system understanding and a long-term research approach for a given environment, or a particular research area and appropriate dataset(s) with which to model a distinct set of parameters.

Some outcomes of this study are embedded in the IMPETUS computational framework. This framework consists of a set of programmes each defined on a specific research object, for example, the resilience of rangelands. These are combined in a project tool base. In this case these tools are comprehensive and include user-adapted information and spatial decision support systems (IS and SDSS) on local and regional pasture management. These tools are based on the visualisation and transfer of local to scientific knowledge (or vice-versa) on the rangeland characteristics and their specific performances on the PFT's grazed by animals. Our predicted output datasets on vegetation cover serve as input for detailed simulations of, for example, soil characteristics and hydrological modelling.

8 Literature

Ainsworth E. A. and Rogers A. (2007): The response of photosynthesis and stomatal conductance to rising [CO2]: mechanisms and environmental interactions. *Plant Cell and Environment* **30**(3): 258-270.

Allen-Diaz B. and Bartolome J. W. (1998): Sagebrush-grass vegetation dynamics: Comparing classical and state-transition models. *Ecological Applications* **8**(3): 795-804.

Alrababah M. A., Alhamad M. A., Suwaileh A. and Al-Gharaibeh M. (2007): Biodiversity of semi-arid Mediterranean grasslands: Impact of grazing and afforestation. *Applied Vegetation Science* **10**(2): 257-264.

Alverson K. D., Bradley R. S. and Pederson T. (2000): Environmental variability and climate change. International Geosphere-Biosphere Program Global Changes (IGBP Secretariat). Stockholm. Sweden.

Ansley R. J., Dugas W. A., Heuer M. L. and Trevino B. A. (1994): Stemflow and porometer measurements of transpiration from Honey Mesquite (Prosopis-Glandulosa). *Journal of Experimental Botany* **45**(275): 847-856.

Asner G. P., Elmore A. J., Olander L. P., Martin R. E. and Harris A. T. (2004): Grazing systems, ecosystem responses, and global change. *Annual Review of Environment and Resources* **29**: 261-299.

Ball J.T., Woodrow I.E. and Berry J.A. (1987): A model predicting stomatal conductance and its contribution to the control of photosynthesis under different environmental conditions. *Progress in Photosynthesis Research*. Nijhoff M. and Biggins J. (Ed.) Dordrecht. **4:** 221-224.

Bates J. D., Svejcar T., Miller R. F. and Angell R. A. (2006): The effects of precipitation timing on sagebrush steppe vegetation. *Journal of Arid Environments* **64**(4): 670-697.

Benabid A and Fennane M. (1994): Connaissances sur la végétation du Maroc. Phytogéographie, phytosociologie et séries de végétation. *Lazaroa* **14**: 21-97.

Benchekroun F. (1988): Forests in social and economic development of Moroccan Middle Atlas. Institut Agronomique et Veterinaire. Université Hassan II. Rabat. Maroc.

Boer M. and Stafford Smith D. M. (2003): A plant functional approach to the prediction of changes in Australian rangeland vegetation under grazing and fire. *Journal of Vegetation Science* **14**(3): 333-344.

Bonan G. B. (1993): Analysis of neighborhood competition among annual plants - Implications of a plant-growth model. *Ecological Modelling* **65**(1-2): 123-136.

Boone R. B., Coughenour M. B., Galvin K. A. and Ellis J. E. (2002): Addressing management questions for Ngorongoro Conservation Area, Tanzania, using the SAVANNA modelling system. *African Journal of Ecology* **40**(2): 138-150.

Boujenane I. and Kansari J. (2002): Lamb production and its components from purebred and crossbred mating types. *Small Ruminant Research* **43**(2): 115-120.

Boulain N., Cappelaere B., Seguis L., Gignoux J. and Peugeot C. (2006): Hydrologic and land use impacts on vegetation growth and NPP at the watershed scale in a semi-arid environment. *Regional Environmental Change* **6**(3): 147-156.

Bremer D. J., Auen L. M., Ham J. M. and Owensby C. E. (2001): Evapotranspiration in a prairie ecosystem: Effects of grazing by cattle. *Agronomy Journal* **93**(2): 338-348.

Brovkin V., Ganopolski A. and Svirezhev Y. (1997): A continuous climate- vegetation classification for use in climate-biosphere studies. *Ecol. Modell.* **101**: 251-261.

Canadell J., Jackson R. B., Ehleringer J. R., Mooney H. A., Sala O. E. and Schulze E. D. (1996): Maximum rooting depth of vegetation types at the global scale. *Oecologia* **108**(4): 583-595.

CBTHA (2002): Étude relative à l´inventaire participatif de la biodiversité dans le versant sud du Haut Atlas (document de synthese). Projet de Conservation de la Biodiversité par la Transhumance dans le versant sud du Haut Atlas (CBTHA). Ouarzazate. Maroc.

Chaves M. M., Maroco J. P. and Pereira J. S. (2003): Understanding plant responses to drought - from genes to the whole plant. *Functional Plant Biology* **30**(3): 239-264.

Chen D. X., Hunt H. W. and Morgan J. A. (1996): Responses of a C-3 and C-4 perennial grass to CO2 enrichment and climate change: Comparison between model predictions and experimental data. *Ecological Modelling* **87**(1-3): 11-27.

Choukri A. (2005): Landwirtschaftliche Produktivität und Wasserverbrauch verschiedener Kulturpflanzenarten im Hohen Atlas (Süd-Marokko). Unveröffentlichte Diplomarbeit an der Landwirtschaftlichen Fakultät der Rheinischen Friedrich-Wilhelms-Universität Bonn: 64 S. Germany.

Christensen L., Coughenour M. B., Ellis J. E. and Chen Z. Z. (2003): Sustainability of inner Mongolian grasslands: Application of the Savanna model. *Journal of Range Management* **56**(4): 319-327.

Christoph M. and Speth P. (2000): IMPETUS Westafrica: An integrated approach to the efficient management of scarce water resources in West Africa. *International Workshop on Climatic Change: Implications for the Hydrological Cycle and for Water Management*. Wengen. Germany.

Coughenour M. B. (1993): The SAVANNA landscape model–documentation and user´s guide. Natural Resource Ecological Laboratory-NREL. Colorado State University. Ft. Collins. USA.

Coughenour M. B. and Chen D. X. (1997): Assessment of grassland ecosystem responses to atmospheric change using linked plant-soil process models. *Ecological Applications* **7**(3): 802-827.

Coughenour M. (2005): Bison and elk carrying capacity in Yellowstone National Park – An assessment based upon spatial ecosystem modelling. Final Report to U.S. Geological Survey-Biological Resources Division. Bozeman. Montana. USA.

Drey T., Poete P., Thamm H.-P., Pannenbecker A. and Menz G. (2004): Generation of a high resolution DEM with ASTER Stereo Data for the river Draa Catchment in Morocco. Presentation at the IMPETUS and ORMVAO Conference 2004. Ouarzazate. Maroc.

DRH (2004): Aktuelle Klimadaten der Stationen im Drâatal. Unveröffentliche Studie der Direction Régionale de l´Hydraulique. Agadir-Ouarzazate. Maroc

Dumont B. and Hill D. R. C. (2001): Multi-agent simulation of group foraging in sheep: effects of spatial memory, conspecific attraction and plot size. *Ecological Modelling* **141**(1-3): 201-215.

Edwards D., Abbott G. D. and Raven J. A. (1996): *Cuticles of early land plants: a palaeoecophysiological evaluation.* Plant cuticles - An integrated functional approach. BIOS Sci. Publ. Oxford.

El Moudden M. (2005): Impact du prélèvement du boi de feu sur les parcours steppiques, cas d´Ighil M´goun, province de Ouarzazate. Thèse. Institut Agronomique et Vétérinaire. Université Hassan II. Rabat. Maroc.

Ellis J.E., Weins J.A., Rodell D.F. and Anway J.C. (1976): A conceptional model of diet selection as an ecosystem process. *J. Theor. Biol.* **60**: 49-55.

Emberger L. (1938): La définition phytogéographique du climate désertique. *La Vie dans la région désertique nord-tropicale de l'Ancien Monde*: 9-14.

FAO (2000): *The State of Food and Agriculture 2000*. Rome. FAO. Italy.

Finckh M. and Staudinger M. (2002): Micro- und makroskalige Ansätze zu einer Vegetationsgliederung des Draa-Einzugsgebietes (Südmarokko). *Ber. d. Rheinh.-Tüxen.-Ges.* **14**: 81 - 92. Hanover. Germany.

Finckh M. (2006): Klima- und Landnutzungsgetriebene Dynamik von Vegetationsmustern in Südmarokko. *Ber. d. Reinh.-Tüxen.-Ges*. **18**. 83–99. Hanover. Germany.

Finckh M. and Poete P. (2008): Vegetation Map of the Drâa Basin. in: Schulz O. and Judex M. (ed.): IMPETUS Atlas Morocco. Research Results 2000–2007. Department of Geography. University of Bonn. Germany.

Floret C., Pontanier R. and Rambal S. (1982): Measurement and modeling of primary production and water-use in a South Tunisian steppe. *Journal of Arid Environments* **5**(1): 77-90.

Foetzky A. (2002): Wasserhaushalt und Wassernutzungseffizienz von vier perennierenden Pflanzenarten im Vorland einer zentralasiatischen Flussoase. Dissertation der Mathematisch-Naturwissenschaftlichen Fakultät der Georg-August-Universität Göttingen. Germany.

Freeman M. C., Pringle C. M. and Jackson C. R. (2007): Hydrologic connectivity and the contribution of stream headwaters to ecological integrity at regional scales. *Journal of the American Water Resources Association* **43**(1): 5-14.

Giertz S. (2004): Analyse der hydrologischen Prozesse in den sub-humiden Tropen Westafrikas unter besonderer Berücksichtigung der Landnutzung am Beispiel des Aguima-Einzugsgebietes in Benin. Dissertation der Mathematisch-Naturwissenschaftlichen Fakultät der Rheinischen Friedrich-Wilhelms-Universität Bonn. URN: urn:nbn:de:hbz:5N-04068;
URL: http://hss.ulb.uni-bonn.de/diss_online/math_nat_fak/2004/giertz_simone/

Gillet F., Besson O. and Gobat J. M. (2002): PATUMOD: a compartment model of vegetation dynamics in wooded pastures. *Ecological Modelling* **147**(3): 267-290.

Granier A., Bobay V., Gash J. H. C., Gelpe J., Saugier B. and Shuttleworth W. J. (1990): Vapour flux density and transpiration rate comparisons in a stand of Maritime pine (*Pinus pinaster Ait.*) in Les Landes forest. *Agricultural and Forest Meteorology* **51**(3-4): 309-319.

Grant W. E., Hamilton W. T. and Quintanilla E. (1999): Sustainability of agroecosystems in semi-arid grasslands: simulated management of woody vegetation in the Rio Grande Plains of southern Texas and northeastern Mexico. *Ecological Modelling* **124**(1): 29-42.

Gresens F. (2006): Untersuchungen zum Wasserhaushalt ausgewählter Pflanzenarten im Drâa-Tal, Südost Marokko. Dissertation am Institut für Nutzpflanzenwissenschaften und Ressourcenschutz der Rheinischen Friedrich-Wilhelms-Universität Bonn. *Bonner Agrikulturchemische Reihe* Bd. **26**. Bonn. Germany.

Heidecke C. and Schulz T. (2008): Agricultural Land Use. in: Schulz O. and Judex M. (ed.): IMPETUS Atlas Morocco. Research Results 2000–2007. Department of Geography. University of Bonn. Germany.

Henkin Z., Seligman N. G. and Noy-Meir I. (2007): Successional transitions and management of a phosphorus-limited shrubland ecosystem. *Rangeland Ecology & Management* **60**(5): 453-463.

Hiepe C. (2008): Soil degradation by water erosion in a sub-humid West-African catchment: a modelling approach considering land use and climate change in Benin. Dissertation der Mathematisch-Naturwissenschaftlichen Fakultät der Rheinischen Friedrich-Wilhelms-Universität Bonn. URN: urn:nbn:de:hbz:5N-16286; URL: http://hss.ulb.uni-bonn.de/2008/1628/1628.htm

Hinkley T.M., Brooks J.R., Cermák J., Ceulemans R., Kucera J., Meinzer F.C. and Roberts D.A. (1994): Water flux in a hybrid poplar stand. *Tree Phys*. **14**(7-9): 1005-1018.

Hogg E. H. and Hurdle P. A. (1997): Sap flow in trembling aspen: implications for stomatal responses to vapor pressure deficit. *Tree Physiology* **17**(8-9): 501-509.

Howden S. M., White D. H. and Bowman P. J. (1996): Managing sheep grazing systems in southern Australia to minimise greenhouse gas emissions: Adaptation of an existing simulation model. *Ecological Modelling* **86**(2-3): 201-206.

Hübener H., Schmidt M., Sogalla M. and Kerschgens M. (2005): Simulating evapotranspiration in a semi-arid environment. *Theoretical and Applied Climatology* **80**(2-4): 153-167.

Hunt H. W., Trlica M. J., Redente E. F., Moore J. C., Detling J. K., Kittel T. G. F., Walter D. E., Fowler M. C., Klein D. A. and Elliott E. T. (1991): Simulation model for the effects of climate change on temperate grassland ecosystems. *Ecological Modelling* **53**(3-4): 205-246.

Huxman T. E., Wilcox B. P., Breshears D. D., Scott R. L., Snyder K. A., Small E. E., Hultine K., Pockman W. T. and Jackson R. B. (2005): Ecohydrological implications of woody plant encroachment. *Ecology* **86**(2): 308-319.

IFAD (1999): Rural poverty assessment of the Near East and North Africa. International Fund for Agricultural Development. Rome. mimeo. http://www.ifad.org/poverty/region/pn/nena.pdf

IMPETUS (2003): IMPETUS West Africa - An Integrated Approach to the Efficient Management of Scare Water Resources in West Africa: Case studies for selected river catchments in different climatic zones. Final Report, Period: 1.5.2000 - 30.4.2003. http://www.impetus.uni-koeln.de/content/download/EB2003/FinalReport2000_2003.pdf.

IMPETUS (2006): Integratives Management-Projekt für einen effizienten und tragfähigen Umgang mit Süßwasser in Westafrika: Fallstudien für ausgewählte Flußeinzugs-gebiete in unterschiedlichen Klimazonen. - http://www.impetus.uni-koeln.de/.

Iniguez L. (2004): Goats in resource-poor systems in the dry environments of West Asia, Central Asia and the Inter-Andean valleys. *Small Ruminant Research* **51**(2): 137-144.

IPCC (2007a): Climate Change 2007-The Physical Science Basis. Contribution of Working Group I to the Fourth Assessment Report of the IPCC. Cambridge. Cambridge University Press.

IPPC (2007b): Climate Change 2007-Impacts, Adaptation and Vulnerability. Contribution of Working Group I to the Fourth Assessment Report of the IPCC. Cambridge. Cambridge University Press.

IPPC (2007c): Climate Change 2007-Mitigation of Climate Change. Contribution of Working Group I to the Fourth Assessment Report of the IPCC. Cambridge. Cambridge University Press.

Jakob D. (2001): A note to the simulation of the annual and inter-annual variability of the water budget over the Baltic Sea drainage basin. *Meteor. Atm.* **77**(61-73).

Jauffret S. and Lavorel S. (2003): Are plant functional types relevant to describe degradation in arid, southern Tunisian steppes? *Journal of Vegetation Science* **14**(3): 399-408.

Kappen L., Lange O. L., Schulze E. D., Buschbom U. and Evenari M. (1972): Extreme water stress and photosynthetic activity of desert plant *Artemisia-herba-alba* Asso. *Oecologia* **10**(2): 177-182.

Kiker G. A. (1998): Development and comparison of Savanna ecosystem models to explore the concept of carrying capacity. Cornell University-Ithaka. New York.

Klose A. (2009): Soil characteristics and soil erosion by water in a semi-arid catchment (Wadi Drâa, South Morocco) under the pressure of global change. Dissertation der Mathematisch-Naturwissenschaftlichen Fakultät der Rheinischen Friedrich-Wilhelms-Universität Bonn. URN:nbn:de:hbz:5N-19599.

Knippertz P. (2003). Niederschlagsvariabilität in Nordwestafrika und der Zusammenhang mit der großskaligen atmosphärischen Zirkulation und der synoptischen Aktivität, Dissertation. Mitteilungen aus dem Institut für Geophysik und Meteorologie der Universität zu Köln. 136 S. Germany.

Knippertz P., Christoph M. and Speth P. (2003): Long-term precipitation variability in Morocco and the link to large-scale circulation in recent and future climates. *Meteorol. Atmos. Phys.* **83**: 67 - 88.

Kolb K. J. and Sperry J. S. (1999): Differences in drought adaptation between subspecies of sagebrush (*Artemisia tridentata*). *Ecology* **80**(7): 2373-2384.

Körner C. (1994): Leaf diffusive conductances in the mayor vegetation typs of the Globe. *Ecophysiology of photosynthesis*. Schulze E.D. and Caldwell M.M. (Ed.) Berlin, Heidelberg, New York, London, Paris, Tokyo, Hong Kong, Barcelona, Budapest. Springer Verlag.

Latore J., Gould P. and Mortimer A. M. (1999): Effects of habitat heterogeneity and dispersal strategies on population persistence in annual plants. *Ecological Modelling* **123**(2-3): 127-139.

Le Houérou H. N. (1972): *Africa - The Mediterranean region.* McKell C. M.; Blaisdell J.P. and Goodin J.R. (Ed.). Wildland shrubs - their biology and utilization. Ogden-Utah, U.S. Dept. Agic. For. Serv. Gen. Tech. Rep. int-1.

Le Houérou H. N. (1995): Bioclimatologie et biogéographie des steppes aride du Nord de l´Afrique. Diversité biologique, dévelopement durable et désertisation. *Option méditerraneénnes. Serie B,* **10**: 1 - 396.

LI-COR (1999): Using the LI-6400, Manual, Book 1, Part 1: The Basics.

Littleboy G and McKeon G. M. (1997): Subroutine GRASP: Grass production model. Documentation of the Macoola version of subroutine GRASP - Final Project Report for RIRDC project. *Appendix 2 of Evaluation the risk of pasture and land degradation in native pastures in Queensland*. Australia

Ludwig J. A., Coughenour M. B., Liedloff A. C. and Dyer R. (2001): Modelling the resilience of Australian savanna systems to grazing impacts. *Environment International* **27**(2-3): 167-172.

Lundblad M., Lagergren F. and Lindroth A. (2001): Evaluation of heat balance and heat dissipation methods for sapflow measurements in pine and spruce. *Annals of Forest Science* **58**(6): 625-638.

McNaughton S. J., Oesterheld M., Frank D. A. and Williams K. J. (1989): Ecosystem-level patterns of primary productivity and herbivory in terrestrial habitats. *Nature* **341**(6238): 142-144.

Montes N., Bertaudiere-Montes V., Badri W., Zaoui E. H. and Gauquelin T. (2002): Biomass and nutrient content of a semi-arid mountain ecosystem: the *Juniperus thurifera L.* woodland of Azzaden Valley (Morocco). *Forest Ecology and Management* **166**(1-3): 35-43.

Moore A.D., Donnelly J.R. and Freer M. (1997): GrazPlan: Decision support systems for Australian grazing enterprises. 3. Pasture growth and soil miosture submodels, and the GrassGro DSS. *Agric. Sys.* **55**: 537-582.

Mouillot F., Rambal S. and Lavorel S. (2001): A generic process-based Simulator for meditERRanean landscApes (SIERRA): design and validation exercises. *Forest Ecology and Management* **147**(1): 75-97.

Msanda F., El Aboudi, A. and Peltier J. P. (2002): Originalité de la flore et de la végétation de l´Anti-Atlas sud-occidental (Maroc). *Feddes Repertorium* **113**(7-8): 603-615.

Müller-Hohenstein K. and Popp H. (1990): *Marokko - Ein islamisches Entwicklungsland mit kolonialer Vergangenheit. Länderprofile: Geographische Strukturen, Daten, Entwicklungen*. Stuttgart. Ernst Klett Verlag.

Nadezhdina N. (1999): Sap flow index as an indicator of plant water status. *Tree Physiology* **19**(13): 885-891.

Nording C. (2008): Erfassung und Modellierung der weidbaren Biomasse im Jebel Saghro (Anti-Atlas)-Marokko. Diplomarbeit am Institut für Landschaftsökologie der Universtität Münster. Germany.

Noy-Meir I., Tadmor N.H. and Orshan G. (1970): Multivariate analysis of desert vegetation. *Israel Journal of Botany* **19**: 561-591.

Oldeland J. (2006): Vegetationsmodellierung am Südrand des Hohen Atlas, Marokko. Diplomarbeit am Institut für Allgemeine Botanik der Universität Hamburg. Biozentrum Klein Flottbek. Germany.

ORMVAO (2002): Rapport d´Activites - Campagne Agricole 2001-2002. Unveröffentlichte Studie der Office Régional de Mise en Valeur Agricole de Ouarzazate. Maroc.

ORMVAO (2003): Rapport d´Activites - Campagne Agricole 2002-2003. Unveröffentlichte Studie der Office Régional de Mise en Valeur Agricole de Ouarzazate. Maroc.

ORMVAO (2005): Office régionale de Mise en Valeur- *PAGER* - Études des resource en eau. Ouarzazate. Maroc.

Orthmann B. (2005): Vegetation ecology of a woodland-savanna mosaic in central Benin (West Africa): Ecosystem analysis with a focus on the impact of selective logging. Dissertation der Mathematischen-Naturwissenschaftlichen Fakultät der Universität Rostock.

Owens M. K. and Norton B. E. (1990): Survival of juvenile basin big sagebrush under different grazing regimes. *Journal of Range Management* **43**(2): 132-135.

Paeth H. (2004): Key factors in African climate change evaluated by a regional climate model. *Erdkunde* **58**: 290-315.

Palmer M. W. (1994): Variation in species richness: Towards a unification of hypotheses. *Folia Geobotanica* **29**(4): 511-530.

Parton W.J., McKeown B., Kirchner V. and Ojima D. S. (1992): CENTURY Model-Users Manual. *NREL Publication*. Colorado State University. Ft. Collins. Colorado. USA.

Paruelo J. M., Epstein H. E., Lauenroth W. K. and Burke I. C. (1997): ANPP estimates from NDVI for the Central Grassland Region of the United States. *Ecology* **78**(3): 953-958.

Paruelo J. M., Lauenroth W. K., Burke I. C. and Sala O. E. (1999): Grassland precipitation-use efficiency varies across a resource gradient. *Ecosystems* **2**(1): 64-68.

Priestley C. H. B. and Taylor R. J. (1972): On the assessment of surface heat-flux and evaporation using large-scale parameters. *Monthly Weather Review* **100**(2): 81-92.

Puigdefabregas J. and Mendizabal T. (1998): Perspectives on desertification: western Mediterranean. *Journal of Arid Environments* **39**(2): 209-224.

Quézel P. and Santa S. (1962): *Nouvelle flore de l'Algérie et des régions désertiques méridionales*. Paris. Editions du Centre National de la Récherche Scièntifique (CNRS). France.

Quézel P. and Barbero M. (1981): Contribution à l'étude des formations présteppiques à genévriers au Maroc. *Bol. Soc. Brot.* **Sér 2**(53): 1137-1160.

Quézel P., Barbéro M., Benabid A., Loisel R. and Rivas-Martinez S. (1988): Contribution à l'étude des groupements pré-forestiers et des matorrals rifains. *Ecol. mediterranea* **14**: 77-122.

Rachid A. (2004): Etude des interactions entre l´oasis et le parcours avoisinant pour une gestion durable des ressources pastorales dans la palmerais de Fezouata (moyenne vallée du Drâa). Thése. Institut Agronomique et Veterinaire. Université Hassan II. Rabat. Maroc.

Ramdane M. (2006): Grazing and animal metabolic characteristics. Unveröffentlichte Studie des Projet de Conservation de la Biodiversité par la Transhumance dans le versant sud du Haut Atlas (CBTHA). Ouarzazate. Maroc.

Rauh W. (1952): Vegetationsstudien im Hohen Atlas und dessen Vorland. Sitzungsberichte. Jg. 1952. 1. Abhandlung. *Heidelberger Akademie der Wissenschaften*. Heidelberg. Germany.

Reisner M. (2001): *Cadillac desert: the american west and its disappearing water*. Pimlico. London. 582 p.

Retzer V. and Reudenbach C. (2005): Modelling the carrying capacity and coexistence of pika and livestock in the mountain steppe of the South Gobi, Mongolia. *Ecological Modelling* **189**(1-2): 89-104.

Retzer V., Nadrowski K. and Miehe G. (2006): Variation of precipitation and its effect on phytomass production and consumption by livestock and large wild herbivores along an altitudinal gradient during a drought, South Gobi, Mongolia. *Journal of Arid Environments* **66**(1): 135-150.

Riedo M., Grub A., Rosset M. and Fuhrer J. (1998): A pasture simulation model for dry matter production, and fluxes of carbon, nitrogen, water and energy. *Ecological Modelling* **105**(2-3): 141-183.

Ritchie J. T. (1972): A model for predicting evaporation from a row crop with incomplete cover. *Water Resources Research* **8**(5): 1204-1214.

ROSELT (2004). Rapport intermédiaire de surveillance de l´observatoire ROSELT/OSS de l´Oued Mird à l´Haut Commisariat aux Eaux et foréts et à la Lutte Contre la Déserfication. Rabat. Maroc.

Roth A. and Heidecke C. (2008): Drought effects on livestock husbandry. in: Schulz O. and Judex M. (ed.): IMPETUS Atlas Morocco. Research Results 2000–2007. Department of Geography. University of Bonn. Germany.

Roth A. (2008): Agricultural structure in Ouled Yaoub. in: Schulz O. and Judex M. (ed.): IMPETUS Atlas Morocco. Research Results 2000–2007. Department of Geography. University of Bonn. Germany.

Schulz O. (2007): Analyse schneehydrologischer Prozesse und Schneekartierung im Einzugsgebiet des Oued M' Goun, Zentraler Hoher Atlas (Marokko). Dissertation der Mathematisch-Naturwissenschaftliche Fakultät der Rheinischen Friedrich-Wilhelms-Universität Bonn. URN: urn:nbn:de:hbz:5N-11286;
URL: http://hss.ulb.uni-bonn.de/diss_online/math_nat_fak/2007/schulz_oliver/

Schulz O. (2008): Impetus Atlas Morocco-research results 2000 - 2007. Schulz O. and Judex M. (Ed.). 2. major rev. ed. Department of Geography. University of Bonn. Germany.

Schulze E. D. (1972): A new type of climatized gas-exchange chamber for net photosynthesis and transpiration measurements in field. *Oecologia* **10**(3): 243-251.

Schulze E. D., Hall A. E., Lange O. L., Evenari M., Kappen L. and Buschbom U. (1980): Long-term effects of drought on wild and cultivated plants in the Negev Desert.1. Maximal rates of net photosynthesis. *Oecologia* **45**(1): 11-18.

Schulze E. D., Lange O. L., Evenari M., Kappen L. and Buschbom U. (1980): Long-term effects of drought on wild and cultivated plants in the Negev Desert.2. Diurnal Patterns of net photosynthesis and daily carbon gain. *Oecologia* **45**(1): 19-25.

Scurlock J. M. O., Johnson K. and Olson R. J. (2002): Estimating net primary productivity from grassland biomass dynamics measurements. *Global Change Biology* **8**(8): 736-753.

Simioni G., Le Roux X., Gignoux J. and Sinoquet H. (2000): Treegrass: a 3D, process-based model for simulating plant interactions in tree–grass ecosystems. *Ecological Modeling* **131**(1): 47-63.

Smith C., Reynolds J.D. and Sutherland W.J. (2000): Population consequences of reproductive decisions. *Proceedings: Biological Sciences*. **267(**1450): 1327-1334.

Speth P., Diekkrüger B., Christoph M. and Jaeger A. (2005): IMPETUS West Africa-An integrated approach to the efficient management of scarce water resources in West Africa. Case studies for selected river catchments in different climate zones. *GLOWA-German Programme on Global Change in the Hydrological Cycle, Status Report 2005*. Deutsches Luft- und Raumfahrtzentrum (DLR)**:** 86-94.

Staudinger M. and Finckh M. (2005): Räumliche Vegetationsmuster in ariden Gebieten Südmarokkos-Klassifizierung zugrunde liegender Mechanismen. Veste M. and Wissel C. (Ed.). *Beiträge zur Vegetationsökologie der Trockengebiete und Desertifikation*. UFZ Bericht 01/2005: 41-53.

Strasburger E., Noll F., Schenck H. and Schimper A.F.W. (1991): *Lehrbuch der Botanik für Hochschulen*. 33. Auflage. New York. Gustav Fischer Verlag.

Tielborger K. and Kadmon R. (2000): Indirect effects in a desert plant community: is competition among annuals more intense under shrub canopies? *Plant Ecology* **150**(1-2): 53-63.

UNEP (1999): Global Environmental Outlook 2000. *http://www.unep.org/geo2000/*.

UNFCCC (1992): United Nations Framework Convention on Climate Change - Articles. United Nations. New York.

UNFCCC (2006): United Nations Framework Convention on Climate Change - Global Observing System for Climate. *Submissions from parties*. Bonn. Germany. http://unfccc.int/resource/docs/2006/sbta/eng/misc05.pdf

UP-GmbH (2000): User Manual PROSALog. *Umweltanalytische Produkte-UP*. Ibbenbühren. Germany.

USDA (1972): U.S. Department of Agriculture-Soil Conservation Service. Section 4 Hydrology. *National Engineering Handbook*. Washington D.C.

Wang S., Grant R. F., Verseghy D. L. and Black T. A. (2001): Modelling plant carbon and nitrogen dynamics of a boreal aspen forest in CLASS - the Canadian Land Surface Scheme. *Ecological Modelling* **142**(1-2): 135-154.

Weber B. (2004): Untersuchungen zum Bodenwasserhaushalt und Modellierung der Bodenwasserflüsse entlang eines Höhen- und Ariditätsgradienten (SE Marokko). Dissertation an der Mathematisch-Naturwissenschaftliche Fakultät der Rheinischen Friedrich-Wilhelms-Universität Bonn.
URN: urn:nbn:de:hbz:5N-05233;
URL. http://hss.ulb.unibonn.de/diss_online/math_nat_fak/2004/weber_benedikt/

Weber G. E., Moloney K. and Jeltsch F. (2000): Simulated long-term vegetation response to alternative stocking strategies in savanna rangelands. *Plant Ecology* **150**(1-2): 77-96.

Weisberg P. J., Hobbs N. T., Ellis J. E. and Coughenour M. B. (2002): An ecosystem approach to population management of ungulates. *Journal of Environmental Management* **65**(2): 181-197.

Weischet W. (1991): *Einführung in die Klimatologie*. Stuttgart. Teubner Verlag. Germany.

White E. G. (1984a): A multispecies Simulation-Model of grassland producers and consumers.1. Validation. *Ecological Modelling* **24**(1-2): 137-157.

White E. G. (1984b): A multispecies Simulation-Model of grassland producers and consumers.2. Producers. *Ecological Modelling* **24**(3-4): 241-262.

White E. G. (1984c): A multispecies Simulation-Model of grassland producers and consumers.3. Consumers. *Ecological Modelling* **24**(3-4): 263-279.

Wiegand T., Snyman H. A., Kellner K. and Paruelo J. M. (2004): Do grasslands have a memory: Modeling phytomass production of a semi-arid South African grassland. *Ecosystems* **7**(3): 243-258.

Wiegand K., Saltz D., Ward D. and Levin S. A. (2008): The role of size inequality in self-thinning: A pattern-oriented simulation model for savannas. *Ecological Modelling* **210**(4): 431-445.

Wight J. R. and Skiles J.W. (1987): SPUR: Simulation of production and utilization of rangelands. Documentation and User guide. *U.S. Dept. of Agriculture. Agric. Res. Serv*. ARS.

Williams C. A. and Albertson J. D. (2005): Contrasting short- and long-timescale effects of vegetation dynamics on water and carbon fluxes in water-limited ecosystems. *Water Resources Research* **41**(6). W06005.

Wook K. J. and Kim J. H. (1997): Modelling the net photosynthetic rate of *Quercus mongolica* stands affected by ambient ozone. *Ecological Modelling* **97**(3): 167-177.

WRI (1998): *World resources 1998-1999*. World Resource Institute. New York, Oxford University Press.

Wraith J. M., Johnson D. A., Hanks R. J. and Sisson D. V. (1987): Soil and plant water relations in a crested wheatgrass pasture: Response to spring grazing by cattle. *Oecologia* **73**: 573–578.

Wu H. I., Li B. L., Stoker R. and Li Y. (1996): A semi-arid grazing ecosystem simulation model with probabilistic and fuzzy parameters. *Ecological Modelling* **90**(2): 147-160.

Yamout H. (2007): The Upper Drâa Basin. in: Schulz O. and Judex M. (ed.): IMPETUS Atlas Morocco. Research Results 2000–2007. 1. Edition. Department of Geography. University of Bonn Germany.

Yessef M. (1996): Diagnostique du système de production fourrager - Rapport no. 32. *Projet Lutte contre la Désertification dans la vallée du Drâa*. Ouarzazate. Maroc.

Zaady E., Yonatan R., Shachak M. and Perevolotsky A. (2001): The effects of grazing on abiotic and biotic parameters in a semiarid ecosystem: A case study from the Northern Negev Desert, Israel. *Arid Land Research and Management* **15**(3): 245-261.

Zhang L., Walker G. R. and Fleming P. M. (2002): Surface water balance for recharge estimation. *CSIRO Publishing*. Melbourne. Australia.

9 Appendix

Table 35 : Soil characteristics of 52 soil types in the study area for soil layer 1, 2 and 3; characteristics are: depth 1-3, wilting point 1-3, field capacity (fcap) 1-3, porosity 1-3, runon, runoff, evaporative capability, Klose (2009) modified

Soil type No.	depth 1	depth 2	total depth	wilting point 1	wilting point 2	wilting point 3	fcap 1	fcap 2	fcap 3	porosity 1	porosity 2	porosity 3	runon	runoff	evaporation
1	192.6	359.5	552.1	0.459	0.349	0.349	2.028	1.569	1.569	0.63	0.57	0.57	90	90	8.2
2	687.3	1405.2	2092.5	0.362	0.346	0.346	1.643	1.510	1.510	0.64	0.6	0.6	50	70	10.4
3	293.3	312	605.3	0.371	0.296	0.296	1.733	1.313	1.313	0.58	0.55	0.55	60	65	8.3
4	388.4	392.7	781.1	0.504	0.369	0.369	2.393	1.838	1.838	0.58	0.55	0.55	75	90	6.4
5	46.3	111	157.3	0.258	0.145	0.145	1.410	0.736	0.736	0.58	0.57	0.57	50	50	6.9
6	316.5	415.4	731.9	0.627	0.405	0.405	2.606	2.007	2.007	0.63	0.56	0.56	70	80	6.8
7	14.9	107.7	122.6	0.383	0.206	0.206	1.816	0.937	0.937	0.63	0.53	0.53	70	80	11.3
8	131.7	141.1	272.8	0.564	0.536	0.536	2.793	2.312	2.312	0.64	0.57	0.57	90	95	8.8
9	56.3	269.7	312	0.578	0.463	0.463	2.806	1.982	1.982	0.58	0.61	0.61	90	95	9.6
10	700.5	791.4	1491.9	0.252	0.286	0.286	1.214	1.135	1.135	0.58	0.54	0.54	80	70	10.4
11	72.9	170.2	243.1	0.424	0.323	0.323	2.186	1.476	1.476	0.64	0.56	0.56	75	65	13
12	1075.4	1173.5	2248.9	0.307	0.371	0.371	1.577	1.482	1.482	0.58	0.59	0.59	50	65	6.6
13	113.4	140.7	254.1	0.341	0.299	0.299	1.881	1.384	1.384	0.58	0.59	0.59	65	65	9.4
14	228.3	686.5	914.8	0.505	0.587	0.587	2.830	2.570	2.570	0.58	0.59	0.59	75	90	10.6
15	575.9	651.8	1227.7	0.222	0.185	0.185	1.024	0.741	0.741	0.58	0.5	0.5	75	80	10.1
16	120.2	341.7	461.8	0.278	0.191	0.191	1.344	0.838	0.838	0.63	0.54	0.54	50	50	12.2
17	436.3	446.8	885.5	0.588	0.686	0.686	2.840	2.752	2.752	0.63	0.59	0.59	60	60	13.1
18	204.1	288.9	493	0.219	0.19	0.19	1.020	0.797	0.797	0.58	0.52	0.52	80	85	7.8
19	31.8	355.2	386.9	0.199	0.11	0.11	0.988	0.459	0.459	0.58	0.49	0.49	85	80	7.2
20	115.7	297	412.7	0.124	0.101	0.101	0.691	0.418	0.418	0.53	0.44	0.44	80	90	8.5
21	561.5	1005.2	1566.7	0.282	0.265	0.265	1.235	1.113	1.113	0.64	0.57	0.57	90	90	4.2
22	14.7	374.4	389.1	0.325	0.091	0.091	1.660	0.416	0.416	0.62	0.5	0.5	55	55	8.4
23	357.7	1036.1	1393.8	0.206	0.172	0.172	0.948	0.731	0.731	0.63	0.55	0.55	60	75	9.1
24	221.1	268.5	489.6	0.189	0.2	0.2	0.985	0.802	0.802	0.53	0.45	0.45	55	65	8.6
25	257.5	467.4	724.9	0.245	0.249	0.249	1.426	1.321	1.321	0.53	0.43	0.43	60	70	8.5
26	115.7	135	250.7	0.251	0.336	0.336	1.437	1.376	1.376	0.52	0.47	0.47	90	80	9.3
27	290.7	499.3	790.1	0.245	0.263	0.263	1.220	1.121	1.121	0.53	0.42	0.42	70	70	9
28	136	308.5	444.5	0.123	0.109	0.109	0.622	0.395	0.395	0.53	0.43	0.43	80	85	7.8
29	235.8	321.4	557.2	0.188	0.186	0.186	0.909	0.679	0.679	0.53	0.44	0.44	60	90	7.4
30	337.8	508.3	846.1	0.32	0.328	0.328	2.162	1.811	1.811	0.52	0.43	0.43	65	75	7.9
31	82.5	164.6	282.1	0.165	0.198	0.198	0.99	0.856	0.856	0.53	0.45	0.45	70	80	8
32	564.2	795.2	1359.4	0.246	0.268	0.268	1.360	1.189	1.189	0.53	0.44	0.44	70	70	9.9
33	1202.5	1305.7	2508.2	0.244	0.36	0.36	1.373	1.313	1.313	0.53	0.47	0.47	80	90	6.3
34	532.4	719	1251.4	0.184	0.197	0.197	0.967	0.794	0.794	0.54	0.44	0.44	85	90	6.9
36	458.9	754.2	1213.2	0.19	0.206	0.206	0.99	0.883	0.883	0.54	0.42	0.42	50	60	11.5
37	329.4	608.1	937.5	0.36	0.358	0.358	1.987	1.750	1.750	0.53	0.42	0.42	70	80	10.7
38	60.7	1158.8	1219.5	0.231	0.078	0.078	1.153	0.35	0.35	0.58	0.45	0.45	60	70	10
39	397	727.8	1124.7	0.104	0.101	0.101	0.586	0.364	0.364	0.53	0.42	0.42	70	80	10.4
40	318.7	875.3	1194	0.121	0.091	0.091	0.628	0.338	0.338	0.53	0.43	0.43	60	60	12.1
41	685.9	982.4	1668.3	0.342	0.347	0.347	1.784	1.539	1.539	0.53	0.47	0.47	80	90	11.4
42	423.3	902.2	1325.5	0.272	0.265	0.265	1.446	1.240	1.240	0.53	0.42	0.42	85	80	6.5
43	274.3	592	866.3	0.472	0.564	0.564	2.908	2.507	2.507	0.52	0.44	0.44	80	85	7.3
44	107.9	170.9	278.8	0.784	0.59	0.59	2.735	2.092	2.092	0.52	0.47	0.47	70	80	8.8
45	87.5	106.4	193.9	0.147	0.204	0.204	0.827	0.794	0.794	0.53	0.42	0.42	70	75	8.1
46	298	1088.1	1386.1	0.132	0.459	0.459	0.662	0.864	0.864	0.54	0.56	0.56	70	80	8.9
47	109	159.7	258.7	0.217	0.388	0.388	1.246	1.280	1.280	0.53	0.42	0.42	65	60	5.7
48	71.7	506.3	577.9	0.186	2.587	2.587	0.912	2.982	2.982	0.54	0.51	0.51	60	70	6.3
49	10	20	30	0.004	0.004	0.004	0.002	0.002	0.002	0.01	0.01	0.01	10	10	5
50	50.9	359.5	410.4	0.096	1.299	1.299	0.5	2.223	2.223	0.54	0.47	0.47	70	80	7.7
51	46.1	1010.5	1056.6	0.159	0.015	0.015	0.832	0.157	0.157	0.51	0.35	0.35	60	70	8.2
52	470.8	496.3	967.1	0.501	0.446	0.446	2.726	2.447	2.447	0.53	0.48	0.48	85	80	9.9

Table 36: Soil fertility characteristics of 52 soil types in the study area for soil layer 1, 2 and 3; characteristics are: C content (%) layer 1-3, N content (%) layer 1-3, Bulk density 1-3, surface litter g C m^{-2}, soil litter g C m^{-2}, surface litter g N m^{-2}, Klose (2009) modified

Soil type no.	%C layer 1	%C layer 2	%C layer 3	% N layer 1	% N layer 2	% N layer 3	Bulk density 1	Bulk density 2	Bulk density 3	surface litter gC/ m^2	soil litter gC/ m^2	surface litter gN/ m^2	soil litter gN/ m^2
1	3.99	3.99	3.99	0.11	0.11	0.11	22.32	21.71	21.71	187	-99	0.047	0.066
2	4.16	4.16	4.16	0.13	0.13	0.13	21.96	21.88	21.88	444	-99	0.036	0.066
3	1.63	1.63	1.63	0.08	0.08	0.08	29.95	28.53	28.53	701	-99	0.045	0.066
4	1.68	1.68	1.68	0.07	0.07	0.07	31.19	30.07	30.07	153	-99	0.024	0.066
5	1.68	1.68	1.68	0.08	0.08	0.08	37.79	34.02	34.02	171	-99	0.031	0.066
6	4.05	4.05	4.05	0.10	0.10	0.10	22.40	22.57	22.57	347	-99	0.031	0.066
7	4.38	4.38	4.38	0.11	0.11	0.11	33.95	30.11	30.11	655	-99	0.028	0.066
8	4.75	4.75	4.75	0.08	0.08	0.08	20.45	23.62	23.62	192	-99	0.034	0.066
9	1.78	1.78	1.78	0.07	0.07	0.07	21.60	24.87	24.87	208	-99	0.045	0.066
10	1.55	1.55	1.55	0.08	0.08	0.08	31.99	25.98	25.98	304	-99	0.041	0.066
11	4.54	4.54	4.54	0.09	0.09	0.09	30.52	29.41	29.41	643	-99	0.041	0.066
12	1.68	1.68	1.68	0.10	0.10	0.10	31.02	24.79	24.79	672	-99	0.042	0.066
13	1.61	1.61	1.61	0.07	0.07	0.07	33.02	32.32	32.32	391	-99	0.044	0.066
14	1.64	1.64	1.64	0.07	0.07	0.07	30.69	22.65	22.65	290	-99	0.044	0.066
15	1.46	1.46	1.46	0.08	0.08	0.08	31.32	25.21	25.21	179	-99	0.044	0.066
16	3.93	3.93	3.93	0.11	0.11	0.11	25.26	29.14	29.14	165	-99	0.041	0.066
17	3.89	3.89	3.89	0.10	0.10	0.10	32.00	24.57	24.57	918	-99	0.041	0.066
18	1.53	1.53	1.53	0.10	0.10	0.10	30.40	29.34	29.34	188	-99	0.043	0.066
19	1.53	1.53	1.53	0.07	0.07	0.07	35.95	33.27	33.27	452	-99	0.022	0.066
20	0.66	0.66	0.66	0.05	0.05	0.05	36.27	37.95	37.95	166	-99	0.022	0.066
21	4.07	4.07	4.07	0.12	0.12	0.12	21.72	22.86	22.86	421	-99	0.022	0.066
22	3.79	3.79	3.79	0.10	0.10	0.10	33.46	42.20	42.20	701	-99	0.033	0.066
23	3.91	3.91	3.91	0.11	0.11	0.11	24.35	28.77	28.77	210	-99	0.039	0.066
24	0.65	0.65	0.65	0.05	0.05	0.05	36.99	35.92	35.92	377	-99	0.042	0.066
25	0.65	0.65	0.65	0.04	0.04	0.04	42.67	37.66	37.66	453	-99	0.027	0.066
26	0.70	0.70	0.70	0.04	0.04	0.04	36.10	33.92	33.92	555	-99	0.027	0.066
27	0.44	0.44	0.44	0.04	0.04	0.04	38.69	37.82	37.82	399	-99	0.023	0.066
28	0.43	0.43	0.43	0.04	0.04	0.04	35.42	38.16	38.16	444	-99	0.020	0.066
29	0.44	0.44	0.44	0.04	0.04	0.04	36.19	37.11	37.11	803	-99	0.025	0.066
30	0.65	0.65	0.65	0.03	0.03	0.03	43.41	36.86	36.86	633	-99	0.026	0.066
31	0.66	0.66	0.66	0.04	0.04	0.04	40.67	37.05	37.05	333	-99	0.026	0.066
32	0.64	0.64	0.64	0.04	0.04	0.04	39.75	37.21	37.21	173	-99	0.033	0.066
33	0.69	0.69	0.69	0.05	0.05	0.05	36.71	32.93	32.93	646	-99	0.038	0.066
34	0.66	0.66	0.66	0.05	0.05	0.05	38.44	36.29	36.29	738	-99	0.040	0.066
35	2.96	2.96	2.96	0.25	0.25	0.25	46.51	36.09	36.09	720	-99	0.041	0.066
36	0.43	0.43	0.43	0.04	0.04	0.04	40.05	40.35	40.35	783	-99	0.042	0.066
37	0.45	0.45	0.45	0.03	0.03	0.03	40.27	33.21	33.21	833	-99	0.048	0.066
38	1.66	1.66	1.66	0.12	0.12	0.12	24.16	30.83	30.83	826	-99	0.037	0.066
39	0.43	0.43	0.43	0.04	0.04	0.04	39.86	39.62	39.62	825	-99	0.036	0.066
40	0.67	0.67	0.67	0.05	0.05	0.05	35.50	37.42	37.42	666	-99	0.044	0.066
41	0.43	0.43	0.43	0.03	0.03	0.03	38.09	35.00	35.00	629	-99	0.047	0.066
42	0.43	0.43	0.43	0.03	0.03	0.03	40.12	38.12	38.12	381	-99	0.023	0.066
43	0.64	0.64	0.64	0.03	0.03	0.03	28.96	32.15	32.15	400	-99	0.024	0.066
44	0.74	0.74	0.74	0.04	0.04	0.04	18.24	27.84	27.84	574	-99	0.028	0.066
45	0.45	0.45	0.45	0.03	0.03	0.03	42.18	36.60	36.60	207	-99	0.030	0.066
46	0.05	0.05	0.05	0.05	0.05	0.05	47.52	7.59	7.59	399	-99	0.041	0.066
47	0.44	0.44	0.44	0.03	0.03	0.03	41.20	33.51	33.51	738	-99	0.022	0.066
48	0.06	0.06	0.06	0.05	0.05	0.05	46.87	4.37	4.37	736	-99	0.037	0.066
49	-99	-99	-99	-99	-99	-99	-99	-99	-99	-99	-99	-99	0.066
50	0.06	0.06	0.06	0.05	0.05	0.05	46.73	34.55	34.55	280	-99	0.042	0.066
51	0.78	0.78	0.78	0.04	0.04	0.04	13.39	56.52	56.52	702	-99	0.044	0.066
52	0.47	0.47	0.47	0.04	0.04	0.04	30.45	32.34	32.34	462	-99	0.047	0.066

Acknowledgements

This work was conducted under the IMPETUS project, and was supported by the Federal German Ministry of Education and Research (BMBF) under grant No. 01 LW 0301A and by the Ministry of Science and Research (MWF) of the federal of Northrhine-Westfalia (grant No. 223-21200200).

I am grateful to PD Dr. Burkhardt, for introducing me to the topic of this PhD.

I am indebted to my supervisor Prof. Dr. H. Goldbach for always providing advice and support and for seeing me through the process of this study. I also thank Prof. Dr. B. Diekkrüger for accepting to be my co-supervisor, for his interest and support throughout this thesis.

I am extremely thankful to Dr. Frank Gresens. He directed me through the field of vegetation eco-physiology and familiarised me with the methods required. His knowledge and passion about this topic as well as his suggestions and answers to all my numerous questions are highly appreciated.

I convey special gratitude to Dr. Michael Coughenour for providing support along the SAVANNA software whenever needed.

My gratitude is also extended to all the former and current staff of the IPE, in particular Dr. Sebastian Wulf, Dr. Thomas Eichert, Yvonne Dills, Sven Berkau, Dr. Thuweba Dibani, Dr. Alice Beining, Christiane Stadler, Dr. Monika Wimmer, Dr. Frank Gresens, Dr. Christian Schneider, Dr. Melanie Hecht, Axel Heck for the inspiring working atmosphere and the wonderful time we had together. My thanks also go to the other staff of this institute who all contributed to this study in one way or the other.

I am indebted to Dr. Anna Klose, Stefan Klose, Dr. Oliver Schulz, Henning Busche, Christina Rademacher, Dr. Manfred Finckh, Jens Oldeland, Dr. Holger Kirscht, Claudia Heidecke, Gero Steup, Pierre Fritzsche, Dr. Thomas Gaiser, Dr. Anja Lindstaedter for pictures, Dr. Kai Born, Ralf Hoffmann, Dr. Sebastien Cappy, Martina Gockel and Jamal Ait El Hadj for inspiring scientific discussions, their assistance to overcome any hurdles and the great time we had together in Morocco. I would like to thank all the staff of the formerly IMPETUS project for their support and assistance whenever needed but foremost for the pleasant team work throughout the project.

Special thanks also to Dr. Maria Thielen for proof-reading this work and providing valuable comments and Dr. Manfred Finckh for his scientific support.

I am extremely grateful to Dr. Therese Hintemann for critically proof-reading major parts of this thesis and meticulously bringing this script into this printable format. Her encouragement kept the spirits up during the entire duration of this study.

Last but not least I would like to thank my family and friends who all have their share in making this study a success.